The Abdus Salam International Centre for Theoretical Physics

United Nations Educational, Scientific and Cultural Organization

IAEA International Atomic Energy Agency

2332

School on Synchrotron and FEL Based Methods and their Multi-Disciplinary Applications

19 - 30 March 2012

Additional information lecture 1

Charles S. Fadley

Univ. of California Davis & LBNL
USA

Characterization of Surfaces, Interfaces, and Complex Materials with Core and Valence Photoemission

Chuck Fadley
Dept. of Physics, UC Davis
and
Materials Sciences Division
Lawrence Berkeley National Laboratory

Supported by: U.S. Dept. of Energy
Humboldt Foundation & Helmholtz Association
Jülich Research Center

School on Synchrotron Radiation and FEL Based Methods and their Multi-Disciplinary Applications
March 26, 2012

Photoelectron spectroscopy = Photoemission: The Basic Elements

Friday, 23 March 2012

Room: Adriatico Guest House Giambiagi Lecture Hall

09:00 10:30	Surfaces, Interfaces & Photoelectron Spectroscopy 01h30'	A. Goldoni *Sincrotrone Trieste*
10:30 11:00	BREAK 30'	
11:00 12:30	ARPES 01h30'	A. Goldoni *Sincrotrone Trieste*
12:30 14:00	LUNCH BREAK 01h30'	
14:00 15:30	Inelastic X-ray Scattering: principles and application 01h30'	F. Bencivenga *Sincrotrone Trieste*
15:30 16:00	BREAK 30'	
16:00 17:00	Electronic structure and atomistic computations for the interpretation of synchrotron experiments 01h00'	N. Binggeli *ICTP*

Monday, 26 March 2012

Room: Adriatico Guest House Giambiagi Lecture Hall

09:00 10:30	Photoelectron Diffraction and holography 01h30'	Charles S. Fadley *Univ. of California Davis & LBNL (USA)*
10:30 11:00	BREAK 30'	
11:00 12:30	Core Level shifts, splitting and dichroism 01h30'	Charles S. Fadley *Univ. of California Davis & LBNL (USA)*
12:30 14:00	LUNCH BREAK 01h30'	
14:00 15:30	Low density matter: spectroscopy and scattering 01h30'	M. Simon *University Pierre et Marie Curie, France*
15:30 16:00	BREAK 30'	
16:00 17:00	Low-density matter: ultrafast dynamics 01h00'	M. Simon *University Pierre et Marie Curie, France*
17:00 18:30	Theoretical spectroscopy of gas-phase systems 01h30'	P. Decleva *University of Trieste*

Link to archive of longer set of lectures in 2010, plus guides to use of SESSA and EDAC simulation programs:
http://www.yousendit.com/download/M3Btb2VDeFU3N0RFdzhUQw

General references on various aspects of photoelectron spectroscopy, diffraction, holography (available at School website and/or Fadley group website: http://www.physics.ucdavis.edu/fadleygroup/ :

Paper [1] "Basic Concepts of X-ray Photoelectron Spectroscopy", C.S.F, in Electron Spectroscopy, Theory, Techniques, and Applications, Brundle and Baker, Eds. (Pergamon Press, 1978) Vol. II, Ch. 1.

Paper [2] "Atomic-Level Characterization of Materials with Core- and Valence-Level Photoemission: Basic Phenomena and Future Directions", C.S. Fadley, Surf. Interface Anal. 2008, 40, 1579–1605.

Paper [3] "X-ray photoelectron spectroscopy: Progress and perspectives"
C.S. Fadley, Journal of Electron Spectroscopy and Related Phenomena 178–179 (2010) 2–32

Key Reference: "X-ray Data Booklet", Center for X-Ray Optics and the Advanced Light Source, LBNL, January, 2001, available online at: http://xdb.lbl.gov/

Additional very useful websites:

X-ray optical calculations: reflectivities, penetration depths for a variety of mirror/surface geometries— http://www-cxro.lbl.gov/optical_constants/

General properties of the elements and their compounds: http://www.webelements.com

Simulation of photoelectron and Auger spectra with program SESSA: See "SESSA: A Brief Manual", with download instructions, etc.

Simulation of x-ray photoelectron diffraction (XPD) with program EDAC: See guide example calculation for CO on Fe.

X-RAY DATA BOOKLET

Center for X-ray Optics and Advanced Light Source
Lawrence Berkeley National Laboratory

http://xdb.lbl.gov/

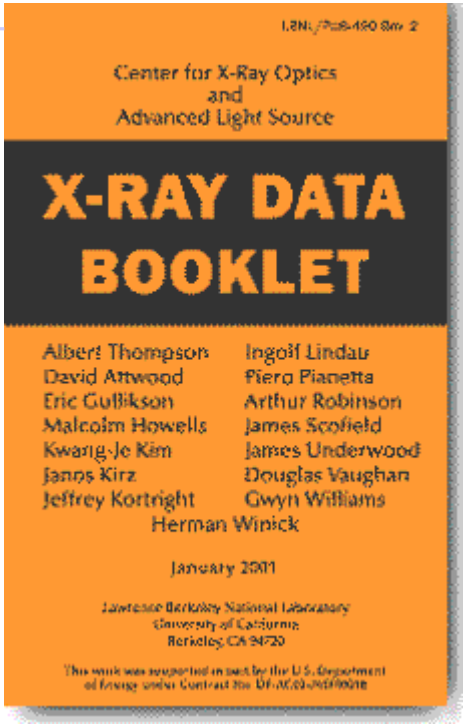

Periodic Table, with the Outer Electron Configurations of Neutral Atoms in Their Ground States

The notation used to describe the electronic configuration of atoms and ions is discussed in all textbooks of introductory atomic physics. The letters s, p, d, . . . signify electrons having orbital angular momentum 0, 1, 2, . . . in units $\hbar$; the number to the left of the letter denotes the principal quantum number of one orbit, and the superscript to the right denotes the number of electrons in the orbit.

H^{1} $1s$																	He^{2} $1s^2$
Li^{3} $2s$	Be^{4} $2s^2$											B^{5} $2s^22p$	C^{6} $2s^22p^2$	N^{7} $2s^22p^3$	O^{8} $2s^22p^4$	F^{9} $2s^22p^5$	Ne^{10} $2s^22p^6$
Na^{11} $3s$	Mg^{12} $3s^2$											Al^{13} $3s^23p$	Si^{14} $3s^23p^2$	P^{15} $3s^23p^3$	S^{16} $3s^23p^4$	Cl^{17} $3s^23p^5$	Ar^{18} $3s^23p^6$
K^{19} $4s$	Ca^{20} $4s^2$	Sc^{21} $3d$ $4s^2$	Ti^{22} $3d^2$ $4s^2$	V^{23} $3d^3$ $4s^2$	Cr^{24} $3d^5$ $4s$	Mn^{25} $3d^5$ $4s^2$	Fe^{26} $3d^6$ $4s^2$	Co^{27} $3d^7$ $4s^2$	Ni^{28} $3d^8$ $4s^2$	Cu^{29} $3d^{10}$ $4s$	Zn^{30} $3d^{10}$ $4s^2$	Ga^{31} $4s^24p$	Ge^{32} $4s^24p^2$	As^{33} $4s^24p^3$	Se^{34} $4s^24p^4$	Br^{35} $4s^24p^5$	Kr^{36} $4s^24p^6$
Rb^{37} $5s$	Sr^{38} $5s^2$	Y^{39} $4d$ $5s^2$	Zr^{40} $4d^2$ $5s^2$	Nb^{41} $4d^4$ $5s$	Mo^{42} $4d^5$ $5s$	Tc^{43} $4d^6$ $5s$	Ru^{44} $4d^7$ $5s$	Rh^{45} $4d^8$ $5s$	Pd^{46} $4d^{10}$ –	Ag^{47} $4d^{10}$ $5s$	Cd^{48} $4d^{10}$ $5s^2$	In^{49} $5s^25p$	Sn^{50} $5s^25p^2$	Sb^{51} $5s^25p^3$	Te^{52} $5s^25p^4$	I^{53} $5s^25p^5$	Xe^{54} $5s^25p^6$
Cs^{55} $6s$	Ba^{56} $6s^2$	La^{57} $5d$ $6s^2$	Hf^{72} $4f^{14}$ $5d^2$ $6s^2$	Ta^{73} $5d^3$ $6s^2$	W^{74} $5d^4$ $6s^2$	Re^{75} $5d^5$ $6s^2$	Os^{76} $5d^6$ $6s^2$	Ir^{77} $5d^9$ –	Pt^{78} $5d^9$ $6s$	Au^{79} $5d^{10}$ $6s$	Hg^{80} $5d^{10}$ $6s^2$	Tl^{81} $6s^26p$	Pb^{82} $6s^26p^2$	Bi^{83} $6s^26p^3$	Po^{84} $6s^26p^4$	At^{85} $6s^26p^5$	Rn^{86} $6s^26p^6$
Fr^{87} $7s$	Ra^{88} $7s^2$	Ac^{89} $6d$ $7s^2$															
			Ce^{58} $4f^2$ $6s^2$	Pr^{59} $4f^3$ $6s^2$	Nd^{60} $4f^4$ $6s^2$	Pm^{61} $4f^5$ $6s^2$	Sm^{62} $4f^6$ $6s^2$	Eu^{63} $4f^7$ $6s^2$	Gd^{64} $4f^7$ $5d$ $6s^2$	Tb^{65} $4f^8$ $5d$ $6s^2$	Dy^{66} $4f^{10}$ $6s^2$	Ho^{67} $4f^{11}$ $6s^2$	Er^{68} $4f^{12}$ $6s^2$	Tm^{69} $4f^{13}$ $6s^2$	Yb^{70} $4f^{14}$ $6s^2$	Lu^{71} $4f^{14}$ $5d$ $6s^2$
			Th^{90} – $6d^2$ $7s^2$	Pa^{91} $5f^2$ $6d$ $7s^2$	U^{92} $5f^3$ $6d$ $7s^2$	Np^{93} $5f^5$ $7s^2$	Pu^{94} $5f^6$ $7s^2$	Am^{95} $5f^7$ $7s^2$	Cm^{96} $5f^7$ $6d$ $7s^2$	Bk^{97}	Cf^{98}	Es^{99}	Fm^{100}	Md^{101}	No^{102}	Lr^{103}

Table 3 Crystal structures of the elements

The data given are at room temperature for the most common form, or at the stated temperature in deg K. For further descriptions of the elements see Wyckoff, Vol. 1, Chap. 2. Structures labeled complex are described there.

H^1 4K hcp 3.75 6.12																	He^4 2K hcp 3.57 5.83
Li 78K bcc 3.491	Be hcp 2.27 3.59											B rhomb.	C diamond 3.567	N 20K cubic 5.66 (N_2)	O complex (O_2)	F	Ne 4K fcc 4.46
Na 5K bcc 4.225	Mg hcp 3.21 5.21	← Crystal structure → ← a lattice parameter, in Å → ← c lattice parameter, in Å →										Al fcc 4.05	Si diamond 5.430	P complex	S complex	Cl complex (Cl_2)	Ar 4K fcc 5.31
K 5K bcc 5.225	Ca fcc 5.58	Sc hcp 3.31 5.27	Ti hcp 2.95 4.68	V bcc 3.03	Cr bcc 2.88	Mn cubic complex	Fe bcc 2.87	Co hcp 2.51 4.07	Ni fcc 3.52	Cu fcc 3.61	Zn hcp 2.66 4.95	Ga complex	Ge diamond 5.658	As rhomb.	Se hex. chains	Br complex (Br_2)	Kr 4K fcc 5.64
Rb 5K bcc 5.585	Sr fcc 6.08	Y hcp 3.65 5.73	Zr hcp 3.23 5.15	Nb bcc 3.30	Mo bcc 3.15	Tc hcp 2.74 4.40	Ru hcp 2.71 4.28	Rh fcc 3.80	Pd fcc 3.89	Ag fcc 4.09	Cd hcp 2.98 5.62	In tetr. 3.25 4.95	Sn (α) diamond 6.49	Sb rhomb.	Te hex. chains	I complex (I_2)	Xe 4K fcc 6.13
Cs 5K bcc 6.045	Ba bcc 5.02	La hex. 3.77 *ABAC*	Hf hcp 3.19 5.05	Ta bcc 3.30	W bcc 3.16	Re hcp 2.76 4.46	Os hcp 2.74 4.32	Ir fcc 3.84	Pt fcc 3.92	Au fcc 4.08	Hg rhomb.	Tl hcp 3.46 5.52	Pb fcc 4.95	Bi rhomb.	Po sc 3.34	At —	Rn —
Fr —	Ra —	Ac fcc 5.31															

Ce fcc 5.16	Pr hex. 3.67 *ABAC*	Nd hex. 3.66	Pm —	Sm complex	Eu bcc 4.58	Gd hcp 3.63 5.78	Tb hcp 3.60 5.70	Dy hcp 3.59 5.65	Ho hcp 3.58 5.62	Er hcp 3.56 5.59	Tm hcp 3.54 5.56	Yb fcc 5.48	Lu hcp 3.50 5.55
Th fcc 5.08	Pa tetr. 3.92 3.24	U complex	Np complex	Pu complex	Am hex. 3.64 *ABAC*	Cm —	Bk —	Cf —	Es —	Fm —	Md —	No —	Lr —

Table 4 Density and atomic concentration

The data are given at atmospheric pressure and room temperature, or at the stated temperature in deg K. (Crystal modifications as for Table 3.)

Atomic radius
= r_{MT}
= 0.5 n-n dist.

Average surface density = $\rho_S \approx (\rho_V)^{2/3}$

H 4K																	He 2K
0.088																	0.205 (at 37 atm)
Li 78K	Be											B	C	N 20K	O	F	Ne 4K
0.542	1.82											2.47	3.516	1.03			1.51
4.700	12.1											13.0	17.6				4.36
3.023	2.22												1.54			1.44	3.16
Na 5K	Mg											Al	Si	P	S	Cl 93K	Ar 4K
1.013	1.74											2.70	2.33			2.03	1.77
2.652	4.30											6.02	5.00				2.66
3.659	3.20											2.86	2.35			2.02	3.76
K 5K	Ca	Sc	Ti	V	Cr	Mn	Fe	Co	Ni	Cu	Zn	Ga	Ge	As	Se	Br 123K	Kr 4K
0.910	1.53	2.99	4.51	6.09	7.19	7.47	7.87	8.9	8.91	8.93	7.13	5.91	5.32	5.77	4.81	4.05	3.09
1.402	2.30	4.27	5.66	7.22	8.33	8.18	8.50	8.97	9.14	8.45	6.55	5.10	4.42	4.65	3.67	2.36	2.17
4.525	3.95	3.25	2.89	2.62	2.50	2.24	2.48	2.50	2.49	2.56	2.66	2.44	2.45	3.16	2.32		4.00
Rb 5K	Sr	Y	Zr	Nb	Mo	Tc	Ru	Rh	Pd	Ag	Cd	In	Sn	Sb	Te	I	Xe 4K
1.629	2.58	4.48	6.51	8.58	10.22	11.50	12.36	12.42	12.00	10.50	8.65	7.29	5.76	6.69	6.25	4.95	3.78
1.148	1.78	3.02	4.29	5.56	6.42	7.04	7.36	7.26	6.80	5.85	4.64	3.83	2.91	3.31	2.94	2.36	1.64
4.837	4.30	3.55	3.17	2.86	2.72	2.71	2.65	2.69	2.75	2.89	2.98	3.25	2.81	2.91	2.86	3.54	4.34
Cs 5K	Ba	La	Hf	Ta	W	Re	Os	Ir	Pt	Au	Hg 227	Tl	Pb	Bi	Po	At	Rn
1.997	3.59	6.17	13.20	16.66	19.25	21.03	22.58	22.55	21.47	19.28	14.26	11.87	11.34	9.80	9.31		
0.905	1.60	2.70	4.52	5.55	6.30	6.80	7.14	7.06	6.62	5.90	4.26	3.50	3.30	2.82	2.67	—	—
5.235	4.35	3.73	3.13	2.86	2.74	2.74	2.68	2.71	2.77	2.88	3.01	3.46	3.50	3.07	3.34		
Fr	Ra	Ac															
—	—	10.07															
		2.66															
		3.76															

Density in g cm^{-3} (10^3kg m^{-3}) ⟶
Concentration in 10^{22} cm^{-3} (10^{28} m^{-3}) ⟶
Nearest-neighbor distance, in Å (10^{-10}m) ⟶

Ce	Pr	Nd	Pm	Sm	Eu	Gd	Tb	Dy	Ho	Er	Tm	Yb	Lu
6.77	6.78	7.00		7.54	5.25	7.89	8.27	8.53	8.80	9.04	9.32	6.97	9.84
2.91	2.92	2.93	—	3.03	2.04	3.02	3.22	3.17	3.22	3.26	3.32	3.02	3.39
3.65	3.63	3.66		3.59	3.96	3.58	3.52	3.51	3.49	3.47	3.54	3.88	3.43
Th	Pa	U	Np	Pu	Am	Cm	Bk	Cf	Es	Fm	Md	No	Lr
11.72	15.37	19.05	20.45	19.81	11.87								
3.04	4.01	4.80	5.20	4.26	2.96	—	—	—	—	—	—	—	—
3.60	3.21	2.75	2.62	3.1	3.61								

Table 1 Debye temperature and thermal conductivity[a]

Low temperature limit of θ, in Kelvin
Thermal conductivity at 300 K, in W $cm^{-1}K^{-1}$

Li	Be											B	C	N	O	F	Ne
344	1440												2230				75
0.85	2.00											0.27	1.29				
Na	Mg											Al	Si	P	S	Cl	Ar
158	400											428	645				92
1.41	1.56											2.37	1.48				
K	Ca	Sc	Ti	V	Cr	Mn	Fe	Co	Ni	Cu	Zn	Ga	Ge	As	Se	Br	Kr
91	230	360.	420	380	630	410	470	445	450	343	327	320	374	282	90		72
1.02		0.16	0.22	0.31	0.94	0.08	0.80	1.00	0.91	4.01	1.16	0.41	0.60	0.50	0.02		
Rb	Sr	Y	Zr	Nb	Mo	Tc	Ru	Rh	Pd	Ag	Cd	In	Sn w	Sb	Te	I	Xe
56	147	280	291	275	450		600	480	274	225	209	108	200	211	153		64
0.58		0.17	0.23	0.54	1.38	0.51	1.17	1.50	0.72	4.29	0.97	0.82	0.67	0.24	0.02		
Cs	Ba	La β	Hf	Ta	W	Re	Os	Ir	Pt	Au	Hg	Tl	Pb	Bi	Po	At	Rn
38	110	142	252	240	400	430	500	420	240	165	71.9	78.5	105	119			
0.36		0.14	0.23	0.58	1.74	0.48	0.88	1.47	0.72	3.17		0.46	0.35	0.08			
Fr	Ra	Ac															

Ce	Pr	Nd	Pm	Sm	Eu	Gd	Tb	Dy	Ho	Er	Tm	Yb	Lu
						200		210				120	210
0.11	0.12	0.16		0.13		0.11	0.11	0.11	0.16	0.14	0.17	0.35	0.16
Th	Pa	U	Np	Pu	Am	Cm	Bk	Cf	Es	Fm	Md	No	Lr
163		207											
0.54		0.28	0.06	0.07									

[a] Most of the θ values were supplied by N. Pearlman; references are given the *A.I.P. Handbook*, 3rd ed; the thermal conductivity values are from R. W. Powell and Y. S. Touloukian, Science **181**, 999 (1973).

X-Ray Data Booklet--Section 1.1 ELECTRON BINDING ENERGIES

The energies are given in eV relative to the <u>vacuum level</u> for the rare gases and for H_2, N_2, O_2, F_2, and Cl_2; relative to the <u>Fermi level</u> for the metals; and relative to the <u>top of the valence bands</u> for semiconductors (and insulators).

Electronic configuration	Element	K 1s	L_1 2s	L_2 $2p_{1/2}$	L_3 $2p_{3/2}$	M_1 3s	M_2 $3p_{1/2}$	M_3 $3p_{3/2}$
$1s$	1 H	13.6						
$1s^2$	2 He	24.6*						
$1s^2\,2s$	3 Li	54.7*						
$1s^2\,2s^2$	4 Be	111.5*						
$1s^2\,2s^2\,2p$	5 B	188*						
$1s^2\,2s^2\,2p^2$	6 C	284.2*						
$1s^2\,2s^2\,2p^3$	7 N	409.9*	37.3*	~ 9	~ 9			
$1s^2\,2s^2\,2p^4$	8 O	543.1*	41.6*	~ 13	~ 13			
$1s^2\,2s^2\,2p^5$	9 F	696.7*	~ 45	~ 17	~ 17			
$1s^2\,2s^2\,2p^6$	10 Ne	870.2*	48.5*	21.7*	21.6*			
[Ne] $3s$	11 Na	1070.8†	63.5†	30.65	30.81			
[Ne] $3s^2$	12 Mg	1303.0†	88.7	49.78	49.50			
[Ne] $3s^2\,3p$	13 Al	1559.6	117.8	72.95	72.55			
[Ne] $3s^2\,3p^2$	14 Si	1839	149.7*b	99.82	99.42			
[Ne] $3s^2\,3p^3$	15 P	2145.5	189*	136*	135*			
[Ne] $3s^2\,3p^4$	16 S	2472	230.9	163.6*	162.5*			
[Ne] $3s^2\,3p^5$	17 Cl	2822.4	270*	202*	200*			
[Ne] $3s^2\,3p^6$	18 Ar	3205.9*	326.3*	250.6†	248.4*	29.3*	15.9*	15.7*
[Ar] $4s$	19 K	3608.4*	378.6*	297.3*	294.6*	34.8*	18.3*	18.3*
[Ar] $4s^2$	20 Ca	4038.5*	438.4†	349.7†	346.2†	44.3 †	25.4†	25.4†
	21 Sc	4492	498.0*	403.6*	398.7*	51.1*	28.3*	28.3*
	22 Ti	4966	560.9†	460.2†	453.8†	58.7†	32.6†	32.6†

Valence levels

Interpolated, extrapolated

Missing valence B.E.s

Valence levels

Adding relativity to the Hamiltonian—spin-orbit coupling

- SPIN-ORBIT SPLITTING OF LEVELS:

$\Rightarrow$ EFFECTIVE $\vec{B}$ (NUCLEUS AROUND e^-) $\propto \vec{L}$

$$\hat{H}_{s\text{-}o} = \xi(r)\,\vec{l}\cdot\vec{s}$$

- SPLITS ALL nl LEVELS $2(2l+1)$ $\rightarrow$ $nlj = l+1/2$ — $2l+2$; $nlj = l-1/2$ — $2l$

- MIXES SPIN + ORBITAL ANGULAR MOM.:

$$\psi_{nljm_j} = C_1\psi_{nl,m_j-1/2}\underbrace{\begin{pmatrix}1\\0\end{pmatrix}}_{m_s=+1/2\ \equiv\ \uparrow} + C_2\psi_{nl,m_j+1/2}\underbrace{\begin{pmatrix}0\\1\end{pmatrix}}_{m_s=-1/2\ \equiv\ \downarrow}$$

WITH C1 AND C2 TABULATED CLEBSCH-GORDAN OR WIGNER 3j SYMBOLS

SOME SPIN-ORBIT SPLITTINGS: (IN eV)

	Z = 13 (Al)	28 (Ni)	46 (Pd)
$2p^6 \to 2p^2_{1/2},\ 2p^4_{3/2}$	0.4	17.8	157.0
$3d^{10} \to 3d^4_{3/2},\ 3d^6_{5/2}$	Z = 30 (Zn)	48 (Cd)	64 (Gd)
	0.1	6.7	32.3
$4f^{14} \to 4f^6_{5/2},\ 4f^8_{7/2}$	Z = 74 (W)	84 (Pb)	92 (U)
	2.2	7.0	64

INCREASE WITH Z FOR A GIVEN LEVEL.

IN GENERAL:

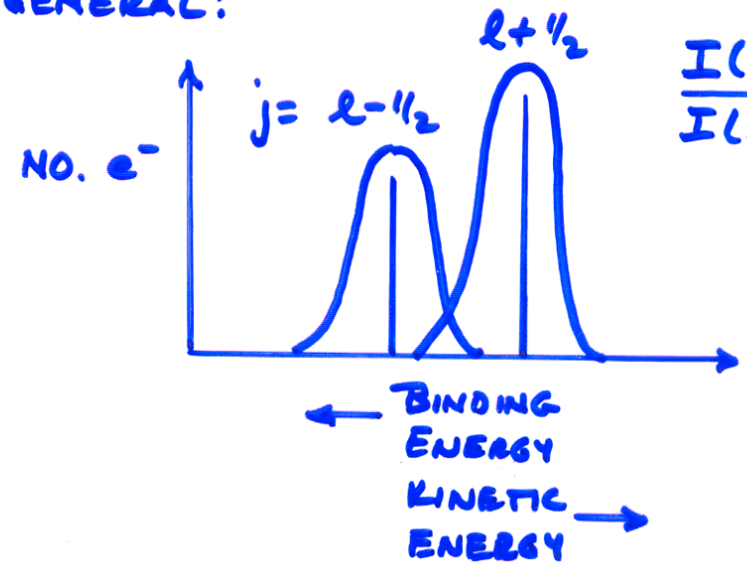

$$\frac{I(l+1/2)}{I(l-1/2)} = \frac{2l+2}{2l}$$

The Photoelectric Effect, Einstein, 1905
Light can behave like a Particle!

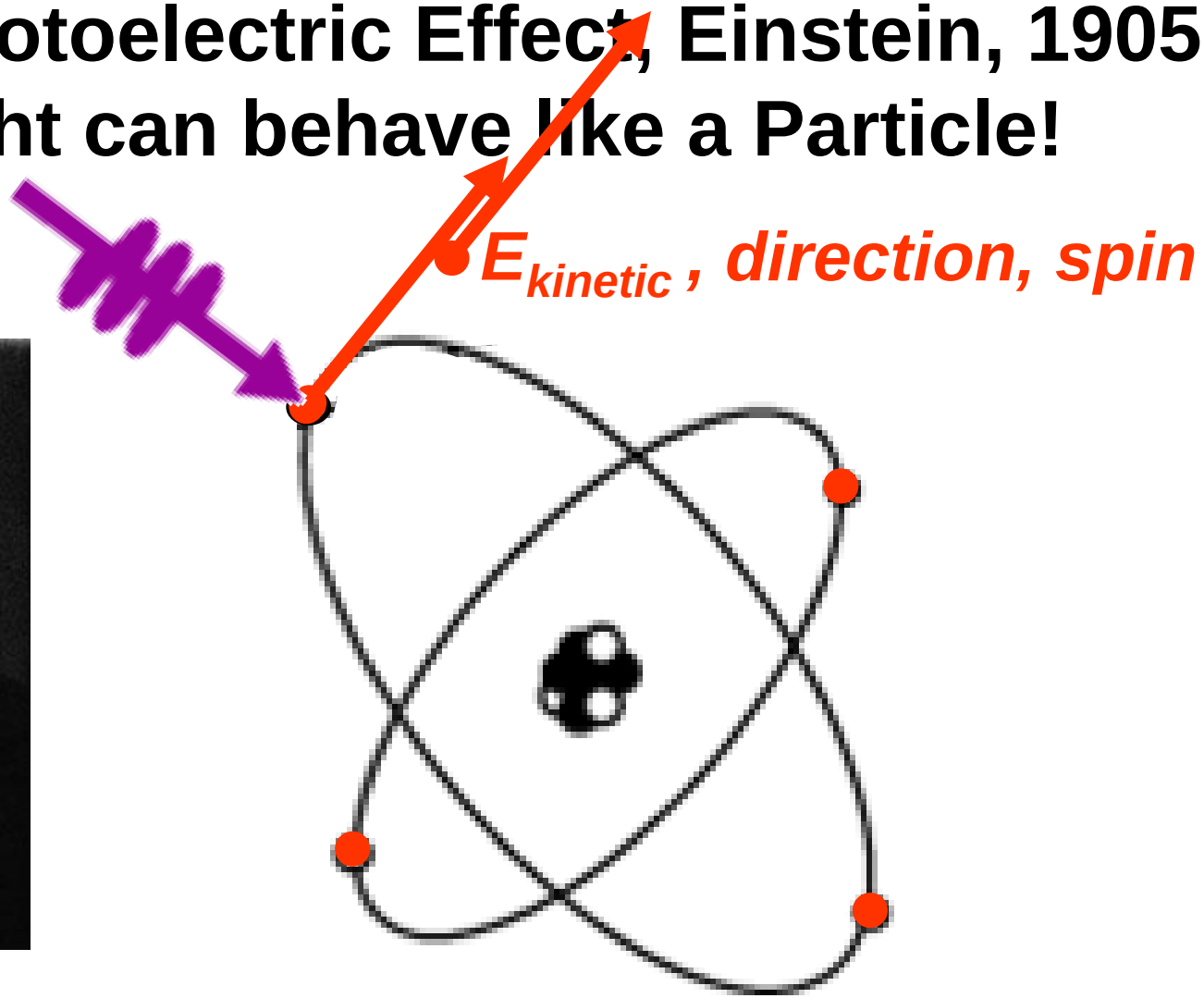

$$h\nu = E_{initial} - E_{final} = E_{binding} + E_{kinetic}$$

Basic Concepts and Experiments

Core-Level Photoemission

Intensities and Quantitative Analysis, the 3-Step Model
Varying Surface and Bulk Sensitivity
Chemical shifts
Multiplet Splittings
Electron Screening and Satellite Structure
Magnetic and Non-Magnetic Dichroism
Resonant Photoemission
Photoelectron Diffraction and Holography

Valence-Level Photoemission

Band-Mapping in the Ultraviolet Photoemission Limit
Densities of States in the X-Ray Photoemission Limit

Some New Directions

Photoemission with Hard X-Rays (throughout lectures)
Photoemission with Standing Wave Excitation
Photoemission with Spatial Resolution/Photoelectron Microscopy
Temporal Resolution
@ Higher Pressures

The Soft X-Ray Spectroscopies

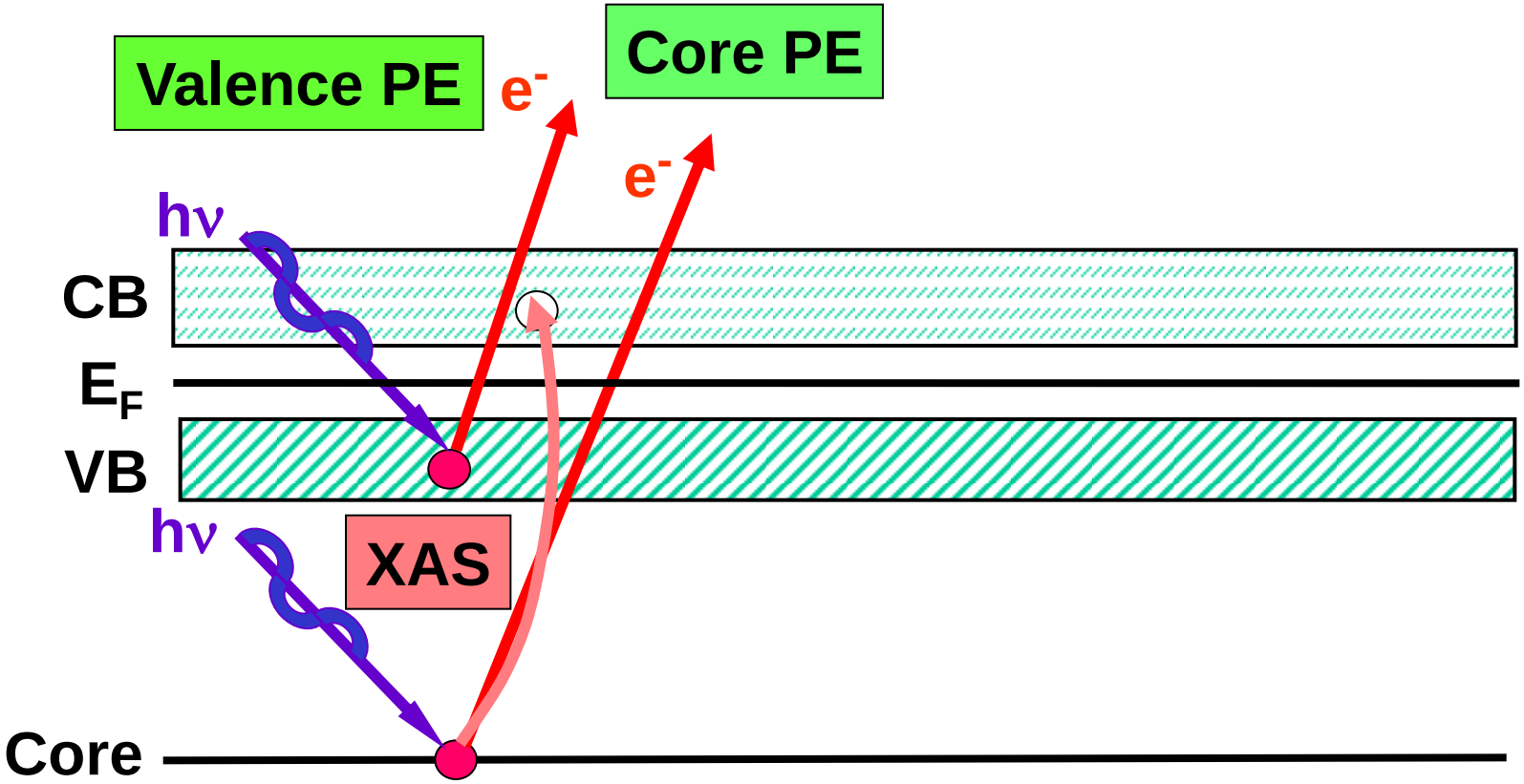

PE = photoemission = photoelectron spectroscopy

XAS = x-ray absorption spectroscopy

AES = Auger electron spectroscopy

XES = x-ray emission spectroscopy

RIXS = resonant inelastic x-ray scattering / x-ray Raman scatt.

MATRIX ELEMENTS IN THE SOFT X-RAY SPECTROSCOPIES: DIPOLE LIMIT

- ***Photoelectron spectroscopy/photoemission:***

$$I \propto \left| \hat{e} \bullet \langle \varphi_f(1) | \vec{r} | \varphi_i(1) \rangle \right|^2$$

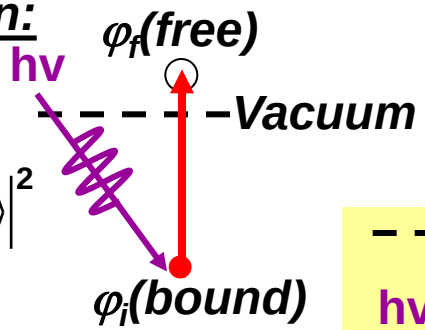

- ***Near-edge x-ray absorption:***

$$I \propto \left| \hat{e} \bullet \langle \varphi_f(1) | \vec{r} | \varphi_i(1) \rangle \right|^2$$

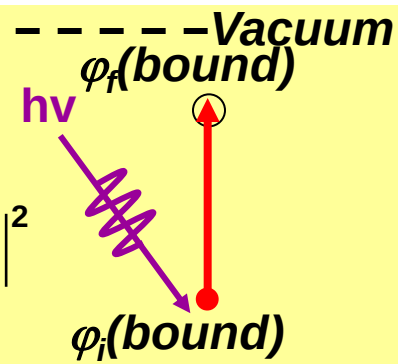

Variation of Near-Edge X-Ray Absorption Fine Structure (NEXAFS) with Atomic No. for Some 3d Transition Metals

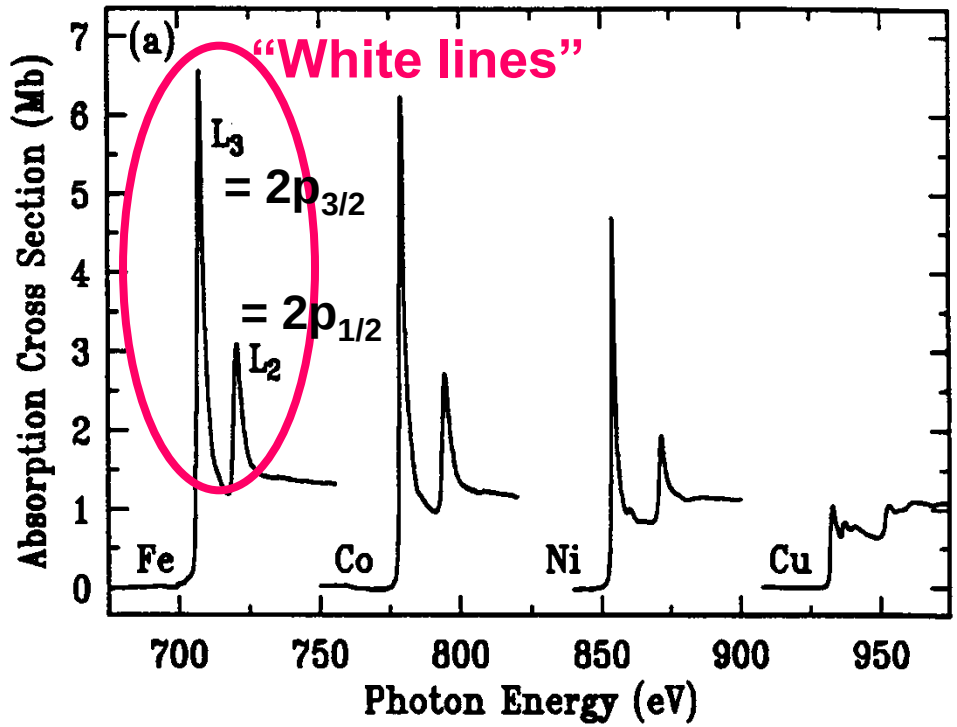

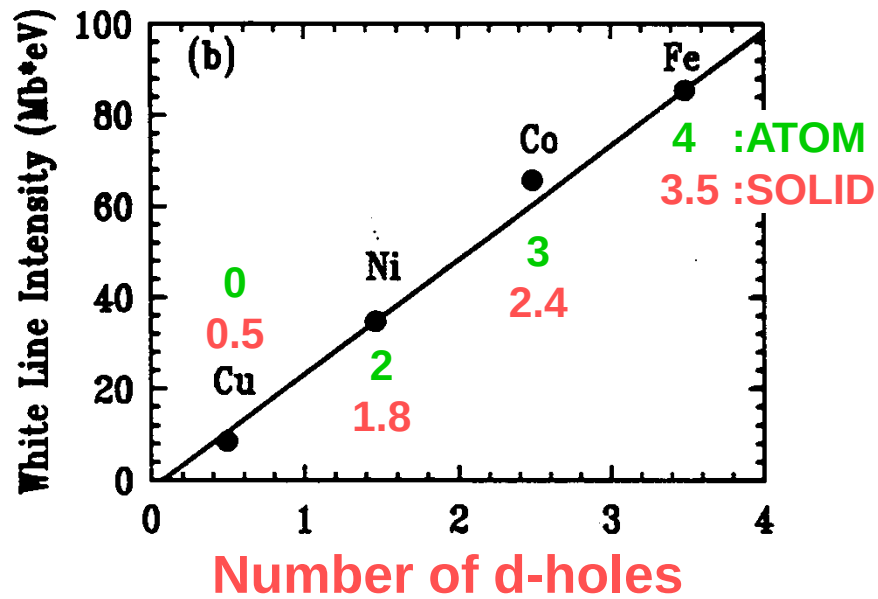

J. Stohr, "NEXAFS Spectroscopy"

Magnetic Circular Dichroism in X-Ray Absorption (XMCD)

Ferromagnetic cobalt with magnetization along incident light direction

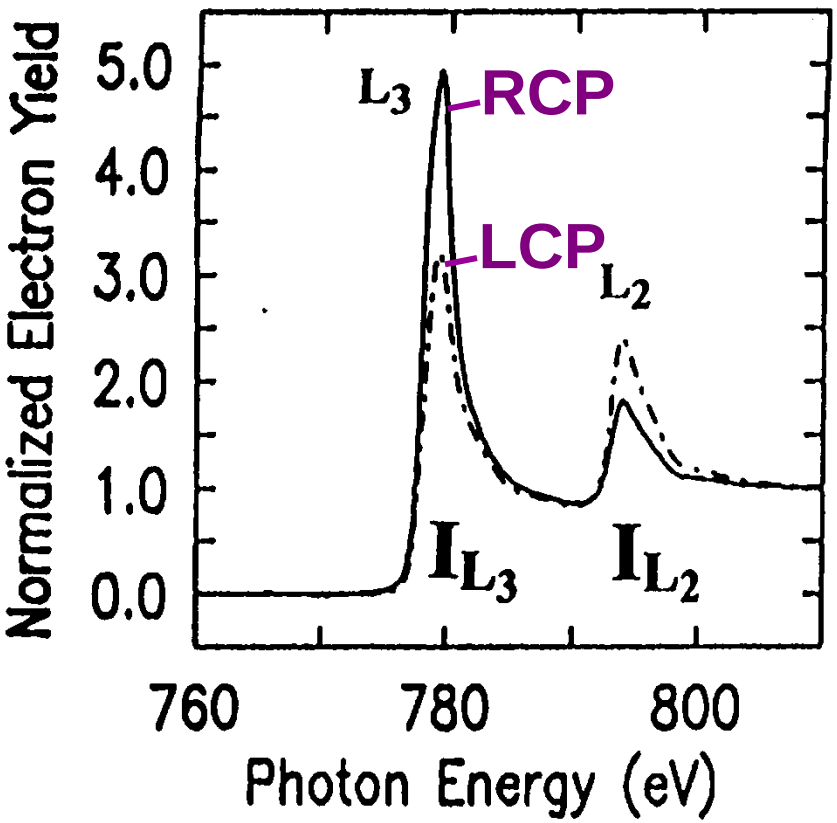

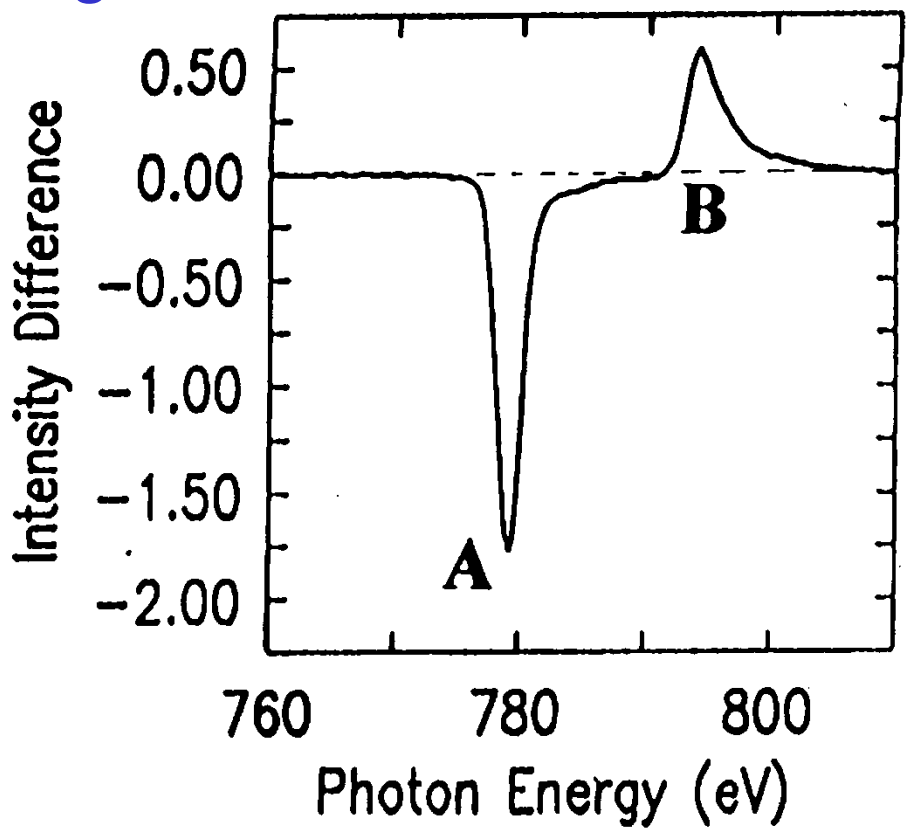

→Sum rules yield spin and orbital magnetic moments on a given atom

Variation of Near-Edge X-Ray Absorption Fine Structure (NEXAFS) for Different Polymers

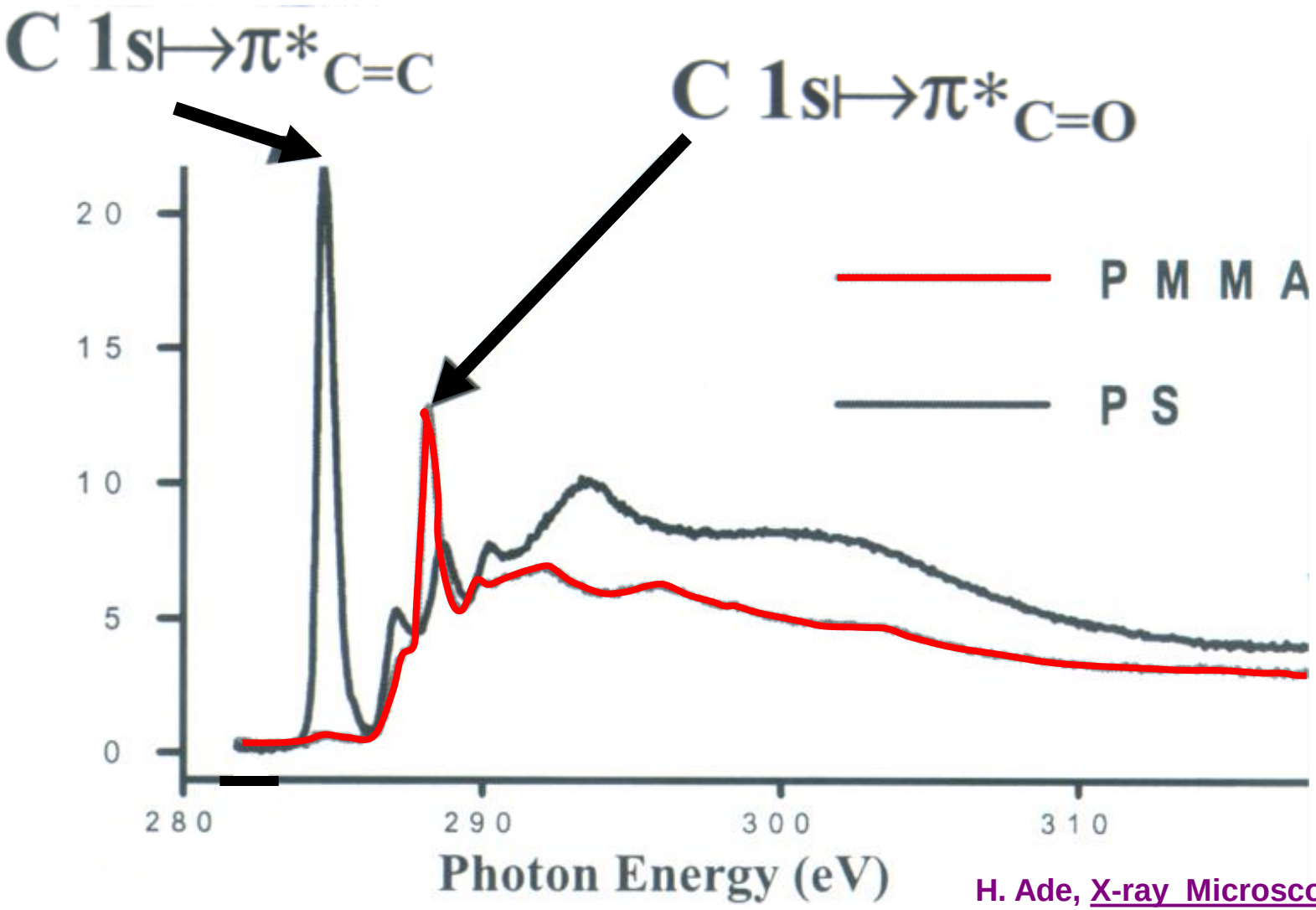

H. Ade, X-ray Microscopy 99, AIP Conf. Proc. 507, p.197

The Soft X-Ray Spectroscopies

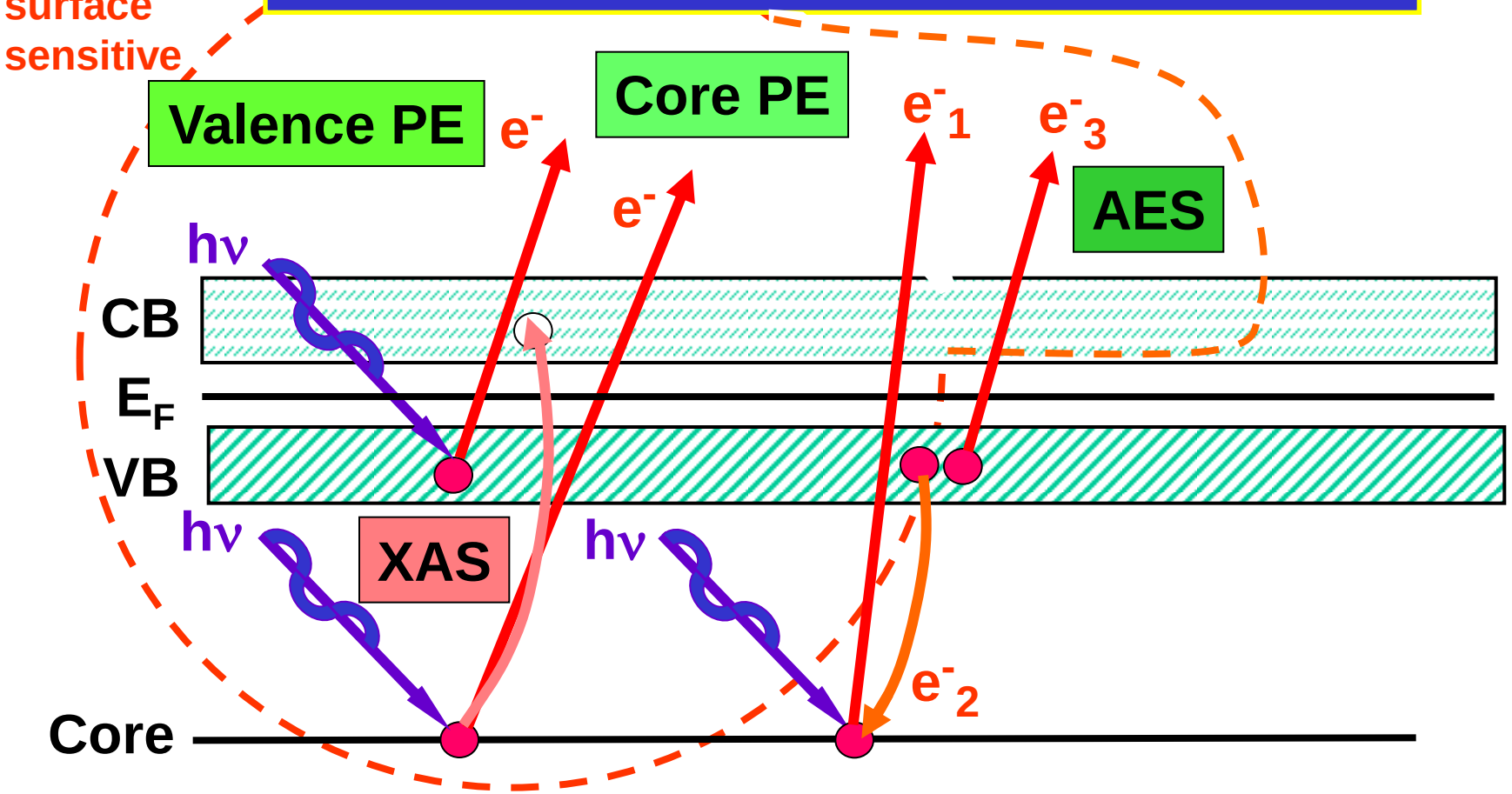

PE = photoemission = photoelectron spectroscopy

XAS = x-ray absorption spectroscopy

AES = Auger electron spectroscopy

XES = x-ray emission spectroscopy

REXS/RIXS = resonant elastic/inelastic x-ray scattering

MATRIX ELEMENTS IN THE SOFT X-RAY SPECTROSCOPIES: DIPOLE LIMIT

- ***Photoelectron spectroscopy/photoemission:***

$$I \propto \left| \hat{e} \bullet \langle \varphi_f(1) | \vec{r} | \varphi_i(1) \rangle \right|^2$$

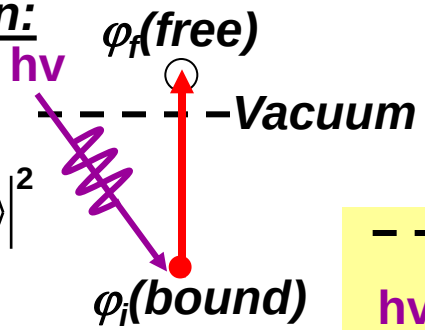

- ***Near-edge x-ray absorption:***

$$I \propto \left| \hat{e} \bullet \langle \varphi_f(1) | \vec{r} | \varphi_i(1) \rangle \right|^2$$

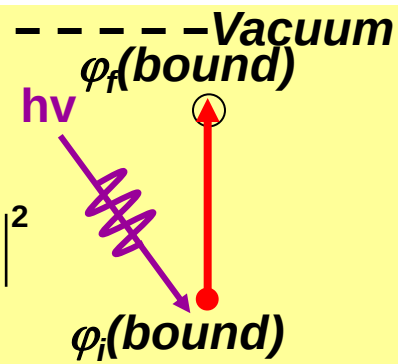

- ***Auger electron emission:***

$$I \propto \left| \langle \varphi_f(1)\varphi_1(2) | \frac{e^2}{r_{12}} | \varphi_3(1)\varphi_2(2) \rangle - \langle \varphi_1(1)\varphi_f(2) | \frac{e^2}{r_{12}} | \varphi_3(1)\varphi_2(2) \rangle \right|^2$$

Direct

Exchange

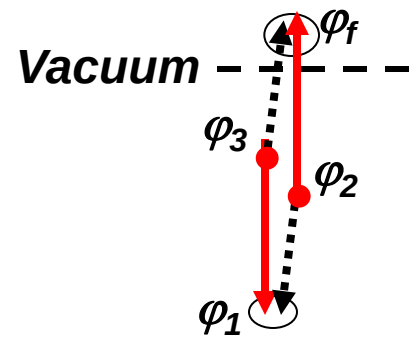

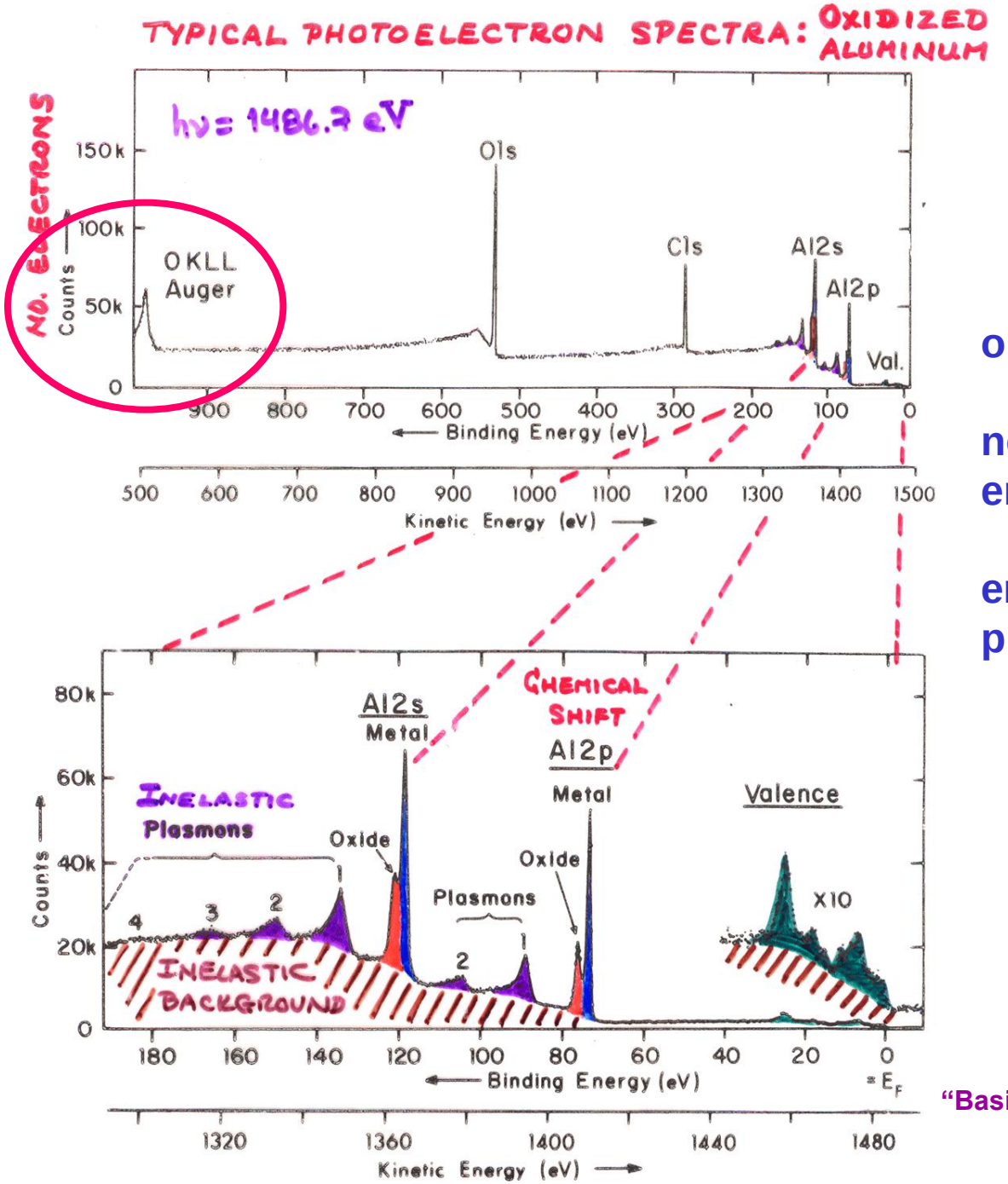

A very useful diagnotic observation:

Auger kinetic energies do not change with photon energy

Photoelectron kinetic energies shift linearly with photon energy

"Basic Concepts of XPS"
Figure 1

THE AUGER PROCESS

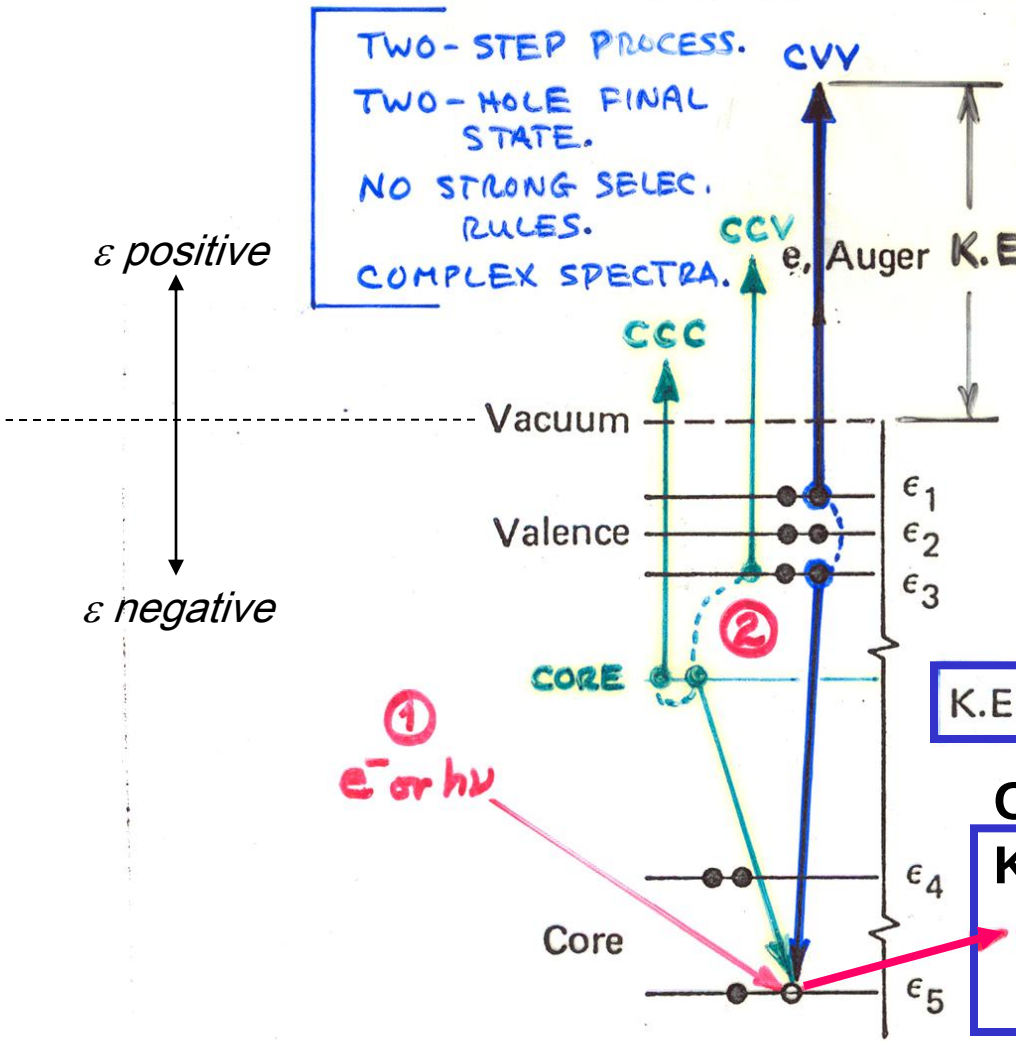

N core = N $1s^2$ = N^{5+}

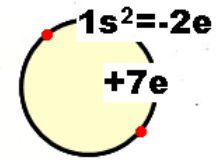

Assume:
N^{6+*} core with
1s hole = N^{6+*} =

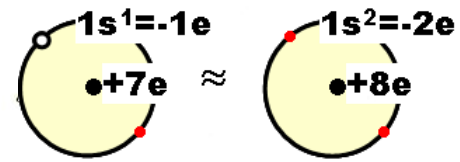

= O^{6+} core

The equivalent core or Z+1 approximation

$$\boxed{K.E. \sim -\epsilon_5 + \epsilon_3 + \epsilon_1}$$

DOES NOT DEPEND ON hν!

Or more accurately:

$$K.E. \approx B.E._5^{Z} - B.E._3^{Z+1} - B.E._1^{Z}$$
$$\approx B.E._5^{Z} - B.E._3^{Z} - B.E._1^{Z+1}$$
$$\approx \text{(average of two above)}$$

Figure 2. Scheme of the Auger process. A valence-level involved Auger emission is illustrated here, but the two electrons involved also could have come from core level, ϵ_4, provided $\epsilon_5 - 2\epsilon_4 > 0$.

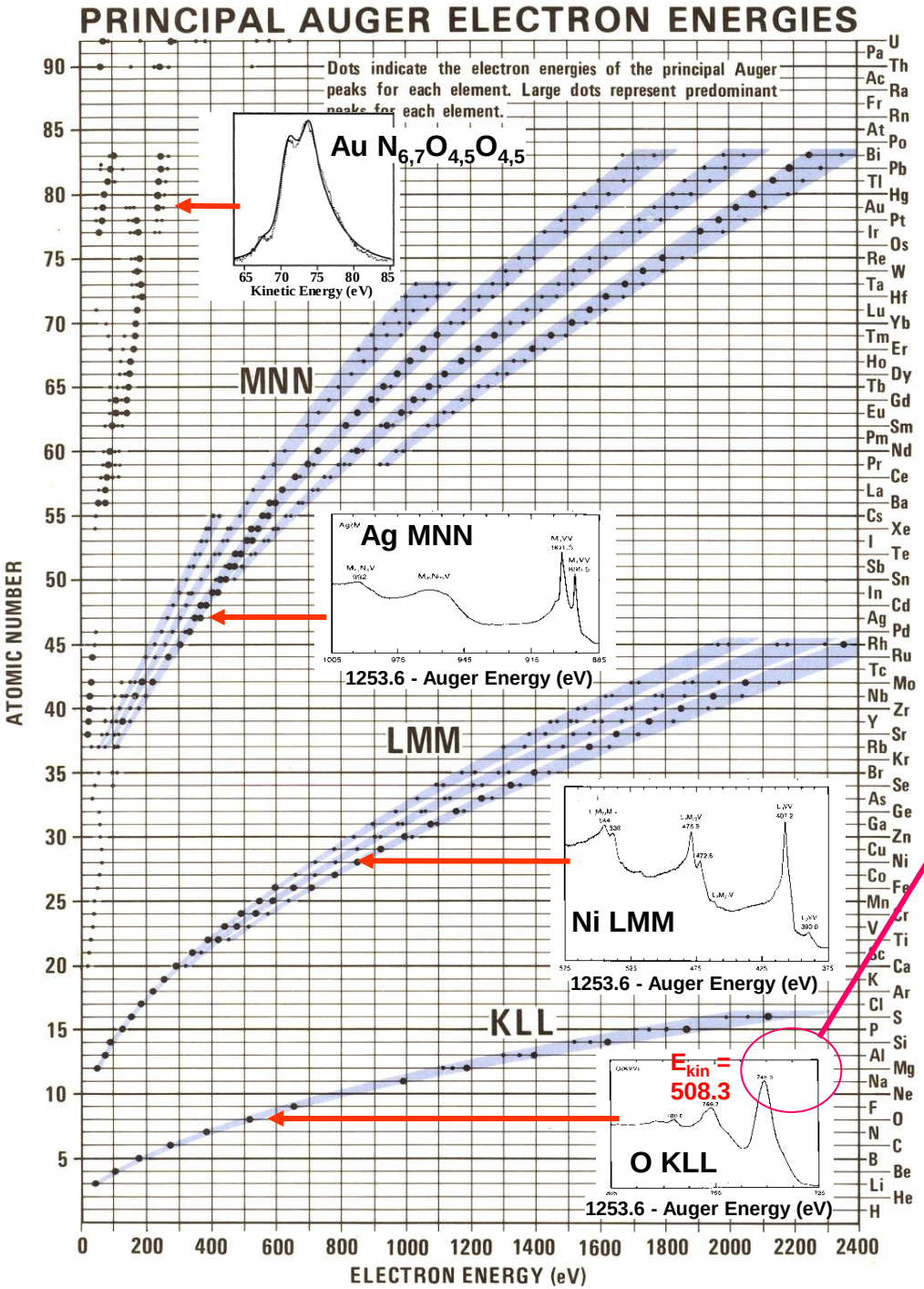

X-Ray Data Booklet Fig. 1.4

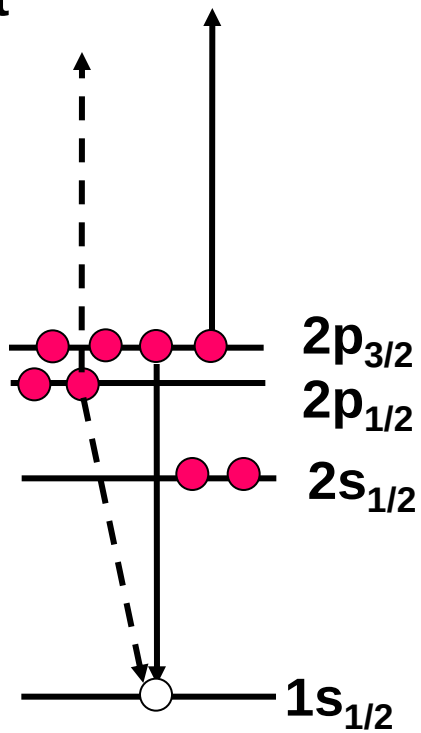

$$K.E. \approx B.E._{1s}^{Z=8} - B.E._{2p}^{9} - B.E._{2p}^{8}$$
$$\approx B.E._{1s}^{8} + B.E._{2p}^{8} - B.E._{2p}^{9}$$
$$\approx 543.1 - 17 - 13 \approx 513 \text{ eV}$$

X-Ray Data Booklet--Section 1.1 ELECTRON BINDING ENERGIES

The energies are given in eV relative to the <u>vacuum level</u> for the rare gases and for H_2, N_2, O_2, F_2, and Cl_2; relative to the <u>Fermi level</u> for the metals; and relative to the <u>top of the valence bands</u> for semiconductors (and insulators).

Electronic configuration	Element	K 1s	L_1 2s	L_2 $2p_{1/2}$	L_3 $2p_{3/2}$	M_1 3s	M_2 $3p_{1/2}$	M_3 $3p_{3/2}$
$1s$	1 H	13.6						
$1s^2$	2 He	24.6*						
$1s^2\,2s$	3 Li	54.7*						
$1s^2\,2s^2$	4 Be	111.5*						
$1s^2\,2s^2\,2p$	5 B	188*						
$1s^2\,2s^2\,2p^2$	6 C	284.2*						
$1s^2\,2s^2\,2p^3$	7 N	409.9*	37.3*	~ 9	~ 9			
$1s^2\,2s^2\,2p^4$	8 O	543.1*	41.6*	~ 13	~ 13			
$1s^2\,2s^2\,2p^5$	9 F	696.7*	~ 45	~ 17	~ 17			
$1s^2\,2s^2\,2p^6$	10 Ne	870.2*	48.5*	21.7*	21.6*			
[Ne] $3s$	11 Na	1070.8†	63.5†	30.65	30.81			
[Ne] $3s^2$	12 Mg	1303.0†	88.7	49.78	49.50			
[Ne] $3s^2\,3p$	13 Al	1559.6	117.8	72.95	72.55			
[Ne] $3s^2\,3p^2$	14 Si	1839	149.7*b	99.82	99.42			
[Ne] $3s^2\,3p^3$	15 P	2145.5	189*	136*	135*			
[Ne] $3s^2\,3p^4$	16 S	2472	230.9	163.6*	162.5*			
[Ne] $3s^2\,3p^5$	17 Cl	2822.4	270*	202*	200*			
[Ne] $3s^2\,3p^6$	18 Ar	3205.9*	326.3*	250.6†	248.4*	29.3*	15.9*	15.7*
[Ar] $4s$	19 K	3608.4*	378.6*	297.3*	294.6*	34.8*	18.3*	18.3*
[Ar] $4s^2$	20 Ca	4038.5*	438.4†	349.7†	346.2†	44.3 †	25.4†	25.4†
	21 Sc	4492	498.0*	403.6*	398.7*	51.1*	28.3*	28.3*
	22 Ti	4966	560.9†	460.2†	453.8†	58.7†	32.6†	32.6†

Valence levels

Interpolated, extrapolated

Missing valence B.E.s

Valence levels

The Soft X-Ray Spectroscopies

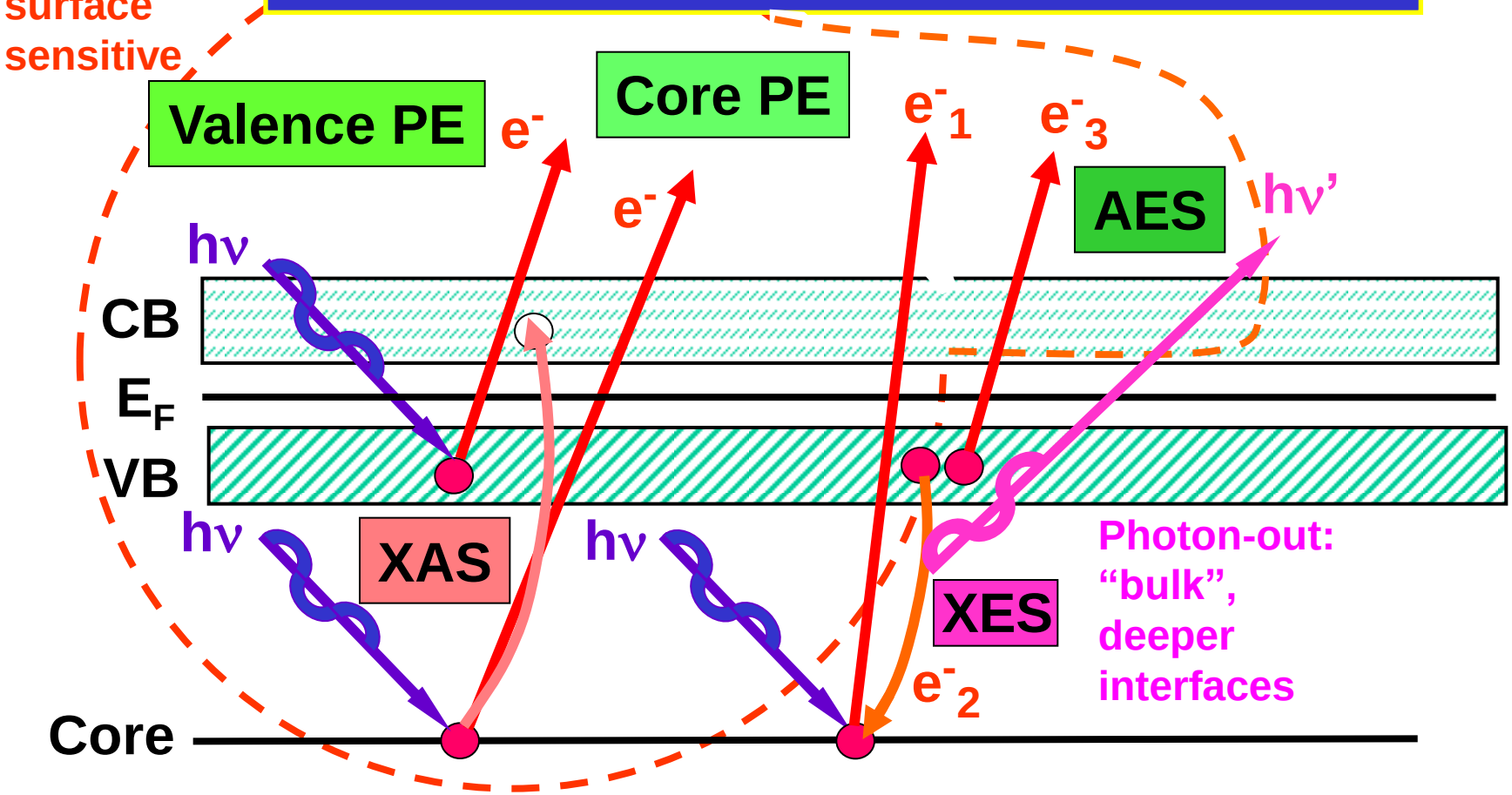

PE = photoemission = photoelectron spectroscopy

XAS = x-ray absorption spectroscopy

AES = Auger electron spectroscopy

XES = x-ray emission spectroscopy

REXS/RIXS = resonant elastic/inelastic x-ray scattering

THE AUGER PROCESS

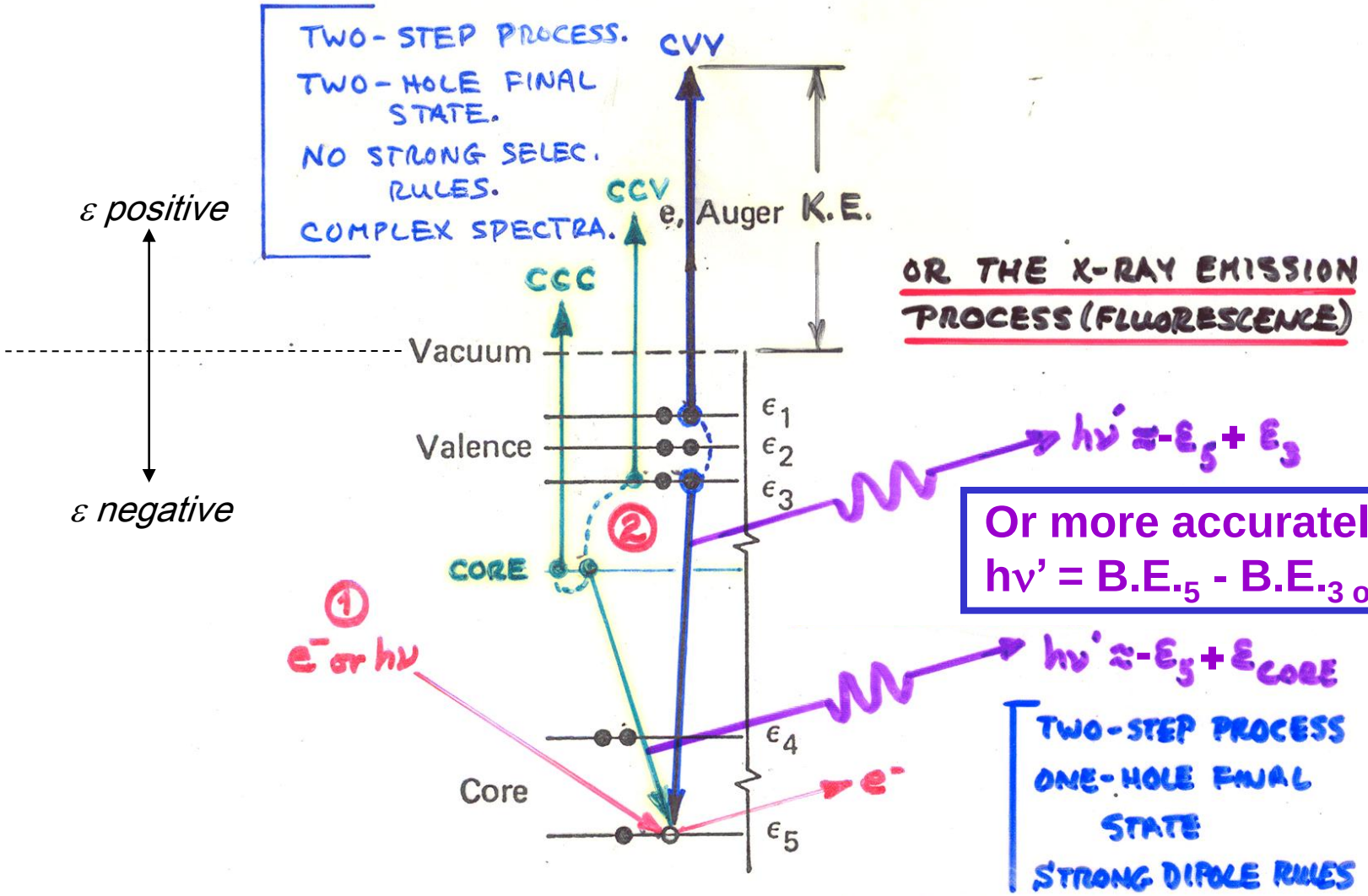

Or more accurately:
$h\nu' = B.E._5 - B.E._{3\ or\ core}$

Figure 2. Scheme of the Auger process. A valence-level involved Auger emission is illustrated here, but the two electrons involved also could have come from core level, ϵ_4, provided $\epsilon_5 - 2\epsilon_4 > 0$.

MATRIX ELEMENTS IN THE SOFT X-RAY SPECTROSCOPIES: DIPOLE LIMIT

- ***Photoelectron spectroscopy/photoemission:***

$$I \propto \left|\hat{e} \bullet \langle \varphi_f(1) | \vec{r} | \varphi_i(1) \rangle\right|^2$$

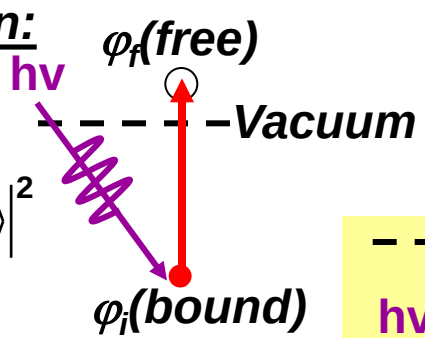

- ***Near-edge x-ray absorption:***

$$I \propto \left|\hat{e} \bullet \langle \varphi_f(1) | \vec{r} | \varphi_i(1) \rangle\right|^2$$

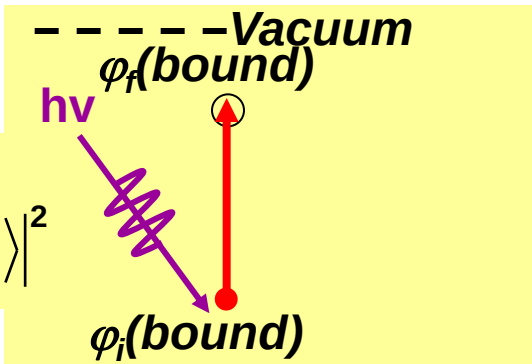

- ***Auger electron emission:***

$$I \propto \left|\langle \varphi_f(1)\varphi_1(2) | \frac{e^2}{r_{12}} | \varphi_3(1)\varphi_2(2) \rangle - \langle \varphi_1(1)\varphi_f(2) | \frac{e^2}{r_{12}} | \varphi_3(1)\varphi_2(2) \rangle\right|^2$$

Direct

Exchange

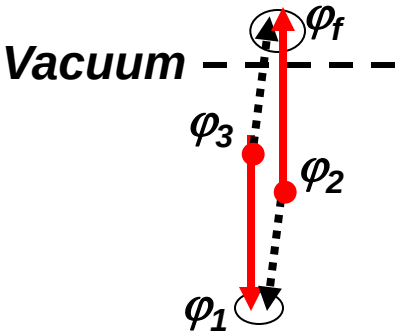

- ***X-ray emission:***

$$I \propto \left|\hat{e} \bullet \langle \varphi_f(1) | \vec{r} | \varphi_i(1) \rangle\right|^2$$

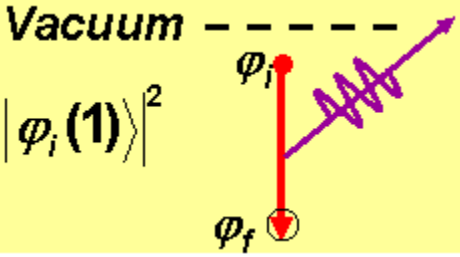

1.3 FLUORESCENCE YIELDS FOR *K* AND *L* SHELLS

Jeffrey B. Kortright

Fluorescence yields for the *K* and *L* shells for the elements $5 \leq Z \leq 110$ are plotted in Fig. 1-2; the data are based on Ref. 1. These yields represent the probability of a core hole in the *K* or *L* shells being filled by a radiative process, in competition with nonradiative processes. Auger processes are the only nonradiative processes competing with fluorescence for the *K* shell and

If fluorescence yield ≡ FY

FY = probability of radiative decay → x-ray emission)

1 - FY = probability of non-radiative decay → Auger electron emission

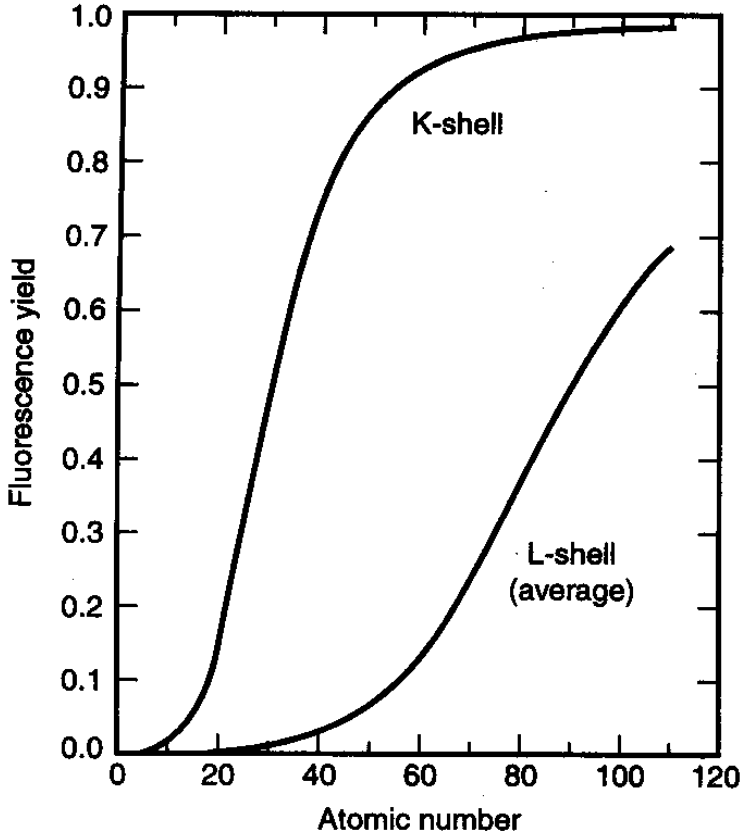

Fig. 1-2. Fluorescence yields for K and L shells fo 110. The plotted curve for the L shell rep average of L_1, L_2, and L_3 effective yields

"X-Ray Data Booklet"
Section 1.3

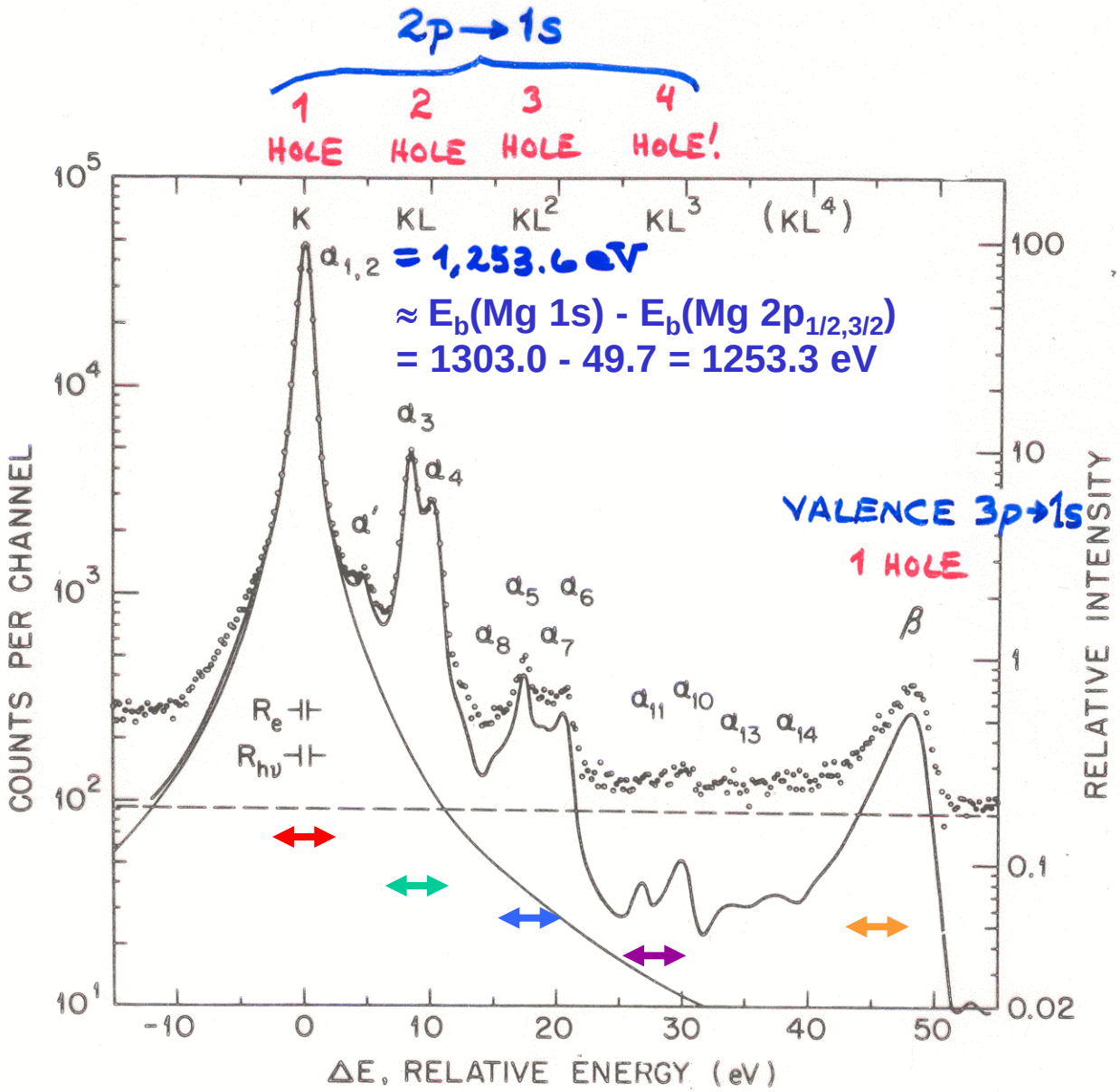

A STANDARD LABORATORY X-RAY SOURCE

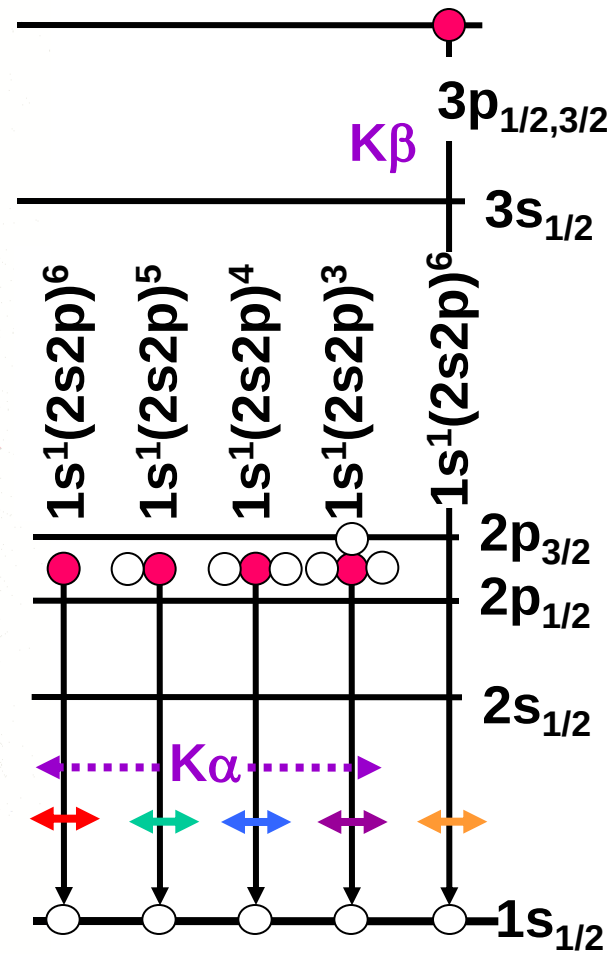

Mg K series of x-rays:
atomic no. = 12
Fluorescence Yield ≈ 0.03

"Basic Concepts of XPS"
Figure 2

The Soft X-Ray Spectroscopies

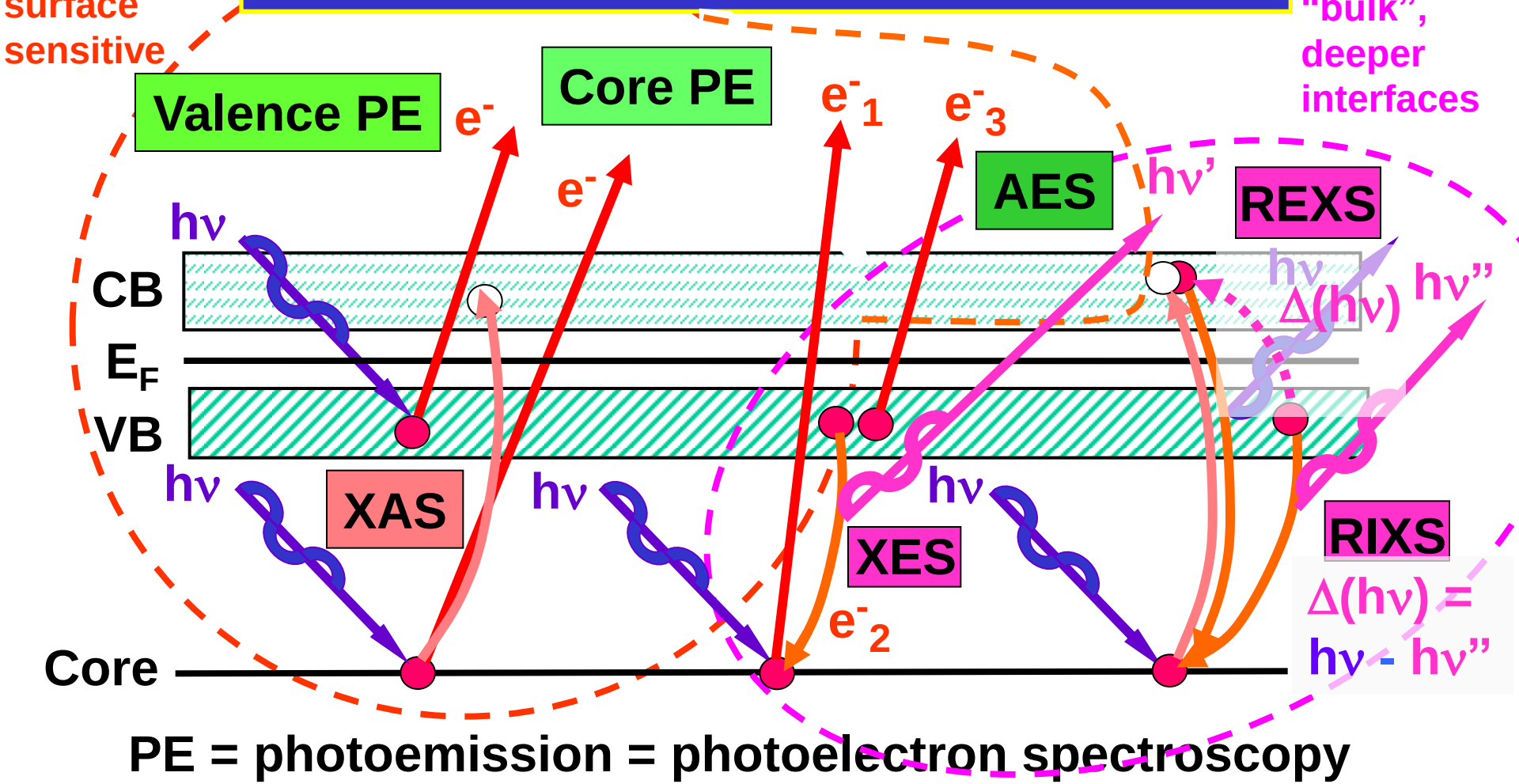

PE = photoemission = photoelectron spectroscopy

XAS = x-ray absorption spectroscopy

AES = Auger electron spectroscopy

XES = x-ray emission spectroscopy

REXS/RIXS = resonant elastic/inelastic x-ray scattering

MATRIX ELEMENTS IN THE SOFT X-RAY SPECTROSCOPIES: RESONANT EFFECTS

- ***X-ray emission:***

$$I \propto \left| \hat{e} \bullet \langle \varphi_f(1) | \vec{r} | \varphi_i(1) \rangle \right|^2$$

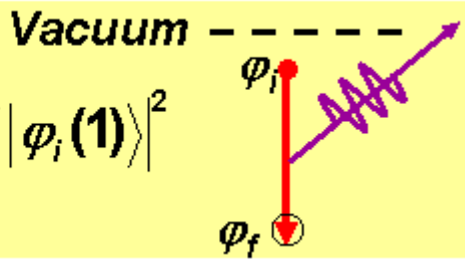

- ***Resonant inelastic x-ray scattering:***

$$I \propto \sum_f \left| \sum_m \frac{\langle \Psi_f(N) | \hat{e}_{emi} \bullet \vec{r} | \Psi_m(N) \rangle \langle \Psi_m(N) | \hat{e}_{inc} \bullet \vec{r} | \Psi_i(N) \rangle}{h\nu + E_i(N) - E_m(N) - i\Gamma_m} \right|^2 \times \delta(h\nu - (E_m(N) - E_i(N)))$$

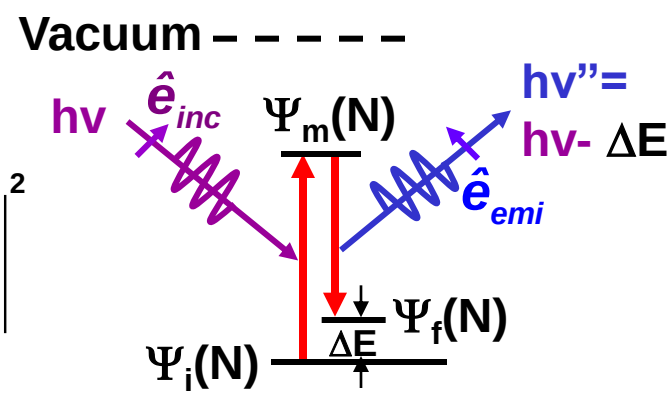

$$N_m(t) = N_m(0) e^{-\frac{2\Gamma_m t}{\hbar}} = N_m(0) e^{-\frac{t}{\tau_{lifetime}}}$$

X-ray fluorescence spectroscopy =X-ray emission spectroscopy (XES)

Resonant inelastic x-ray scattering (RIXS) and Resonant elastic x-ray scattering (REXS)

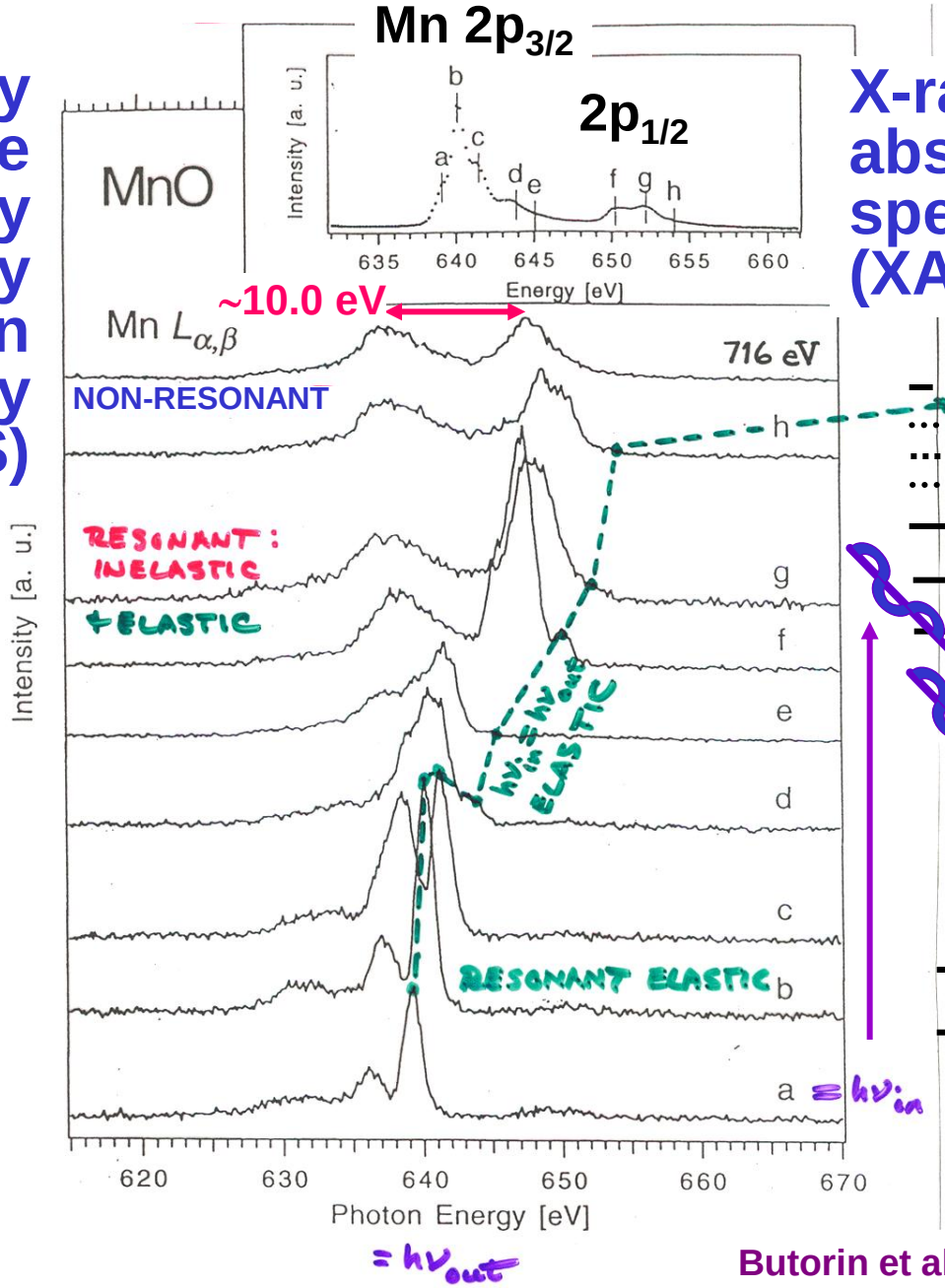

X-ray absorption spectroscopy (XAS)

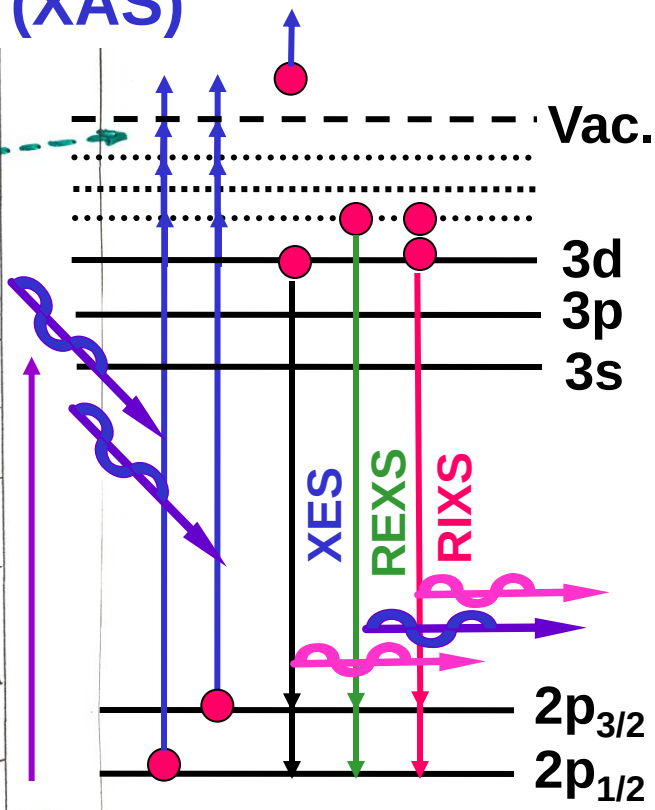

Butorin et al., Phys. Rev. B 54, 4405 ('96)

X-Ray Nomenclature (from "X-Ray Data Booklet")

In general:

nl — Spin-orbit: $nl_{j=l+1/2}$, $nl_{j=l-1/2}$

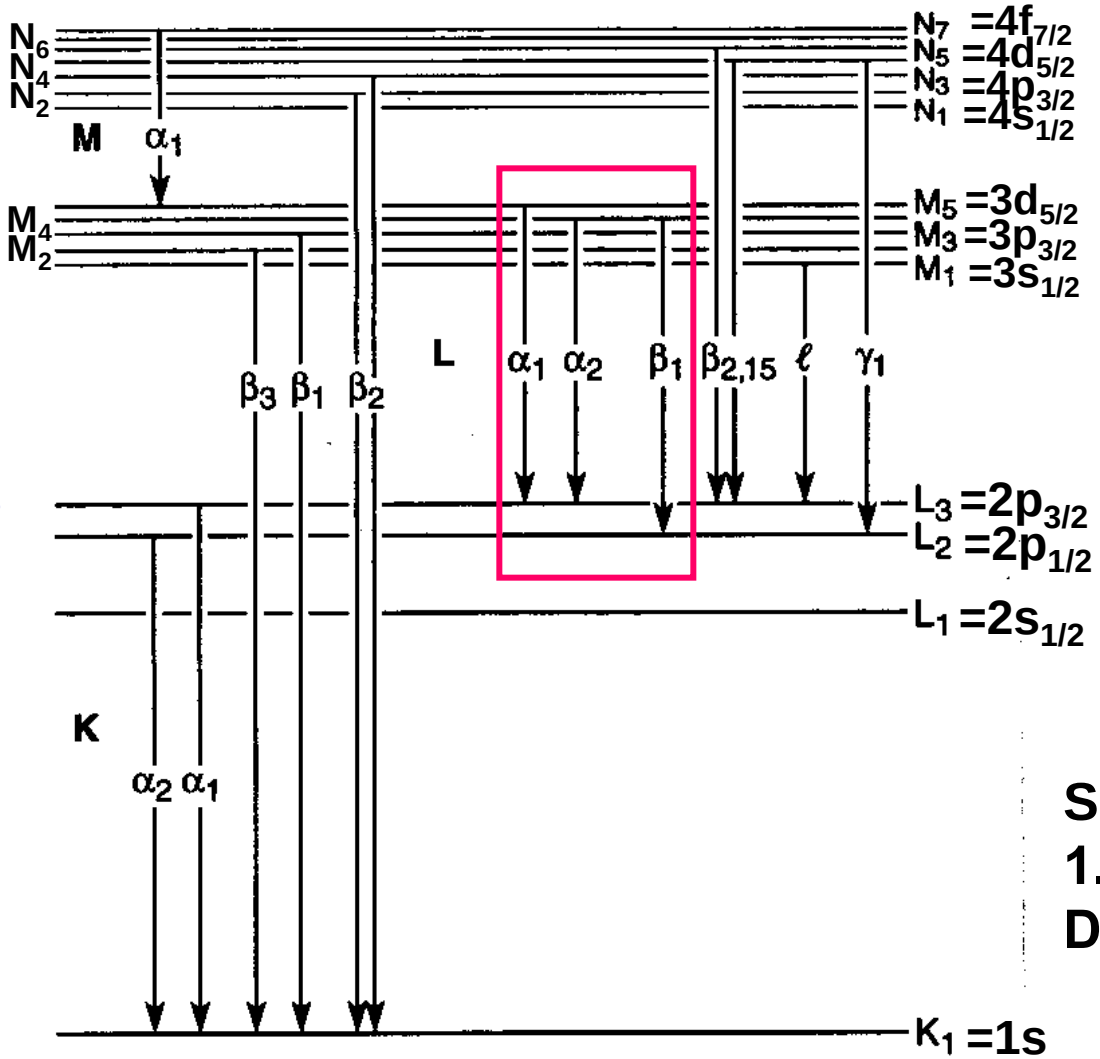

Fig. 1-1. Transitions that give rise to the emission lines in Table 1-3.

Δj=0,±1

See Section 1.2 in "X-Ray Data Booklet"

Basic energetics

$$h\nu = E^{Vacuum}_{binding} + E_{kinetic} = E^{Fermi}_{binding} + \varphi_{spectrometer} + E_{kinetic}$$

One-Electron Picture of Photoemission from a Surface

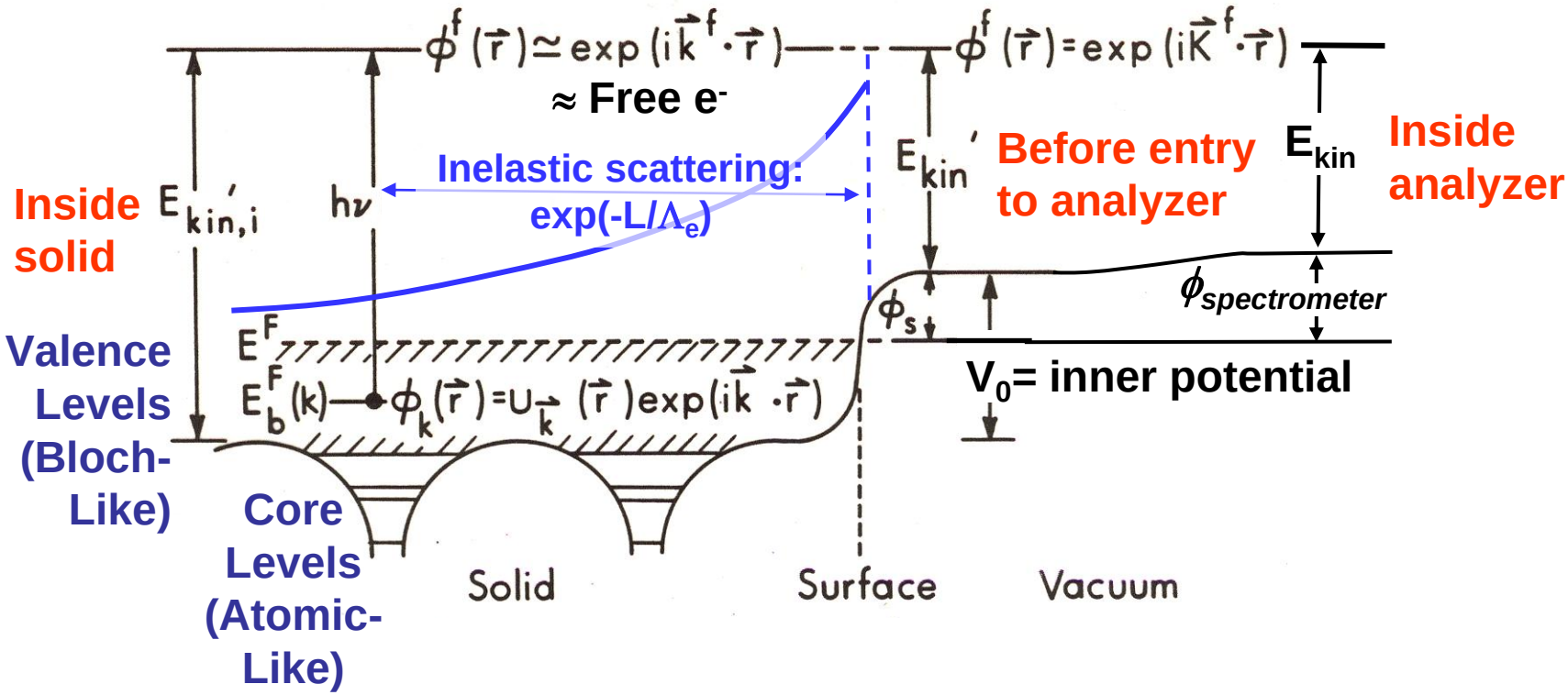

Surface sensitivity and why we may want to go to 5-10 keV in XPS

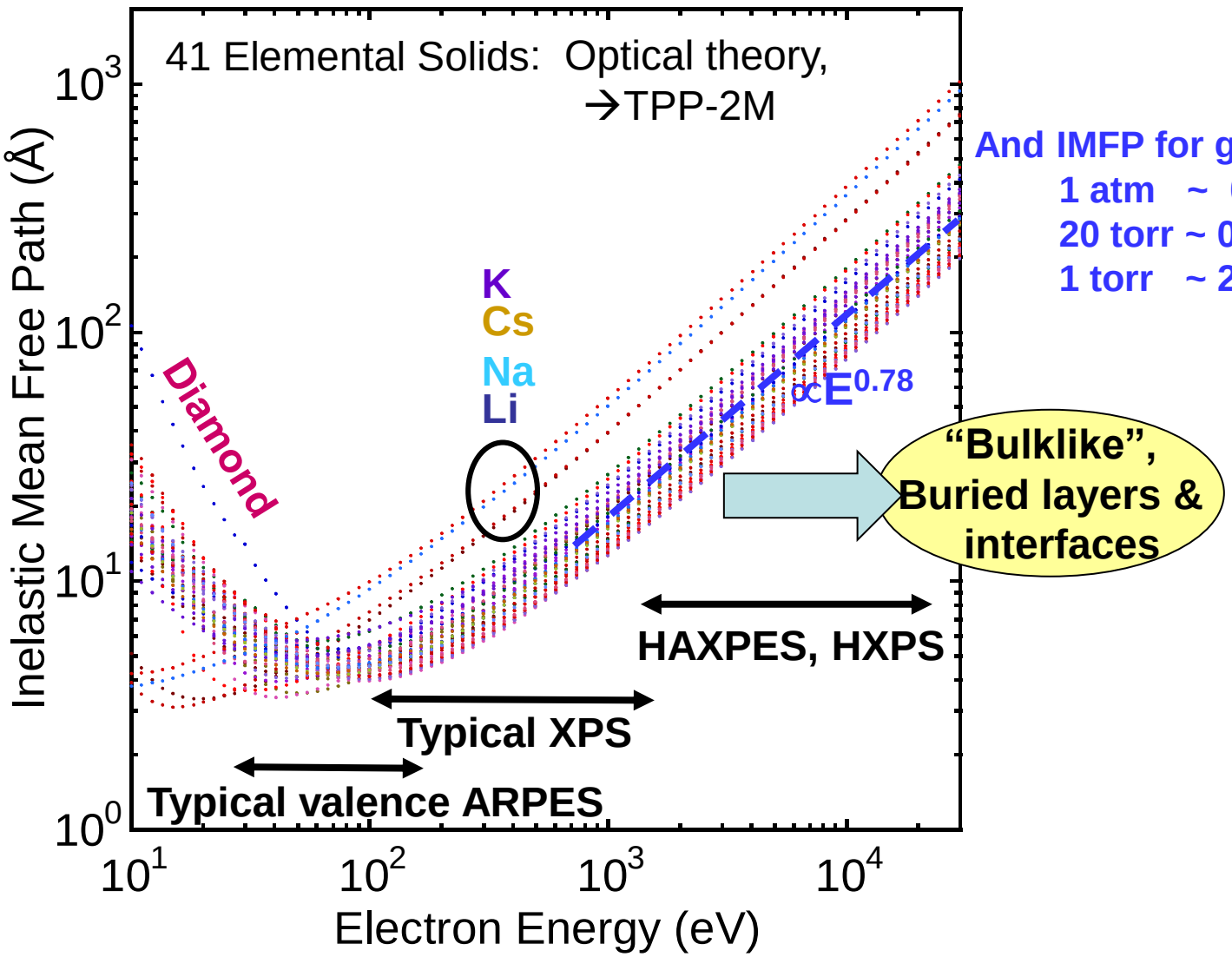

And IMFP for gases: N_2, e^- @ 500 eV
1 atm ~ 0.003 mm = 3 microns
20 torr ~ 0.1 mm = 100 microns
1 torr ~ 2 mm

Tanuma, Powell, Penn, Surf. and Interf. Anal. 43, 689 (2011)

The Advanced Light Source

One of 40→50 synchrotron radiation facilities in the world

Inside a synchrotron radiation source

Electron speed near c: ALS-0.99999997c, very relativistic

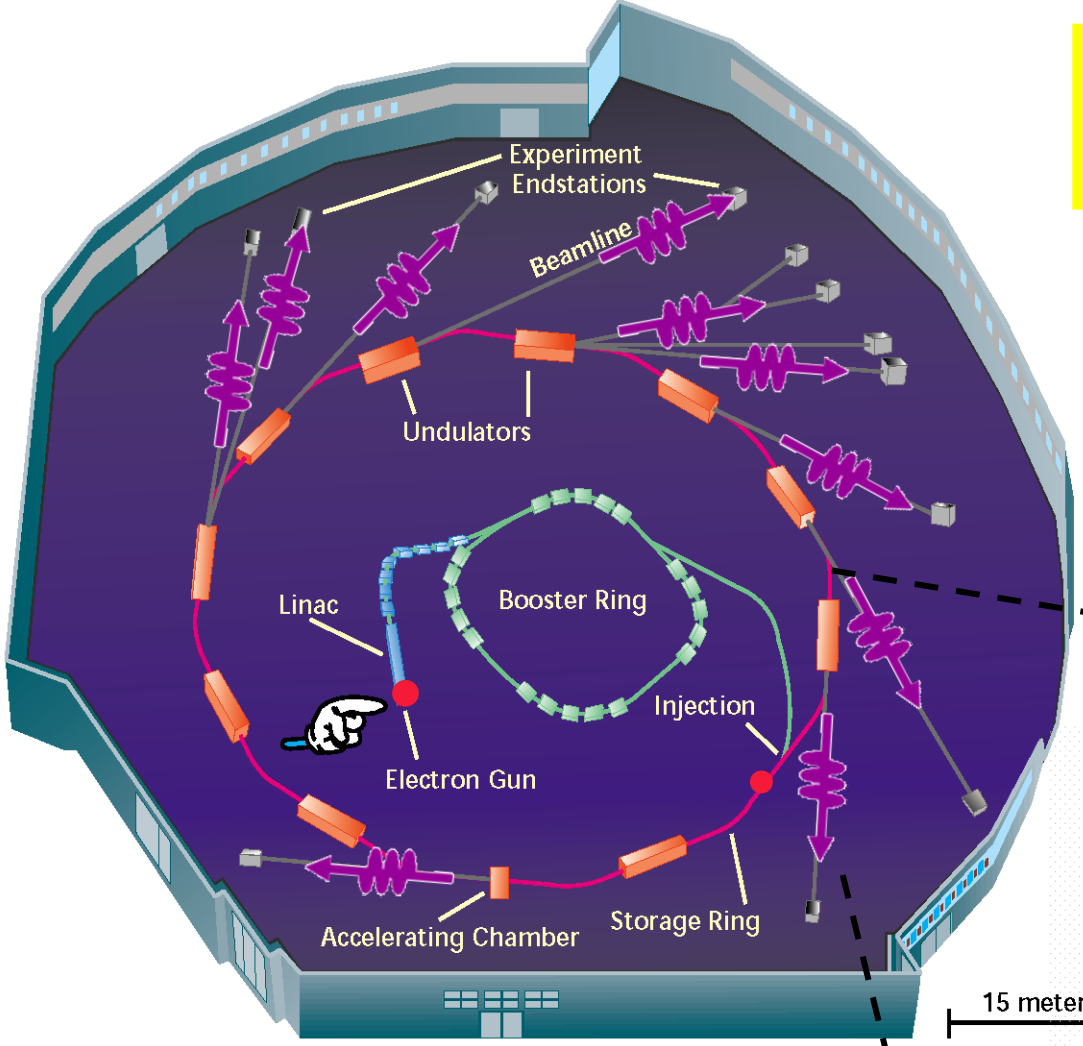

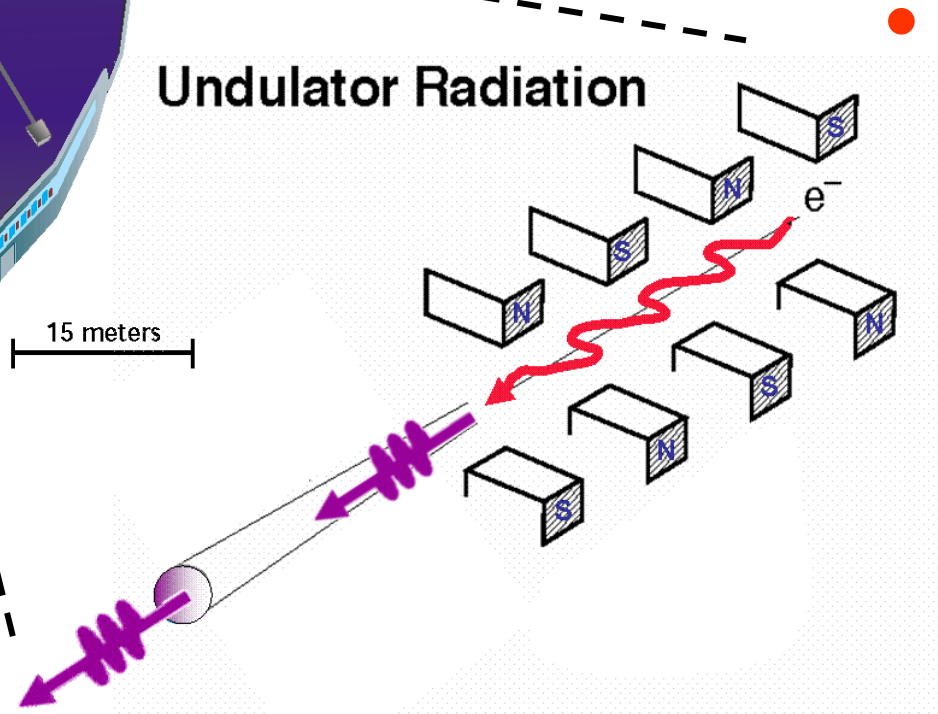

+FELs: FLASH, LCLS, Fermi (seeded),…

EXPERIMENTAL STATION: MULTI-TECHNIQUE SPECTROMETER/ DIFFRACTOMETER (MTSD)

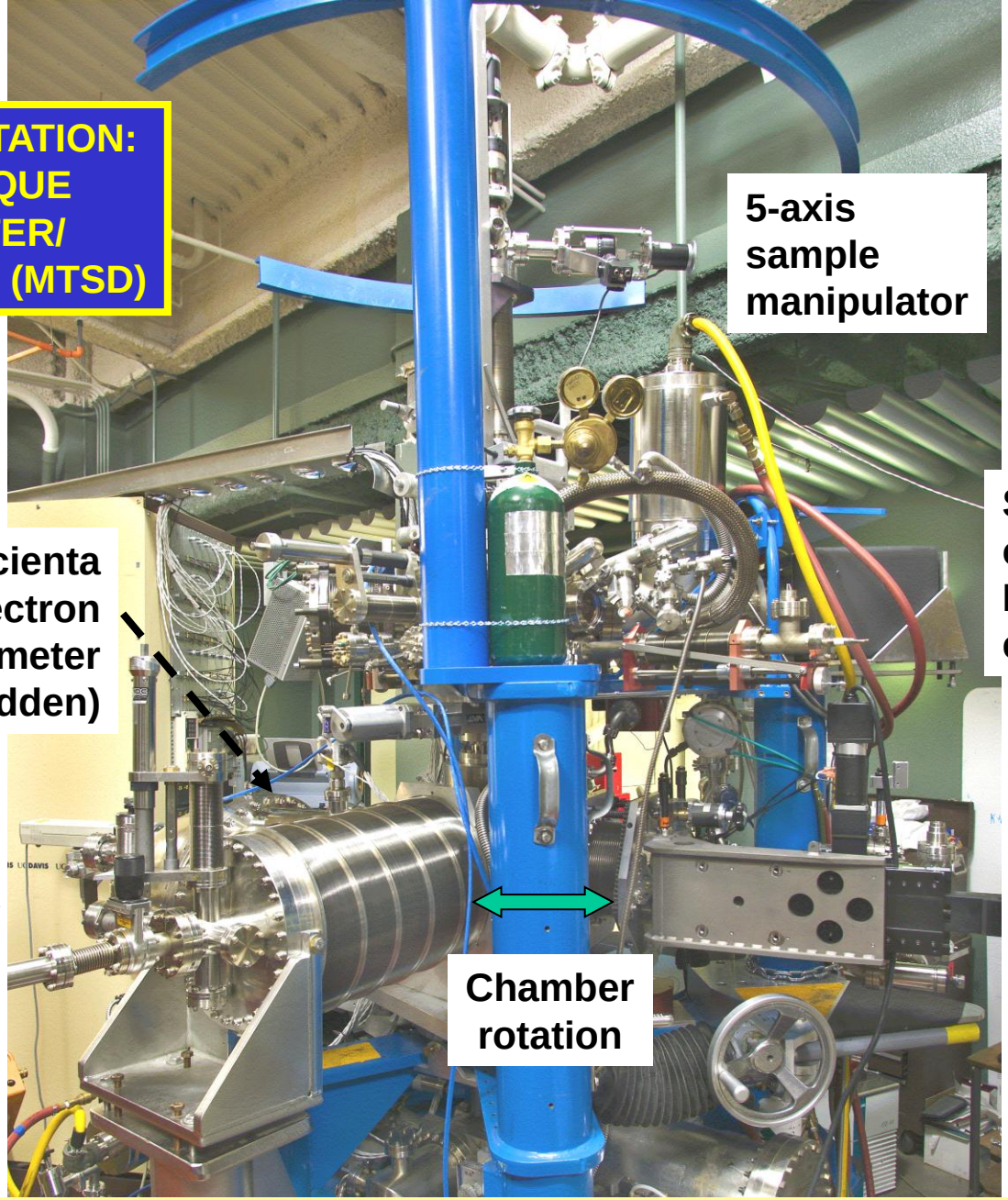

ALS
BL 9.3.1
hν = 2-5 keV

Permits using all relevant soft and hard x-ray spectroscopies on a single sample: PS, PD, PH; XAS (e^- or photon detection), XES/RIXS, with MCD, MLD

Multi-Technique Spectrometer/ Diffractometer

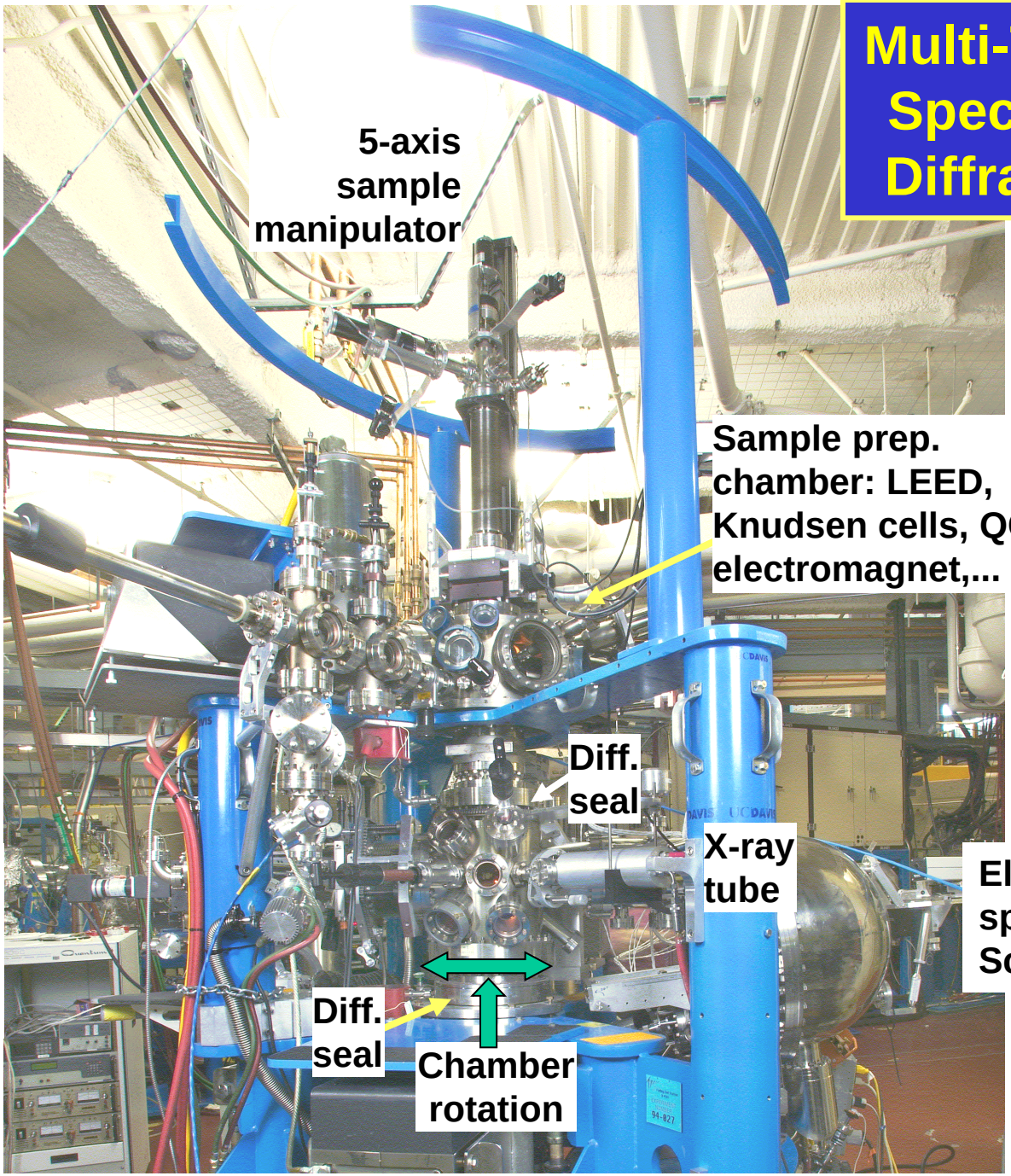

Hard X-Ray Photoemission (HXPS, HAXPES, HX-PES, HIKE...) in the World

Past workshops:

HAXPES03, ESRF--Nucl. Inst. and Meth. A, Volume 547, Issue 1, Pages 1-238 (2005)

HAXPES06, SPring8-- http://haxpes2006.spring8.or.jp/program.html

HAXPES-ALS User Meeting-- http://ssg.als.lbl.gov/ssgdirectory/fedorov/workshops/index.html

HAXPES09-NSLS-- http://www.nsls.bnl.gov/newsroom/events/workshops/2009/haxpes/

HAXPES11-Hasylab-- http://indico.desy.de/conferenceDisplay.py?confId=3713

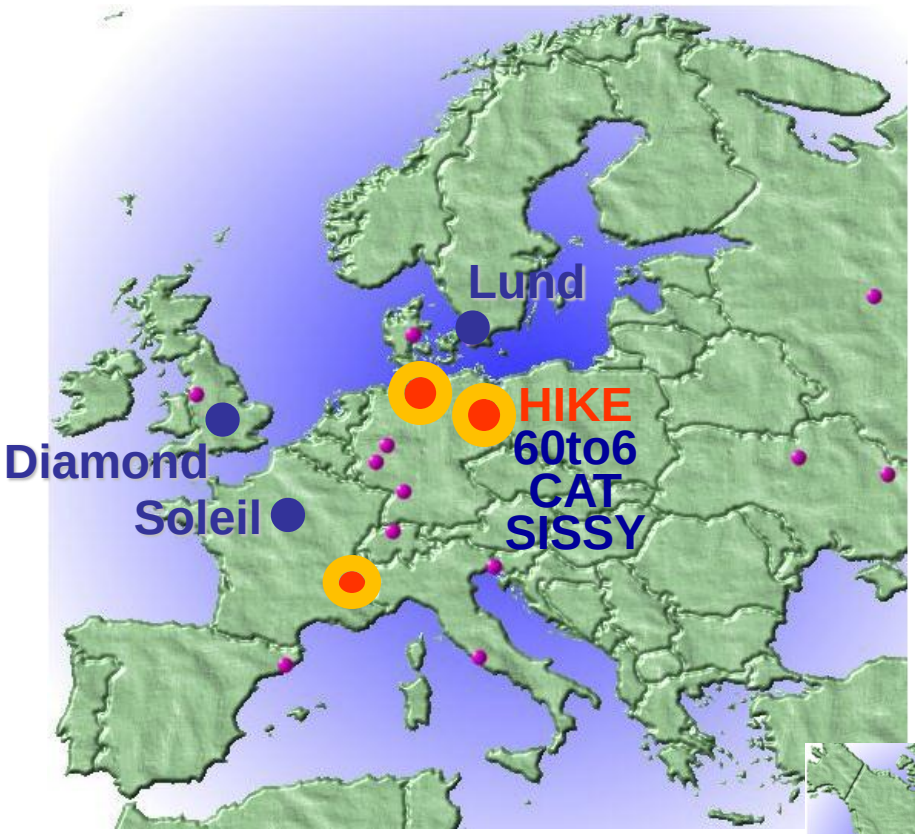

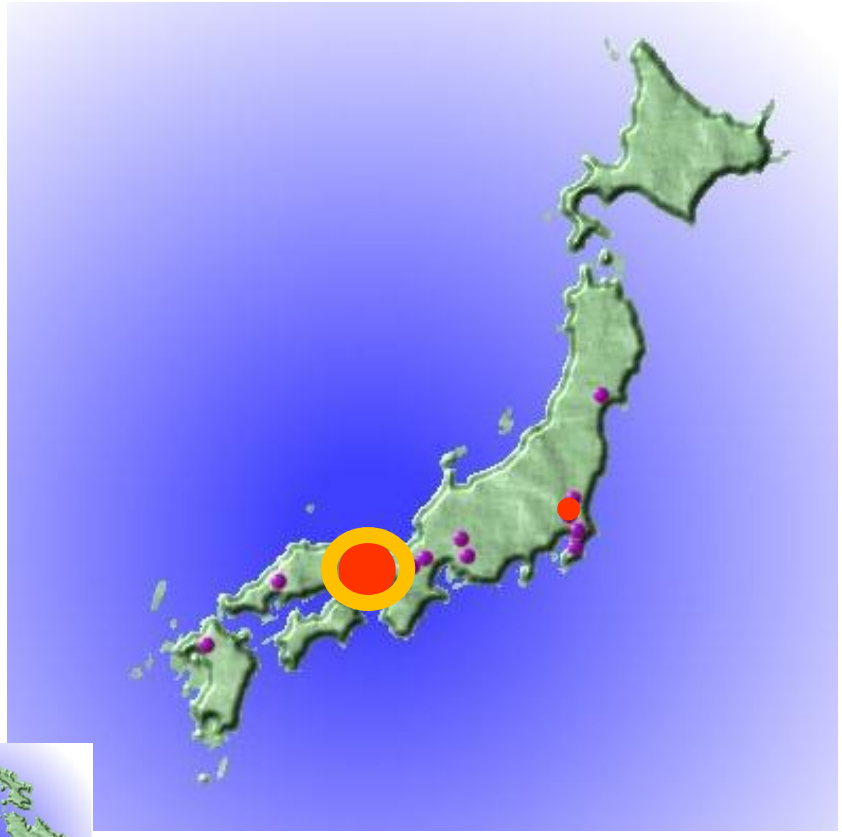

● Existing

● Under construction

○ Our group

Some key elements in Spintronics/Semiconductors/ Sensors—multilayer nanostructures

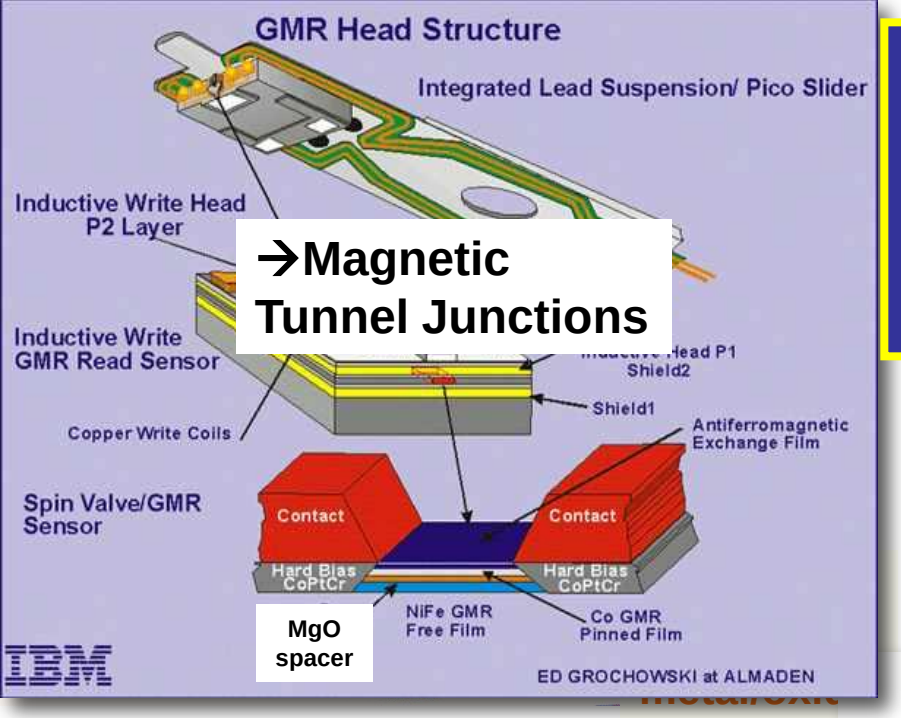

→Magnetic Tunnel Junctions

Magnetic Random Access Memory (MRAM-Non Volatile)

→Race Track Memory?

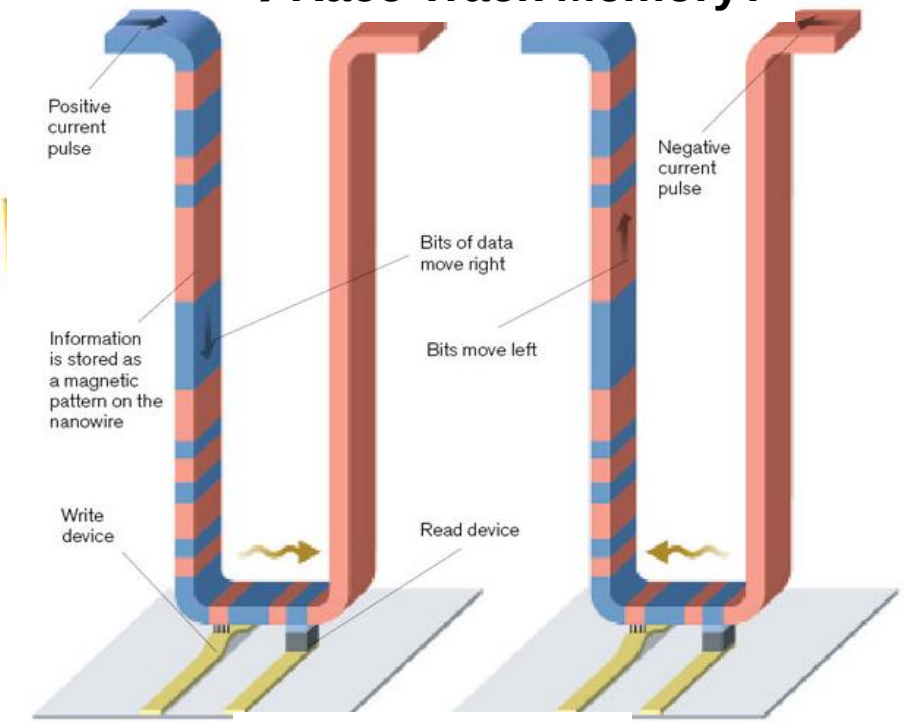

S. Parkin, IBM Almaden

Crucial buried functional layers & interfaces everywhere-

What do we want to know:

- **Interface mixing/roughness/ concentration profiles**
- **Depth-dependent magnetization profiles**
- **Depth-dependent densities of states**
- **Depth-dependent band structure?**

Photoemission from surfaces, interfaces, bulk materials

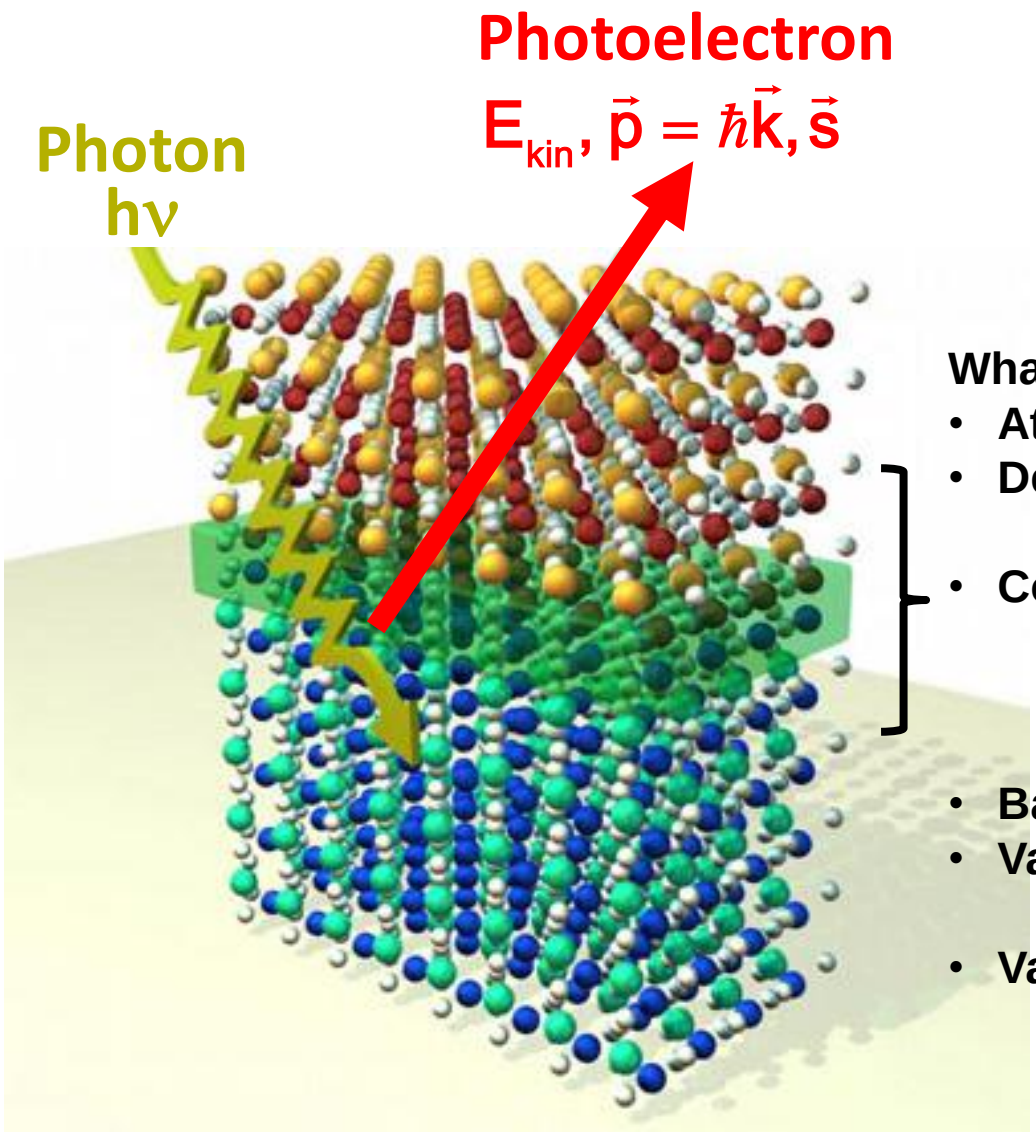

What do we want to know?

- **Atomic structure, lattice distortions**
- **Depth profiles of composition and optical properties**
- **Core-levels→element specific binding energies, charge states magnetic moments, electronic configurations**
- **Band offsets**
- **Valence-band densities of states bandgaps, behavior near E_F**
- **Valence-band dispersions, via depth-resolved ARPES**

X-ray photoemission: some key elements

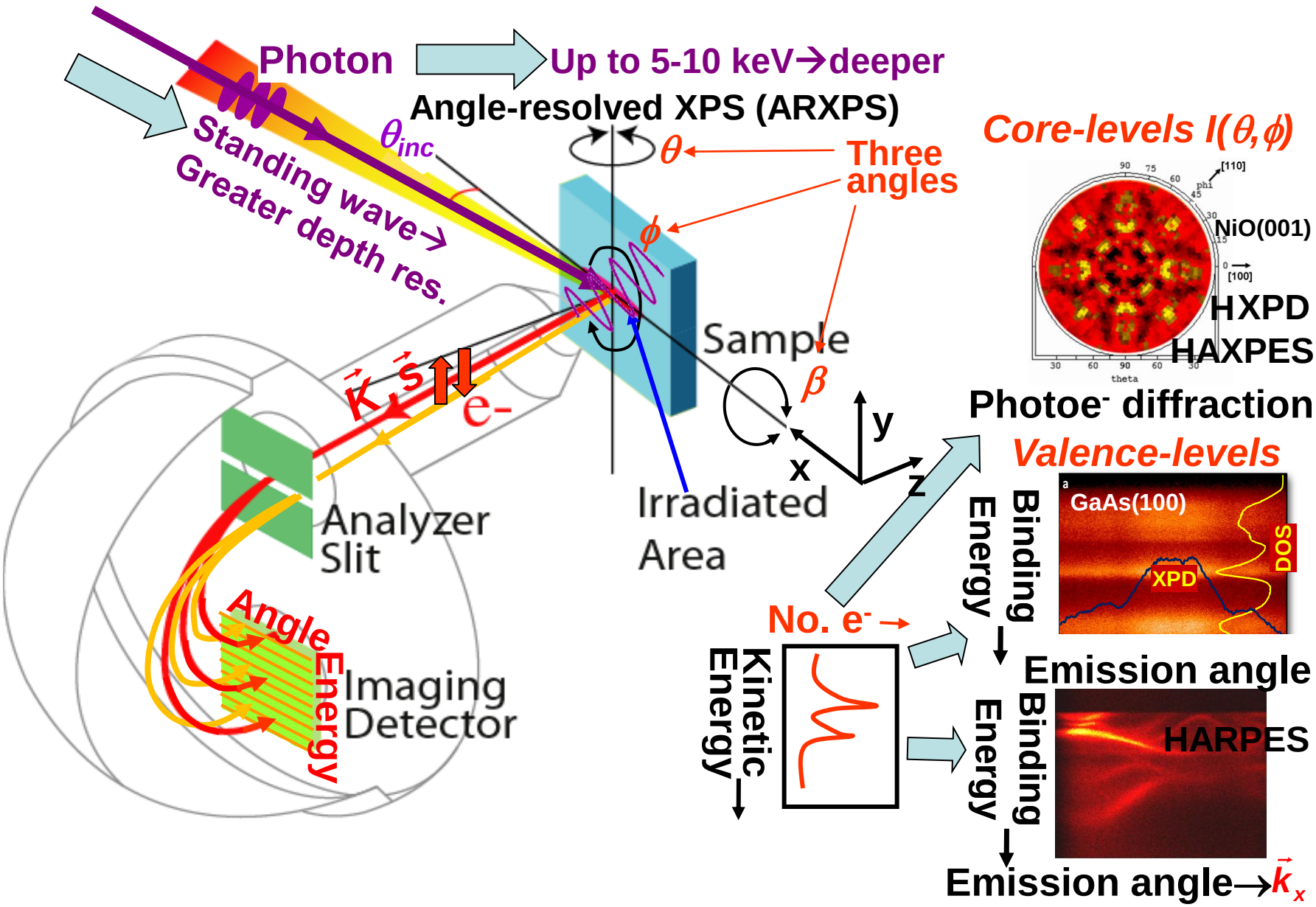

Typical experimental geometry for energy- and angle-resolved photoemission measurements

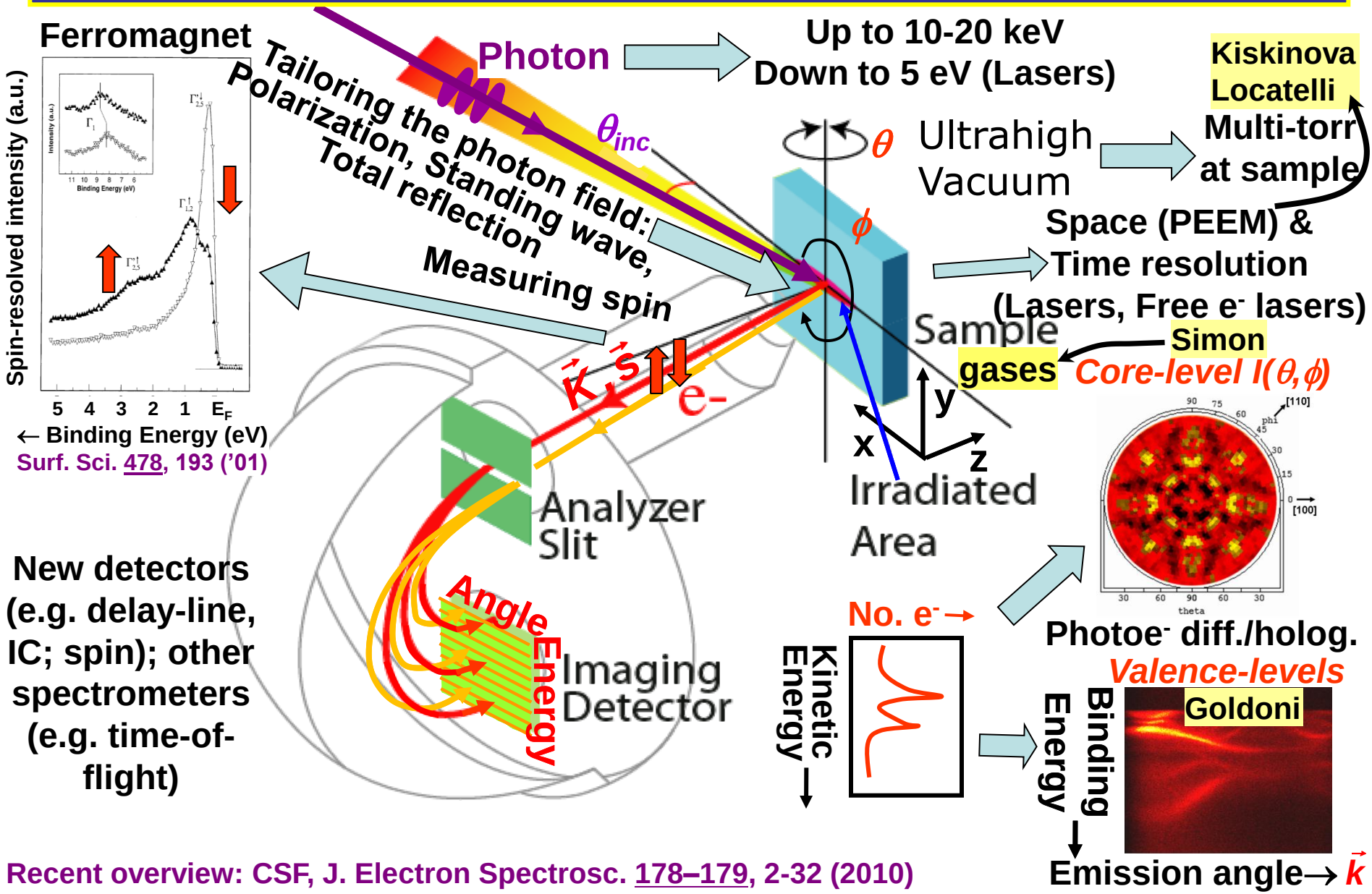

Recent overview: CSF, J. Electron Spectrosc. 178–179, 2-32 (2010)

Photoemission with time-of-flight analysis

UPPSALA

Andreas, Svensson,…

Hemisphere

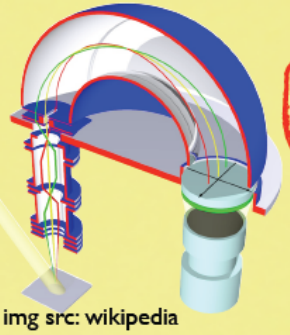

img src: wikipedia

$$\frac{\Delta E}{E} \propto E_{\text{pass}} \left[\frac{W_{\text{slit}}}{2 \cdot r} + \frac{\alpha^2}{2} \right]$$

- Resolution set by: slitwidth, hemisphere's mean radius and angular acceptance.
- Transmission limited by slitwidth and angular acceptance.

- Measures energy and only one momentum component (k_x)

High resolution & High transmission

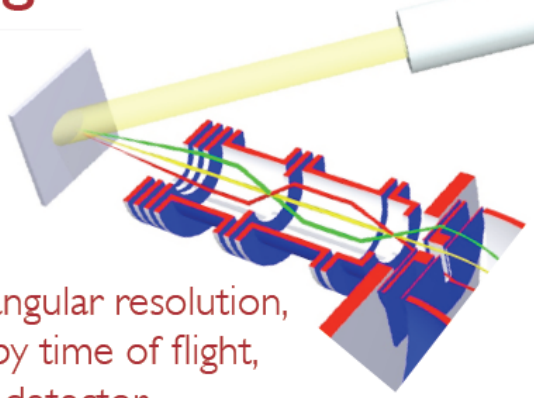

- Get rid of slit,
- Lens system for angular resolution,
- Energy analyzed by time of flight,
- Position sensitive detector

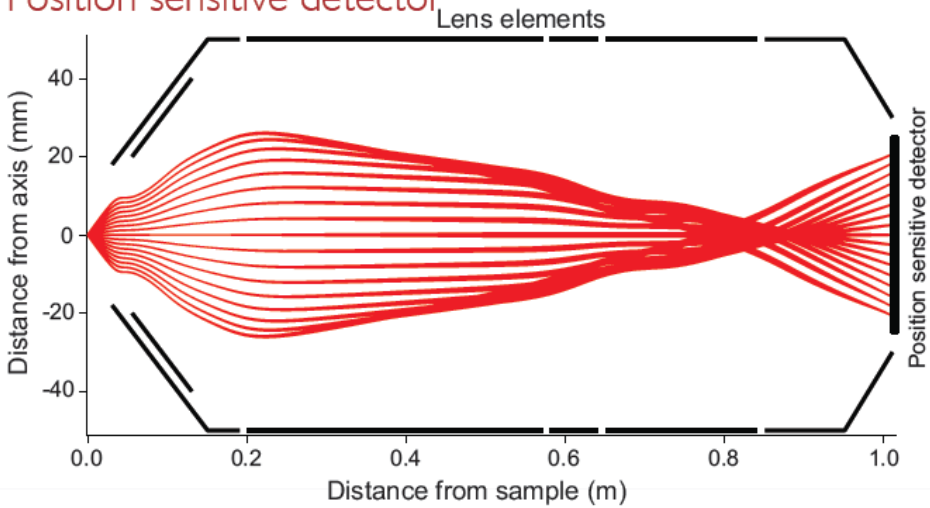

- Measures energy and two momentum components (k_x and k_y)

ARTOF (+ Themis, LBNL,…)

King, … et al. Phys. Rev. Lett. 107, 096802 (2011)

Photoemission with time-of-flight analysis: A topological insulator

UPPSALA UNIVERSITET

ARToF spectroscopy: Bi_2Se_3

High resolution & High transmission

- Full 3d-bandstructure in ~15 min

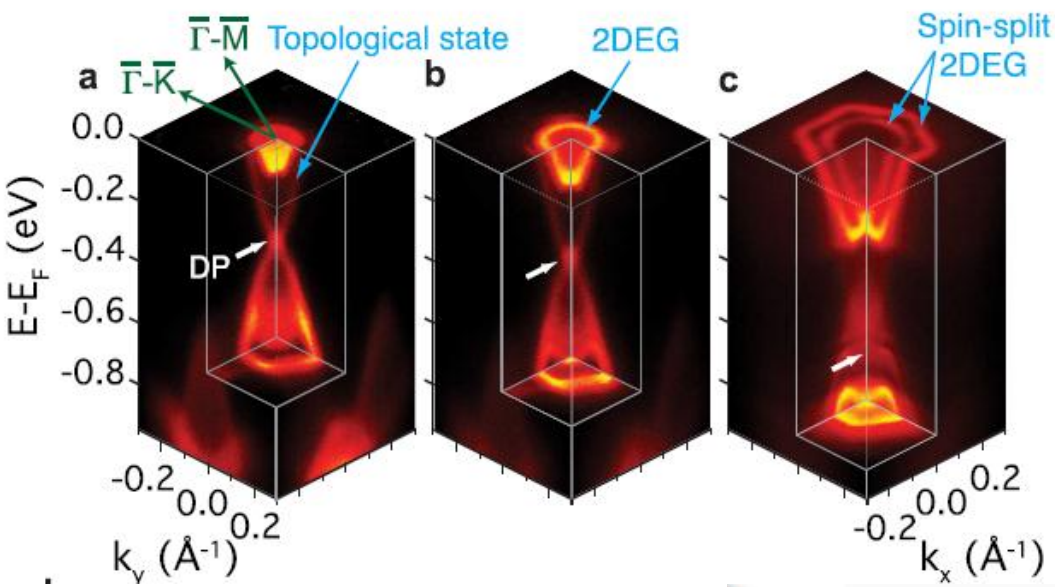

$E-E_F = -810$ meV

Time-resolved video in UHV

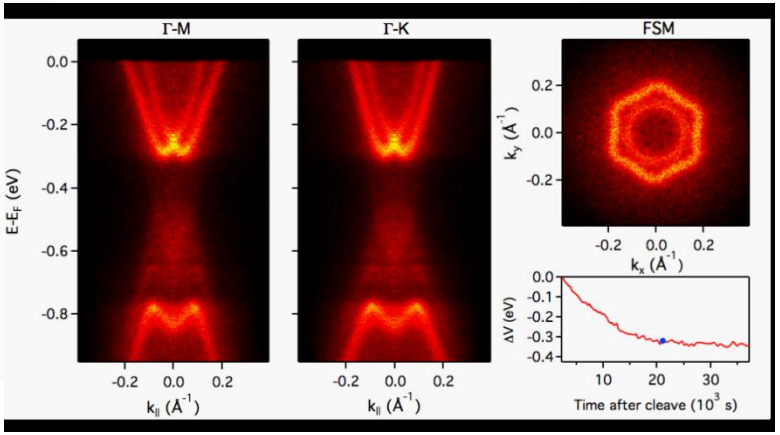

Basic energetics—Many e⁻ picture

$$h\nu = E_{binding}^{Vacuum} + E_{kinetic} = E_{binding}^{Fermi} + \varphi_{spectrometer} + E_{kinetic}$$

$$E_{binding}^{Vacuum}(Qn\ell j, K) = E_{final}(N-1, Qn\ell j\ hole, K) - E_{initial}(N)$$

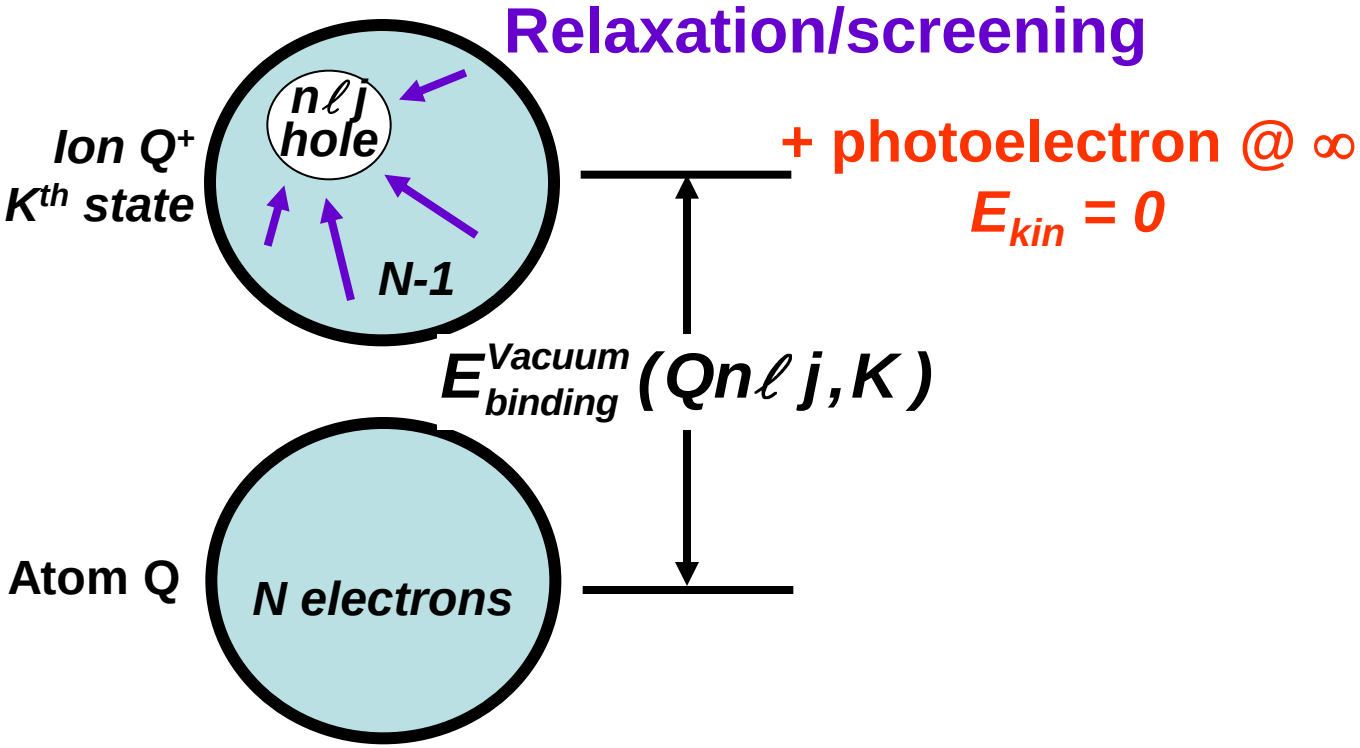

Typical experimental geometry for energy- and angle-resolved photoemission measurements

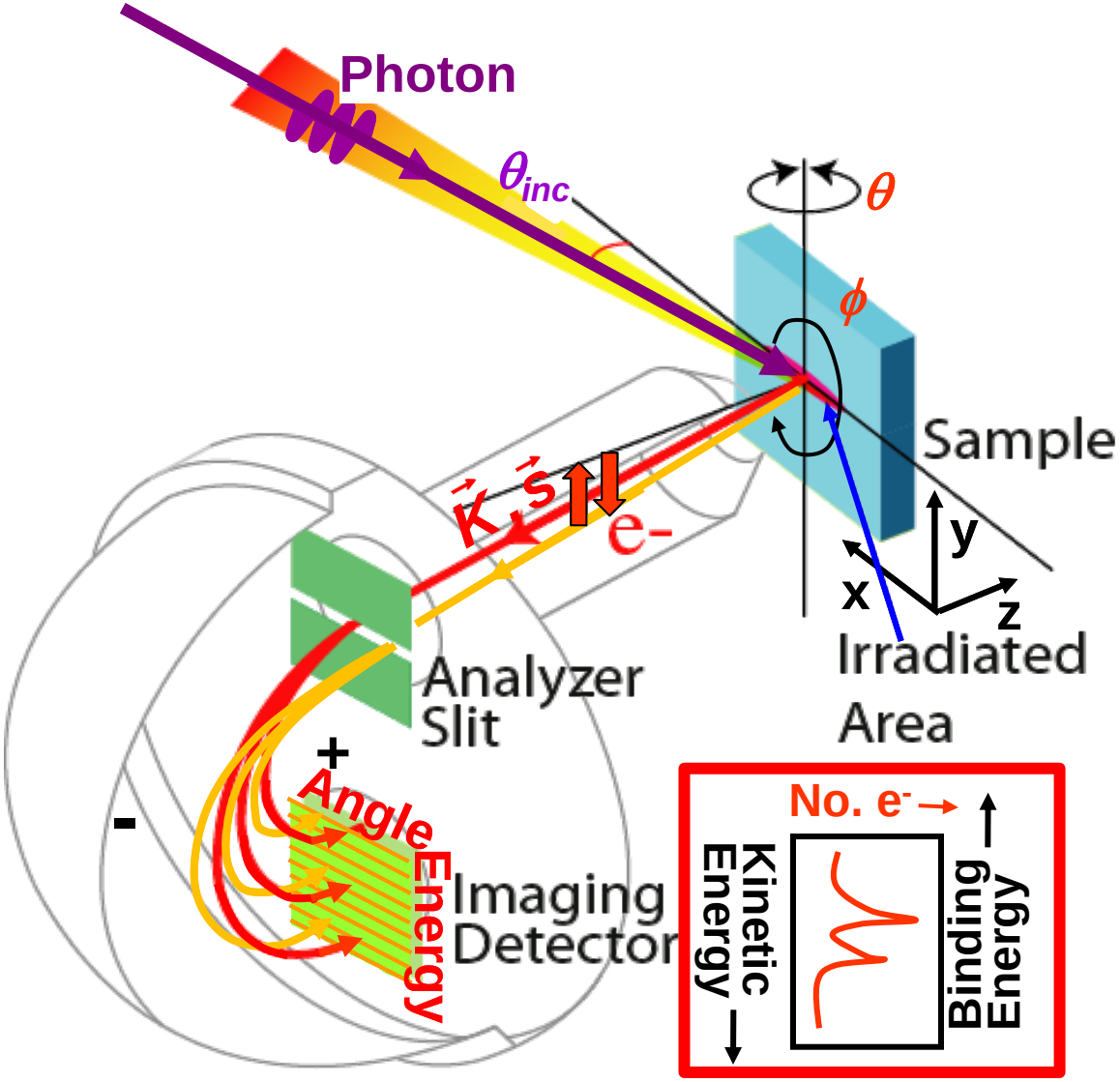

Core and valence photoemission

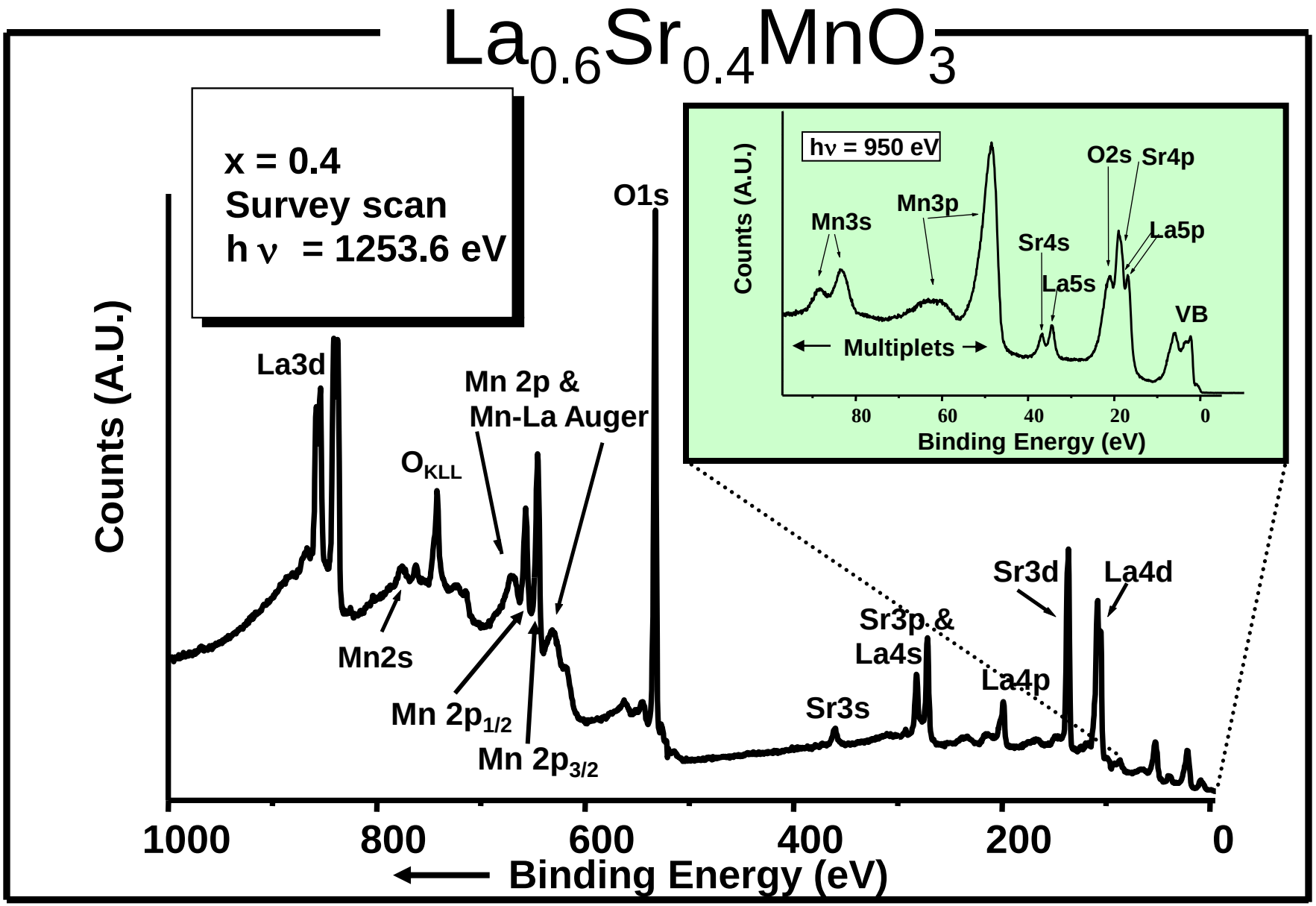

Basic Concepts and Experiments

Core-Level Photoemission

- Intensities and Quantitative Analysis, the 3-Step Model
- Varying Surface and Bulk Sensitivity
- Chemical shifts
- Multiplet Splittings
- Electron Screening and Satellite Structure
- Magnetic and Non-Magnetic Dichroism
- Resonant Photoemission
- Photoelectron Diffraction and Holography

Valence-Level Photoemission

- Band-Mapping in the Ultraviolet Photoemission Limit
- Densities of States in the X-Ray Photoemission Limit

Some New Directions

- Photoemission with Hard X-Rays (throughout lectures)
- Photoemission with Standing Wave Excitation
- Photoemission with Spatial Resolution/Photoelectron Microscopy
  - Temporal Resolution
  - @ Higher Pressures

PHOTOELECTRON INTENSITIES—THE 3-STEP MODEL

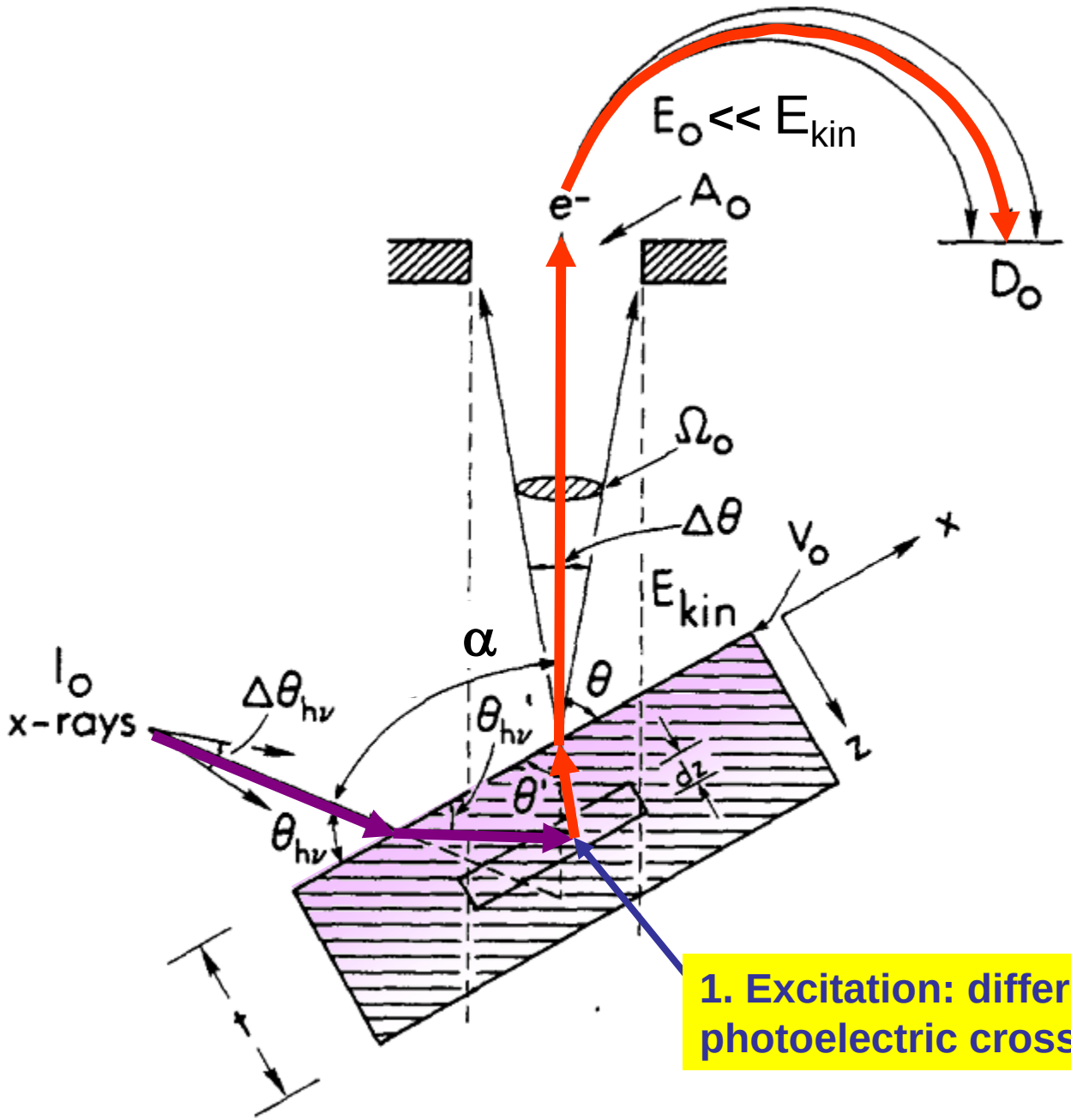

1. Excitation: differential photoelectric cross section ($d\sigma/d\Omega$)

PHOTOELECTRON EMISSION – BASIC MATRIX ELEMENTS + SELECTION RULES:

ATOMIC-LIKE (LOCALIZED) STATES ⇒ CORE:

$$\varphi_i(\vec{r}) = \varphi_{n_i l_i m_i}(r,\theta,\phi) = R_{n_i l_i}(r)\, Y_{l_i m_i}(\theta,\phi)$$

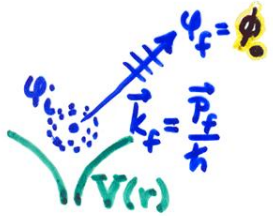

$$\varphi_f(\vec{r},\vec{k}_f) = \varphi_{E_f}(\vec{r},\vec{k}_f)$$

PHASE SHIFT OF l_f WAVE IN $V(r)$

$$= 4\pi \sum_{l_f, m_f} i^{l_f} e^{-i\delta_{l_f}} Y^*_{l_f m_f}(\theta_{k_f}, \phi_{k_f})\, Y_{l_f m_f}(\theta,\phi)\, R_{E_f, l_f}(r)$$

DIPOLE APPROX.: INT. $\propto |\langle \varphi_f | \hat{\varepsilon}\cdot\vec{r} | \varphi_i \rangle|^2 = |\hat{\varepsilon}\cdot\langle \varphi_f | \vec{r} | \varphi_i \rangle|^2 \Rightarrow$

- $\Delta l = l_f - l_i = \pm 1$ TWO CHANNELS
- $\Delta m = m_f - m_i = 0, \pm 1$ LINEAR POLARIZ.
- $\Delta m = \pm 1$, CIRCULAR POLARIZATION

EQUIVALENT WITHIN CONSTANT FACTOR

$$\vec{r} \leftrightarrow \vec{p} \leftrightarrow \vec{\nabla} V(r)$$

The differential photoelectric cross section—dipole limit

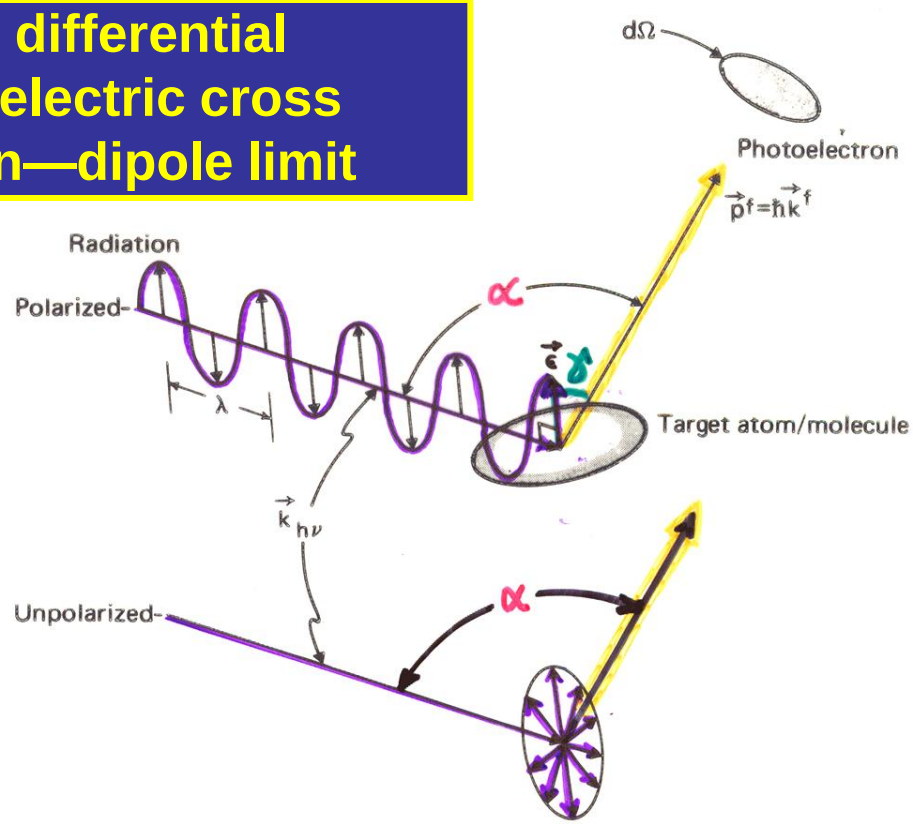

FOR ATOMIC-LIKE EMISSION:

LIN. POLARIZED: $\frac{d\sigma_{n\ell}(E_f)}{d\Omega} = \frac{\sigma_{n\ell}(E_f)}{4\pi}\left[1 + \beta_{n\ell}(E^f)\left(\frac{3}{2}\cos^2\gamma - \frac{1}{2}\right)\right]$

UNPOLARIZED: $\frac{d\sigma_{n\ell}(E_f)}{d\Omega} = \frac{\sigma_{n\ell}(E_f)}{4\pi}\left[1 + \frac{1}{2}\beta_{n\ell}(E^f)\left(\frac{3}{2}\sin^2\alpha - 1\right)\right]$

Figure 7 -- General geometry for defining the differential cross section $d\sigma/d\Omega$, showing both polarized and unpolarized incident radiation. The polarization vector $\vec{\epsilon}$ is parallel to the electric field $\vec{E}$ of the radiation. In order for the dipole approximation to be valid, the radiation wave length λ should be much larger than typical target dimensions (that is, the opposite of what is shown here).

WITH:

$\sigma_{n\ell}$ = TOTAL CROSS SECTION

$\beta_{n\ell}$ = ASYMMETRY PARAMETER

$\sigma_{n\ell}$, $\beta_{n\ell}$ TABULATIONS IN: GOLDBERG ET AL., J. ELECT. SPECT. & YEH, LINDAU, AT. NUC. DATA 32, 1 ('85) \ 21, 285 ('81)

http://ulisse.elettra.trieste.it/services/elements/WebElements.html

PHOTOELECTRIC CROSS SECTIONS FOR Mn

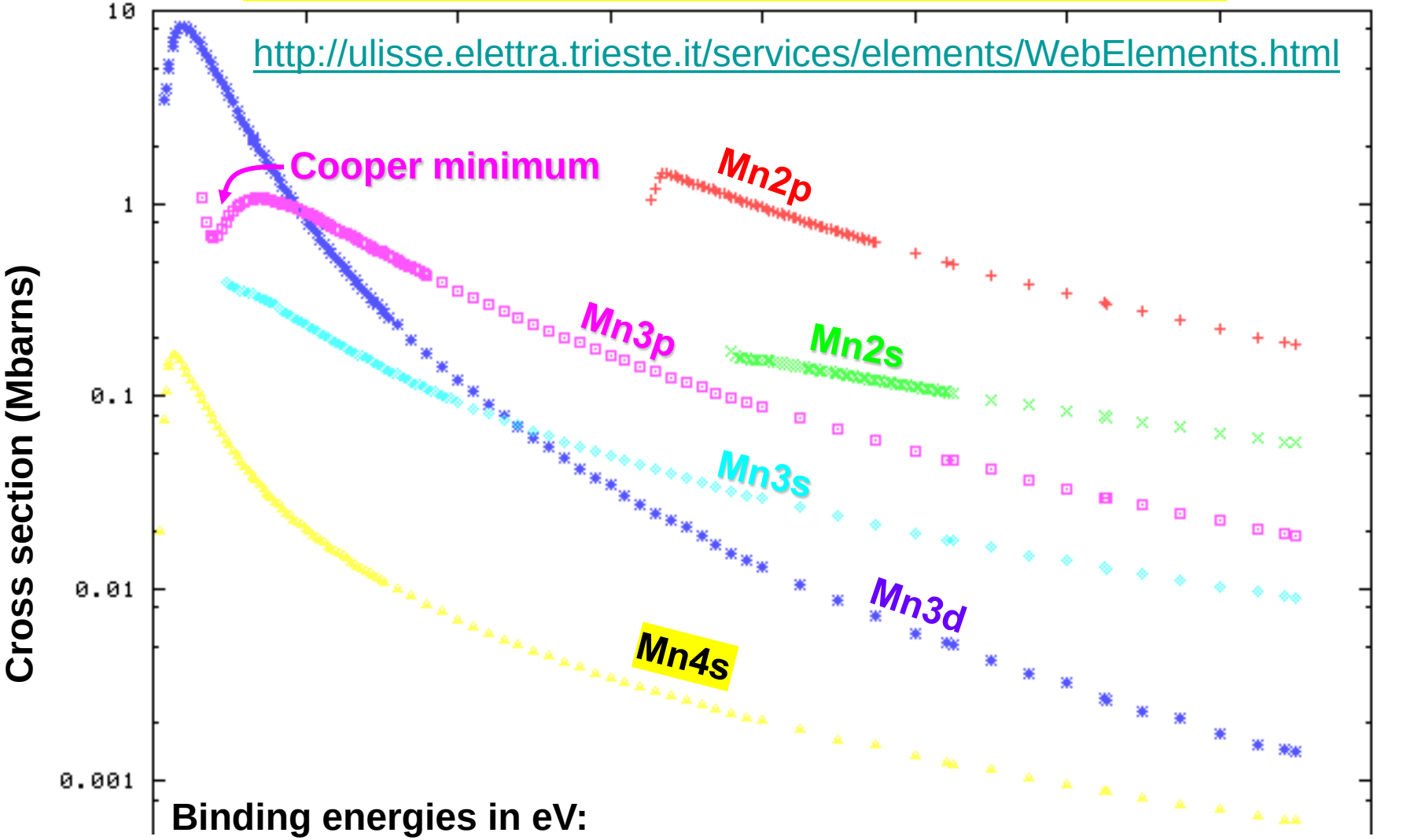

Binding energies in eV:

		K1s	L_1 2s	L_2 $2p_{1/2}$	L_3 $2p_{3/2}$	M_1 3s	M_2 $3p_{1/2}$	M_3 $3p_{3/2}$	M_{4-5} 3d	N_1 4s
25	Mn	6539	769.1	649.9	638.7	82.3	47.2	47.2	≈5	≈5

The differential subshell photoelectric cross section—dipole limit

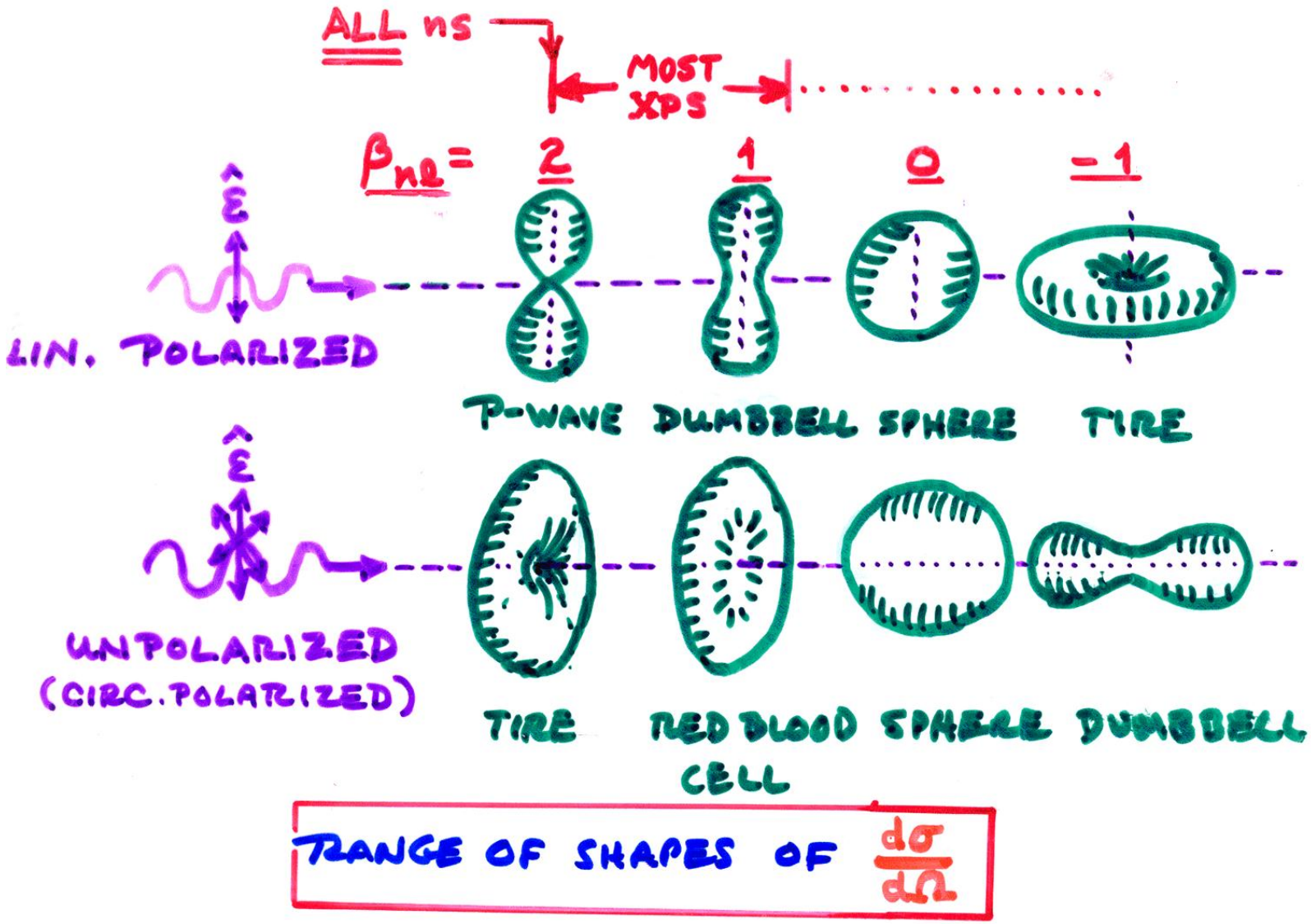

→Higher energies: Nondipolar Angular Distributions

$$\frac{d\sigma(h\nu)}{d\Omega} = \frac{\sigma(h\nu)}{4\pi}\left[1 + \frac{\beta}{2}(3\cos^2\theta - 1) + (\delta + \gamma\cos^2\theta)\sin\theta\cos\phi\right]$$

Dipole Non-dipole

β = 2

1

0

-0.5

-1

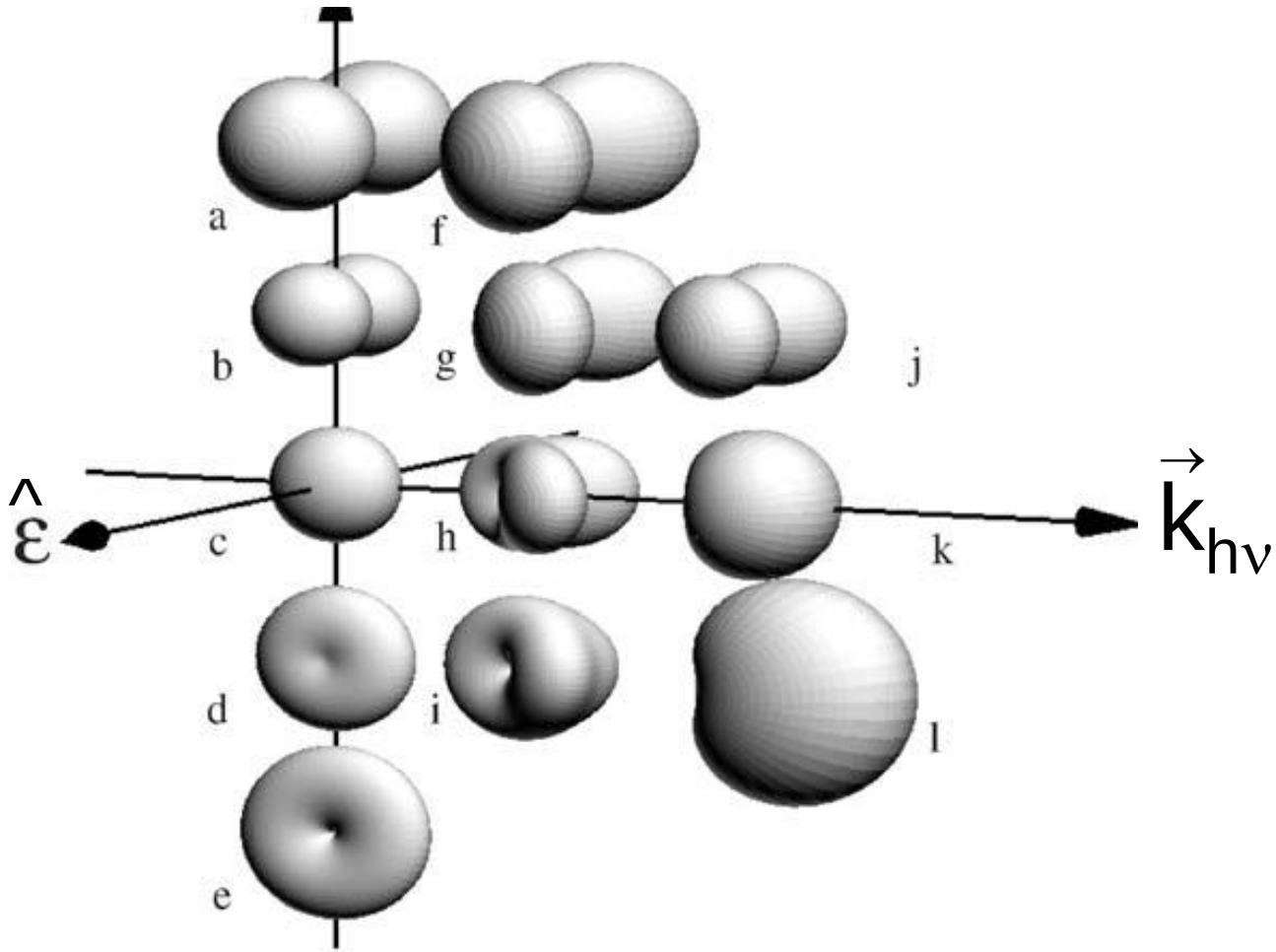

γ,δ=0 γ large δ large

D.W. Lindle

PHOTOELECTRON INTENSITIES—THE 3-STEP MODEL

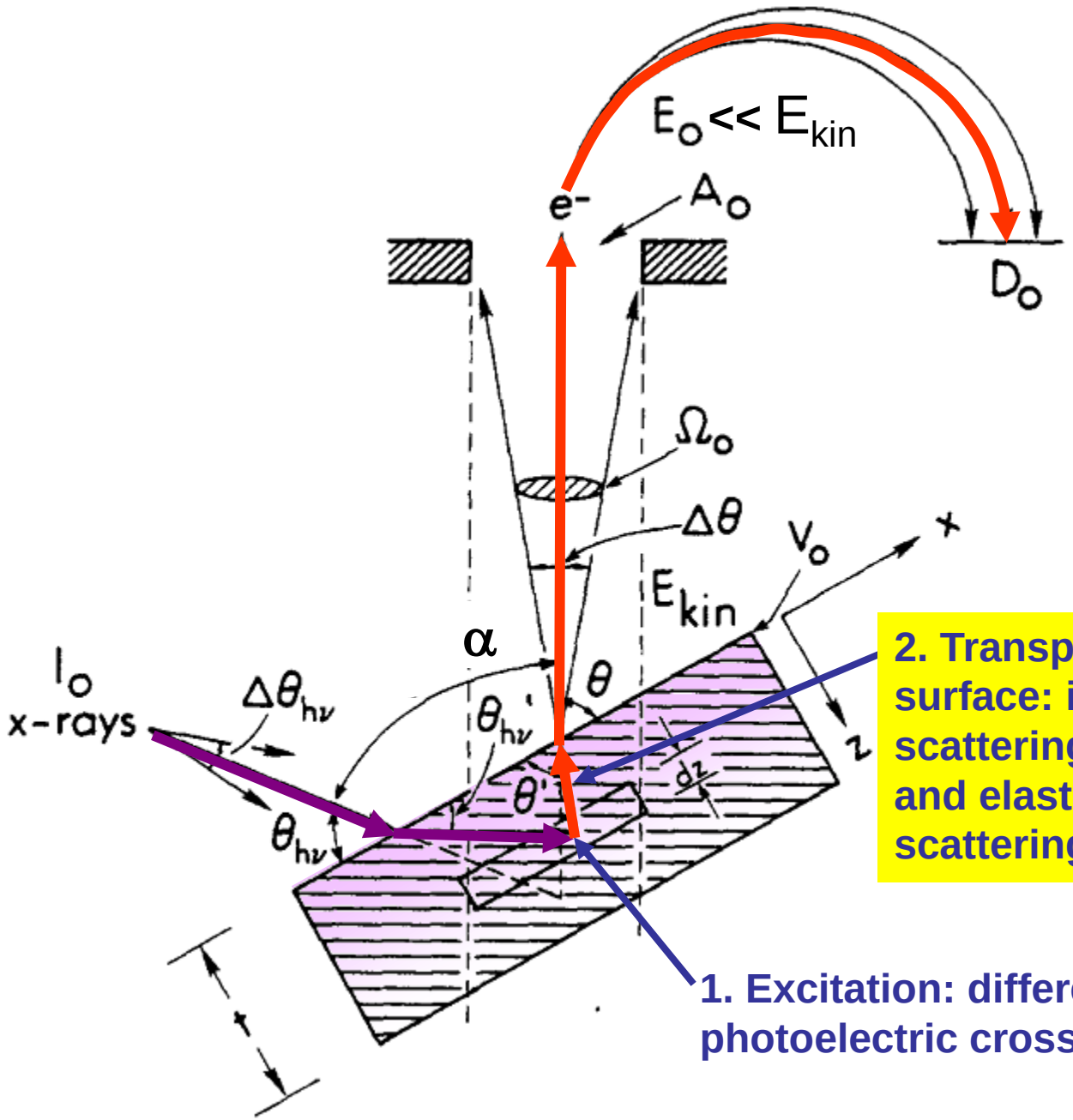

2. Transport to the surface: inelastic scattering (Λ_e) and elastic scattering ($f(\theta)$--later)

1. Excitation: differential photoelectric cross section ($d\sigma/d\Omega$)

Surface sensitivity and why we may want to go to 5-10 keV in XPS

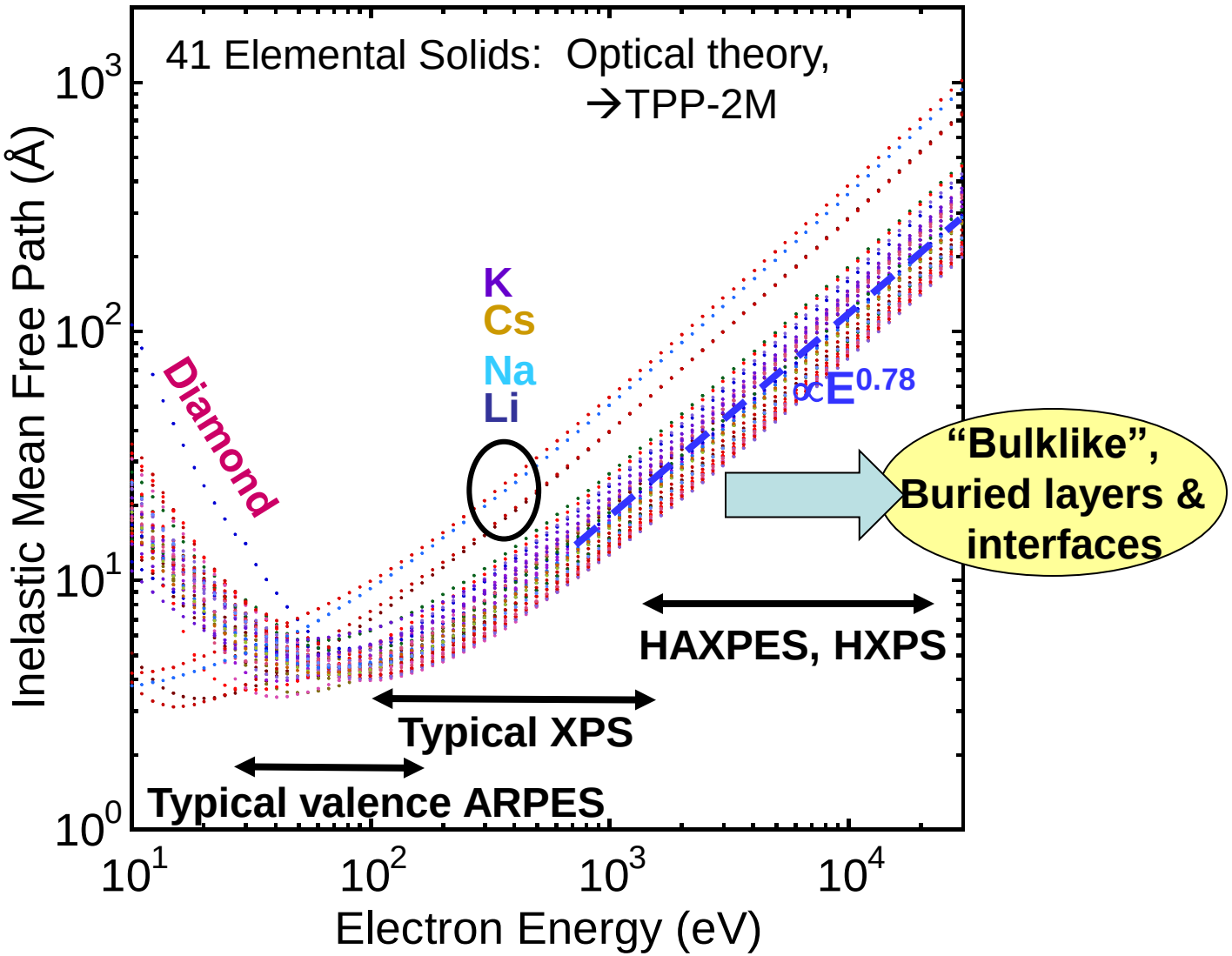

Tanuma, Powell, Penn, Surf. and Interf. Anal. 43, 689 (2011)

Electron inelastic attenuation length in solids—the "universal curve"
Photoemission is a surface sensitive experiment

Changing angle:
1st way to vary surface sensitivity

$$I(z) = I_0 e^{-\frac{z}{\Lambda_e \sin\Theta}}$$

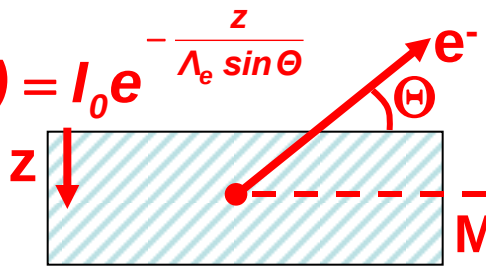

$\Lambda_e \sin\Theta$ = Mean depth

Graphite

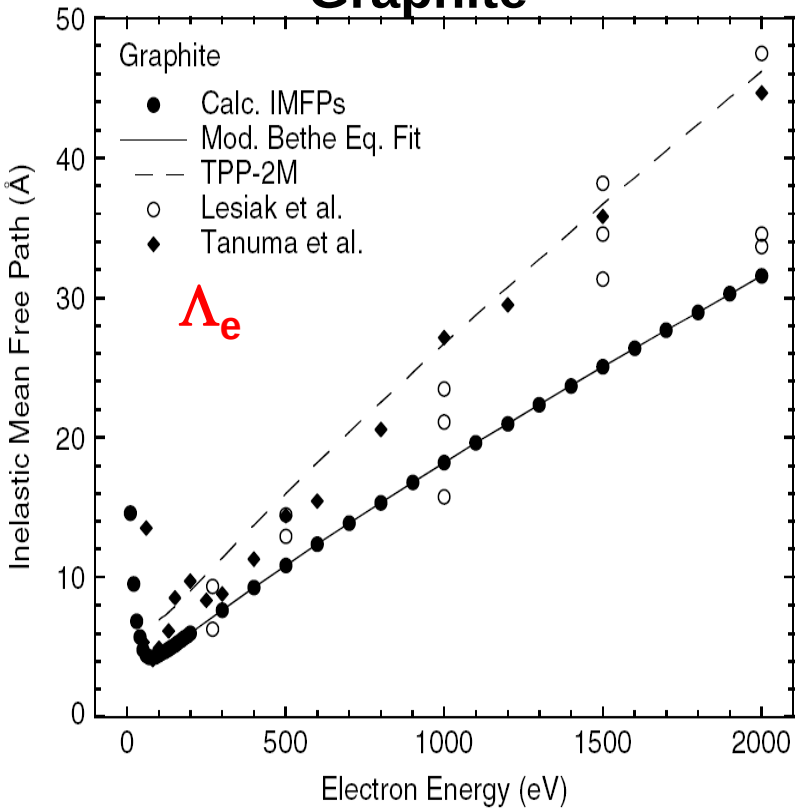

Germanium

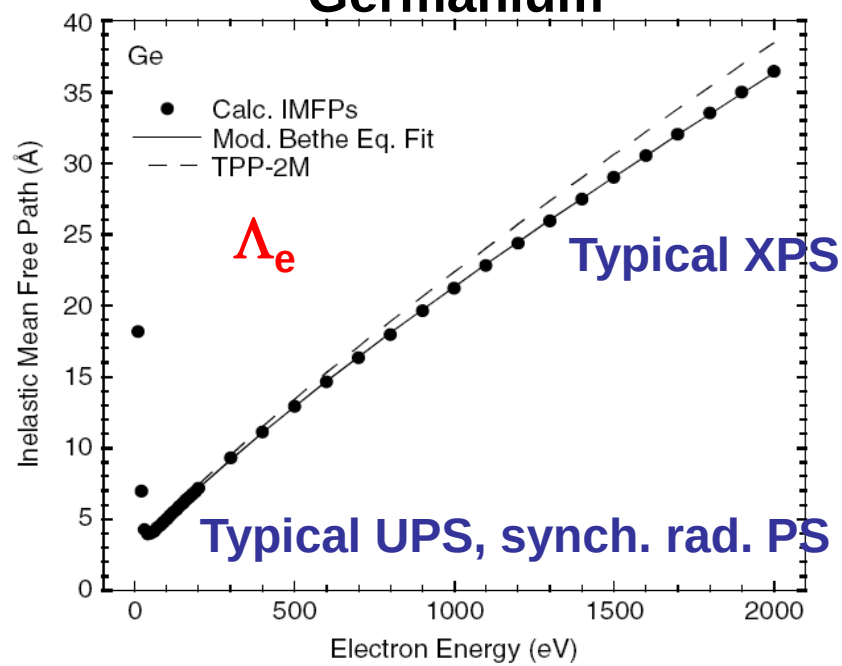

Changing photon energy:
2nd way to vary surface sensitivity

Basic Concepts and Experiments

Core-Level Photoemission

- Intensities and Quantitative Analysis, the 3-Step Model
- Varying Surface and Bulk Sensitivity
- Chemical shifts
- Multiplet Splittings
- Electron Screening and Satellite Structure
- Magnetic and Non-Magnetic Dichroism
- Resonant Photoemission
- Photoelectron Diffraction and Holography

Valence-Level Photoemission

- Band-Mapping in the Ultraviolet Photoemission Limit
- Densities of States in the X-Ray Photoemission Limit

Some New Directions

- Photoemission with Hard X-Rays (throughout lectures)
- Photoemission with Standing Wave Excitation
- Photoemission with Spatial Resolution/Photoelectron Microscopy
  - Temporal Resolution
  - @ Higher Pressures

CORE PHOTOELECTRON INTENSITIES AND COMPOSITION

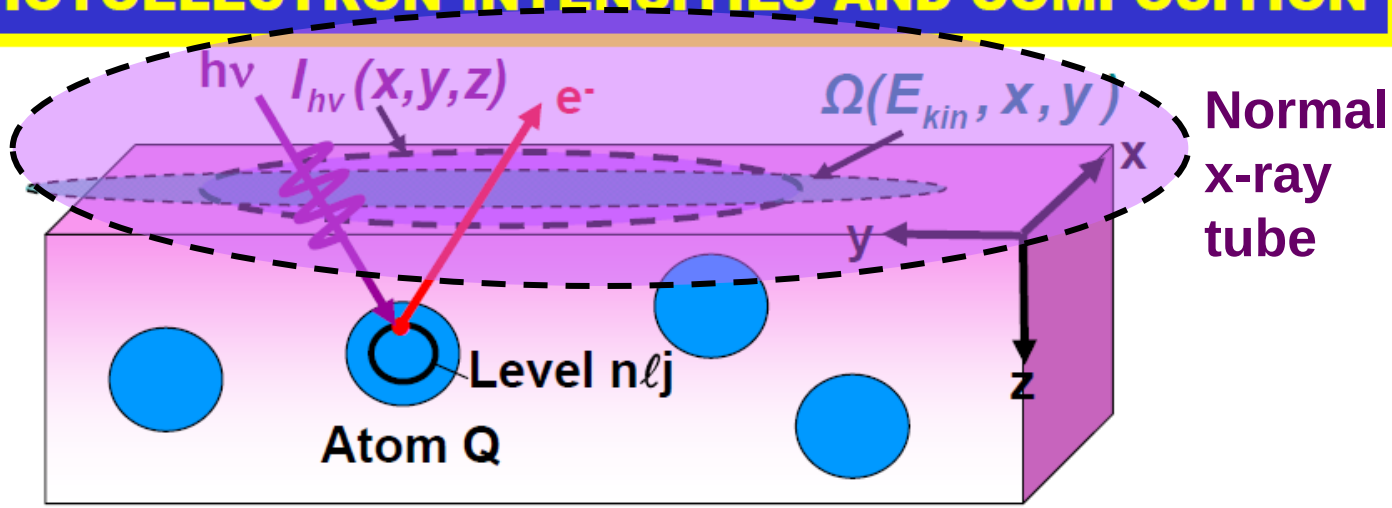

$I(Qn\ell j) =$

$$C\int_0^\infty I_{hv}(x,y,z)\rho_Q(x,y,z)\frac{d\sigma_{Qn\ell j}(hv)}{d\Omega}\exp\left[-\frac{z}{\Lambda_e(E_{kin})\sin\theta}\right]\Omega(E_{kin},x,y)dxdydz$$

$I_{hv}(x,y,z)$ = x-ray flux

$\rho_Q(x,y,z)$ = density of atoms Q → quantitative analysis

$\frac{d\sigma_{Qn\ell j}(hv)}{d\Omega}$ = energy-dependent differential photoelectric cross section for subshell $Qn\ell j$

$\Lambda_e(E_{kin})$ = energy-dependent inelastic attenuation length

→ Effective Attenuation Length (EAL) → Mean Emission Depth (MED)

$\Omega(E_{kin}, x, y)$ = energy-dependent spectrometer acceptance solid angle

C.S.F., Journal of Electron Spectroscopy and Related Phenomena 178–179 (2010) 2–32

CO Atomic orbital makeup

$$\varphi_j^{MO}(\vec{r}) = \sum_{\substack{\text{Atoms } A \\ \text{Orbitals } i}} c_{Ai,j}\varphi_{Ai}^{AO}(\vec{r})$$

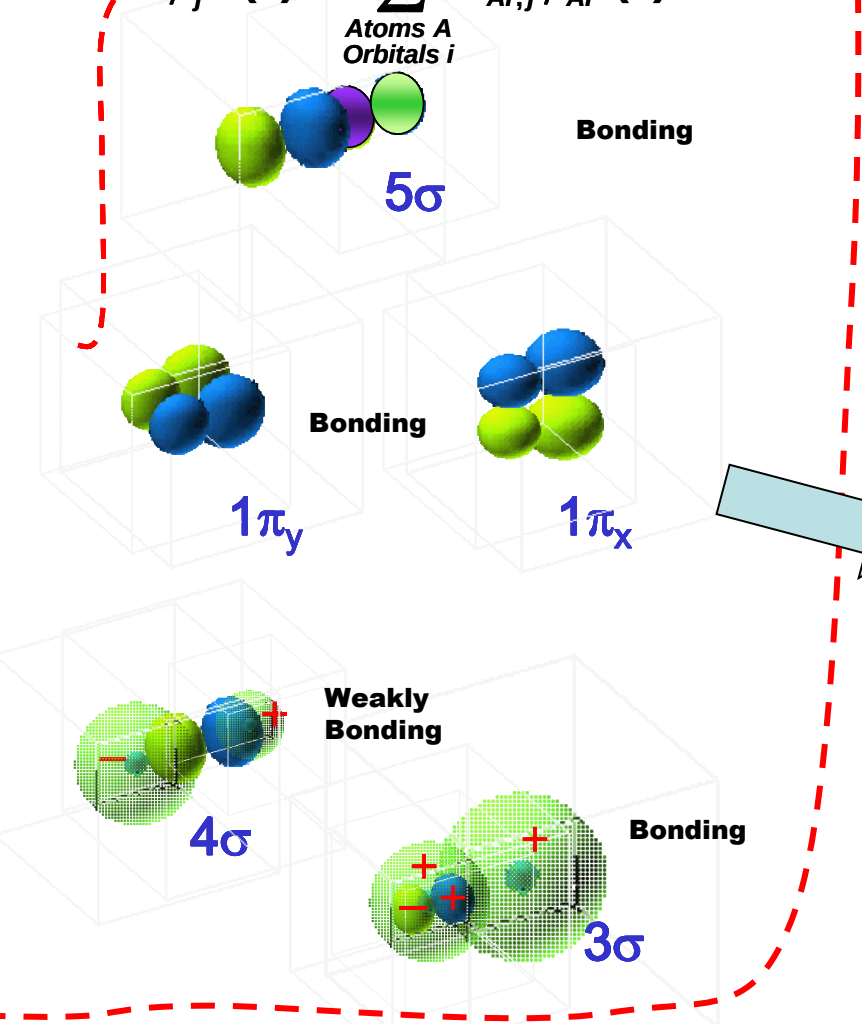

Solid state tight-binding approach

Crystal potential-1D

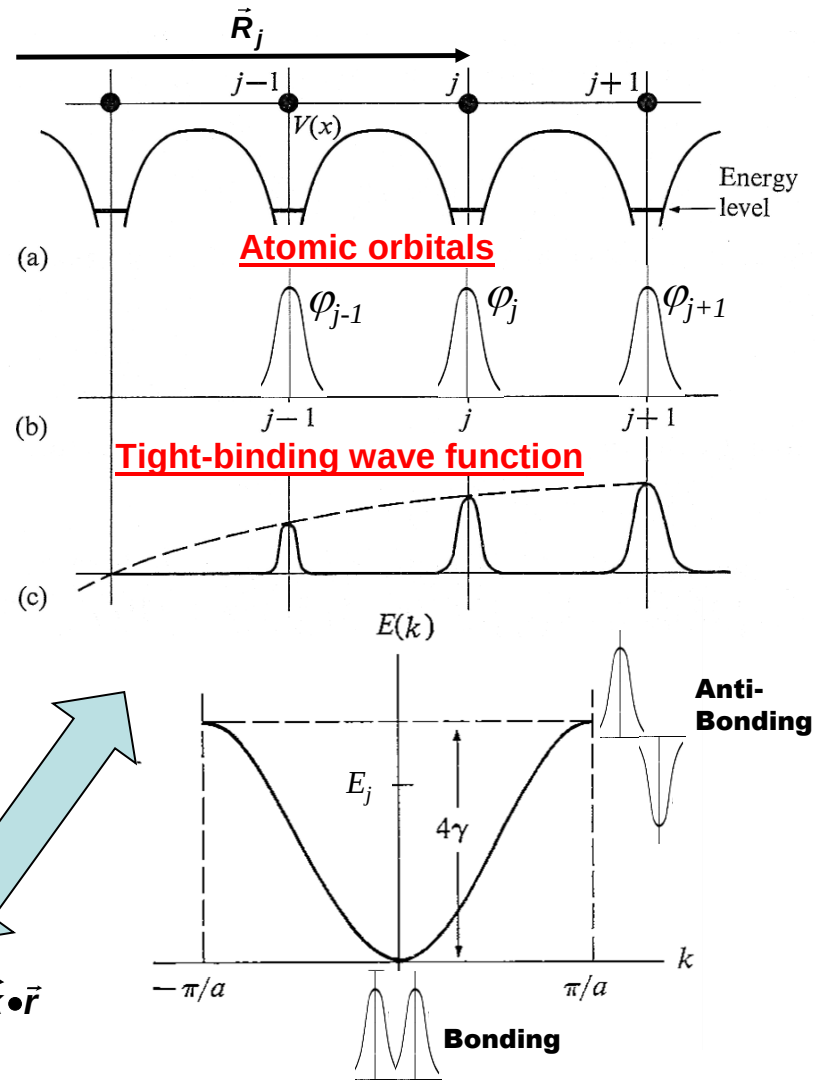

$$\varphi_{\vec{k}}^{TB}(\vec{r}) = \text{a Bloch function} = u_{\vec{k}}^{TB}(\vec{r})e^{i\vec{k}\bullet\vec{r}}$$

$$\propto \frac{1}{N^{1/2}} \sum_{j=1.....N \text{ unit cells at } \vec{R}_j} e^{i\vec{k}\bullet\vec{R}_j} \sum_{\substack{Ai = \text{basis set of AOs} \\ \text{in unit cell}}} c_{Ai,\vec{k}}\varphi_{Ai}^{AO}(\vec{r}-\vec{R}_j)$$

The d orbitals

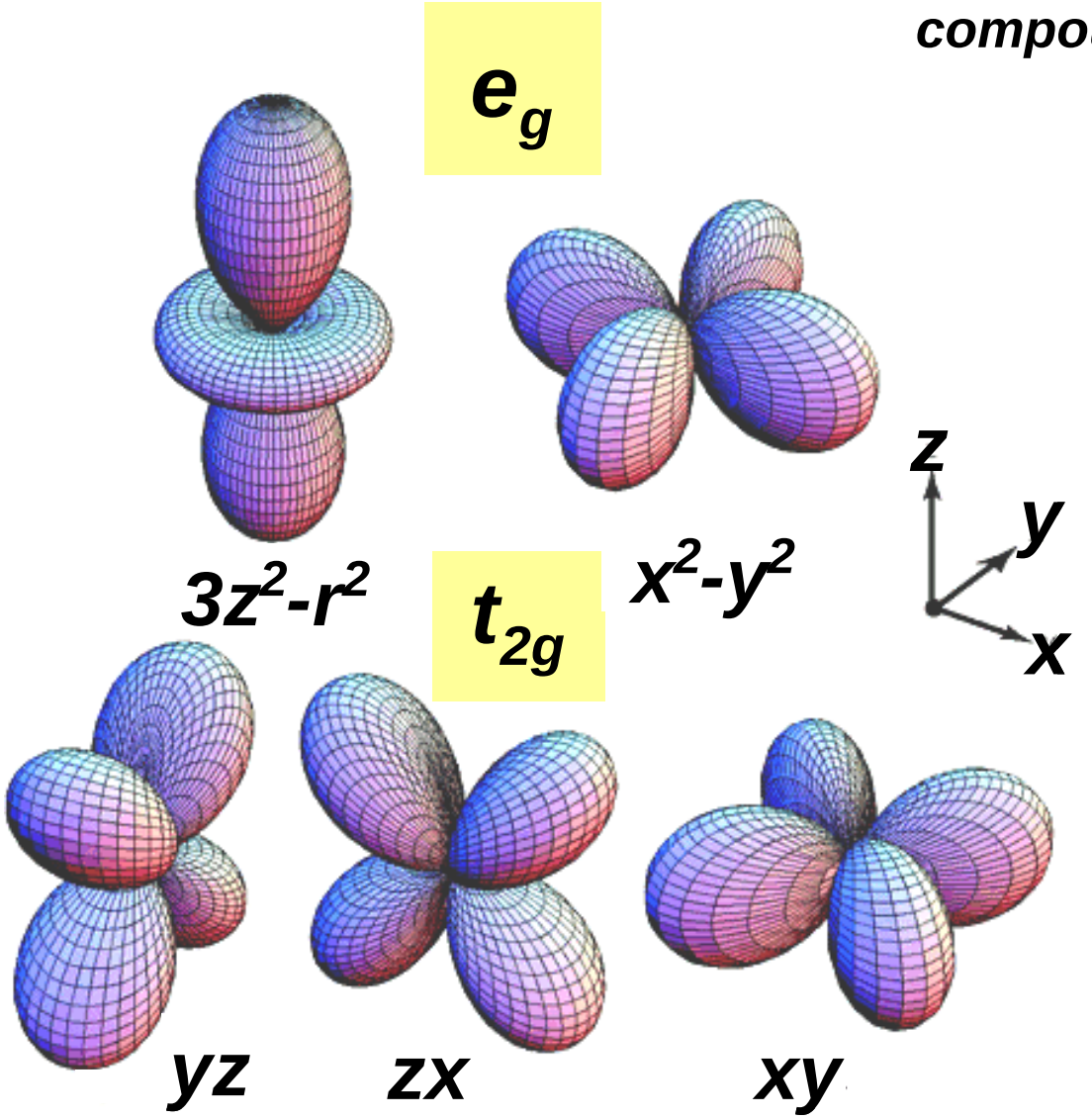

Some Transition-Metal (TM) compounds:

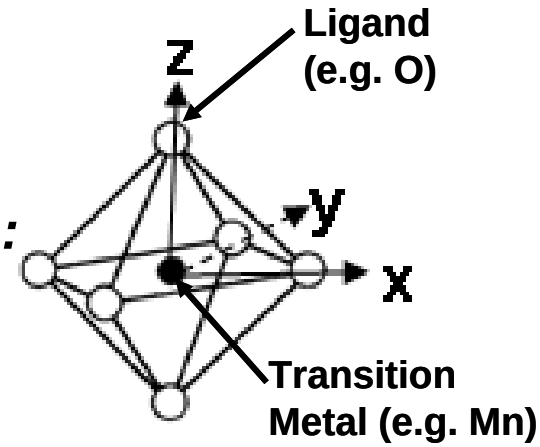

e_g and t_{2g} not equivalent in octahedral (cubic) environment

Some TMs:

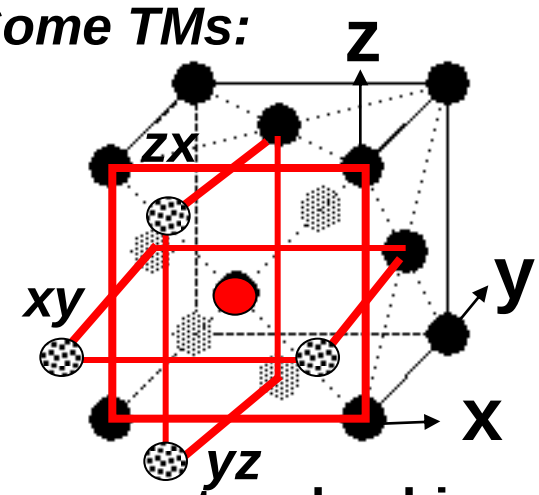

Face-centered cubic—12 nearest neighbors

Electronic bands and density of states for a transition metal-Copper

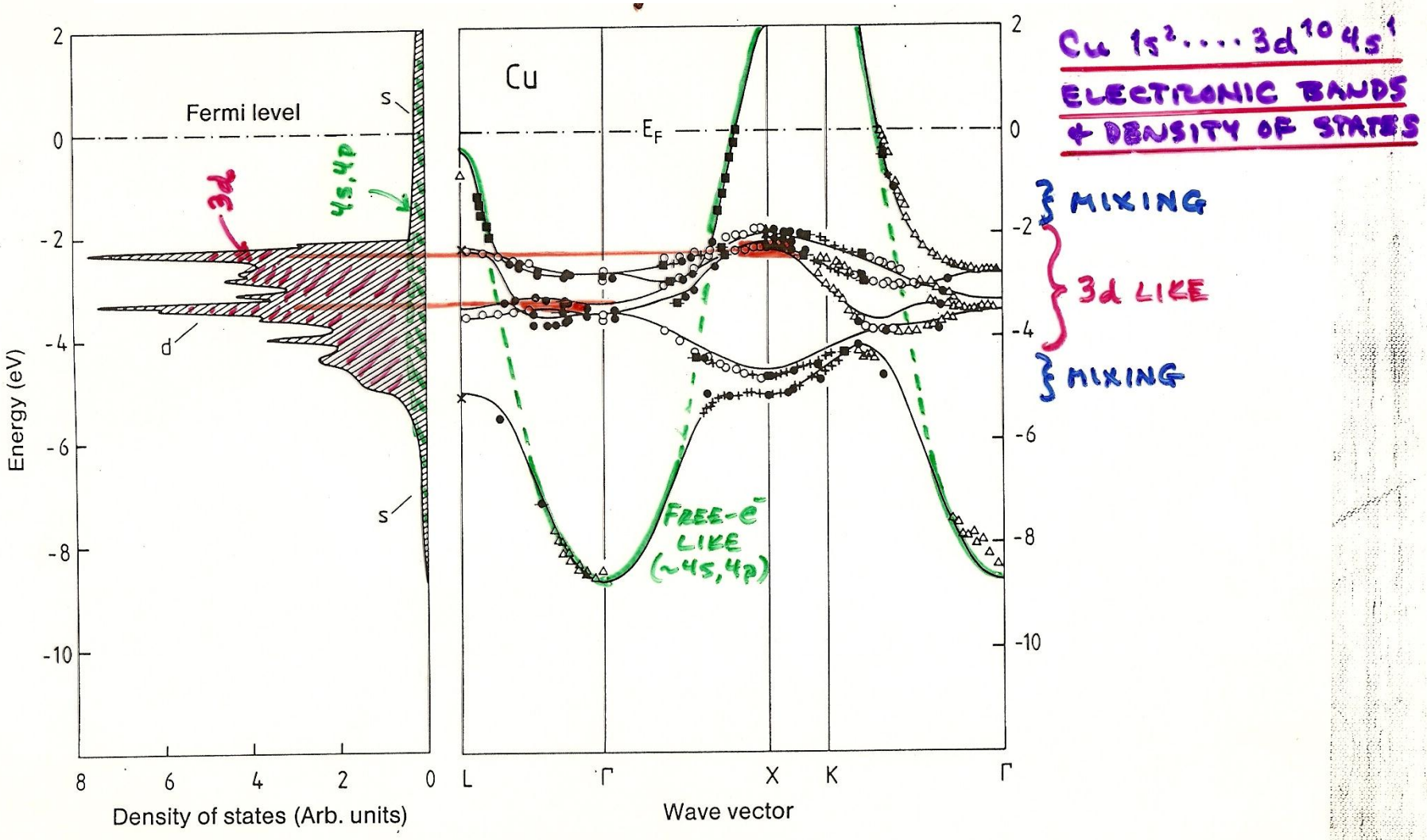

Fig. 7.12. Bandstructure $E(k)$ for copper along directions of high crystal symmetry (*right*). The experimental data were measured by various authors and were presented collectively by Courths and Hüfner [7.4]. The full lines showing the calculated energy bands and the density of states (*left*) are from [7.5]. The experimental data agree very well, not only among themselves, but also with the calculation

Copper projected densities of states-total and by orbital type

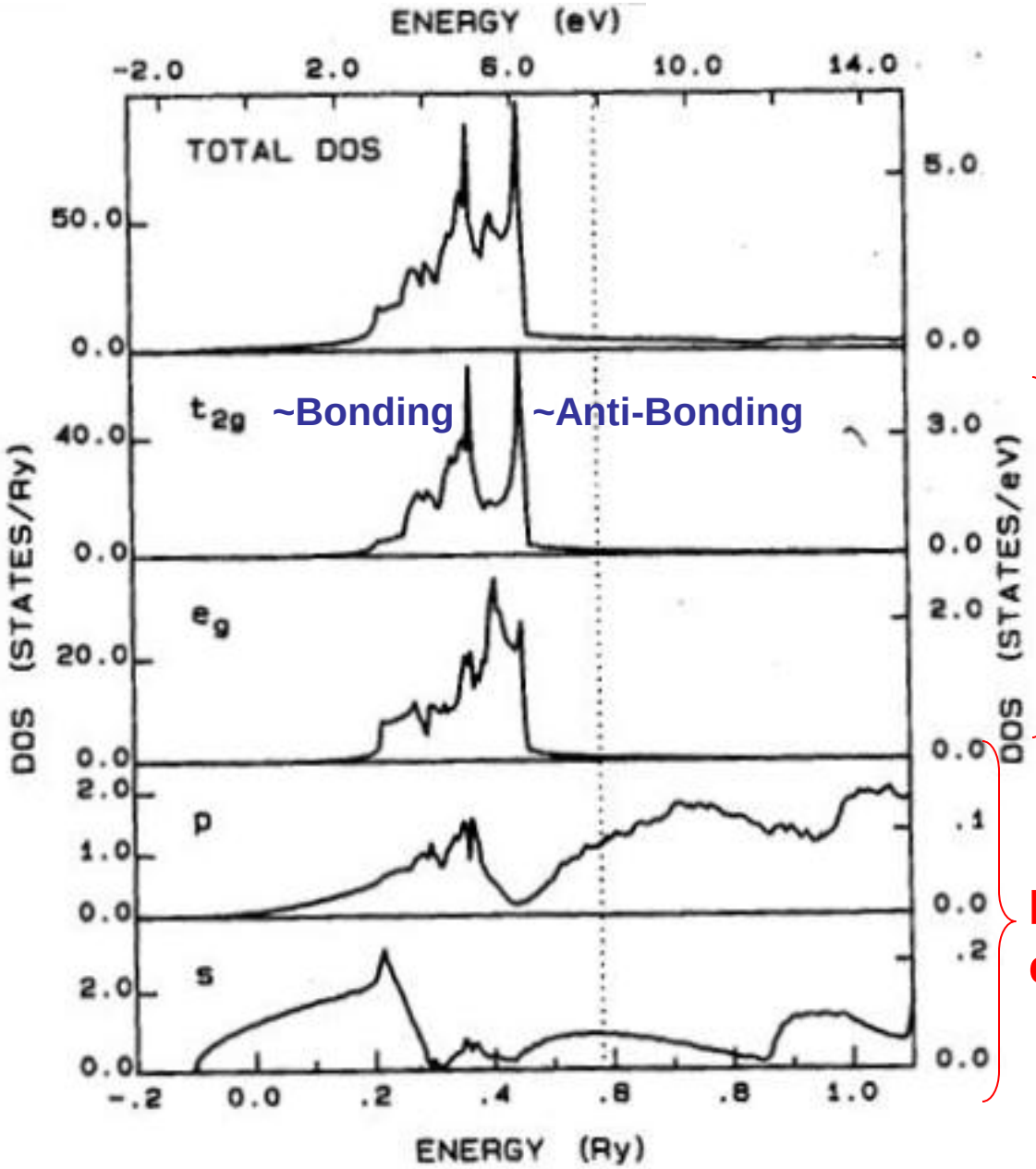

More localized 3d-like

Delocalized free electron-like

$SrTiO_3$ and $La_{0.67}Sr_{0.33}MnO_3$ band structures and DOS

$SrTiO_3$-insulator

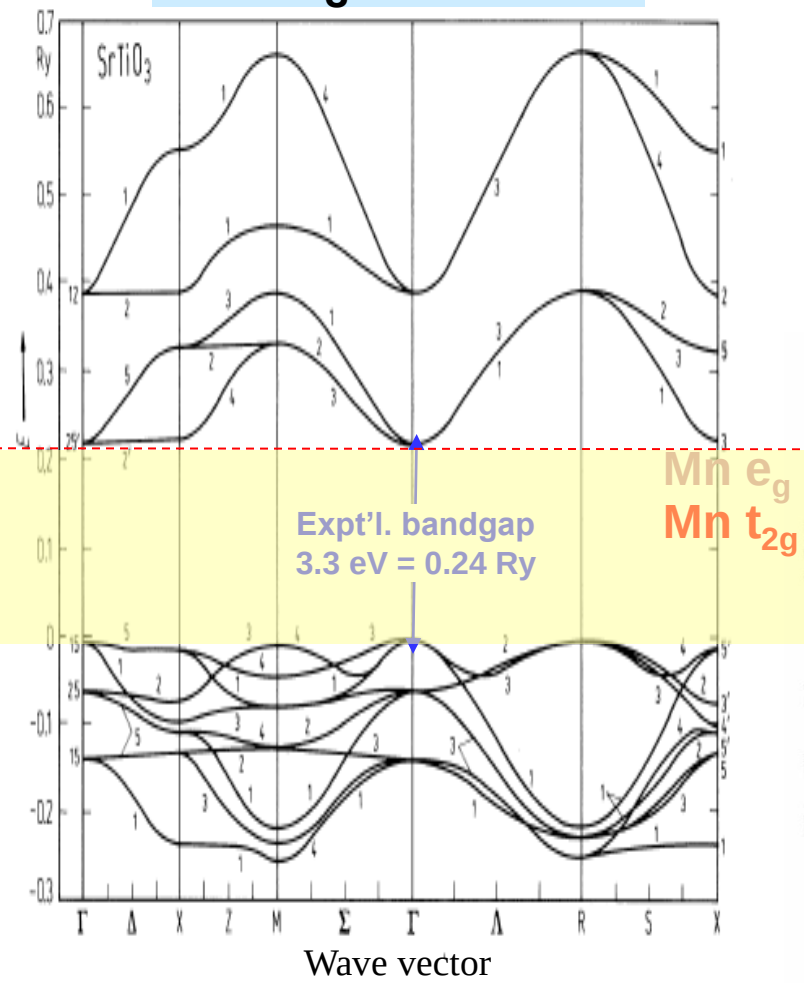

Mattheiss, PRB 6, 4718 (1972)

$La_{0.67}Sr_{0.33}MnO_3$- Half-Metallic Ferromagnetic metal

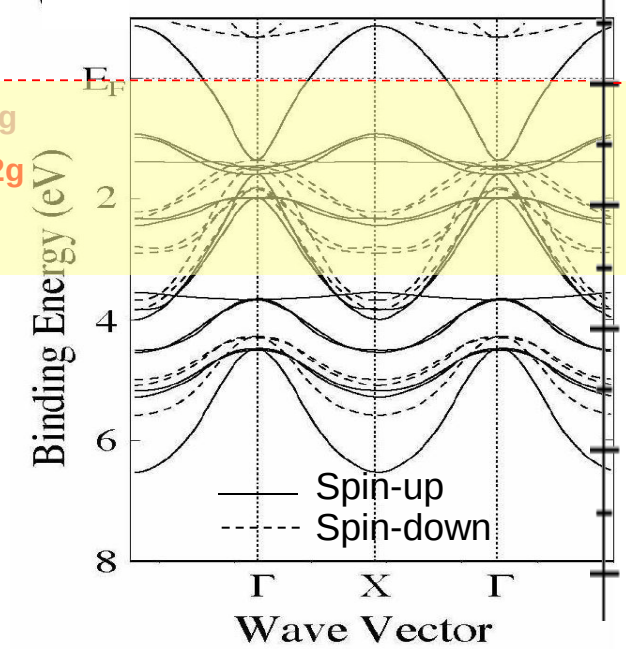

Chikamatsu et al., PRB 73, 195105 (2006)

Zheng, Binggeli, J. Phys. Cond. Matt. 21, 115602 (2009)

Projected DOSs

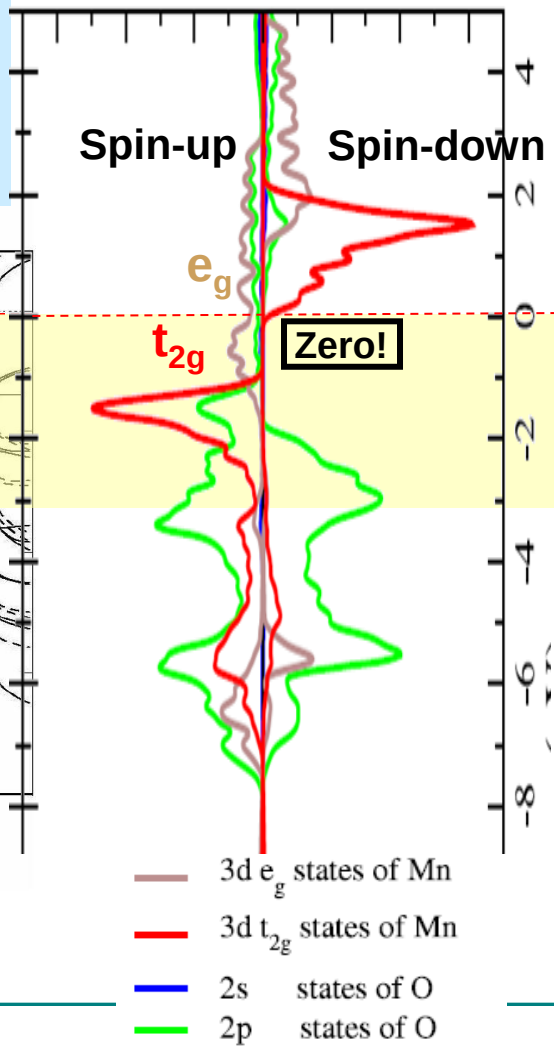

VALENCE-BAND PHOTOELECTRON INTENSITIES AND DENSITIES OF STATES

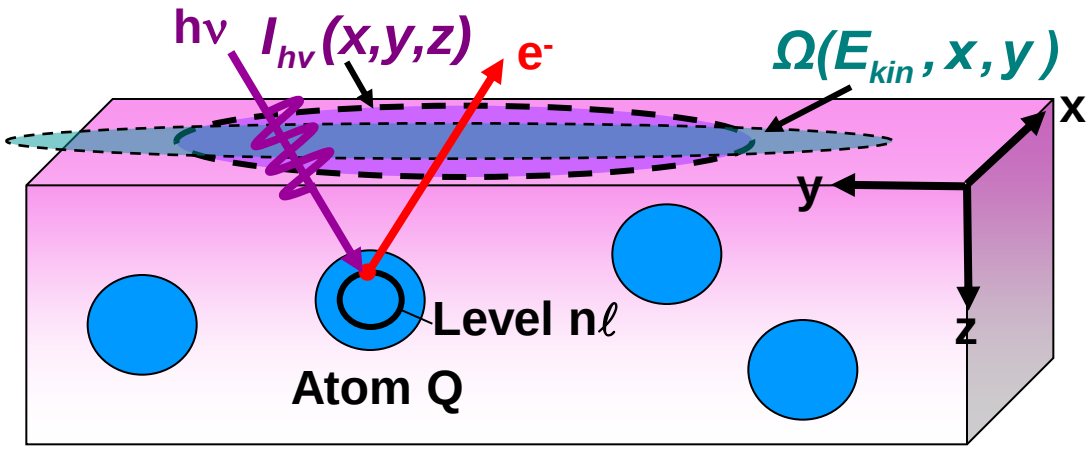

$$I(E_{kin}, Qn\ell) =$$

$$C' \int_0^\infty I_{hv}(x,y,z)\rho_{Qn\ell}(E_b,x,y,z)\frac{d\sigma_{Qn\ell}(hv)}{d\Omega}\exp\left[-\frac{z}{\Lambda_e(E_{kin})\sin\theta}\right]\Omega(E_{kin},x,y)dxdydz$$

$I_{hv}(x,y,z)$ = x-ray flux

$\rho_{Qn\ell}(E_b,x,y,z)$ = density of states, projected onto $Qn\ell$ character

$\frac{d\sigma_{Qn\ell}(hv)}{d\Omega}$ = energy-dependent differential photoelectric cross section for subshell $Qn\ell$

$\Lambda_e(E_{kin})$ = energy-dependent inelastic attenuation length

→ Mean Emission Depth

$\Omega(E_{kin}, x, y)$ = energy-dependent spectrometer acceptance solid angle

PHOTOELECTRON INTENSITIES—THE 3-STEP MODEL

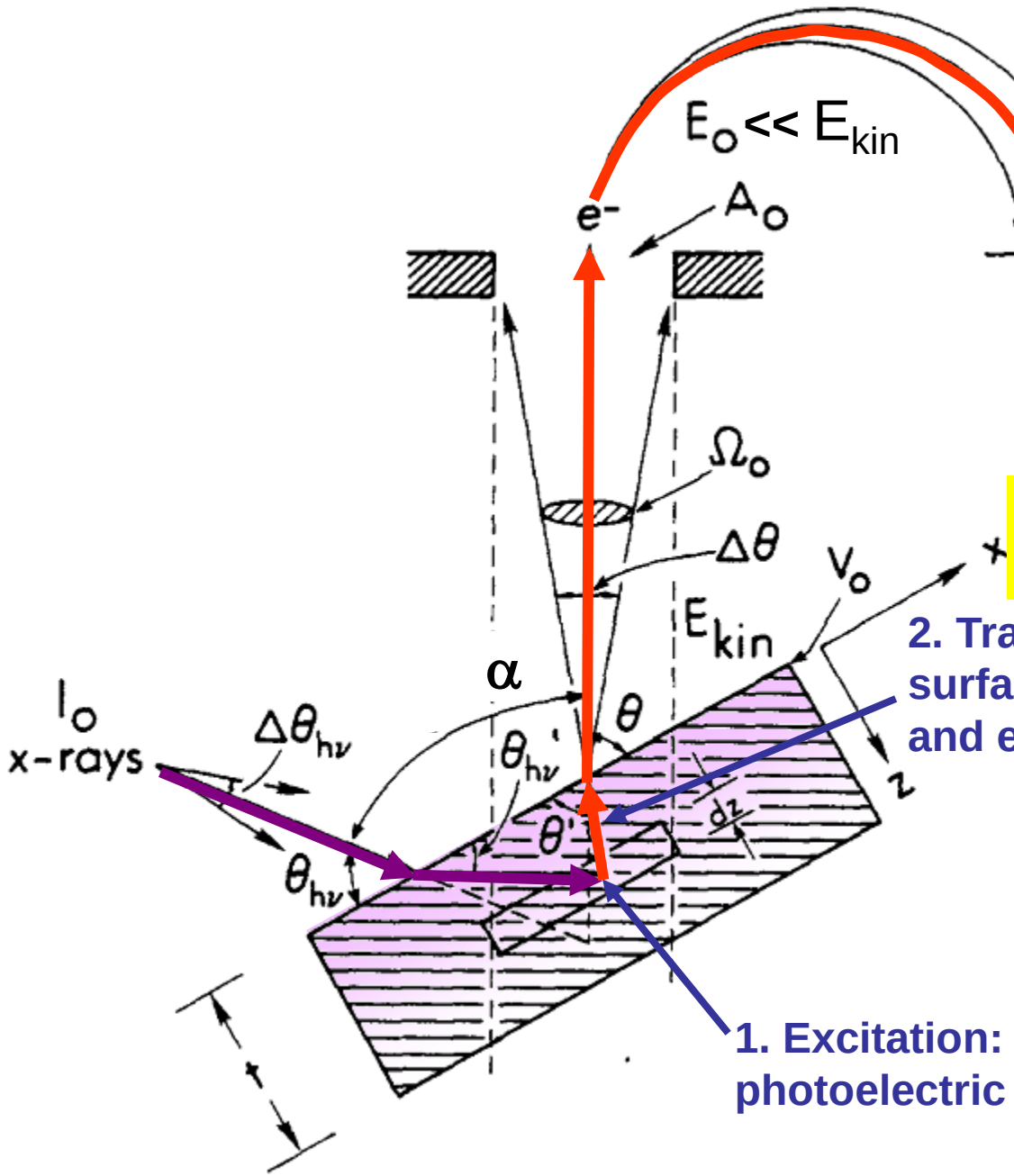

3. Escape across the surface barrier (V_0)

2. Transport to the surface: inelastic (Λ_e) and elastic ($f(\theta)$) scattering

1. Excitation: differential photoelectric cross section ($d\sigma/d\Omega$)

One-Electron Picture of Photoemission from a Surface

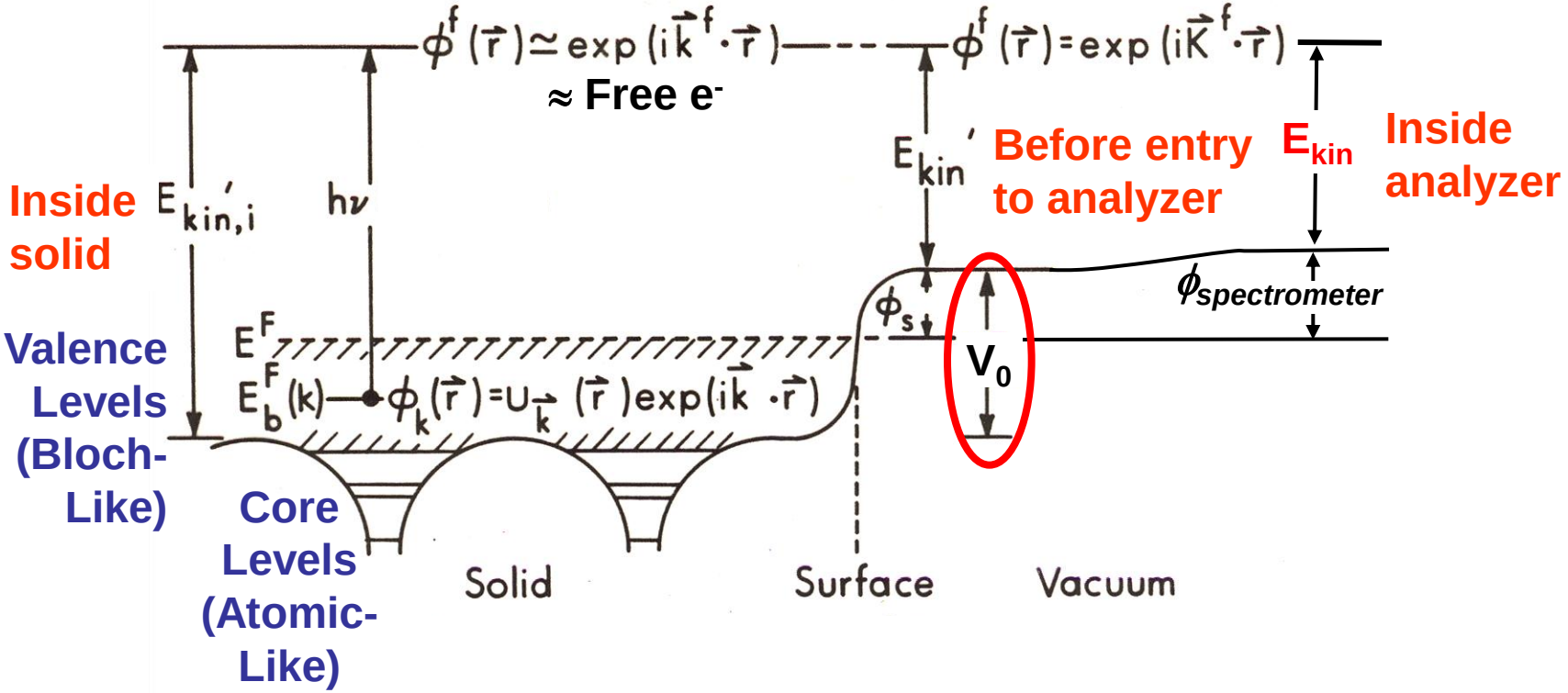

Electron Refraction at the Surface Due to the Inner Potential

$$\theta = \tan^{-1}\left[\sqrt{\sin^2\theta' - \frac{V_o}{E_{kin}}} \Big/ \cos\theta'\right]$$, θ_{IR} = total internal reflection

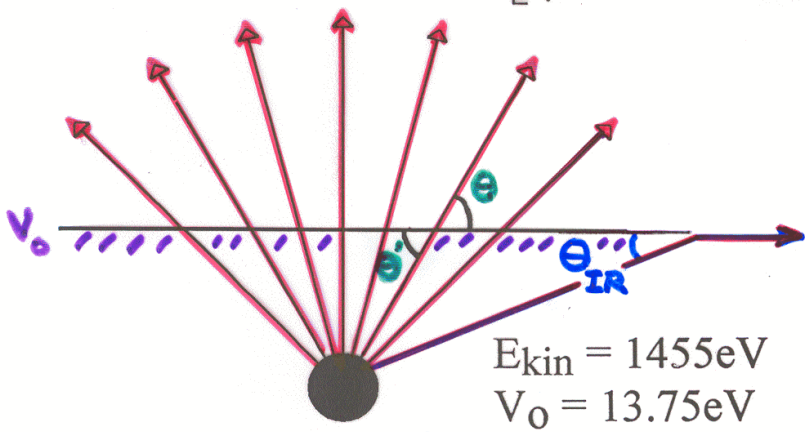

E_{kin} = 1455eV
V_o = 13.75eV
$\theta'_{min} = \theta_{IR} \approx 6°$

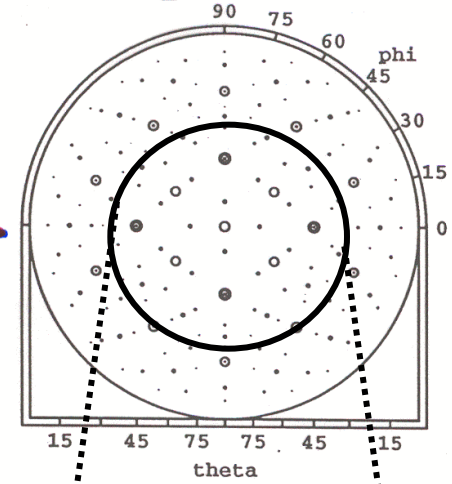

Observed Low-Index Directions Above W(110)

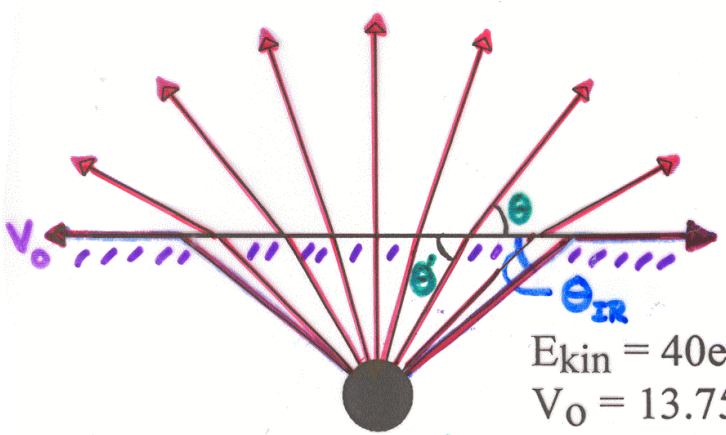

E_{kin} = 40eV
V_o = 13.75eV
$\theta'_{min} = \theta_{IR} \approx 39°$

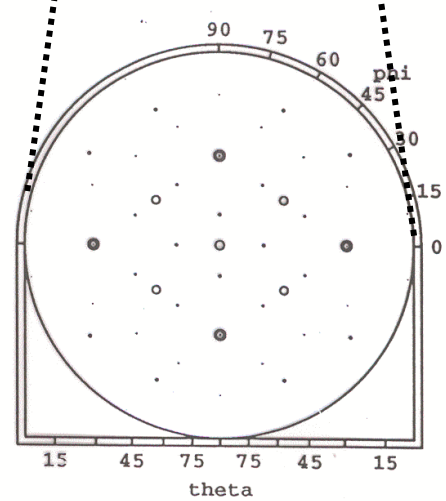

Electron Refraction at the Surface Due to the Inner Potential

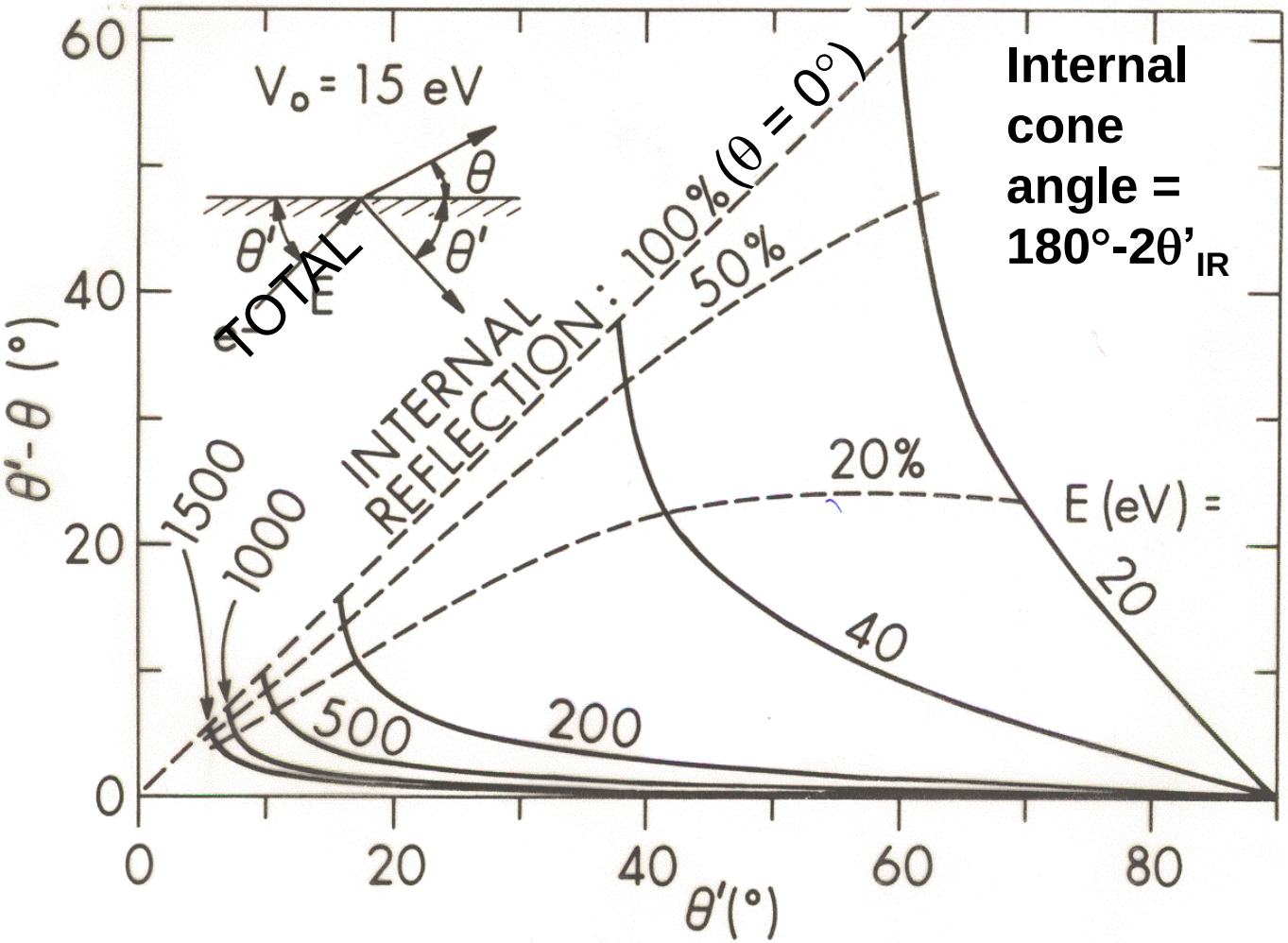

Internal cone angle = 180°-2θ'$_{IR}$

Plus total reflection for lower energies as:

E(eV)	θ'$_{IR}$	Int. Cone Ang.
1500	5.5°	169°
1000	7°	166°
500	9.5°	161°
200	15.5°	149°
40	37.5°	105°
20	60°	60°
19	63°	54°
18	66°	48°
17	70°	40°
16	76°	28°
15.1	86°	8°
15	90°	0°

(Nothing gets out!)

C. S. F., *Prog. Surf. Sci.* 1984, *16*, 275

PHOTOELECTRON INTENSITIES—THE 3-STEP MODEL

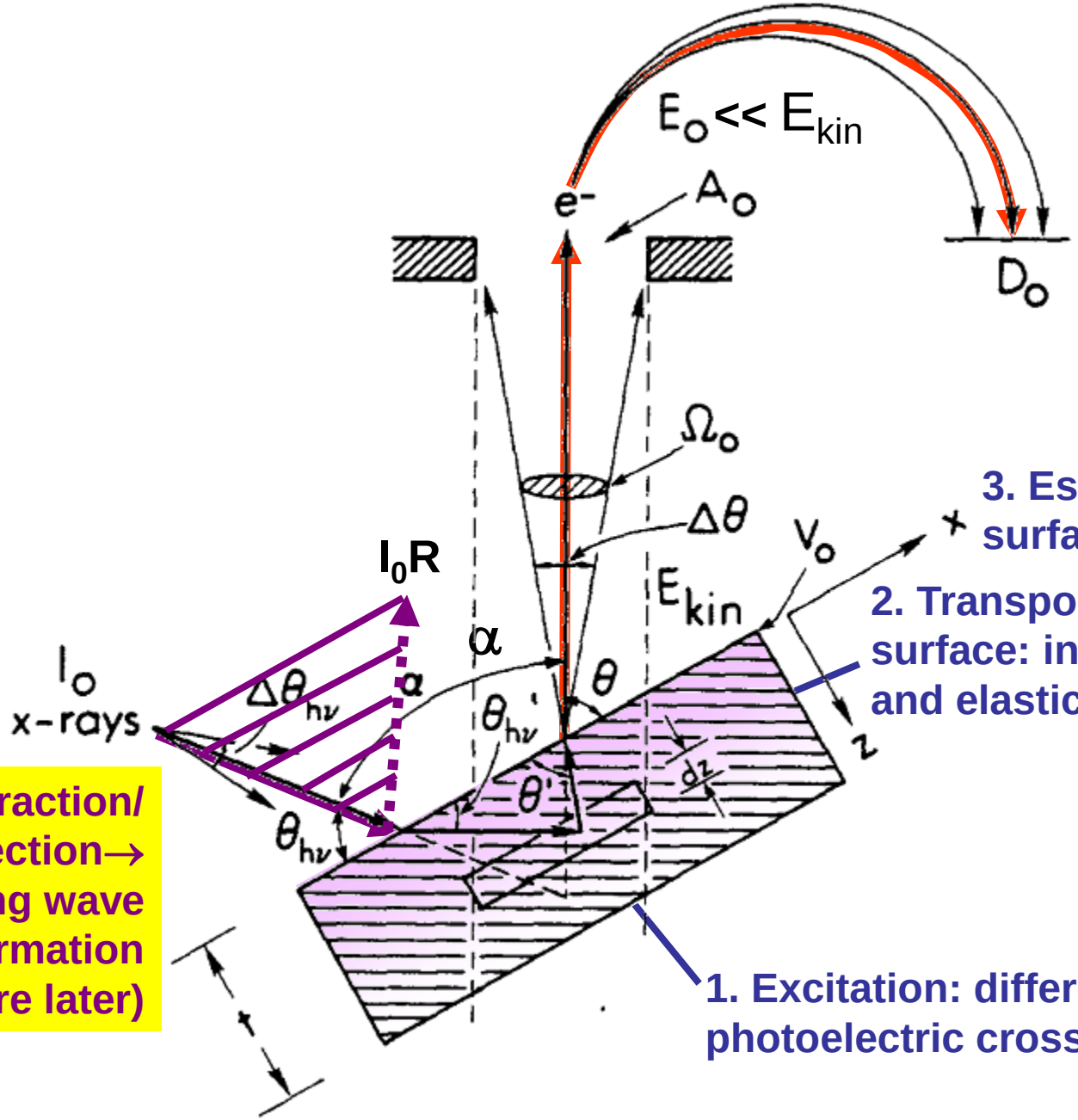

3. Escape across the surface barrier (V_0)

2. Transport to the surface: inelastic (Λ_e) and elastic ($f(\theta)$) scattering

1. Excitation: differential photoelectric cross section ($d\sigma/d\Omega$)

+X-ray refraction/ reflection→ standing wave formation (more later)

Some basic measurements:

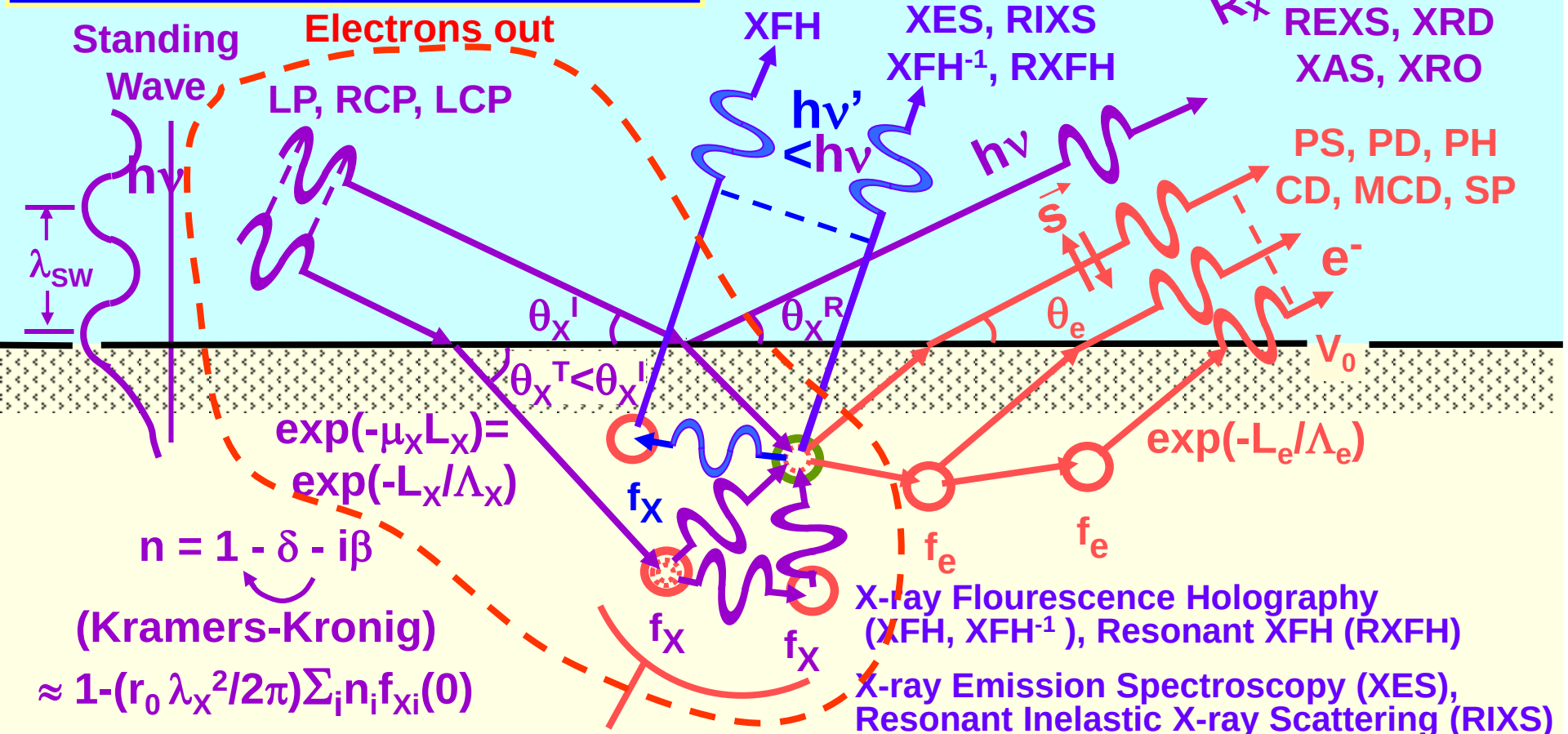

$n = 1 - \delta - i\beta$

(Kramers-Kronig)

$\approx 1-(r_0 \lambda_X^2/2\pi)\Sigma_i n_i f_{Xi}(0)$

$\mu_X = 4\pi\beta/\lambda_X$

$\theta_X^R = \theta_X^I$

$\lambda_{SW} = \lambda_X/(2\sin\theta_X^I)$

$\theta_{CRIT}^I = (2\delta)^{1/2}$

Multi-atom resonant photoemission (MARPE)

X-ray Flourescence Holography (XFH, XFH^{-1}), Resonant XFH (RXFH)

X-ray Emission Spectroscopy (XES), Resonant Inelastic X-ray Scattering (RIXS)

Resonant Elastic X-ray Scattering (REXS)

X-Ray Diffraction (XRD)

X-ray Absorption Spectroscopy (XAS)

X-Ray Optical measurements (XRO)

Photoelectron Spectroscopy (PS), Diffraction (PD), Holography (PH)
+ Circular Dichroism (CD), Magnetic CD (MCD), Spin Polarization (SP)

X-ray scattering factor:
$f_i = Ref_i + i(Imf_i)$

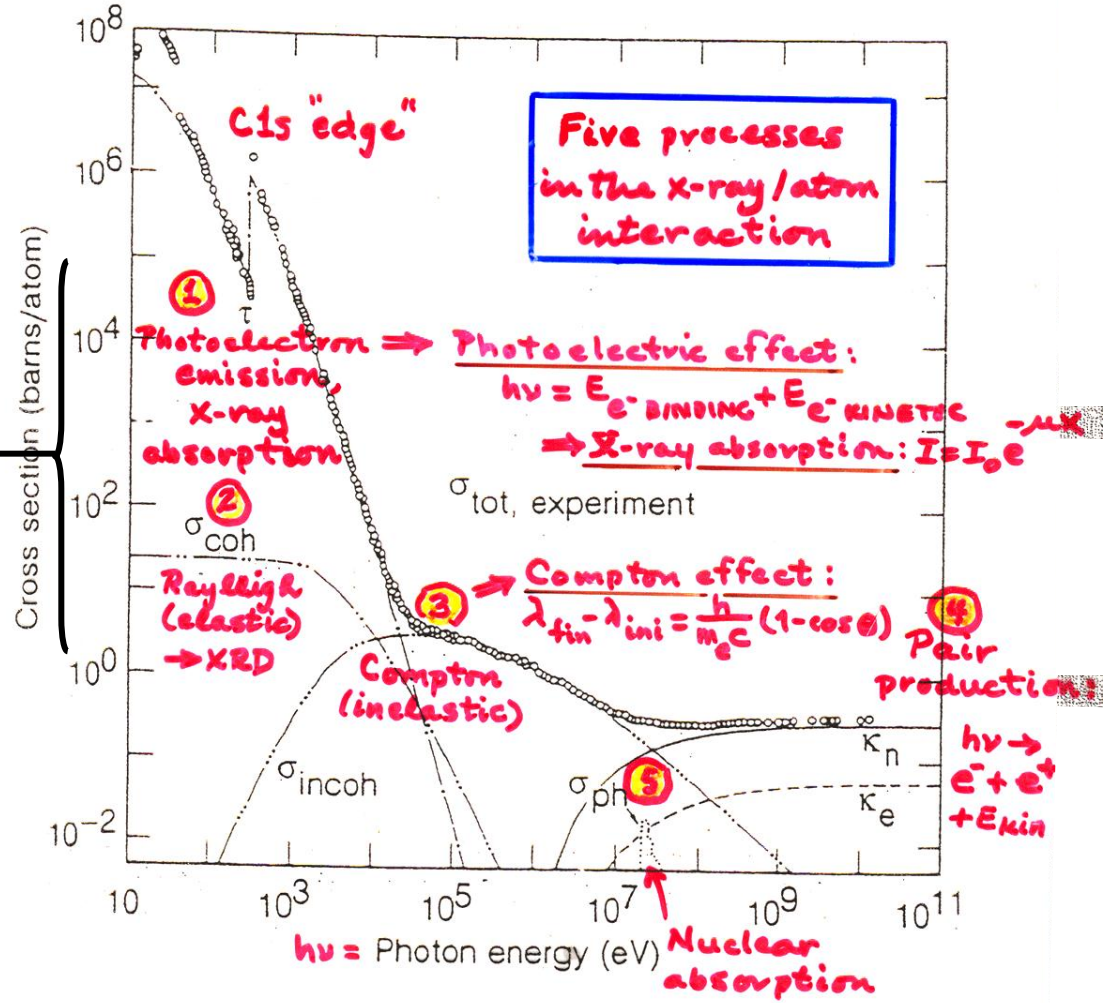

Fig. 3-1. *Total photon cross section σ_{tot} in carbon, as a function of energy, showing the contributions of different processes: τ, atomic photo-effect (electron ejection, photon absorption); σ_{coh}, coherent scattering (Rayleigh scattering—atom neither ionized nor excited); σ_{incoh}, incoherent scattering (Compton scattering off an electron) κ_n, pair production, nuclear field; κ_e, pair production, electron field; σ_{ph}, photonuclear absorption (nuclear absorption usually followed by emission of a neutron or other particle). (From Ref. 3; figure courtesy of J. H. Hubbell.)*

A LITTLE X-RAY OPTICS

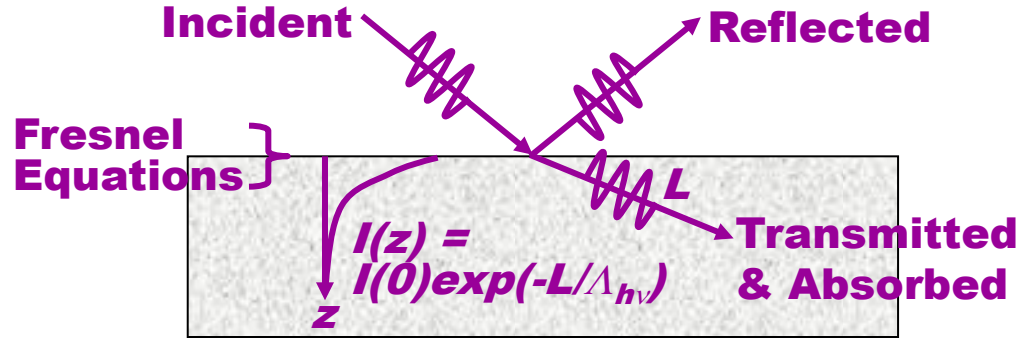

(E.G. See pp. 1-38, 1-44, 5-18-5-19 in X-Ray Data Booklet)

Index of refraction = $n = 1 - \delta - i\beta$

δ = + no. = refractive decrement << 1 **(Sometimes negative through absorption resonances)**

β = + no. = absorptive decrement << 1

δ and β linked by Kramers-Kronig transform

n also = $1 - (r_e/2\pi)\lambda_{h\nu}^2 \sum n_i f_i$(0=fwd. scatt.)

r_e = classical electron radius
$= e^2/4\pi\varepsilon_0 m_e e^2 = 2.817 \times 10^{-15}$ m
$\lambda_{h\nu}$ = x-ray wavelength

n_i = no. i atoms per unit volume

f_i = x-ray scattering factor for ith type of atom, in forward direction

Exponential absorption length = $l_{abs} = \lambda_{h\nu}/(4\pi\beta) = \Lambda_{h\nu}$

θ_{CRIT} = **critical grazing angle at which reflectivity begins (R ≈ 0.20)**
$= [2\delta]^{0.5}$

Online data and calculations at:
http://www-cxro.lbl.gov/optical_constants/

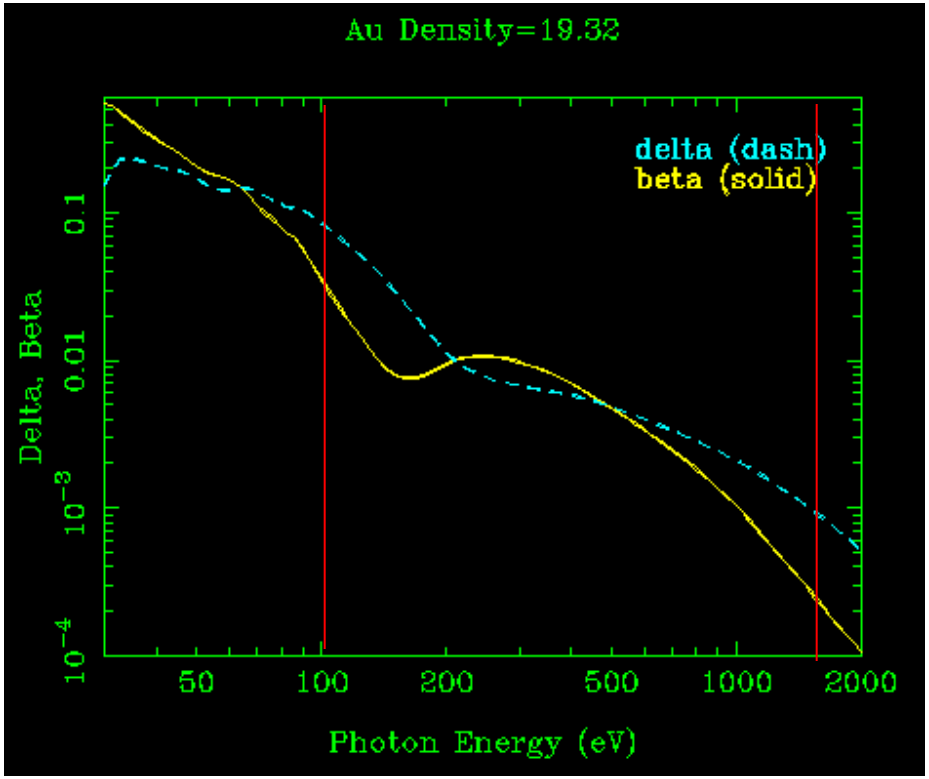

http://www-cxro.lbl.gov/optical_constants/

X-Ray Interactions with Matter

Website

Contents

These pages utilize *JavaScript*, but the decaffeinated versions are still available.

Reference

B.L. Henke, E.M. Gullikson, and J.C. Davis. *X-ray interactions: photoabsorption, scattering, transmission, and reflection at E=50-30000 eV, Z=1-92*, Atomic Data and Nuclear Data Tables Vol. **54** (no.2), 181-342 (July 1993).

By Eric Gullikson. Please direct any comments to EMGullikson@lbl.gov

SOME X-RAY OPTICAL EFFECTS: REDUCED PENETRATION DEPTHS AND INCREASED REFLECTIVITY AT GRAZING INCIDENCE ANGLES

θ_{CRIT} = Grazing angle at which reflectivity begins ($R \approx 0.20$)

$= [2\delta]^{0.5}$

ENHANCED SURFACE SENSITIVITY @ GRAZING INCIDENCE

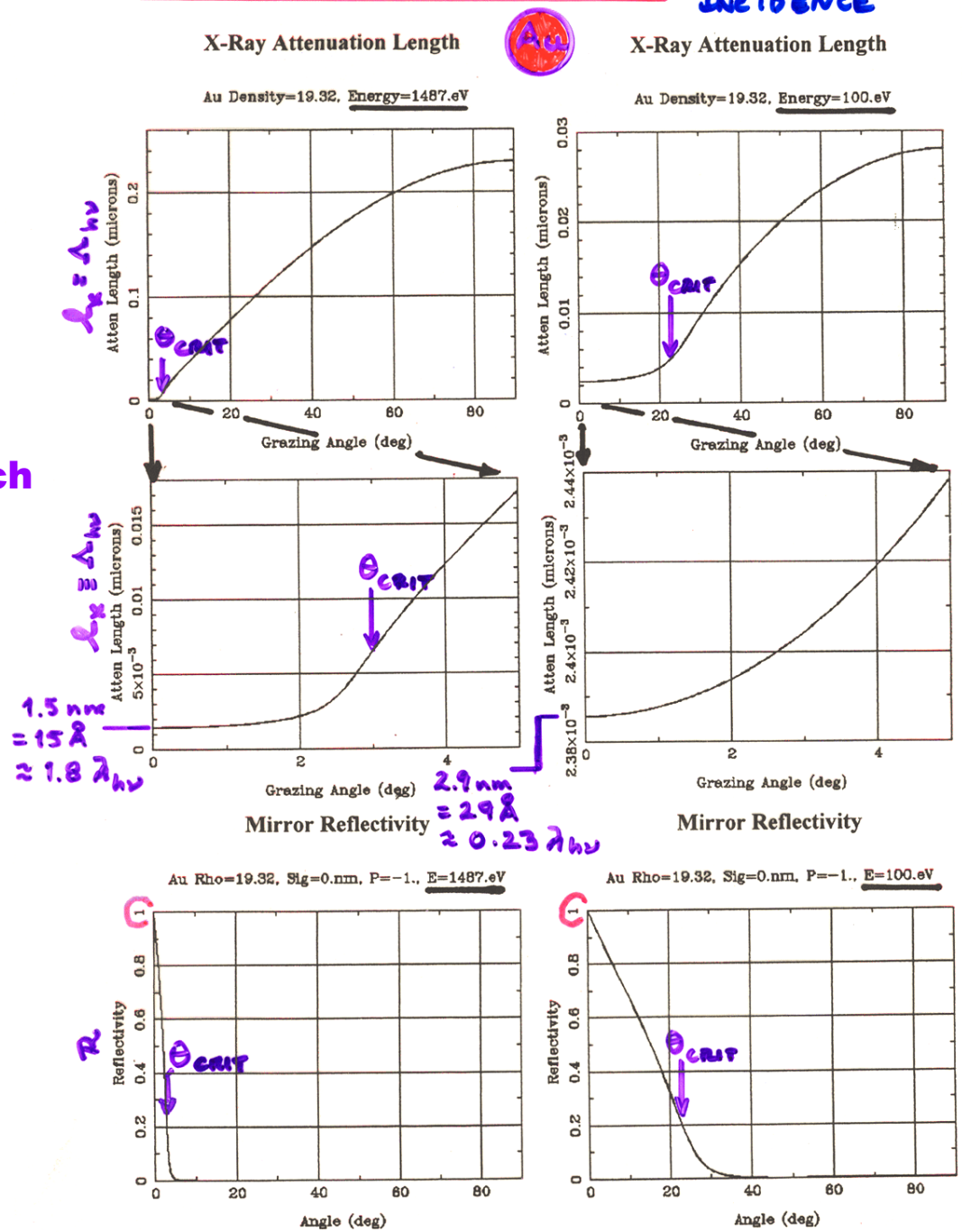

Optical constants through Mn 2p edges of MnO—
Web data <u>without absorption peaks</u>

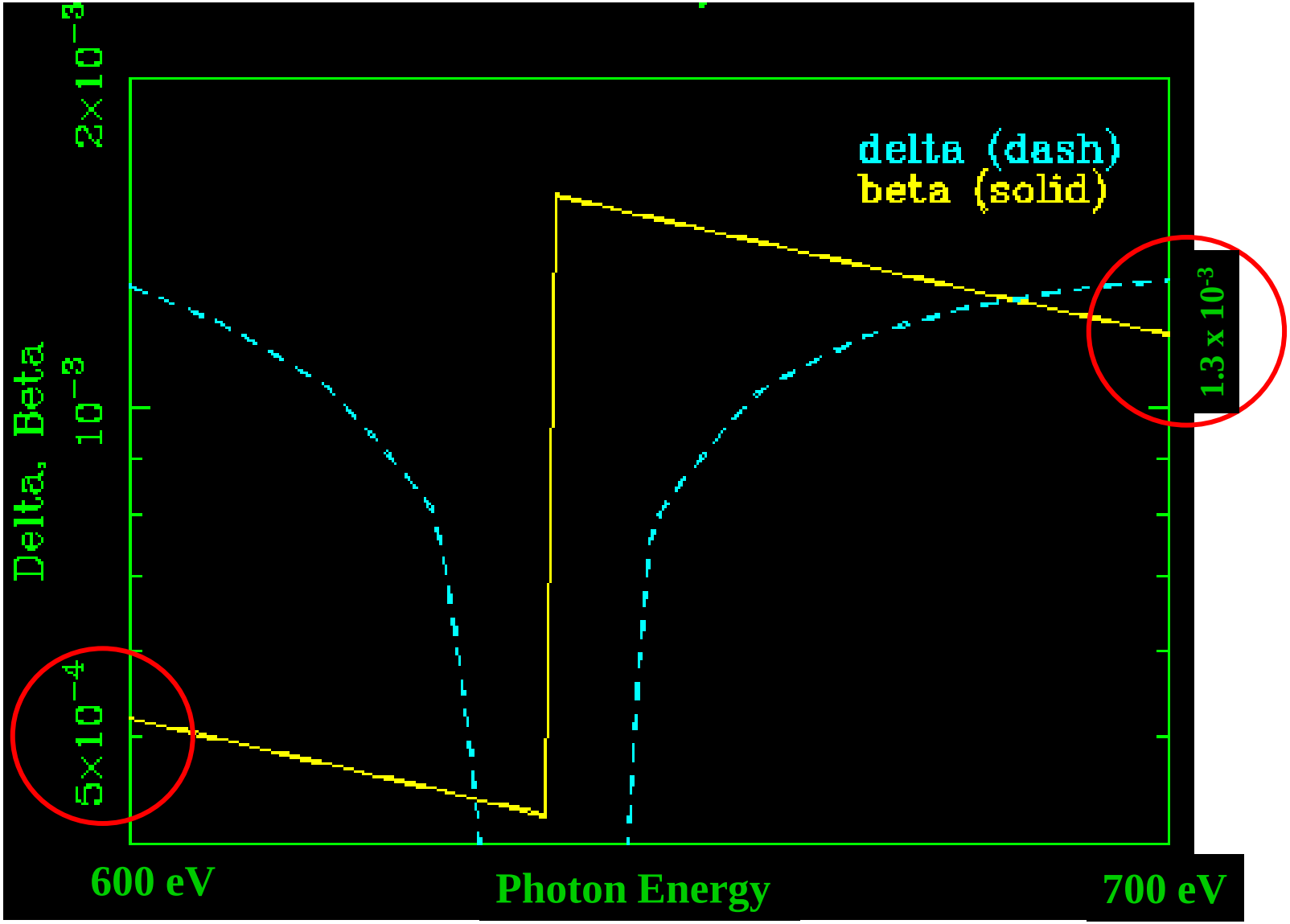

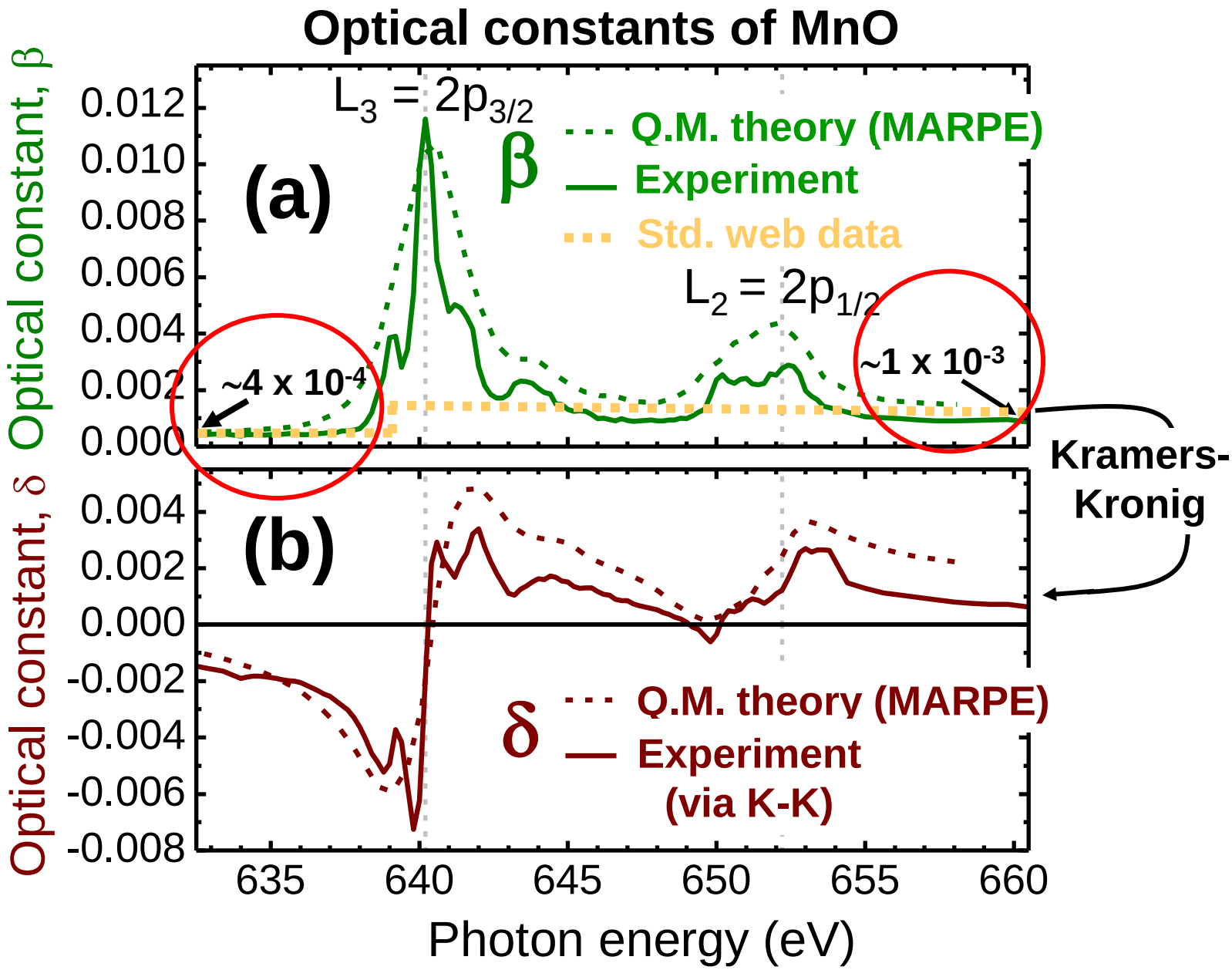
Optical constants of MnO
Optical constant, β
Optical constant, δ
(a)
(b)
L3 = 2p3/2
L2 = 2p1/2
β
δ
Q.M. theory (MARPE)
Experiment
Std. web data
Q.M. theory (MARPE)
Experiment
(via K-K)
~4 x 10-4
~1 x 10-3
Kramers-Kronig
0.012
0.010
0.008
0.006
0.004
0.002
0.000
0.004
0.002
0.000
-0.002
-0.004
-0.006
-0.008
635
640
645
650
655
660
Photon energy (eV)

Basic Concepts and Experiments

Core-Level Photoemission

Intensities and Quantitative Analysis, the 3-Step Model
Varying Surface and Bulk Sensitivity
Chemical shifts
Multiplet Splittings
Electron Screening and Satellite Structure
Magnetic and Non-Magnetic Dichroism
Resonant Photoemission
Photoelectron Diffraction and Holography

Valence-Level Photoemission

Band-Mapping in the Ultraviolet Photoemission Limit
Densities of States in the X-Ray Photoemission Limit

Some New Directions

Photoemission with Hard X-Rays (throughout lectures)
Photoemission with Standing Wave Excitation
Photoemission with Spatial Resolution/Photoelectron Microscopy
Temporal Resolution
@ Higher Pressures

Chemical shifts:
Looking into the silicon dioxide layer with photoelectron spectroscopy

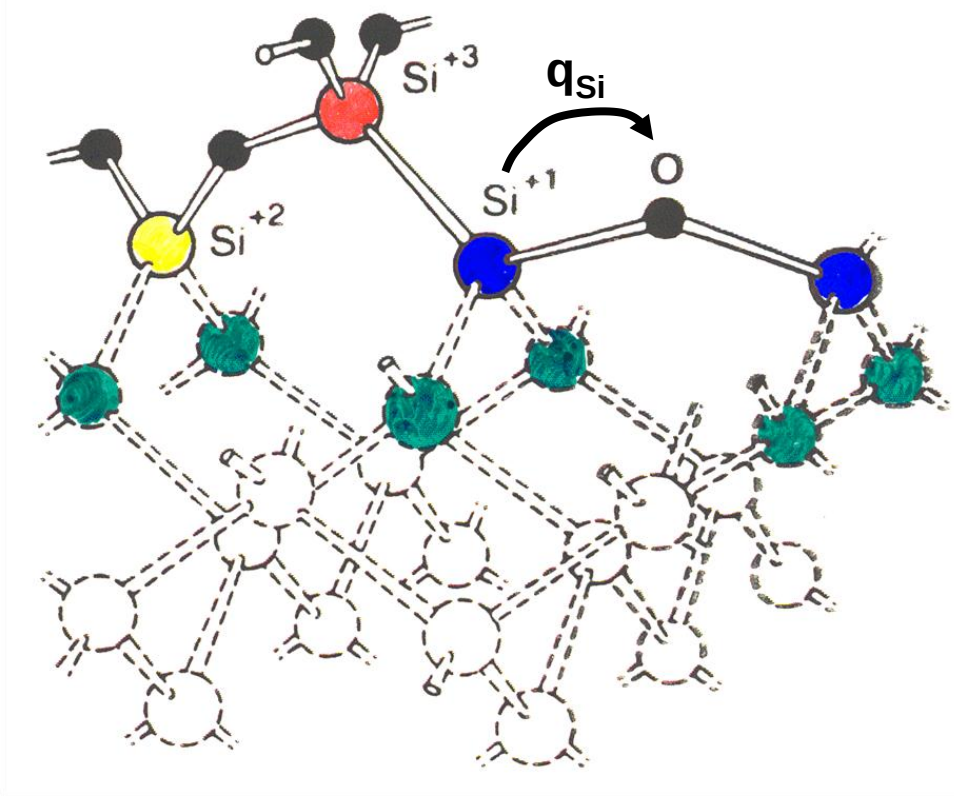

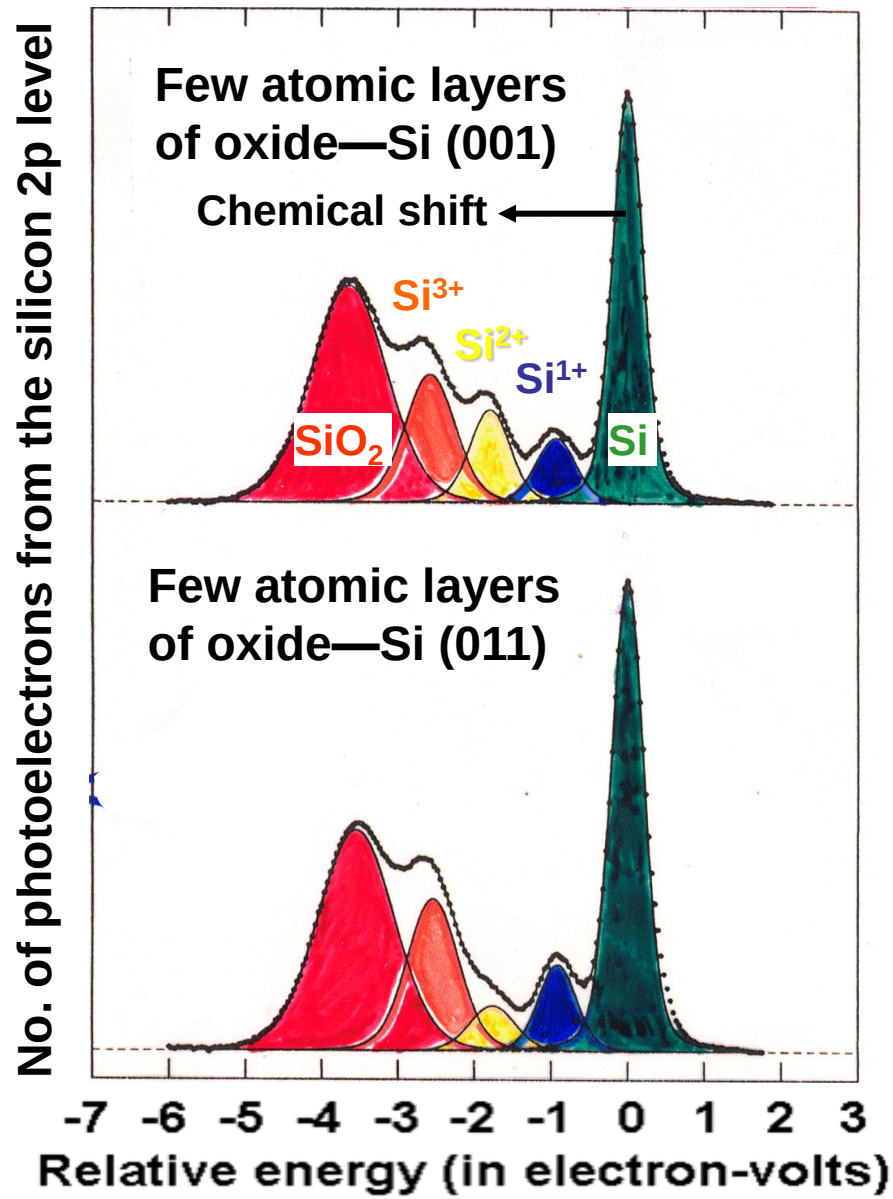

Charge transfer, e^-- e^- coulomb integral:

$$Shift \approx q_{Si} K_{Si2p,Si3p} =$$

$$q_{Si} \int \varphi^*_{2p}(\vec{r}_1)\varphi^*_{3p}(\vec{r}_2)\frac{e^2}{r_{12}}\varphi_{2p}(\vec{r}_1)\varphi_{3p}(\vec{r}_2)dV_1 dV_2$$

Himpsel et al., Phys. Rev. B 38, 6086 ('88)

Enhancing surface sensitivity at grazing exit angles

$$I(z) = I_0 e^{-\frac{z}{\Lambda_e \sin\Theta}}$$

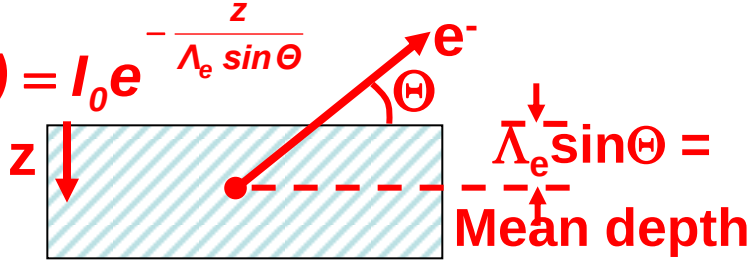

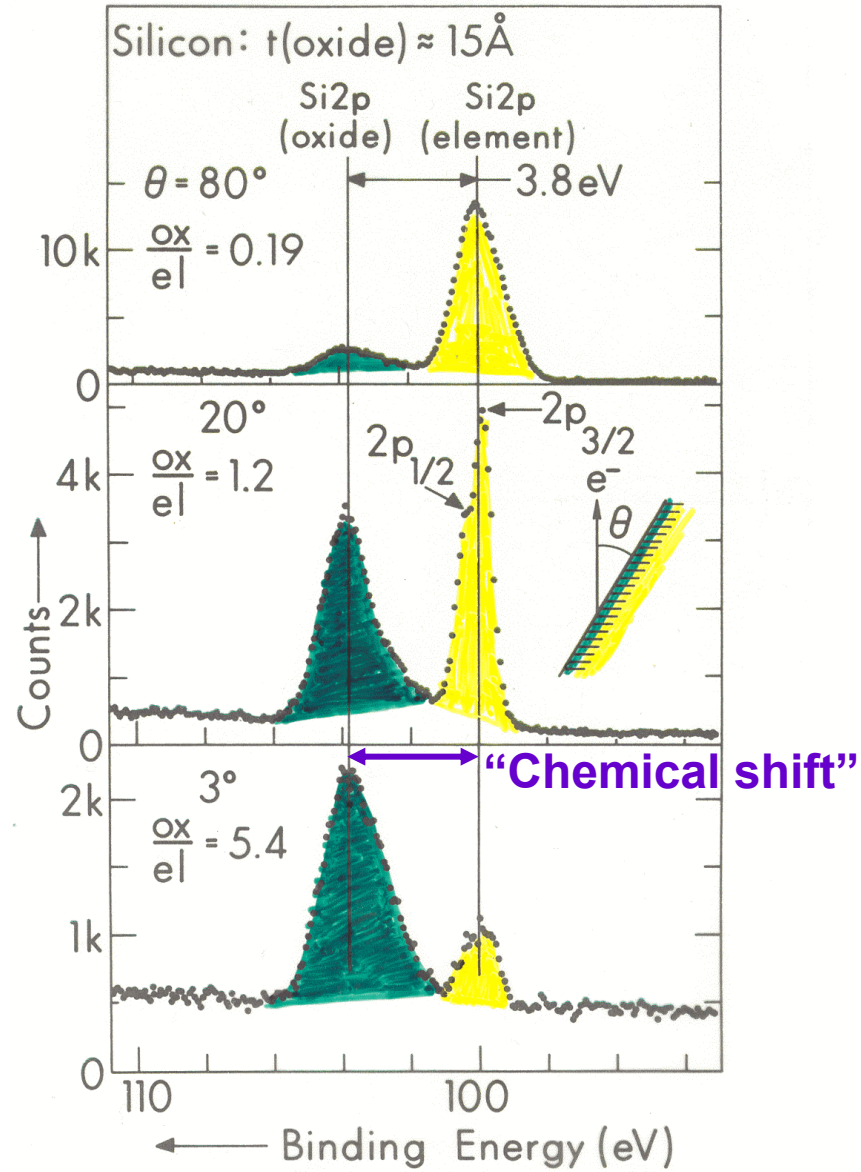

CSF, Prog. in Surf. Sci. 16, 275 (1984)

W(110)/O—W $4f_{7/2}$ Chemical Shifts

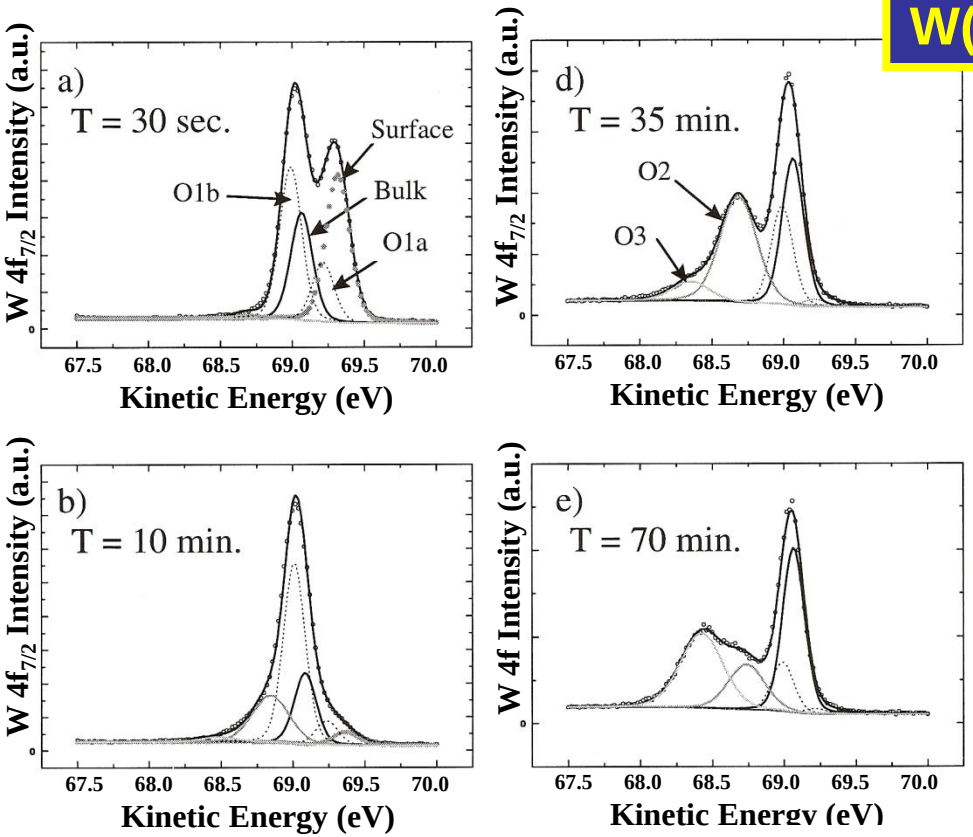

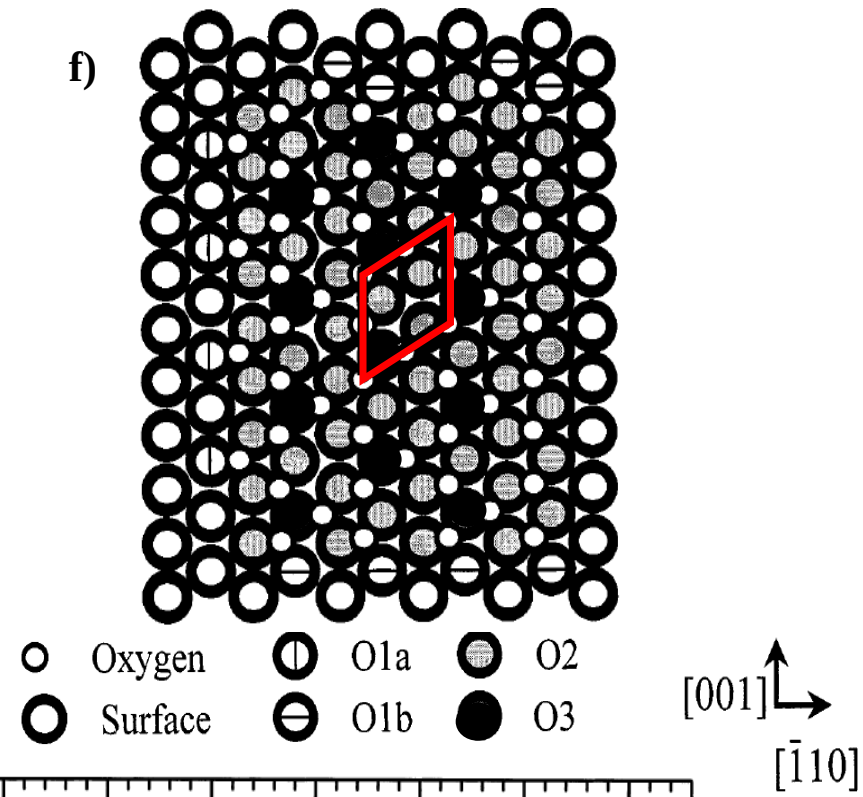

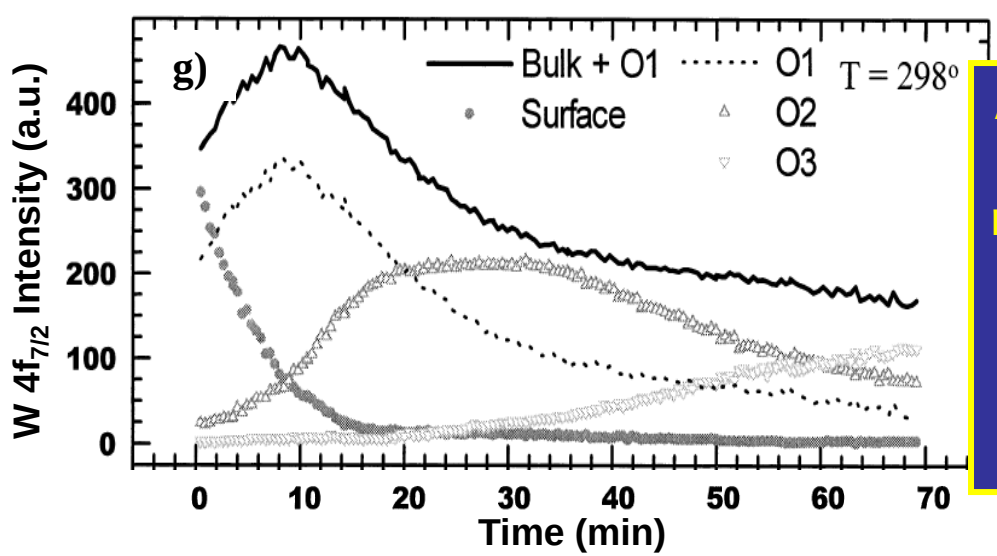

An early time-resolved reaction study (more later)

Ynzunza et al.,
Surf. Sci. 459 (2000) 69

Core and valence photoemission

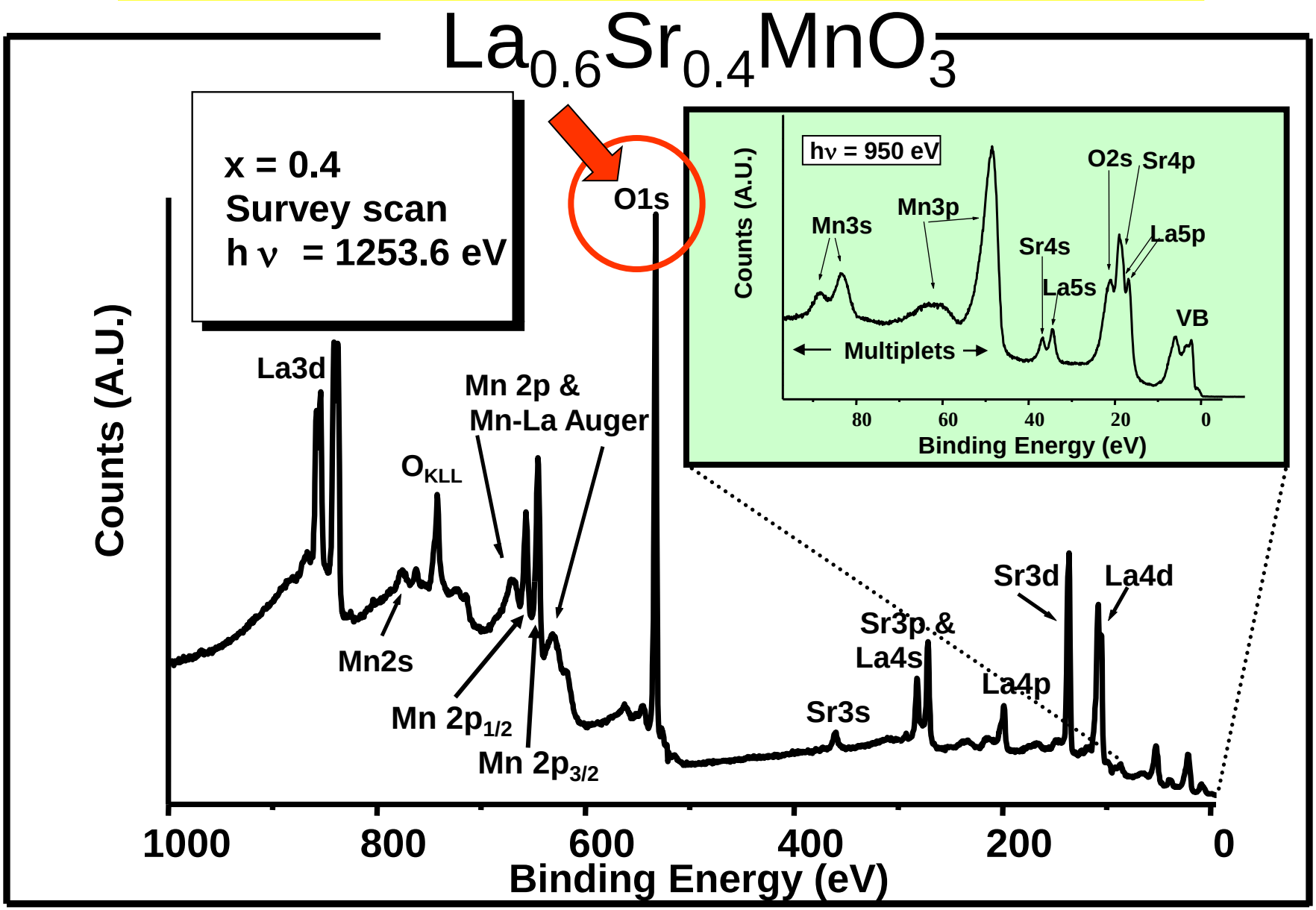

N. Mannella et al., Phys. Rev. Lett. 92, 166401 (2004)

Temperature dependence of Mn3s and O1s spectra: $La_{0.7}Sr_{0.3}MnO_3$

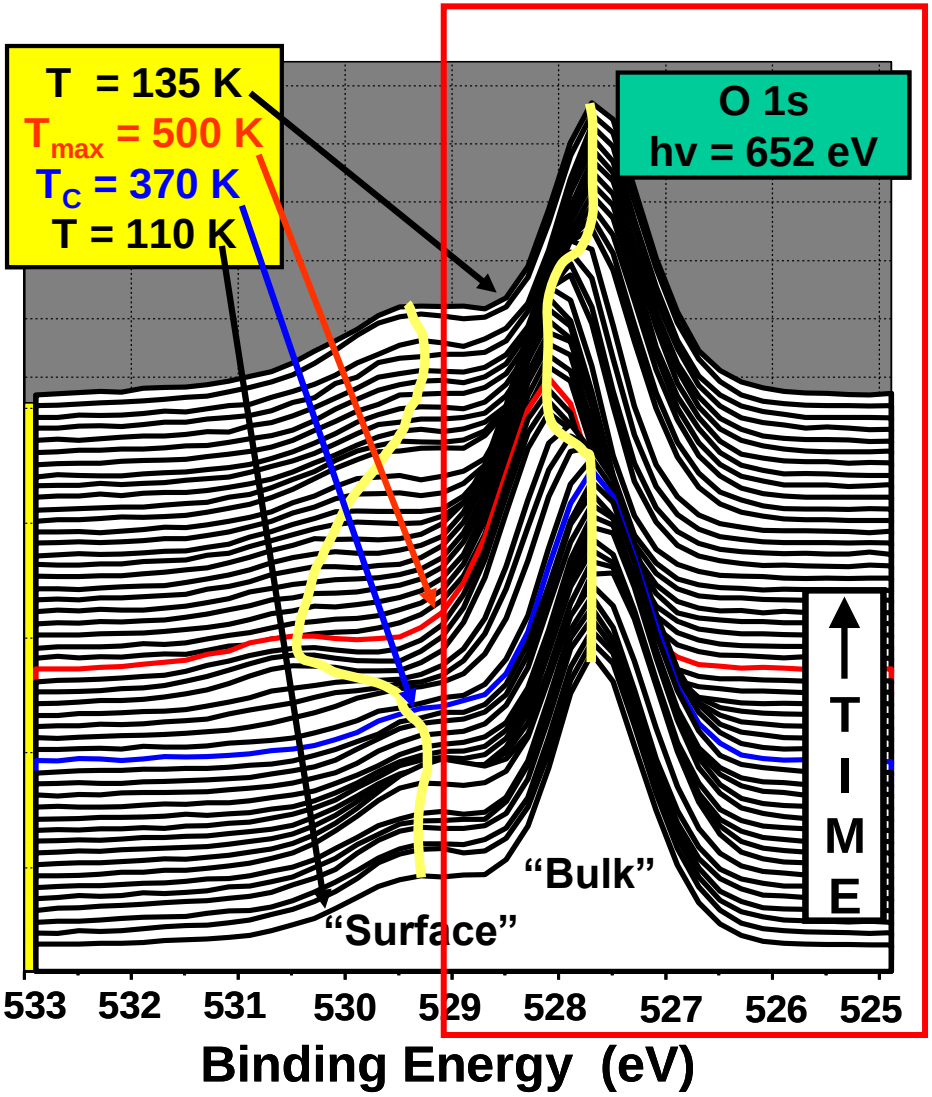

N. Mannella et al., Phys. Rev. Lett. 92, 166401 (2004)

Core and valence photoemission

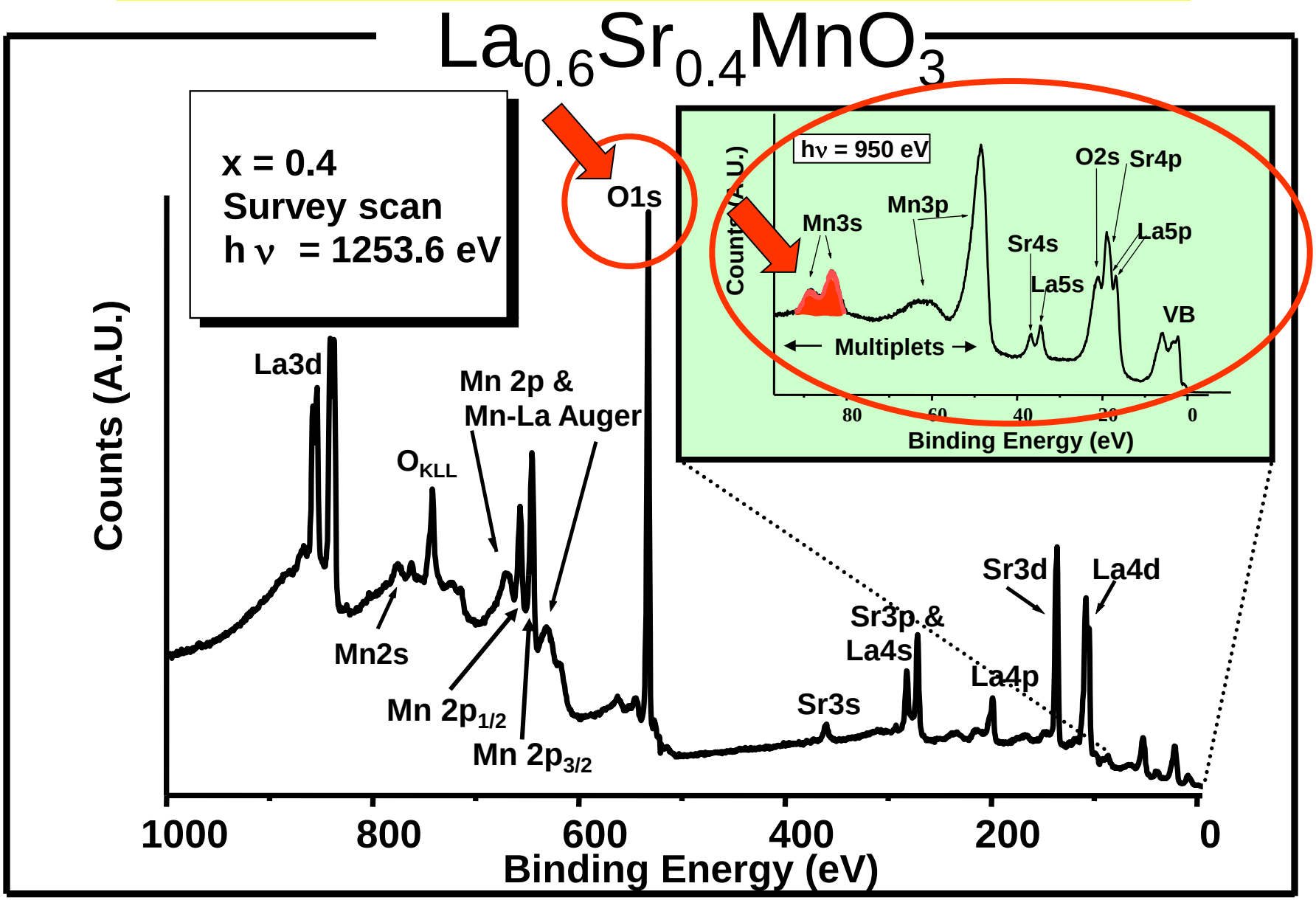

N. Mannella et al., Phys. Rev. Lett. 92, 166401 (2004)

Basic Concepts and Experiments

Core-Level Photoemission

Intensities and Quantitative Analysis, the 3-Step Model
Varying Surface and Bulk Sensitivity
Chemical shifts
Multiplet Splittings
Electron Screening and Satellite Structure
Magnetic and Non-Magnetic Dichroism
Resonant Photoemission
Photoelectron Diffraction and Holography

Valence-Level Photoemission

Band-Mapping in the Ultraviolet Photoemission Limit
Densities of States in the X-Ray Photoemission Limit

Some New Directions

Photoemission with Hard X-Rays (throughout lectures)
Photoemission with Standing Wave Excitation
Photoemission with Spatial Resolution/Photoelectron Microscopy
Temporal Resolution
@ Higher Pressures

Multiplet splitting in core levels of transition metal oxides

$$BE = h\nu - E_{kin} = \underbrace{E^*(N-1)}_{\text{Final state}} - \underbrace{E_0(N)}_{\text{Initial state}}$$

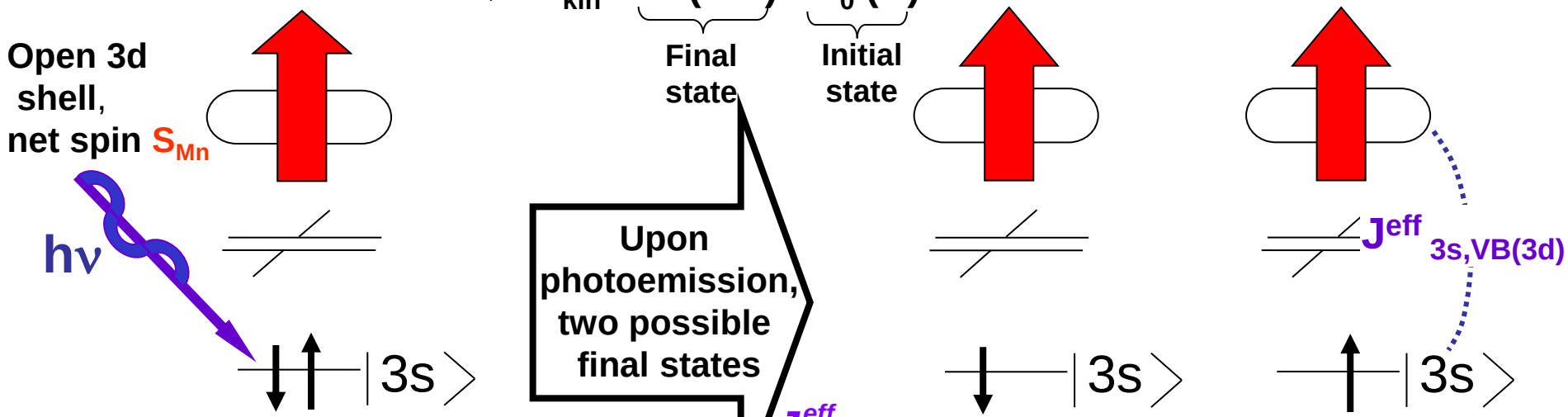

$$J^{eff}_{3s,VB(3d)} \approx \int \varphi_{3s}(\vec{r}_1)\varphi_{3d}(\vec{r}_2)\frac{e^2}{r_{12}}\varphi_{3d}(\vec{r}_1)\varphi_{3s}(\vec{r}_2)dV_1dV_2$$

The splitting between the two peaks is given by

$\Delta E_{3s} \approx (2S_{Mn} + 1)\, J^{eff}_{3s,VB(3d)}$

(Van Vleck Theorem)

For the cubic manganites in simplest doping model,

$S_{Mn}=1/2(4-x) \rightarrow$

$\Delta E_{3s} \approx [5-x]\, J^{eff}_{3s,\, VB)3d)}$

with $J^{eff}_{3s,\, VB} \approx 1.1$ eV

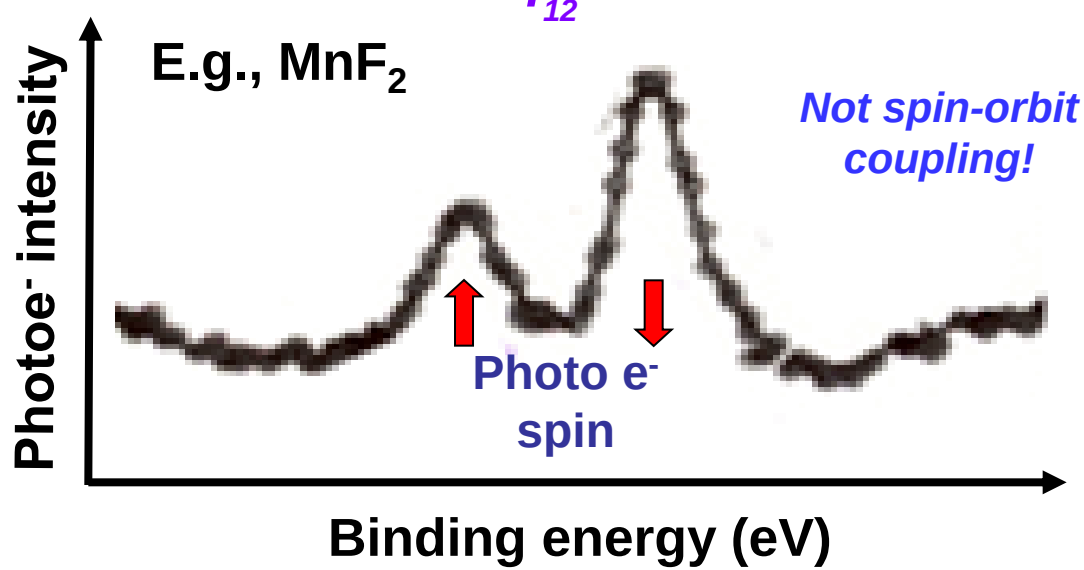

INTENSITIES IN PHOTOELECTRON SPECTRA:

- GENERAL: FINAL STATE K (K-SUBSHELL + ALL OTHER DESIG.)

$$\text{INT.}_K \propto \left|\hat{e}\cdot\langle\Psi^f_{tot}(N,K)|\sum_{i=1}^{N}\vec{r}_i|\Psi^i(N)\rangle\right|^2 \quad \text{(DIPOLE APPROX.}$$

- BORN-OPPENHEIMER: e^-'s FAST, VIBRATIONS SLOW

$$\text{INT.}_K \propto \underbrace{|\langle\psi^f_{vib,v'}|\psi^i_{vib,v}\rangle|^2}_{\text{FRANCK-CONDON FACTOR}}\left|\hat{e}\cdot\langle\Psi^f_{e^-}(N,K)|\sum_{i=1}^{N}\vec{r}_i|\psi^i_{e^-}(N)\rangle\right|^2$$

- SUDDEN APPROXIMATION: $\varphi_K \to \varphi_f$ = PHOTOe^- (FAST)

$$\left.\begin{array}{l}\varphi_1 \to \varphi_1' \\ \vdots \\ \varphi_{K-1} \to \varphi'_{K-1} \\ \varphi_{K+1} \to \varphi'_{K+1} \\ \vdots \\ \varphi_N \to \varphi_N'\end{array}\right\} \text{(SLOW)}$$

K HOLE →

$$\text{INT.}_K \propto |\langle\psi^f_{vib,v'}|\psi^i_{vib,v}\rangle|^2 \underbrace{|\langle\psi^f_{e^-}(N-1,K)|\psi_K(N-1,K)\rangle|^2}_{\text{SAME SUBSHELL COUPLING + TOTAL L,S→"MONOPOLE"}}$$

K MISSING

$$|\hat{e}\cdot\langle\varphi_f|\vec{r}|\varphi_K\rangle|^2$$

↳ NORMAL $\frac{d\sigma_K}{d\Omega}$

- SLATER DETS. FOR $\psi^f_{e^-} = \det(\varphi_1'\varphi_2'\cdots\varphi'_{K-1}\varphi'_{K+1}\cdots\varphi_N')$

$$\psi_K = \det(\varphi_1\varphi_2\cdots\varphi_{K-1}\varphi_{K+1}\cdots\varphi_N)$$

$$\text{INT.}_K \propto |\langle\psi^f_{vib,v'}|\psi^i_{vib,v}\rangle|^2|\langle\varphi_1'|\varphi_1\rangle|^2|\langle\varphi_2'|\varphi_2\rangle|^2\cdots$$
$$|\langle\varphi'_{K-1}|\varphi_{K-1}\rangle|^2|\langle\varphi'_{K+1}|\varphi_{K+1}\rangle|^2\cdots|\langle\varphi_N'|\varphi_N\rangle|^2 \quad \Big\}$$

$$|\hat{e}\cdot\langle\varphi_f|\vec{r}|\varphi_K\rangle|^2$$

1e- DIPOLE→dσ/dΩ

(N-1)e⁻ SHAKE-UP/ SHAKE-OFF→ "MONOPOLE"

- PLUS DIFFRACTION EFFECTS IN φ_f ESCAPE

ORIGIN OF MULTIPLET SPLITTINGS IN Mn^{2+}: "ONE-ELECTRON" THEORY

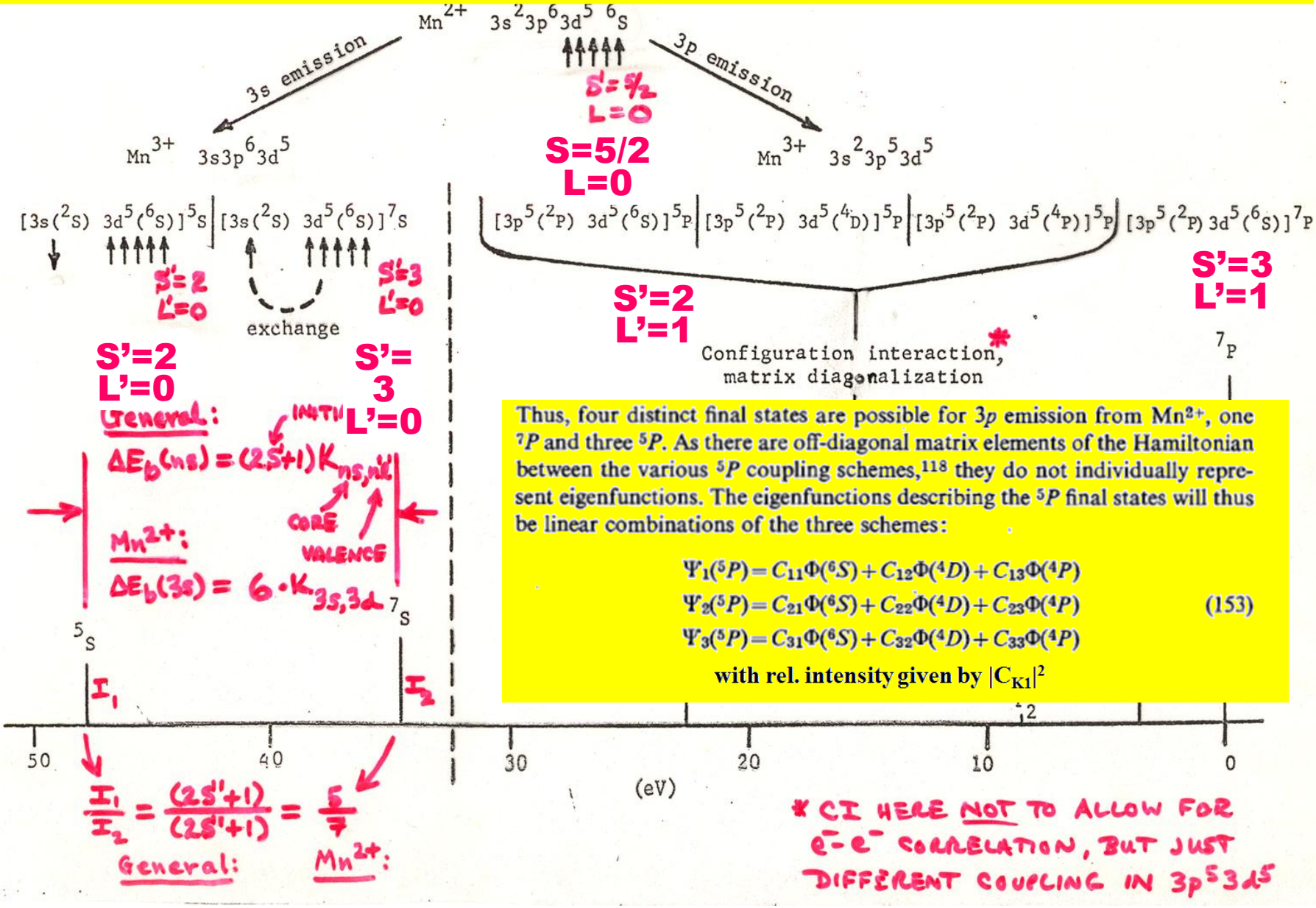

Thus, four distinct final states are possible for $3p$ emission from Mn^{2+}, one ^7P and three ^5P. As there are off-diagonal matrix elements of the Hamiltonian between the various ^5P coupling schemes,[118] they do not individually represent eigenfunctions. The eigenfunctions describing the ^5P final states will thus be linear combinations of the three schemes:

$$\begin{aligned}\Psi_1(^5P) &= C_{11}\Phi(^6S) + C_{12}\Phi(^4D) + C_{13}\Phi(^4P)\\ \Psi_2(^5P) &= C_{21}\Phi(^6S) + C_{22}\Phi(^4D) + C_{23}\Phi(^4P)\\ \Psi_3(^5P) &= C_{31}\Phi(^6S) + C_{32}\Phi(^4D) + C_{33}\Phi(^4P)\end{aligned} \tag{153}$$

with rel. intensity given by $|C_{K1}|^2$

General **Mn^{2+}** **"Basic Concepts of XPS"**

Figure 30

ORIGIN OF MULTIPLET SPLITTINGS IN Mn^{2+}: "ONE-ELECTRON" THEORY

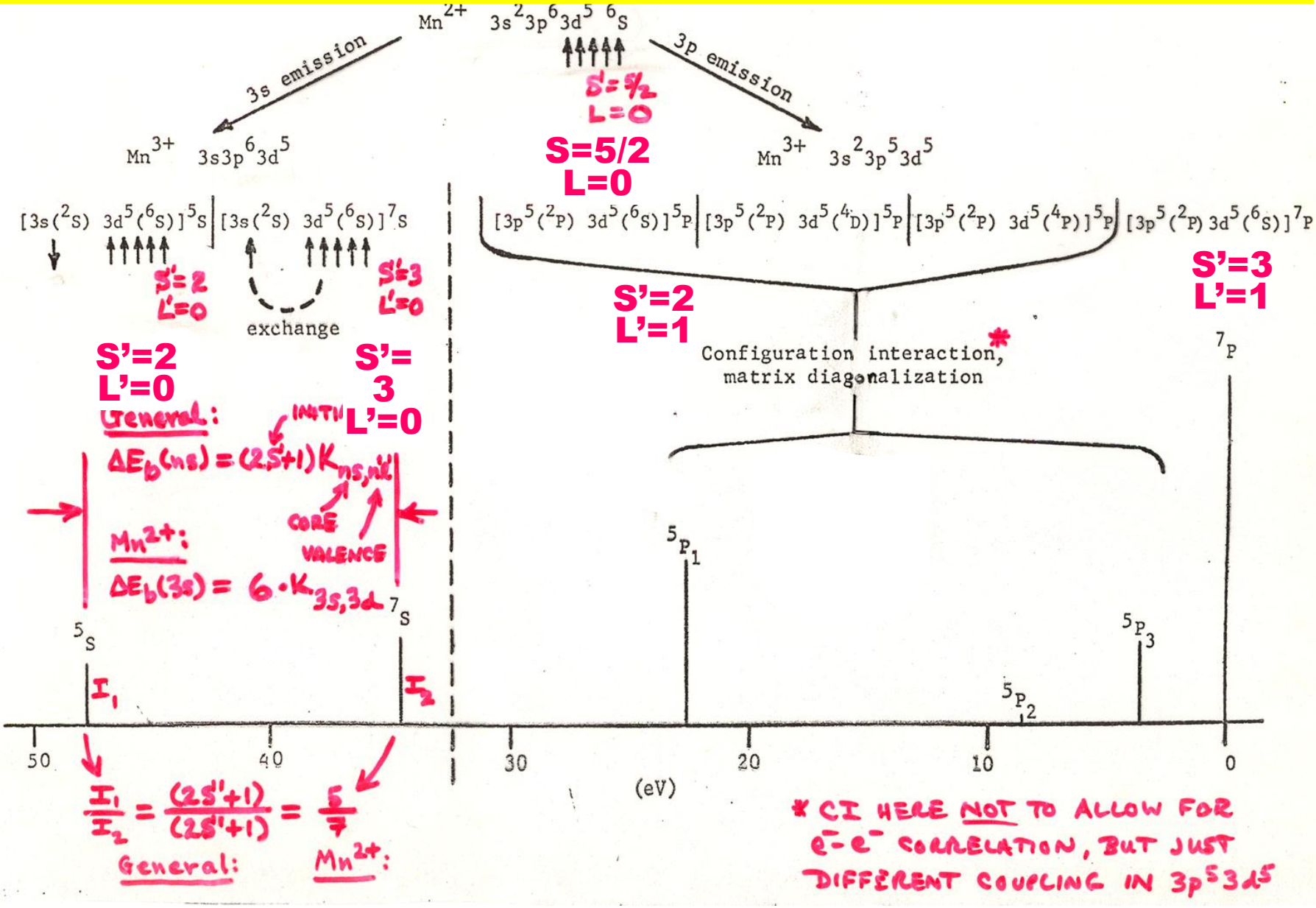

General **Mn^{2+}** **"Basic Concepts of XPS"**

Figure 30

CORE-LEVEL MULTIPLET SPLITTINGS IN Mn COMPOUNDS

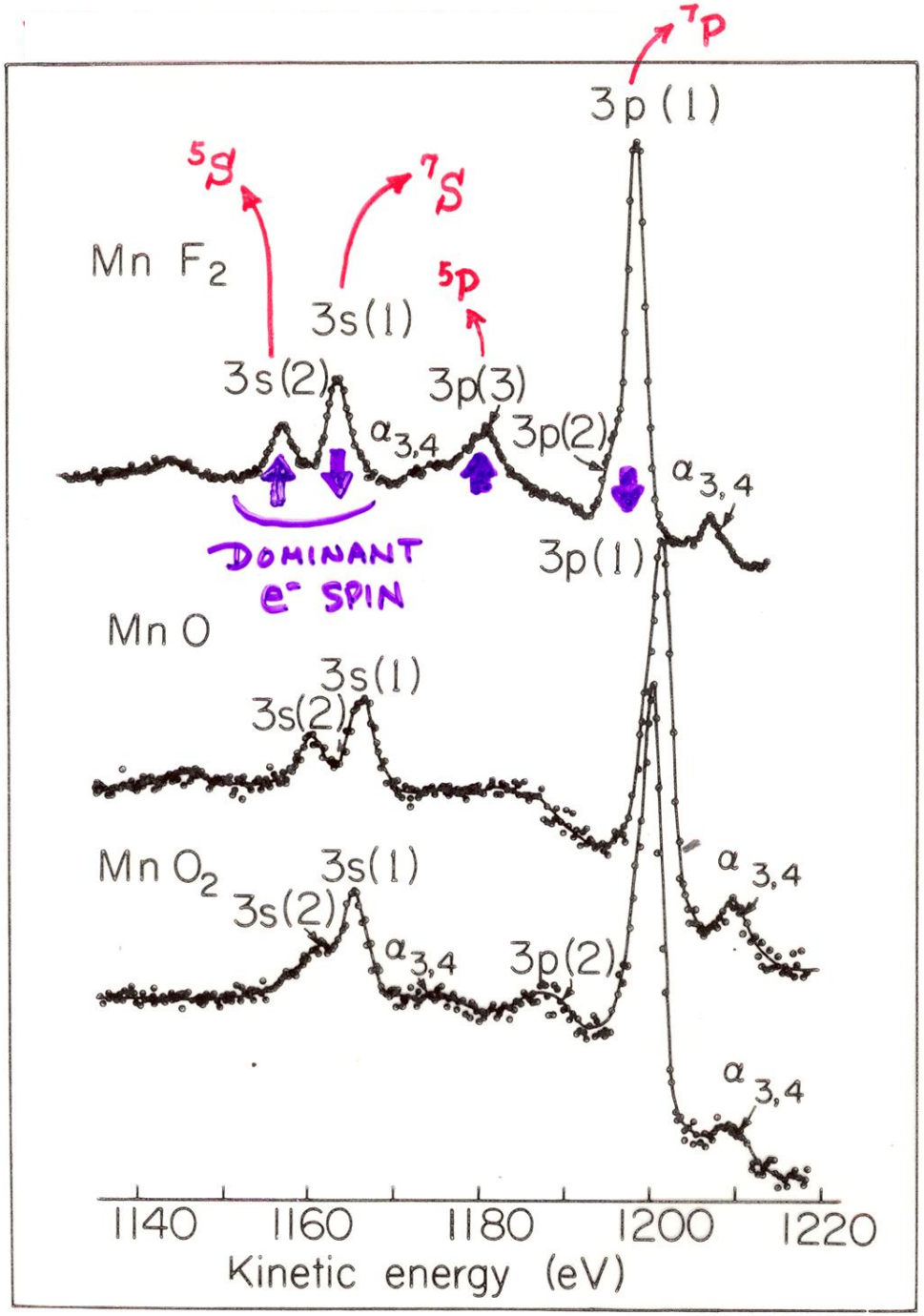

"Basic Concepts of XPS"
Figure 31

COMPARISON OF GAS-PHASE AND SOLID-STATE SPECTRA

EXPT.: (a), (b), (d), HERMSMEIER ET AL., PHYS. REV. LETT. 61, 2592 (1988) (OUR GROUP)

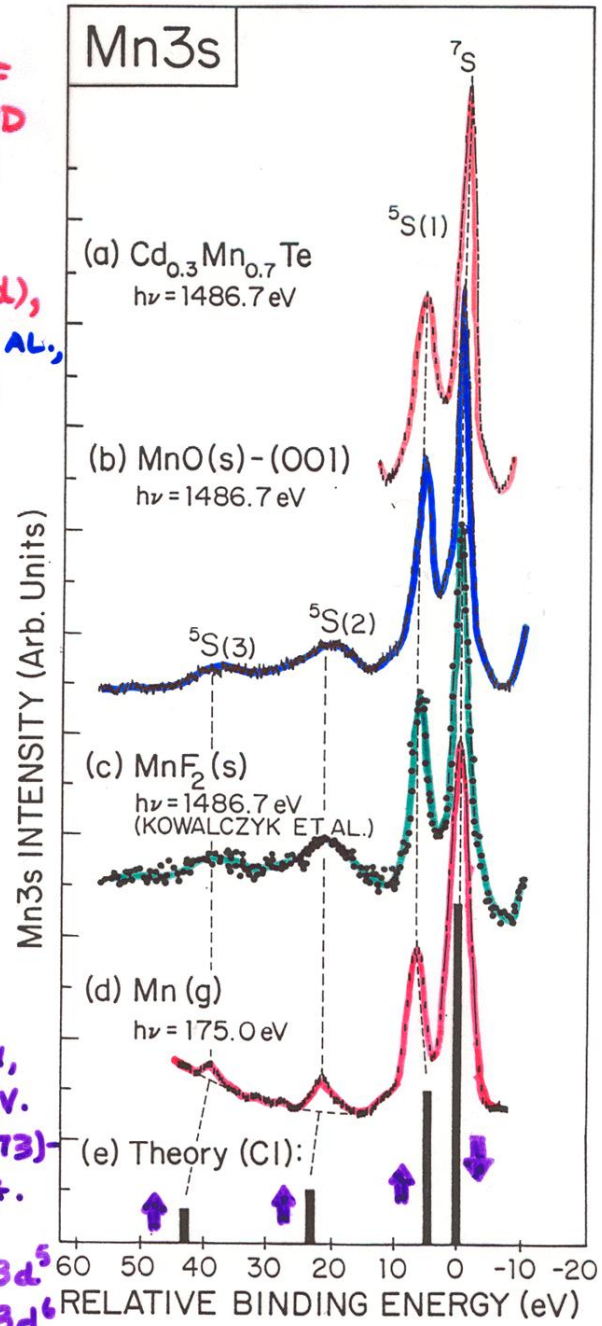

THEORY: BAGUS, FREEMAN, SASAKI, PHYS. REV. LETT. 30, 850 (1973) – ATOMIC CONFIG. INT. IN $Mn^{3+}\ldots 3s^1\ldots 3d^5$ + $Mn^{3+}\ldots 3s^2 3p^4 3d^6$

Correlation CI effects: anti-parallel electrons

"Basic Concepts of XPS"
Figure 33

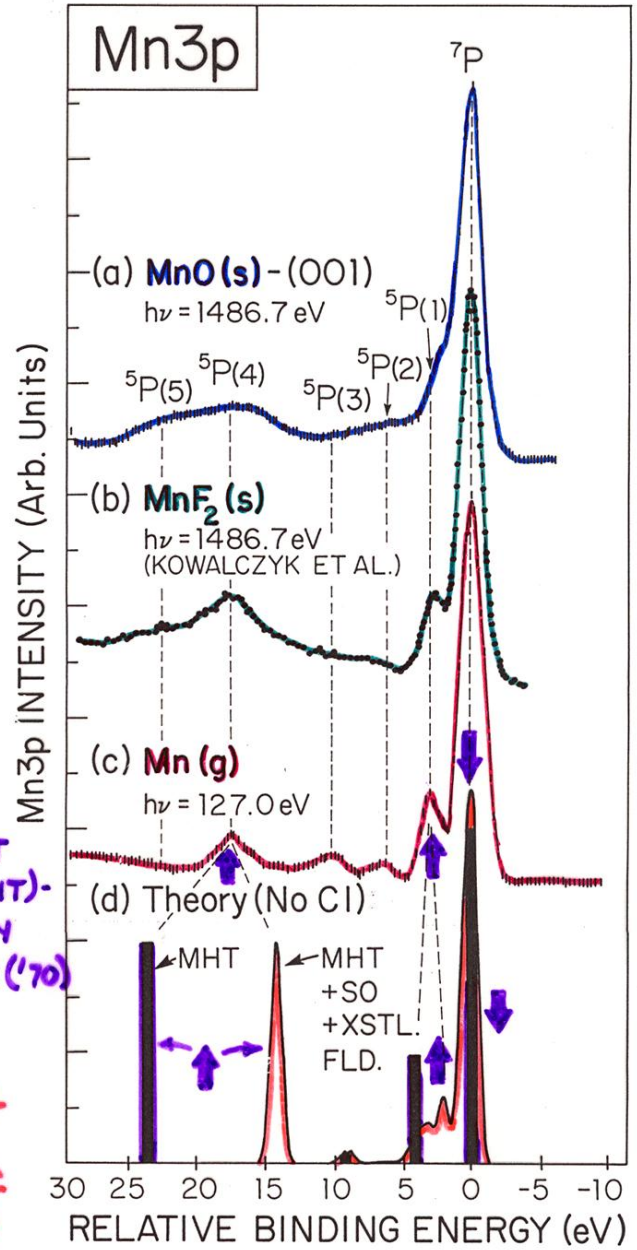

THEORY: NO CI

SIMPLE MULTIPLET HOLE THEORY (MHT) - FADLEY, SHIRLEY PHYS. REV. A2, 1109 ('70)

EMPIRICAL MHT WITH SPIN ORBIT + CRYSTAL FIELD - SUGANO ET AL., J. PHYS. C 15, 2625 (1982)

HERMSMEIER ET AL., P.R.L. 61, 2592 ('88)

Temperature dependence of Mn3s and O1s spectra: $La_{0.7}Sr_{0.3}MnO_3$

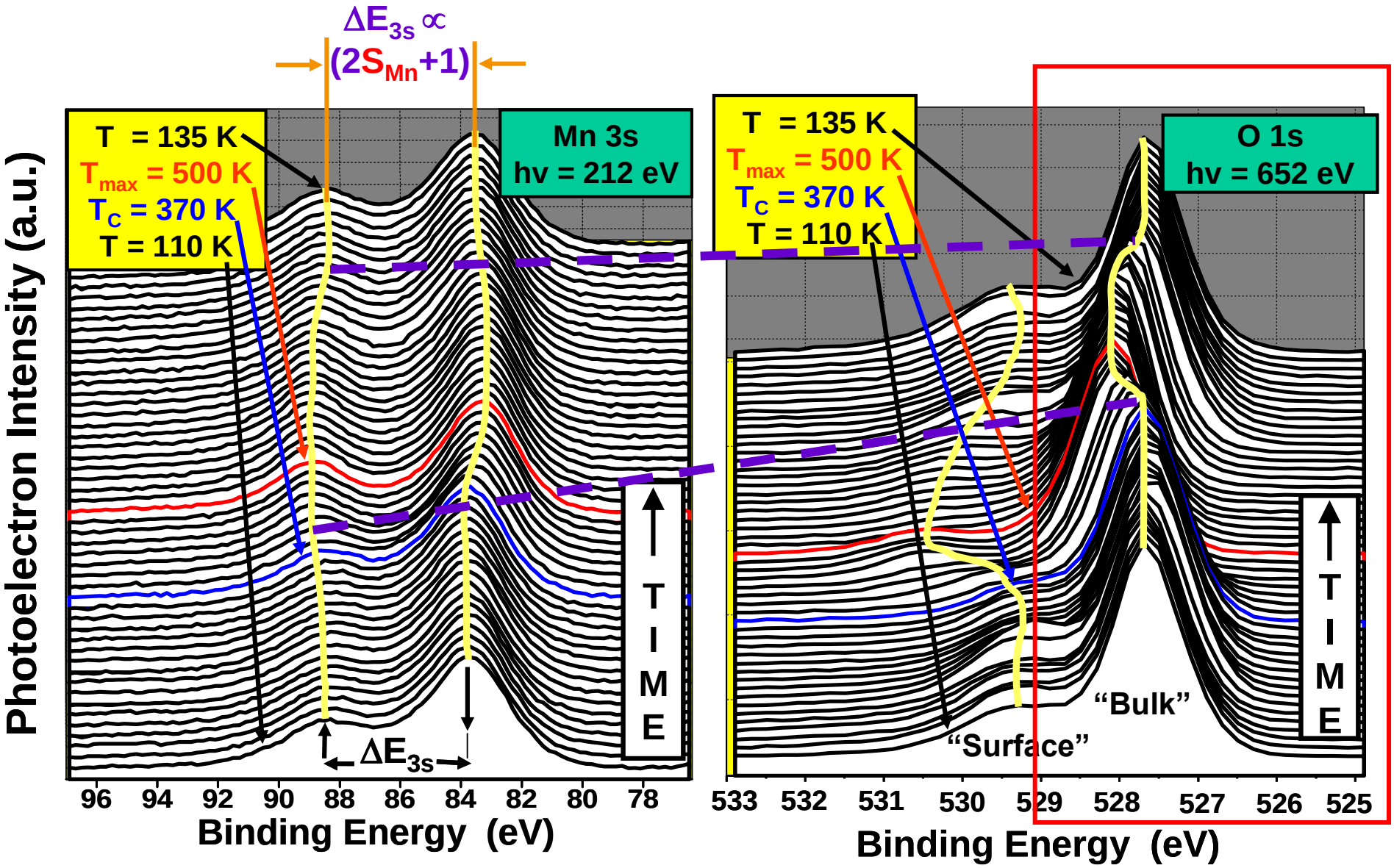

N. Mannella et al., Phys. Rev. Lett. 92, 166401 (2004)

Suggested scenario

Jahn-Teller distortion

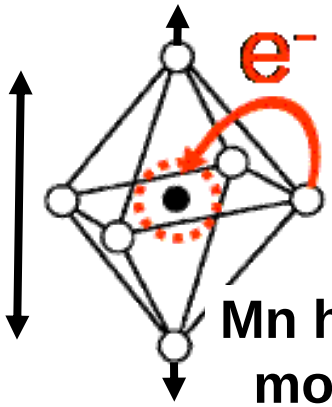

O more positive

Mn higher spin, more negative

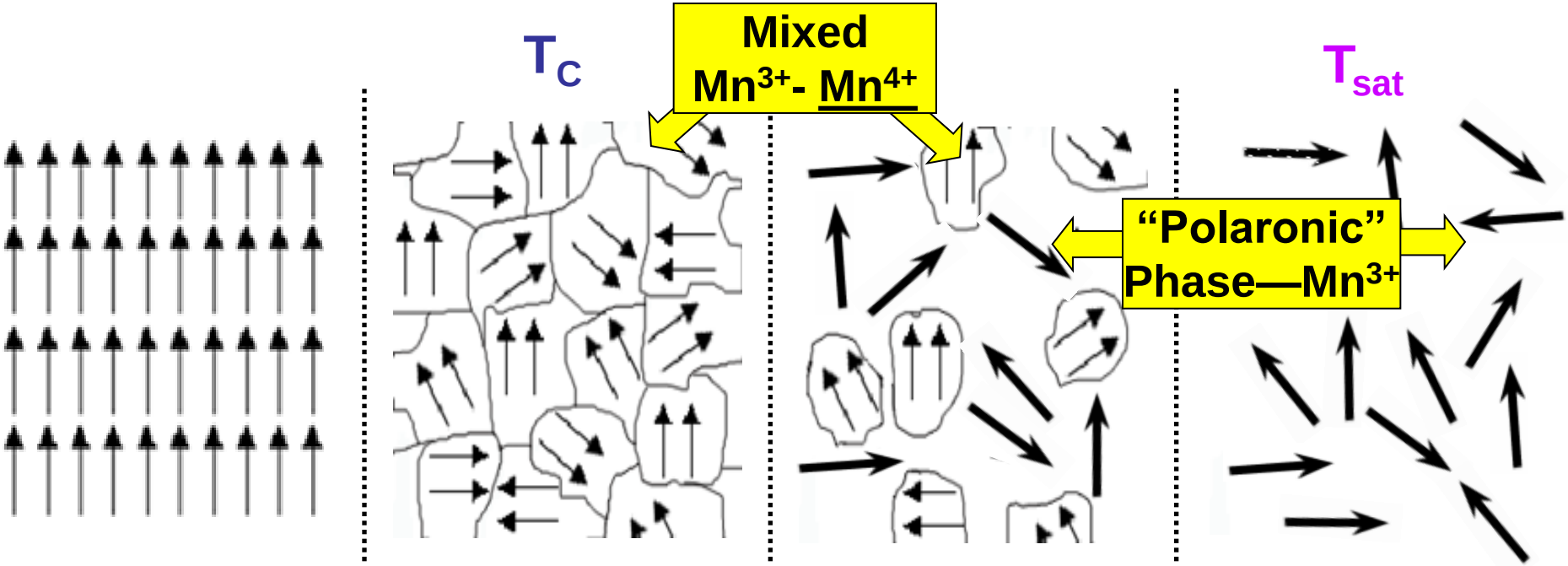

Long-range ferromagnetic order

Loss of long - range order at T_C

Short - range order above T_C up to T_{sat} Jahn-Teller distortion

N. Mannella et al., PRL 92, 166401 ('04); PRB 70, 224433 ('04), and to be publ.

Basic Concepts and Experiments

Core-Level Photoemission

Intensities and Quantitative Analysis, the 3-Step Model
Varying Surface and Bulk Sensitivity
Chemical shifts
Multiplet Splittings
Electron Screening and Satellite Structure
Magnetic and Non-Magnetic Dichroism
Resonant Photoemission
Photoelectron Diffraction and Holography

Valence-Level Photoemission

Band-Mapping in the Ultraviolet Photoemission Limit
Densities of States in the X-Ray Photoemission Limit

Some New Directions

Photoemission with Hard X-Rays (throughout lectures)
Photoemission with Standing Wave Excitation
Photoemission with Spatial Resolution/Photoelectron Microscopy
Temporal Resolution
@ Higher Pressures

Basic energetics—Many e$^-$ & many atom picture

$$h\nu = E_{binding}^{Vacuum} + E_{kinetic} = E_{binding}^{Fermi} + \varphi_{spectrometer} + E_{kinetic}$$

$$E_{binding}^{Vacuum}(Qn\ell j, K) = E_{final}(N-1, Qn\ell j\ hole, K) - E_{initial}(N)$$

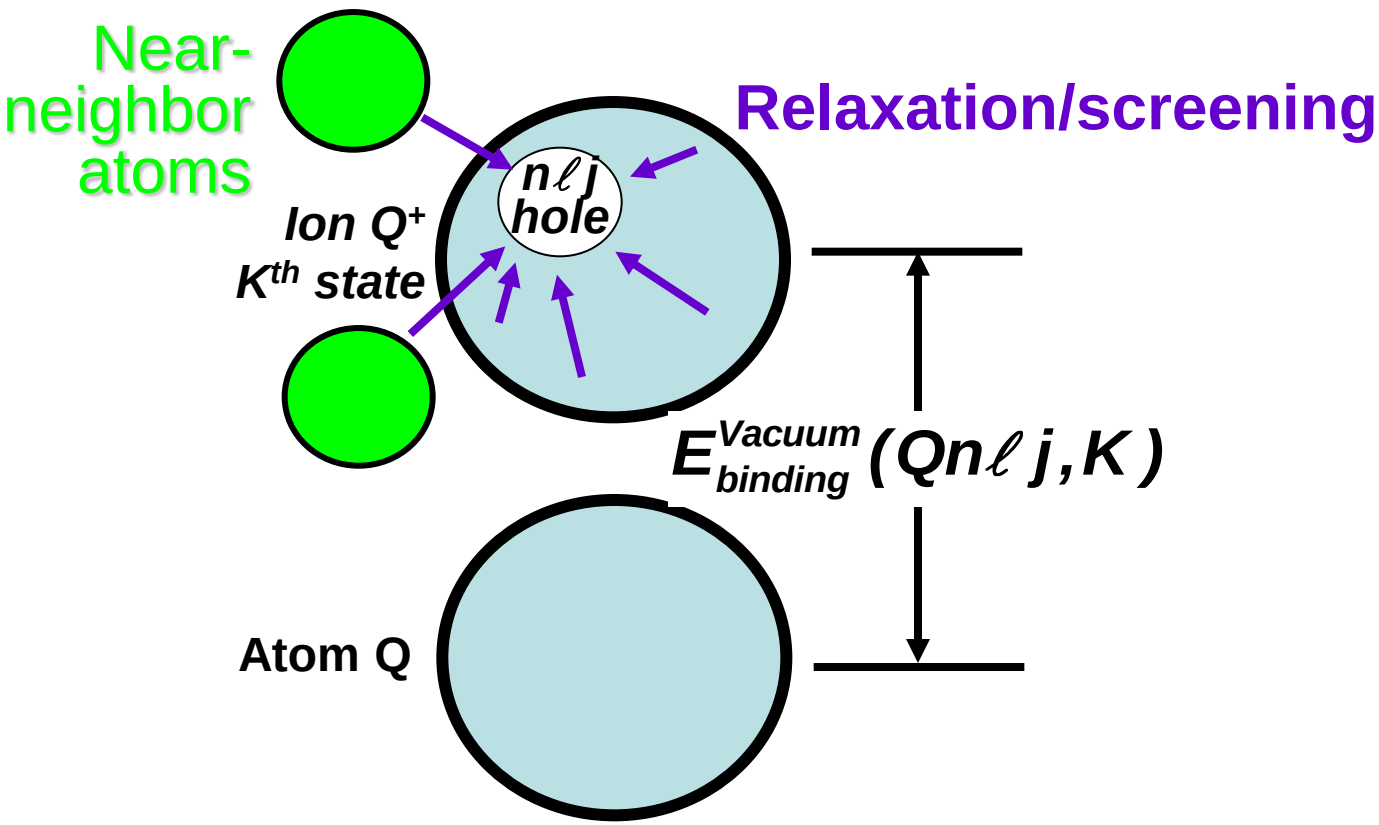

INTENSITIES IN PHOTOELECTRON SPECTRA:

- GENERAL: FINAL STATE K (K-SUBSHELL + ALL OTHER DESIG.)

$$\text{INT.}_K \propto \left|\hat{e}\cdot\langle\Psi^f_{tot}(N,K)|\sum_{i=1}^{N}\vec{r}_i|\Psi^i(N)\rangle\right|^2 \quad \text{(DIPOLE APPROX.}$$

- BORN-OPPENHEIMER: e^-'s FAST, VIBRATIONS SLOW

$$\text{INT.}_K \propto \underbrace{|\langle\psi^f_{vib,v'}|\psi^i_{vib,v}\rangle|^2}_{\text{FRANCK-CONDON FACTOR}}\left|\hat{e}\cdot\langle\Psi^f_{e^-}(N,K)|\sum_{i=1}^{N}\vec{r}_i|\psi^i_{e^-}(N)\rangle\right|^2$$

- SUDDEN APPROXIMATION: $\varphi_K \to \varphi_f$ = PHOTOe^- (FAST)

$$\left.\begin{array}{l}\varphi_1 \to \varphi_1' \\ \vdots \\ \varphi_{K-1} \to \varphi'_{K-1} \\ \varphi_{K+1} \to \varphi'_{K+1} \\ \vdots \\ \varphi_N \to \varphi_N'\end{array}\right\} \text{(SLOW)}$$

K HOLE →

$$\text{INT.}_K \propto |\langle\psi^f_{vib,v'}|\psi^i_{vib,v}\rangle|^2 \underbrace{|\langle\psi^f_{e^-}(N-1,K)|\psi_K(N-1,K)\rangle|^2}_{\text{SAME SUBSHELL COUPLING + TOTAL L,S→"MONOPOLE"}}$$

K MISSING

$$|\hat{e}\cdot\langle\varphi_f|\vec{r}|\varphi_K\rangle|^2$$

↳ NORMAL $\frac{d\sigma_K}{d\Omega}$

- SLATER DETS. FOR $\psi^f_{e^-} = \det(\varphi_1'\varphi_2'\cdots\varphi'_{K-1}\varphi'_{K+1}\cdots\varphi_N')$

$$\psi_K = \det(\varphi_1\varphi_2\cdots\varphi_{K-1}\varphi_{K+1}\cdots\varphi_N)$$

$$\text{INT.}_K \propto |\langle\psi^f_{vib,v'}|\psi^i_{vib,v}\rangle|^2|\langle\varphi_1'|\varphi_1\rangle|^2|\langle\varphi_2'|\varphi_2\rangle|^2\cdots$$
$$|\langle\varphi'_{K-1}|\varphi_{K-1}\rangle|^2|\langle\varphi'_{K+1}|\varphi_{K+1}\rangle|^2\cdots|\langle\varphi_N'|\varphi_N\rangle|^2 \quad \Big\}$$

$$|\hat{e}\cdot\langle\varphi_f|\vec{r}|\varphi_K\rangle|^2$$

1e- DIPOLE→dσ/dΩ

(N-1)e⁻ SHAKE-UP/ SHAKE-OFF→ "MONOPOLE"

- PLUS DIFFRACTION EFFECTS IN φ_f ESCAPE

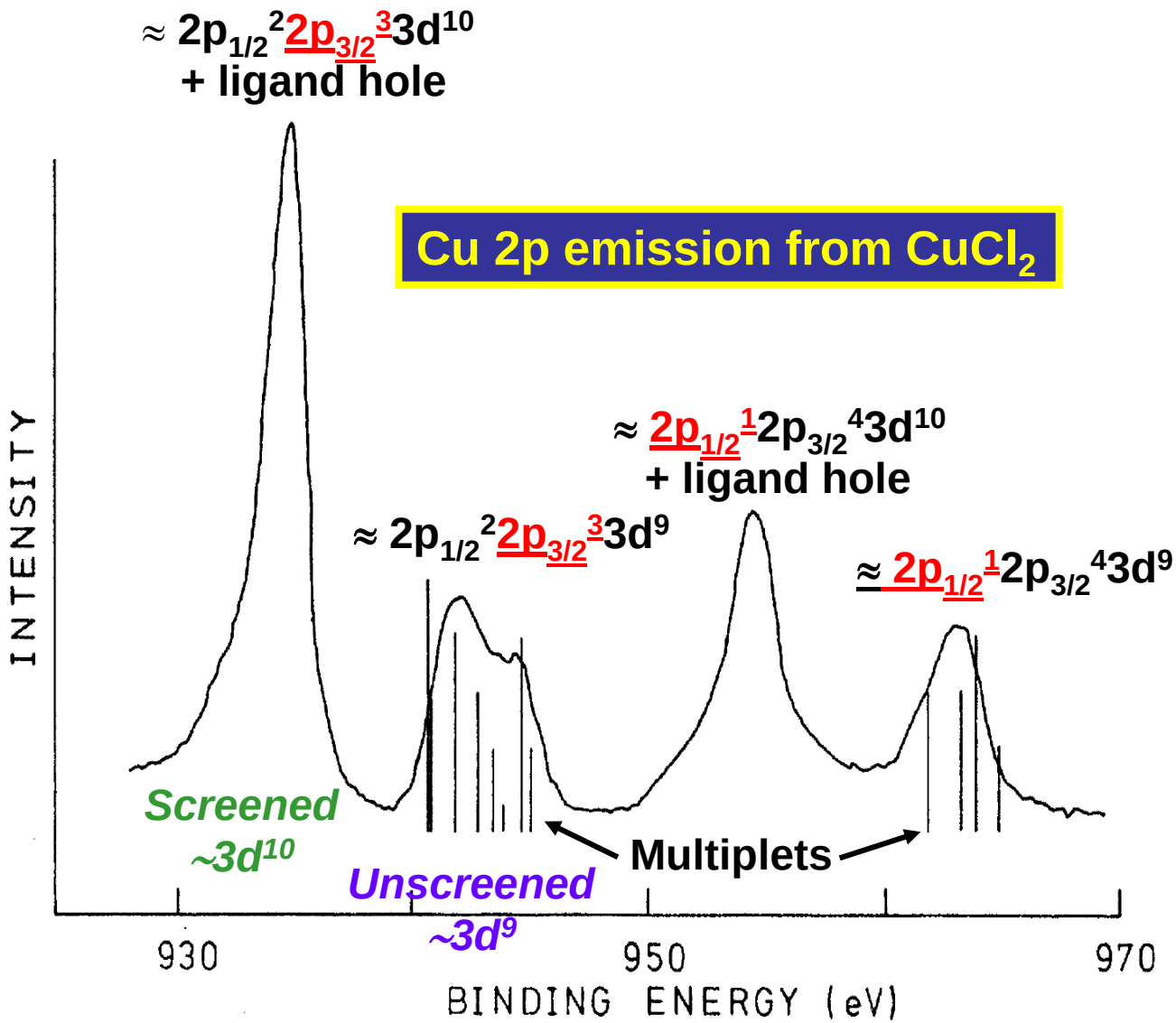

$$\Psi_{final,K}(N-1) = C_{1,K}\Phi_1(2p_{1/2}^2 2p_{3/2}^3 3d^{10} + C\ell\ hole) + C_{2,K}\Phi_2(2p_{1/2}^2 2p_{3/2}^3 3d^9)$$

Van der Laan et al., Phys. Rev. B 23 (1981) 4369

Many-electron and screening effects: $La_{0.7}Sr_{0.3}MnO_3$, hν = 7700 eV

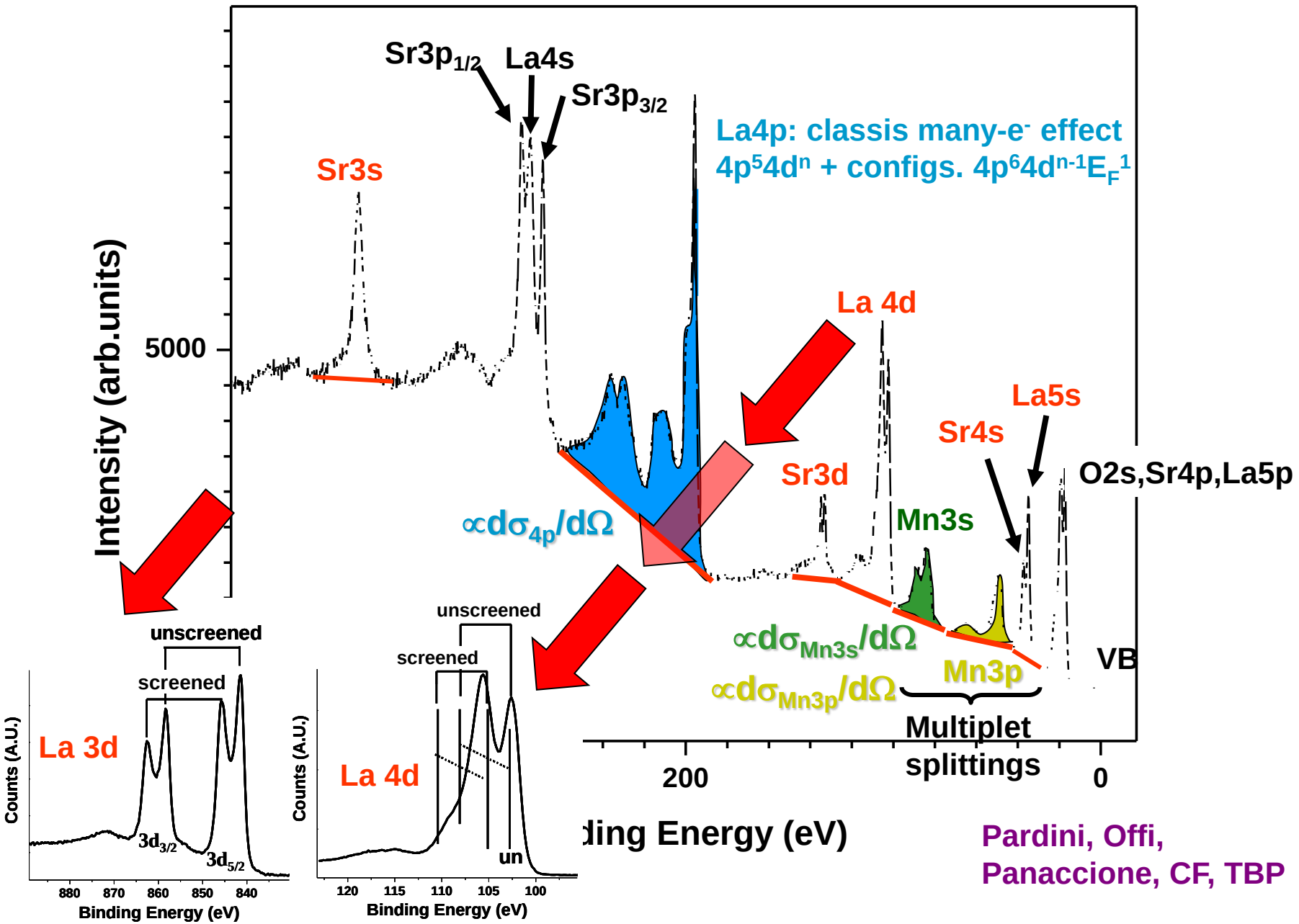

Pardini, Offi, Panaccione, CF, TBP

Basic Concepts and Experiments

Core-Level Photoemission

Intensities and Quantitative Analysis, the 3-Step Model
Varying Surface and Bulk Sensitivity
Chemical shifts
Multiplet Splittings
Electron Screening and Satellite Structure
Magnetic and Non-Magnetic Dichroism
Resonant Photoemission
Photoelectron Diffraction and Holography

Valence-Level Photoemission

Band-Mapping in the Ultraviolet Photoemission Limit
Densities of States in the X-Ray Photoemission Limit

Some New Directions

Photoemission with Hard X-Rays (throughout lectures)
Photoemission with Standing Wave Excitation
Photoemission with Spatial Resolution/Photoelectron Microscopy
Temporal Resolution
@ Higher Pressures

Typical experimental geometry for energy- and angle-resolved photoemission measurements

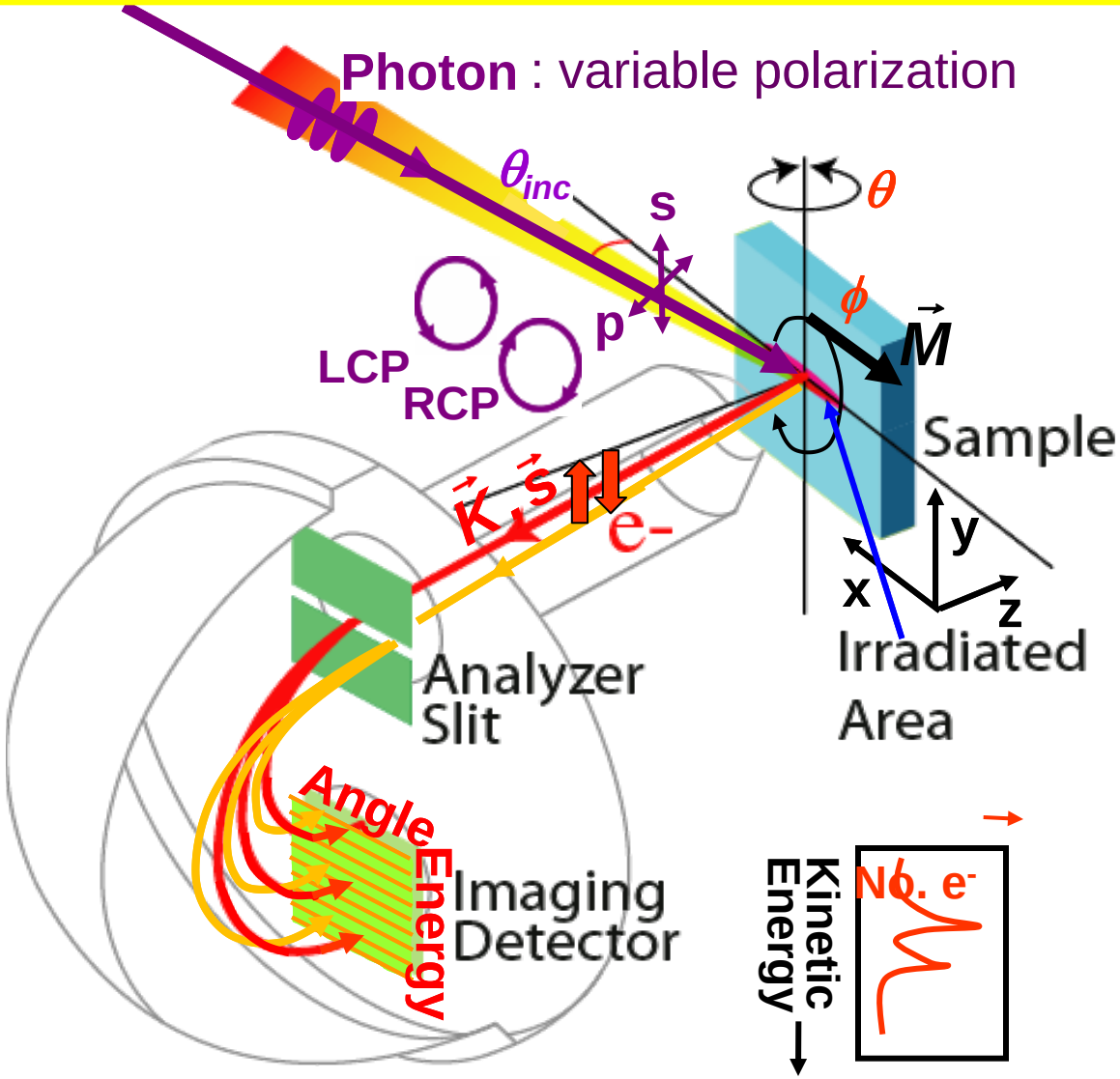

1st Expt. Magnetic Circular Dichroism 1-e- Theo.

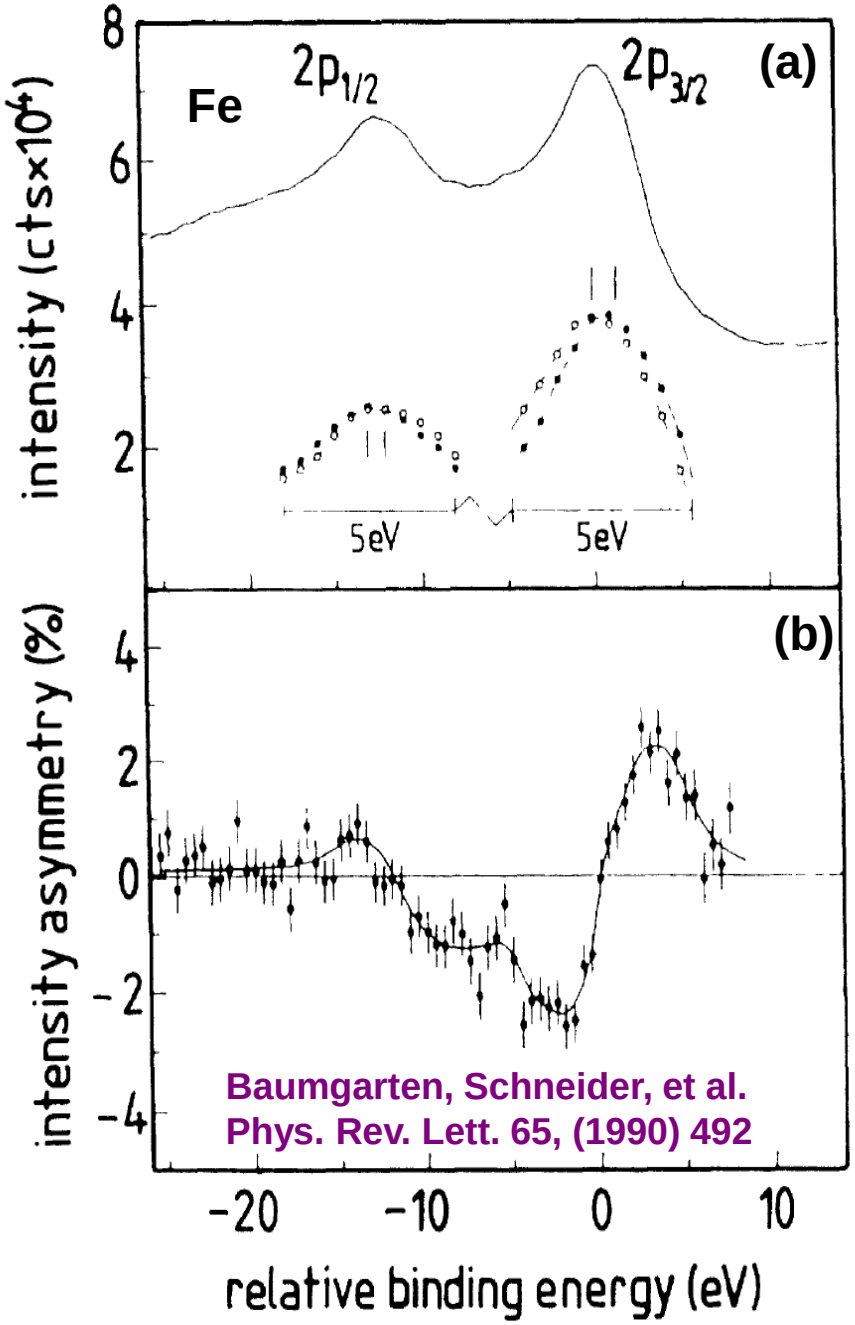

Baumgarten, Schneider, et al.
Phys. Rev. Lett. 65, (1990) 492

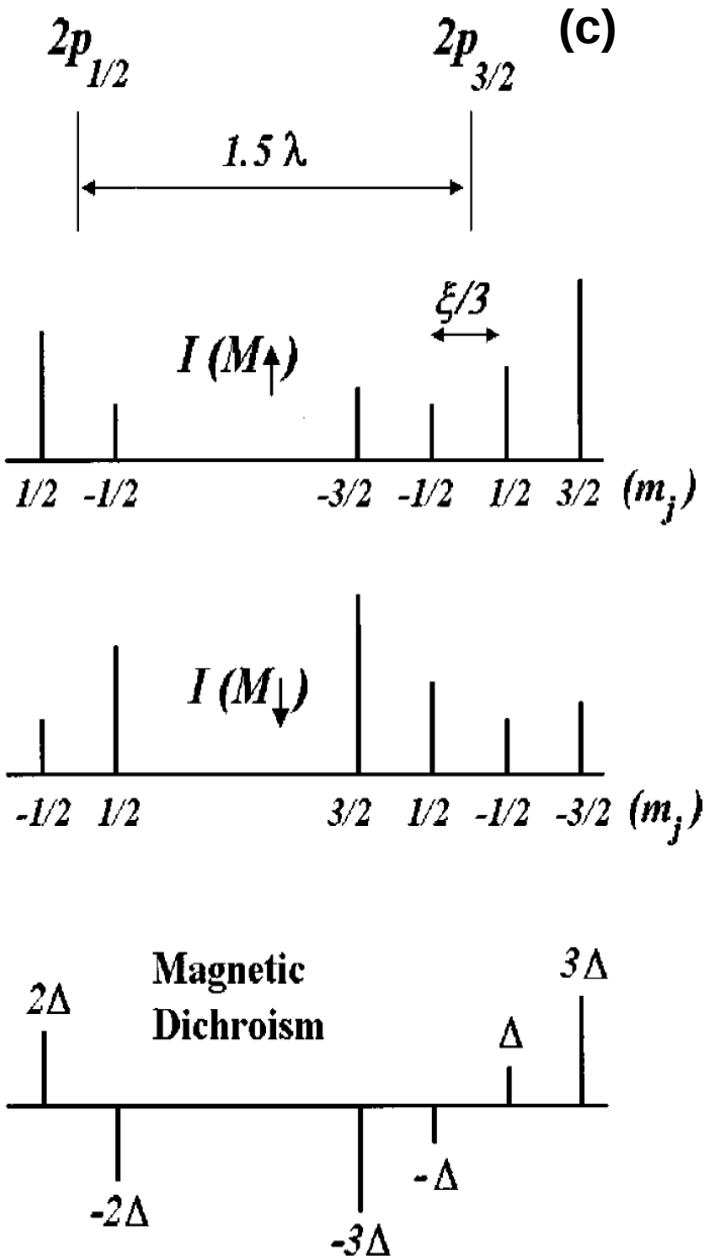

Menchero, Phys. Rev. B 57 (1998)993

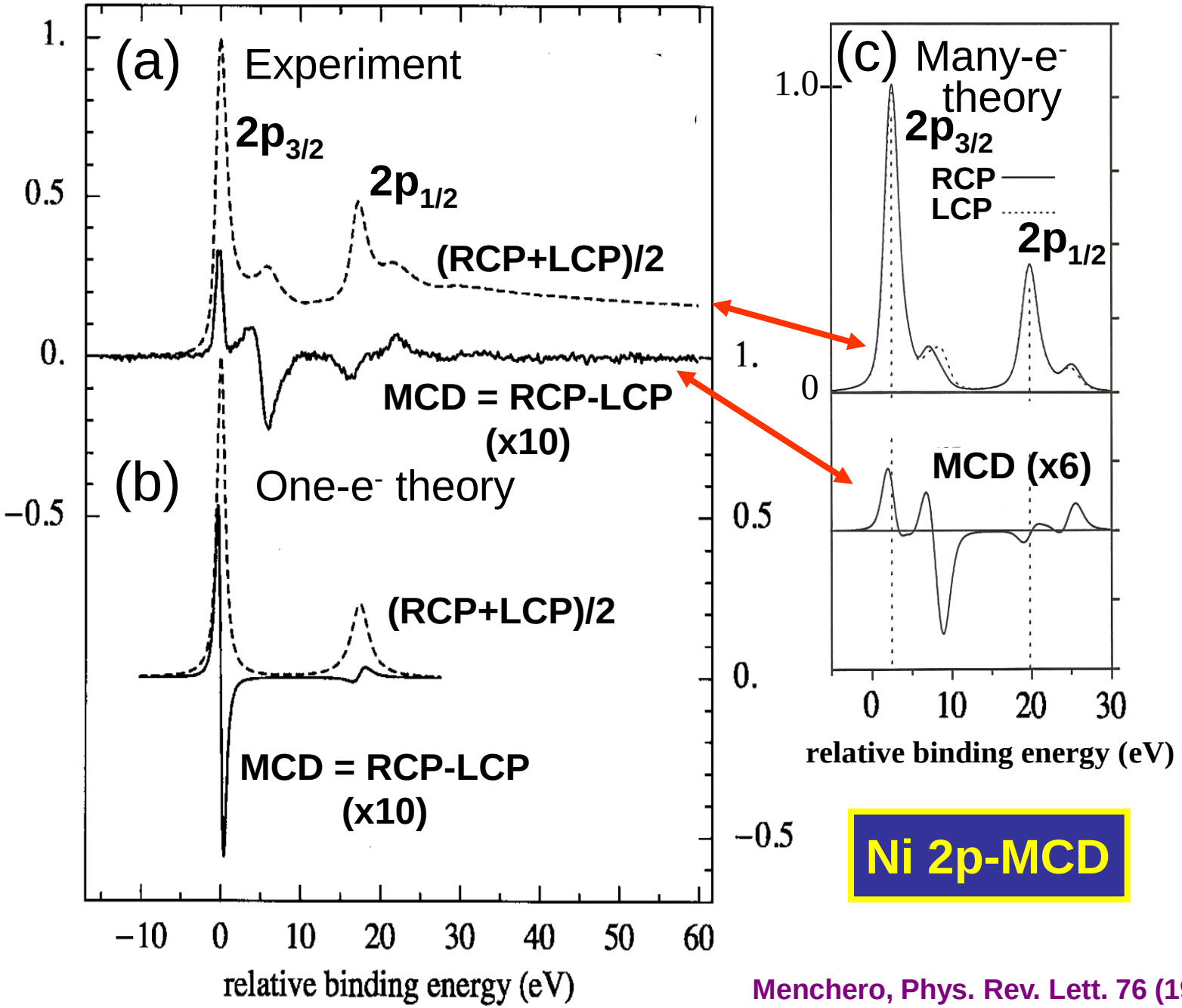

Ni 2p-MCD

Menchero, Phys. Rev. Lett. 76 (1996) 3208

Van der Laan et al., J. Phys. Condens. Matter 12 (2000) L275

Magnetic circular dichroism with soft and hard x-rays

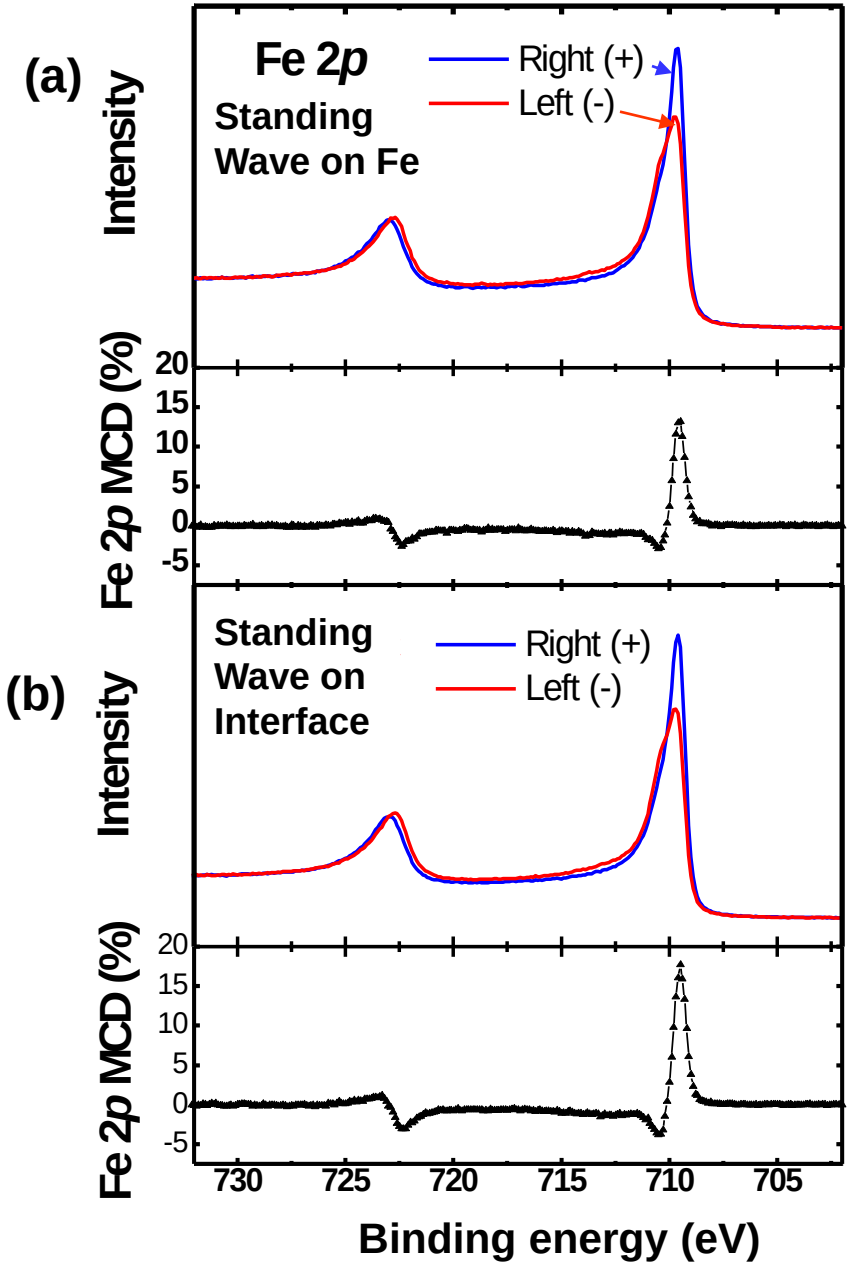

Magnetic circular dichroism in Fe 2p emission. (a) and (b) MCD data for Fe emission from a 16A overlayer of Fe on a Cr wedge, excited by a soft X-ray standing wave at 825 eV that has been positioned either (a) maximally on Fe or (b) maximally on Cr near the Fe/Cr interface. (c) MCD for Fe emission from hematite at 7.94 keV, demonstrating for the first time that these effects can be measured with hard X-rays.

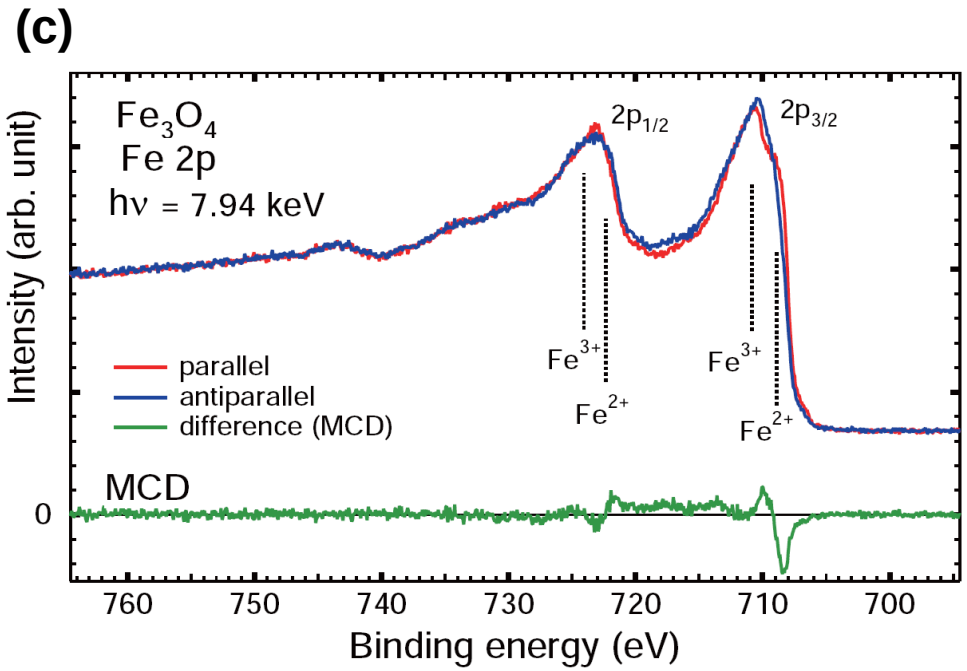

CSF, J. Electron Spectrosc. 178–179, 2-32 (2010)

Basic Concepts and Experiments

Core-Level Photoemission

Intensities and Quantitative Analysis, the 3-Step Model
Varying Surface and Bulk Sensitivity
Chemical shifts
Multiplet Splittings
Electron Screening and Satellite Structure
Magnetic and Non-Magnetic Dichroism
Resonant Photoemission
Photoelectron Diffraction and Holography

Valence-Level Photoemission

Band-Mapping in the Ultraviolet Photoemission Limit
Densities of States in the X-Ray Photoemission Limit

Some New Directions

Photoemission with Hard X-Rays (throughout lectures)
Photoemission with Standing Wave Excitation
Photoemission with Spatial Resolution/Photoelectron Microscopy
Temporal Resolution
@ Higher Pressures

CIRCULAR DICHROISM – NON-MAGNETIC SYSTEMS

Si2p -- 250eV = E_{kin}

EXPERIMENT

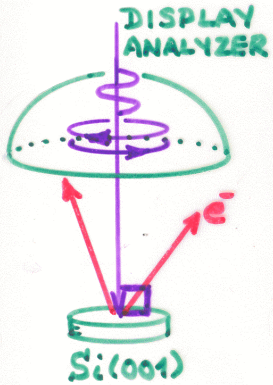

(a) LCP (b) RCP

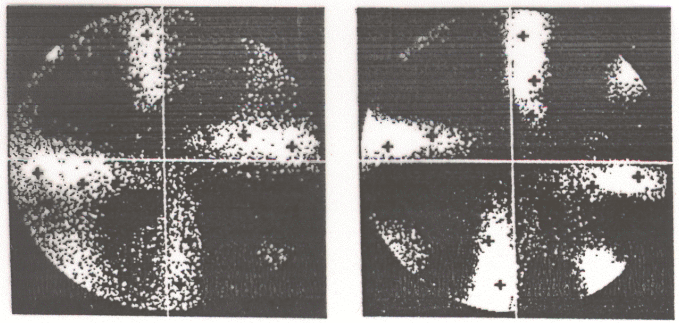

DAIMON ET AL.
JPN. J. APPL. PHYS.
32, L1480 ('93)

THEORY

(c) LCP (d) RCP

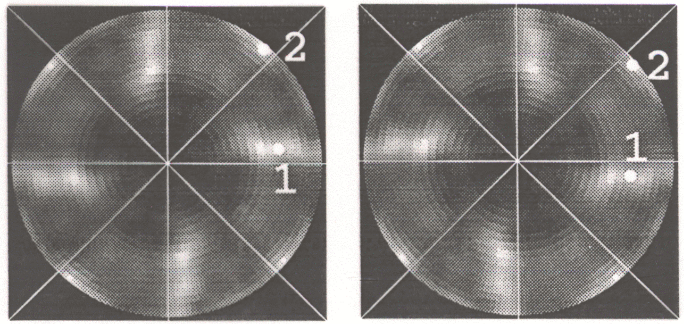

KADUWELA ET AL.
P. R. B 50, 6203 ('94)

(e) UNPOLARIZED

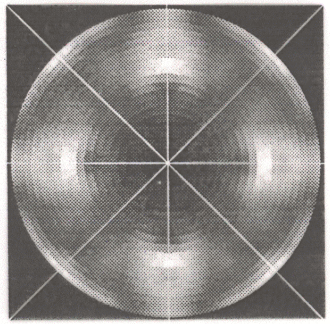

Adding relativity to the Hamiltonian—spin-orbit coupling

- SPIN-ORBIT SPLITTING OF LEVELS:

$\Rightarrow$ EFFECTIVE $\vec{B}$ (NUCLEUS AROUND e^-) $\propto \vec{L}$

$$\hat{H}_{s\text{-}o} = \xi(r)\,\vec{l}\cdot\vec{s}$$

- SPLITS ALL nl LEVELS $2(2l+1)$ $\rightarrow$ $nlj = l+1/2$ — $2l+2$; $nlj = l-1/2$ — $2l$

- MIXES SPIN + ORBITAL ANGULAR MOM.:

$$\psi_{nljm_j} = C_1\psi_{nl,m_j-1/2}\underbrace{\begin{pmatrix}1\\0\end{pmatrix}}_{m_s=+1/2\ \equiv\ \uparrow} + C_2\psi_{nl,m_j+1/2}\underbrace{\begin{pmatrix}0\\1\end{pmatrix}}_{m_s=-1/2\ \equiv\ \downarrow}$$

WITH C1 AND C2 TABULATED CLEBSCH-GORDAN OR WIGNER 3j SYMBOLS

Photoelectron spin polarization from spin-orbit coupling and circularly-polarized radiation—The Fano Effect

$$P_{3/2} = -50\% = \frac{I_{up} - I_{down}}{I_{up} + I_{down}} = \frac{\sqrt{1/3}^2 - 1^2}{\sqrt{1/3}^2 + 1^2} x100$$

$$= \frac{-2/3}{4/3} x100 = -50\%$$

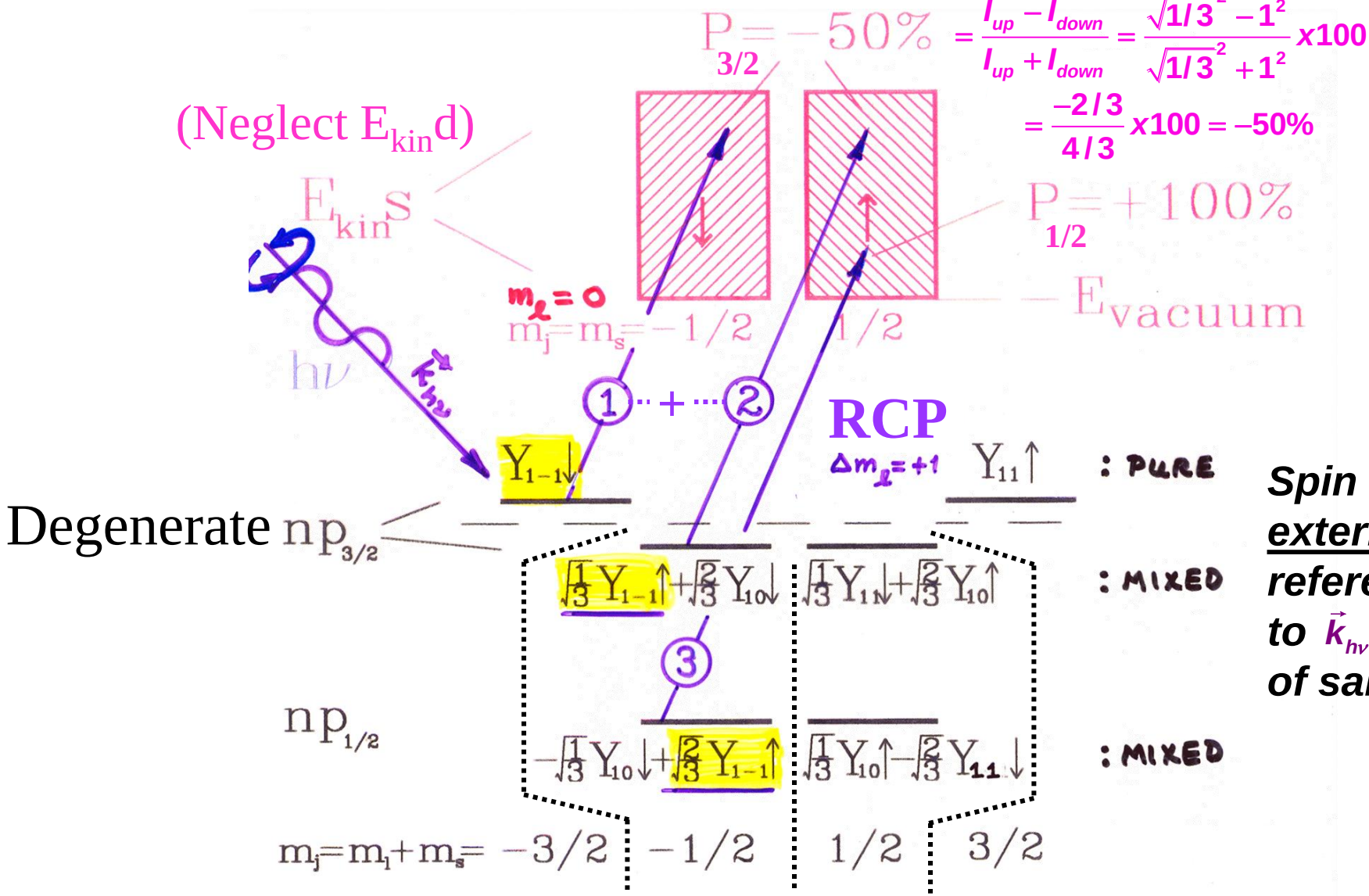

Spin externally referenced to $\vec{k}_{h\nu}$ and $\vec{M}$ of sample

Photoelectron spin polarization from spin-orbit coupling and circularly-polarized radiation—The Fano Effect

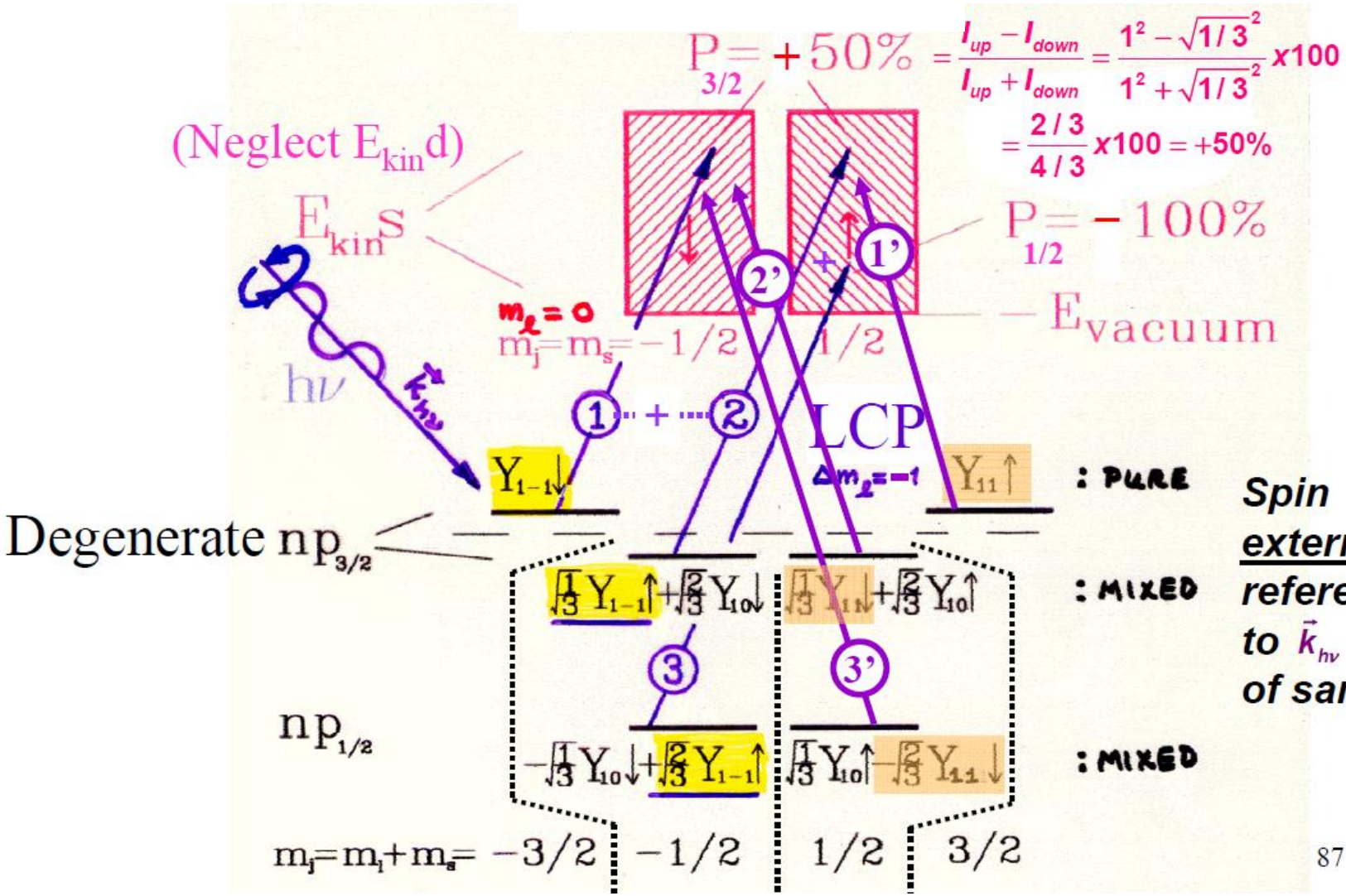

Spin externally referenced to $\vec{k}_{h\nu}$ and $\vec{M}$ of sample

Fano effect and Spin polarization in core photoelect

SPIN-ORBIT SPLIT LEVEL EXCITED WITH CIRCULAR POLARIZATION (FANO EFFECT)

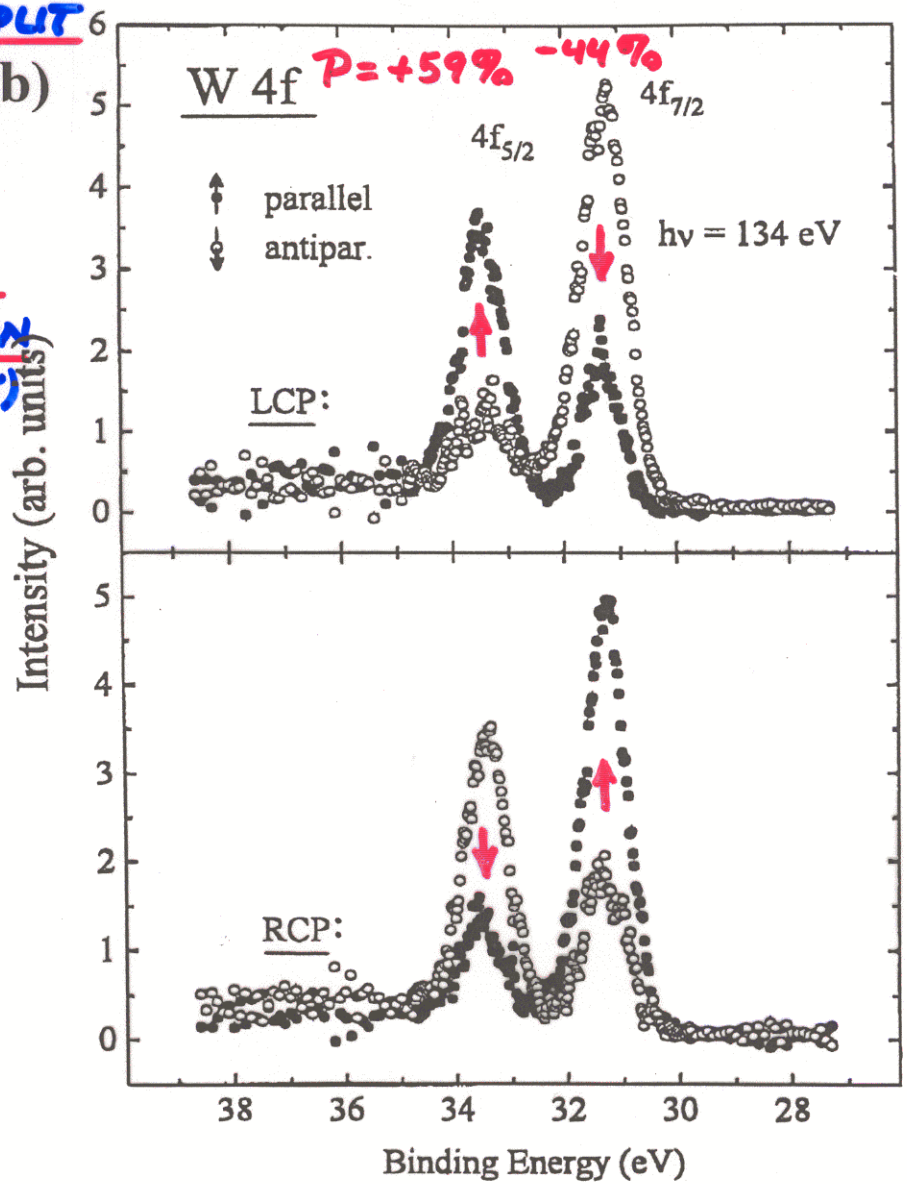

EXPT. - STARKE ET AL. PRB 53, R10544 (1996)

Basic Concepts and Experiments

Core-Level Photoemission

Intensities and Quantitative Analysis, the 3-Step Model
Varying Surface and Bulk Sensitivity
Chemical shifts
Multiplet Splittings
Electron Screening and Satellite Structure
Magnetic and Non-Magnetic Dichroism
Resonant Photoemission
Photoelectron Diffraction and Holography

Valence-Level Photoemission

Band-Mapping in the Ultraviolet Photoemission Limit
Densities of States in the X-Ray Photoemission Limit

Some New Directions

Photoemission with Hard X-Rays (throughout lectures)
Photoemission with Standing Wave Excitation
Photoemission with Spatial Resolution/Photoelectron Microscopy
Temporal Resolution
@ Higher Pressures

Resonant Photoemission—Mn 3d

J. J. YEH and I. LINDAU Subshell Photoionization Cross Sections

ATOMIC + NUCLEAR DATA TABLES 32, 45 (1985)

GRAPH I. Atomic Subshell Photoionization Cross Sections for 0–1500 eV, $1 \leq Z \leq 103$

See page 6 for Explanation of Graphs

THEORETICAL ATOMIC CROSS SECTIONS: ENTIRE PERIODIC TABLE

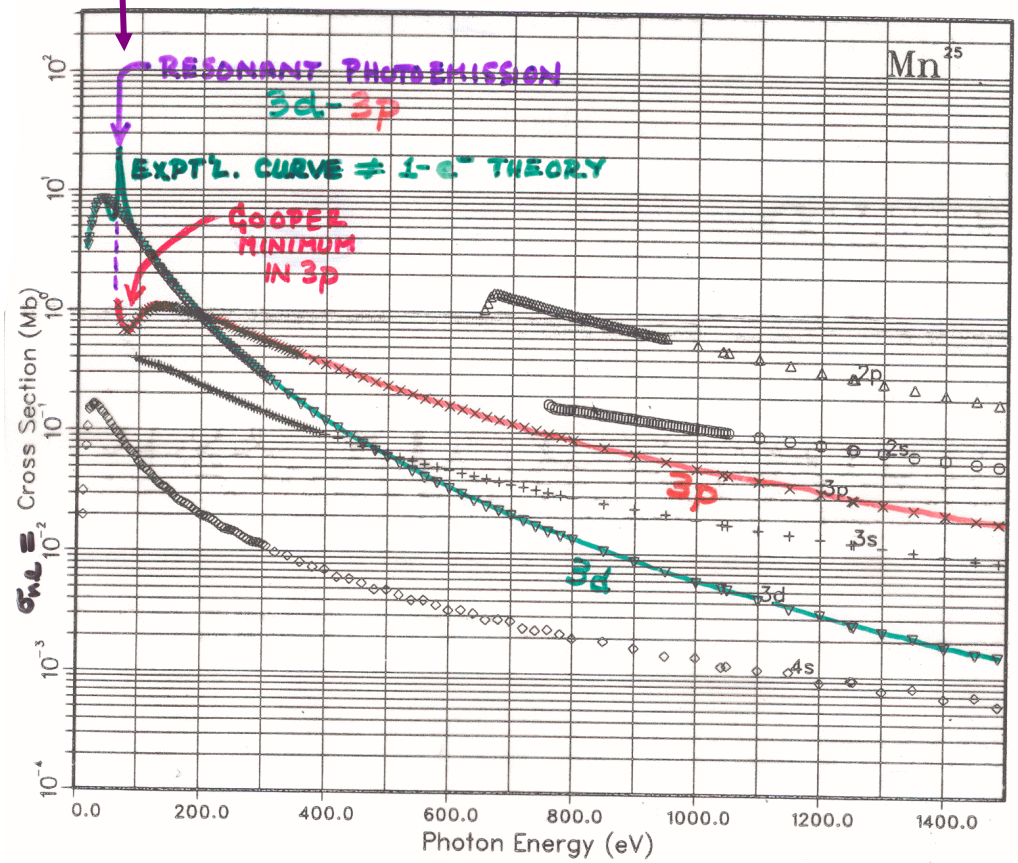

Mn binding energies(eV) are:

1s(2) 6455.26	2s(2) 755.155	2p(6) 653.681
3s(2) 90.8814	3p(6) 60.9150	4s(2) 7.14671
3d(5) 12.0486		

Resonant Photoemission—Mn 3d

Ex. – Mn atom: Mn3d emission, resonance with Mn3p

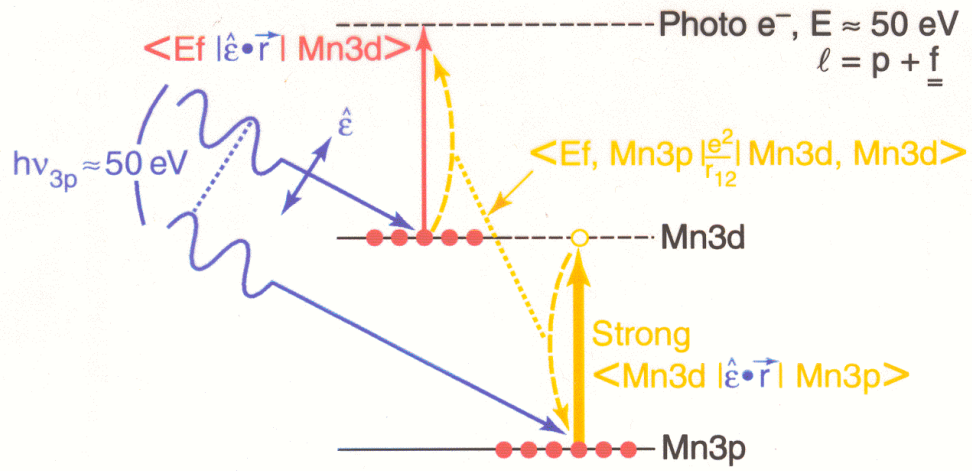

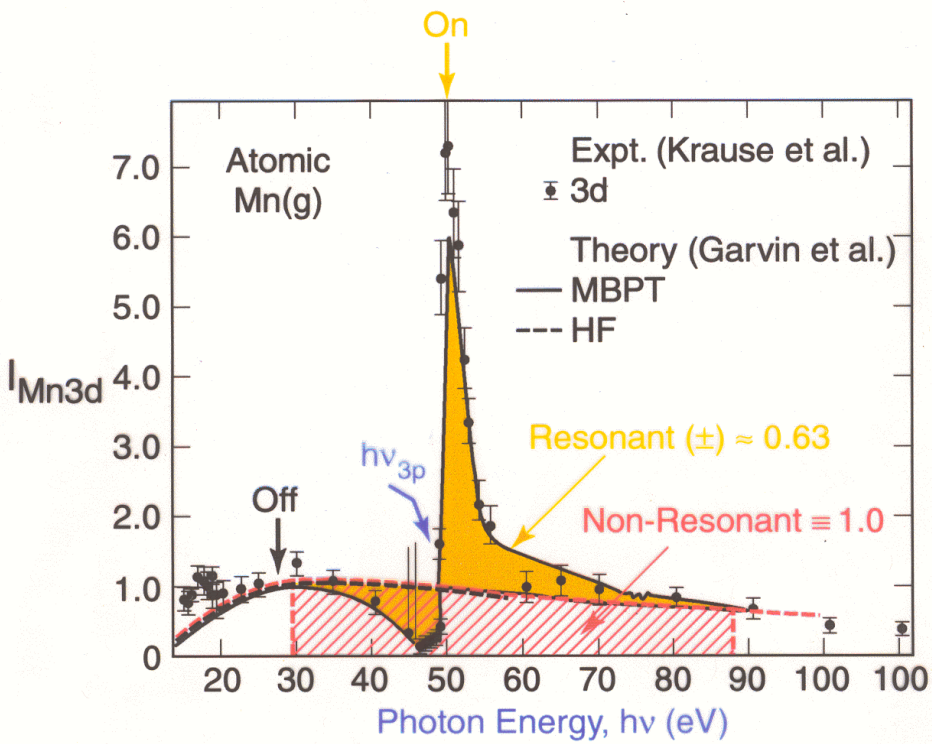

MATRIX ELEMENTS IN THE SOFT X-RAY SPECTROSCOPIES: RESONANT EFFECTS

- ***Resonant photoemission:***

$$I \propto \left| \langle \varphi_f(1) | \hat{e} \bullet \vec{r} | \phi_i(1) \rangle + \sum_m \langle \varphi_f(1)\varphi_1(2) | \frac{e^2}{r_{12}} | \varphi_i(1)\varphi_m(2) \rangle \langle \varphi_m(1) | \hat{e} \bullet \vec{r} | \varphi_1(1) \rangle \right|^2 \times \delta(h\nu - (E_m - E_1))$$

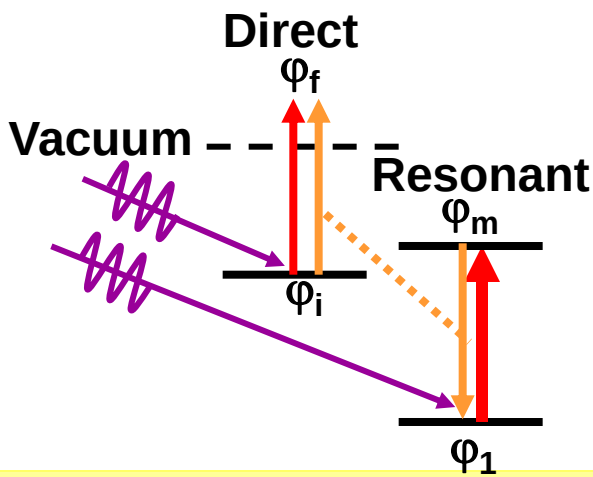

- ***Resonant inelastic x-ray scattering:***

$$I \propto \sum_f \left| \sum_m \frac{\langle \Psi_f(N) | \hat{e} \bullet \vec{r} | \Psi_m(N) \rangle \langle \Psi_m(N) | \hat{e} \bullet \vec{r} | \Psi_i(N) \rangle}{h\nu + E_i(N) - E_m(N) - i\Gamma} \right|^2 \times \delta(h\nu - (E_m(N) - E_i(N)))$$

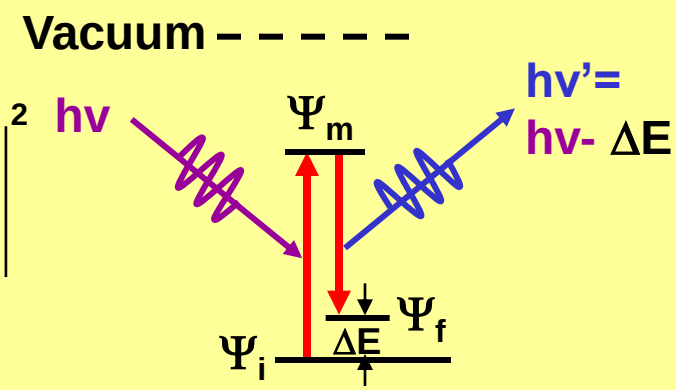

Resonant Photoemission—$La_{0.6}Sr_{0.4}MnO_3$, Mn 3d with Mn 2p

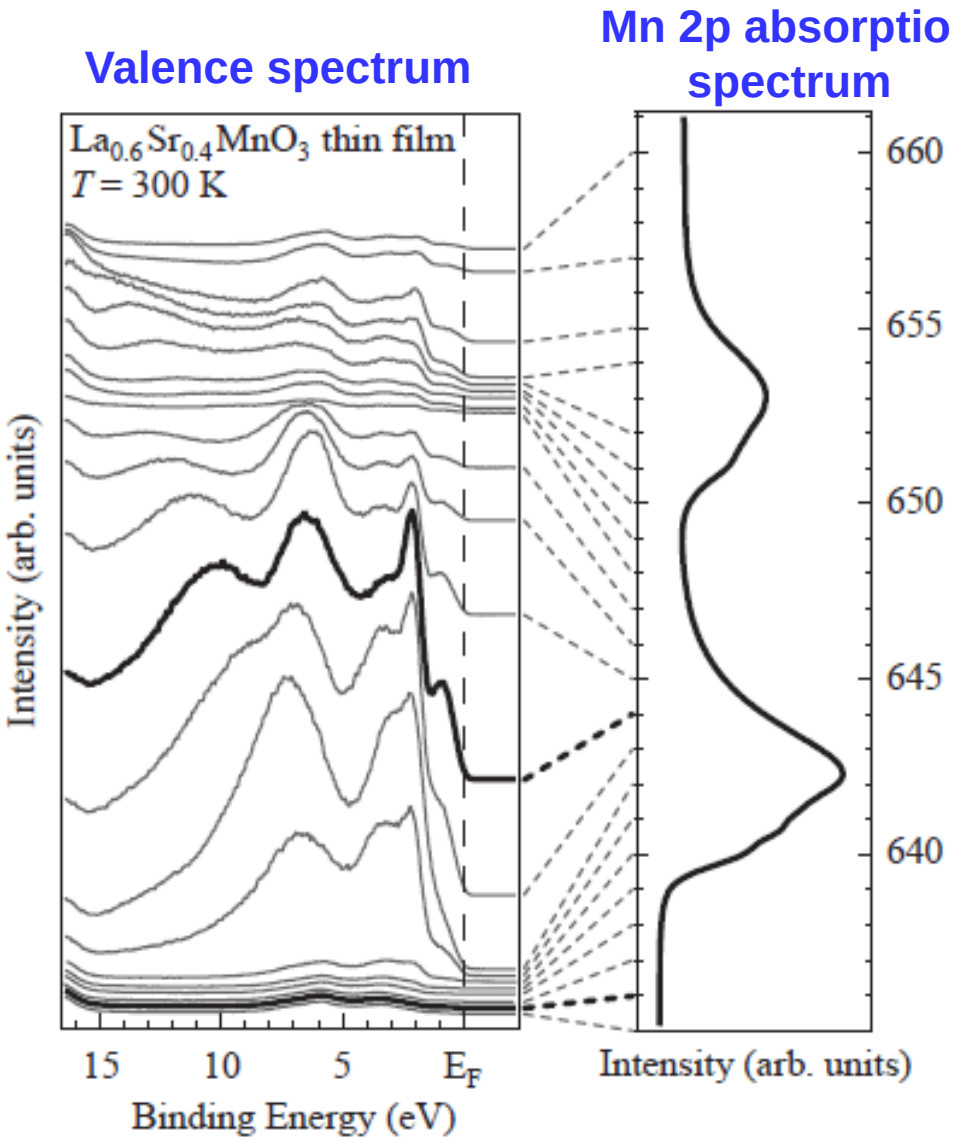

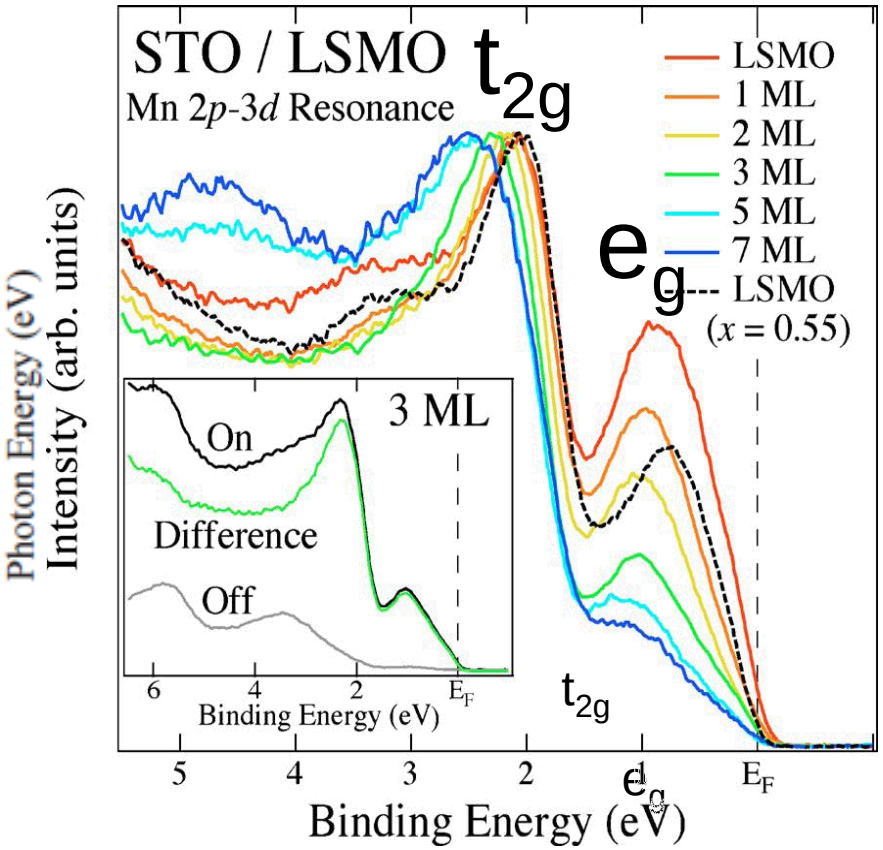

Prior resonant PS: Fujimori et al., J.A.P 99, 08S903 (2006)

K. Horiba et al. / Journal of Magnetism and Magnetic Materials 272–276 (2004) 436–437

Basic Concepts and Experiments

Core-Level Photoemission

Intensities and Quantitative Analysis, the 3-Step Model
Varying Surface and Bulk Sensitivity
Chemical shifts
Multiplet Splittings
Electron Screening and Satellite Structure
Magnetic and Non-Magnetic Dichroism
Resonant Photoemission
Photoelectron Diffraction and Holography

Valence-Level Photoemission

Band-Mapping in the Ultraviolet Photoemission Limit
Densities of States in the X-Ray Photoemission Limit

Some New Directions

Photoemission with Hard X-Rays (throughout lectures)
Photoemission with Standing Wave Excitation
Photoemission with Spatial Resolution/Photoelectron Microscopy
Temporal Resolution
@ Higher Pressures

Typical experimental geometry for energy- and angle-resolved photoemission measurements

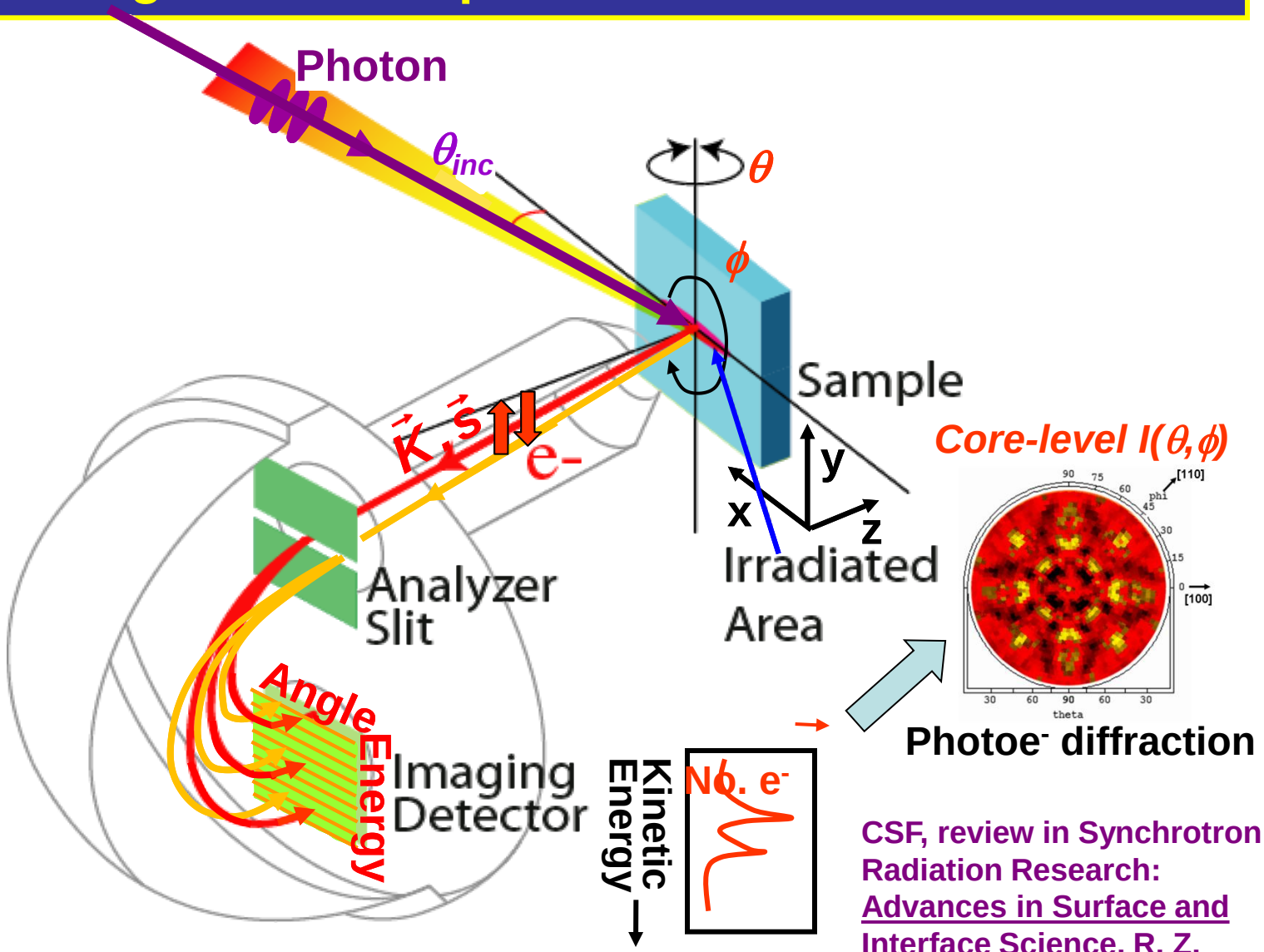

CSF, review in Synchrotron Radiation Research: Advances in Surface and Interface Science, R. Z. Bachrach, Ed. (Plenum Press, New York, 1992).

PHOTOELECTRON INTENSITIES—THE 3-STEP MODEL

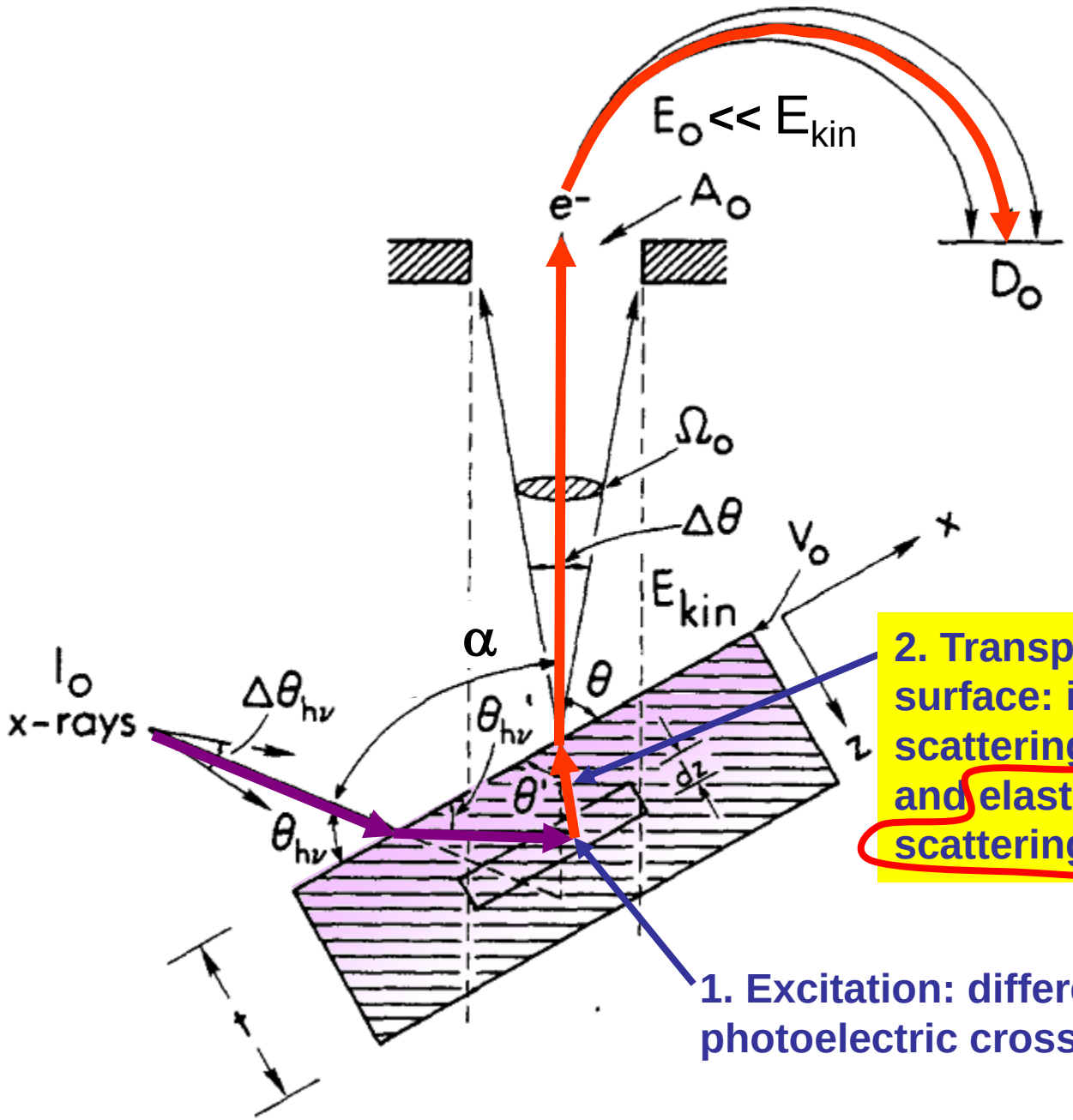

2. Transport to the surface: inelastic scattering (Λ_o) and elastic scattering ($f(\theta)$--later)

1. Excitation: differential photoelectric cross section ($d\sigma/d\Omega$)

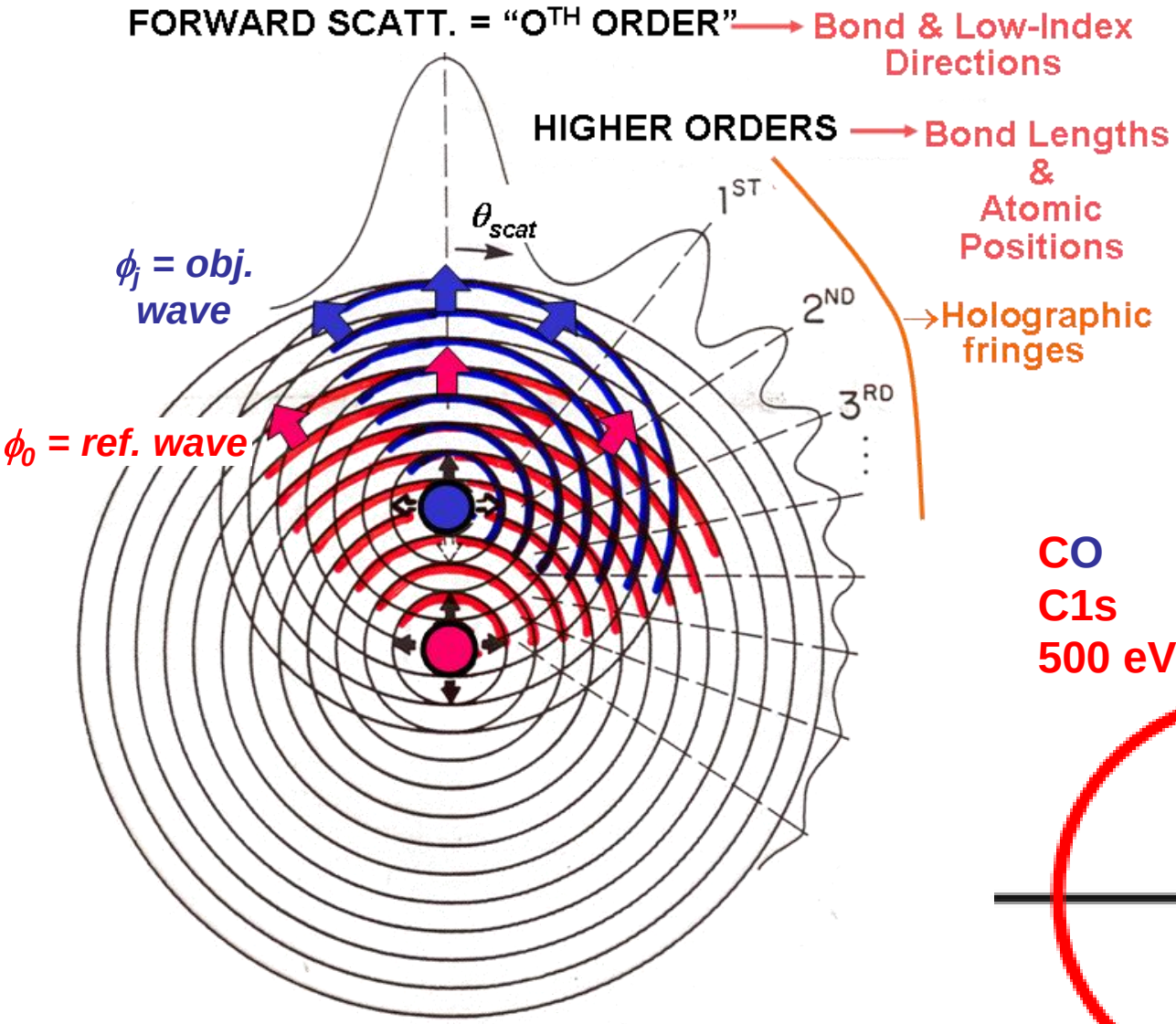

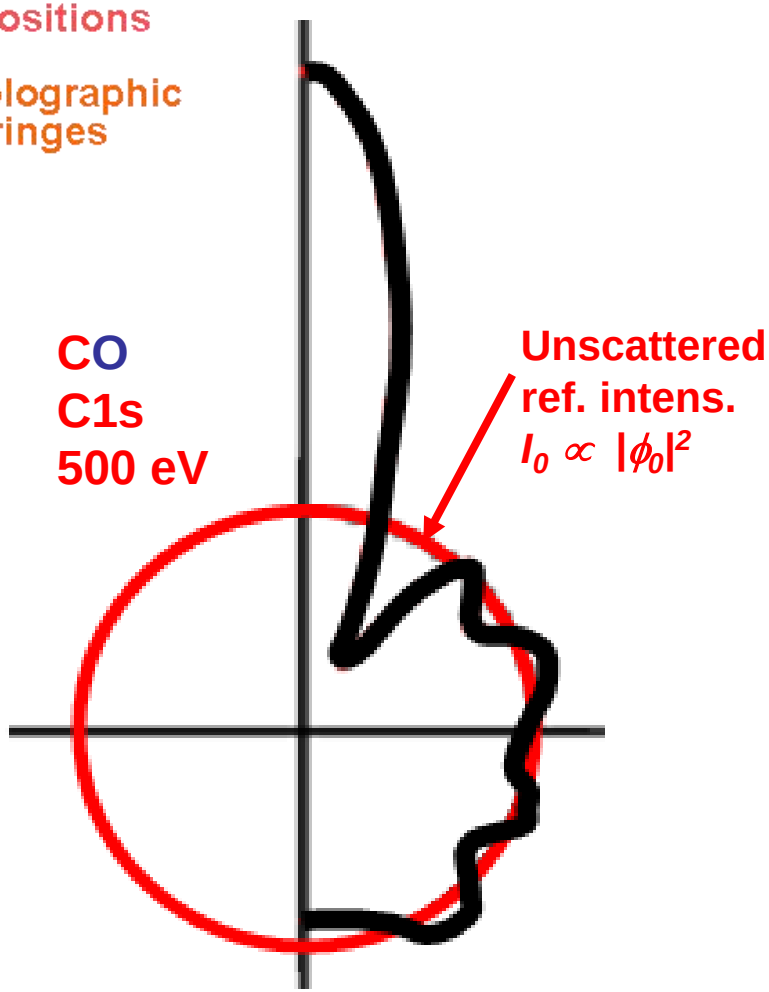

Photoelectron Diffraction

EDAC program: Javier Garcia de Abajo

http://nanophotonics.csic.es/static/widgets/edac/index.html

Photoelectron Diffraction: Single Scattering Theory

$$I(\vec{k}_f) = \left| \varphi_0 + \sum_{Scatterers,\, j} \varphi_j \right|^2$$

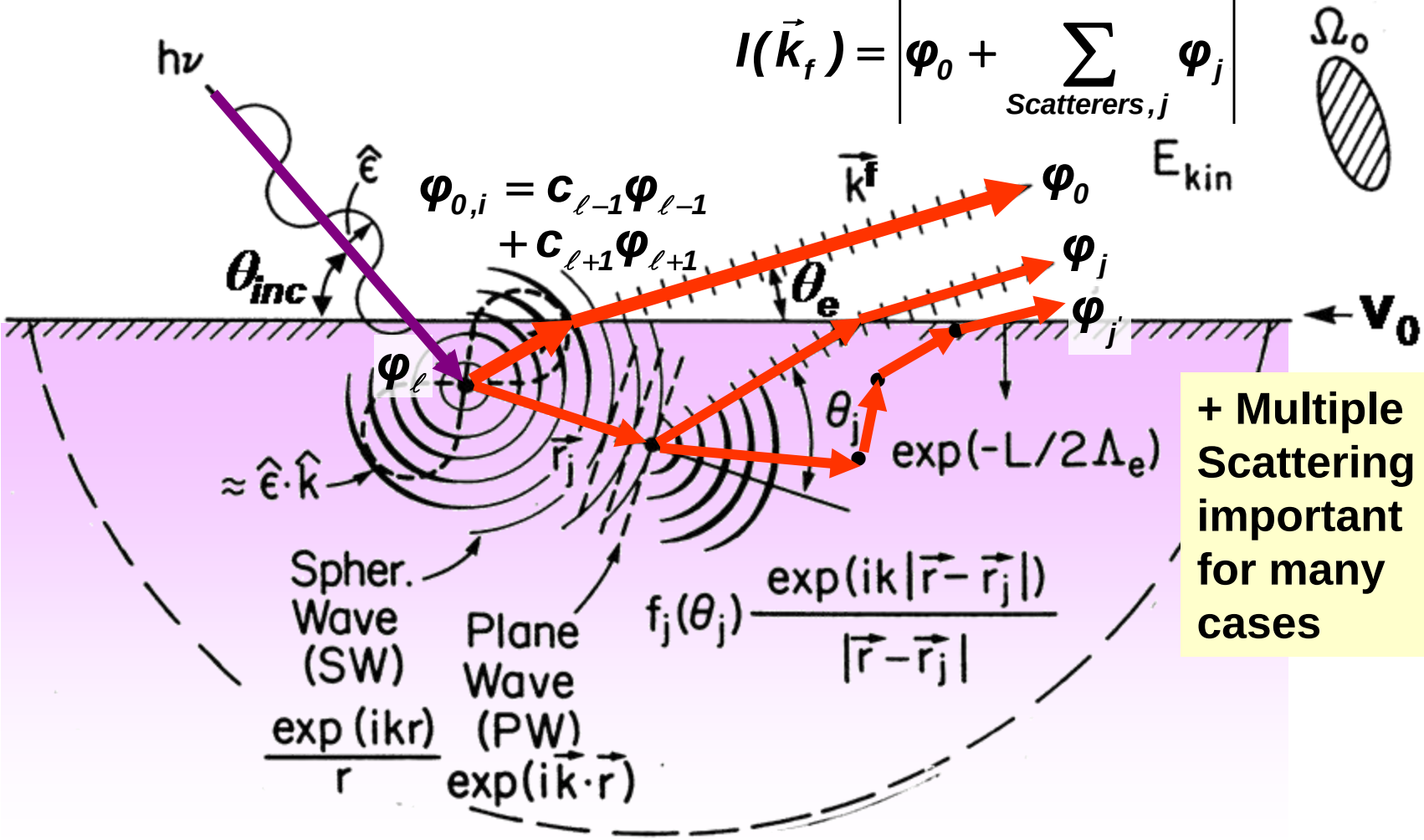

+ Multiple Scattering important for many cases

ENERGY DEPENDENCE OF ELECTRON ELASTIC SCATTERING

$$f(\theta) = |f(\theta)| e^{i\psi(\theta)}$$

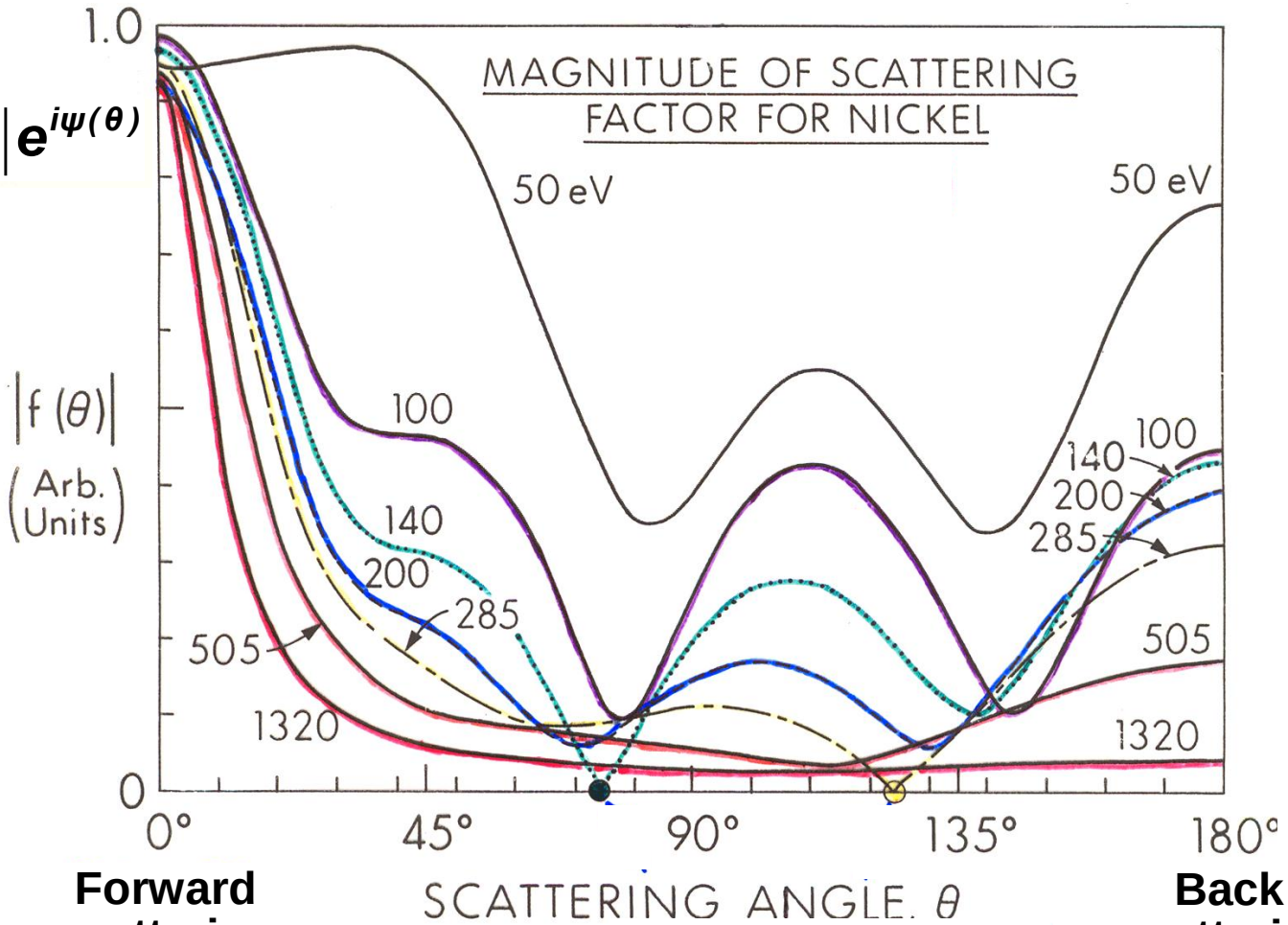

Forward scattering

Back scattering

Sagurton et al.
Surf. Sci. 182, 287 ('84)

X-ray Photoelectron Diffraction:1ML FeO on Pt(111)

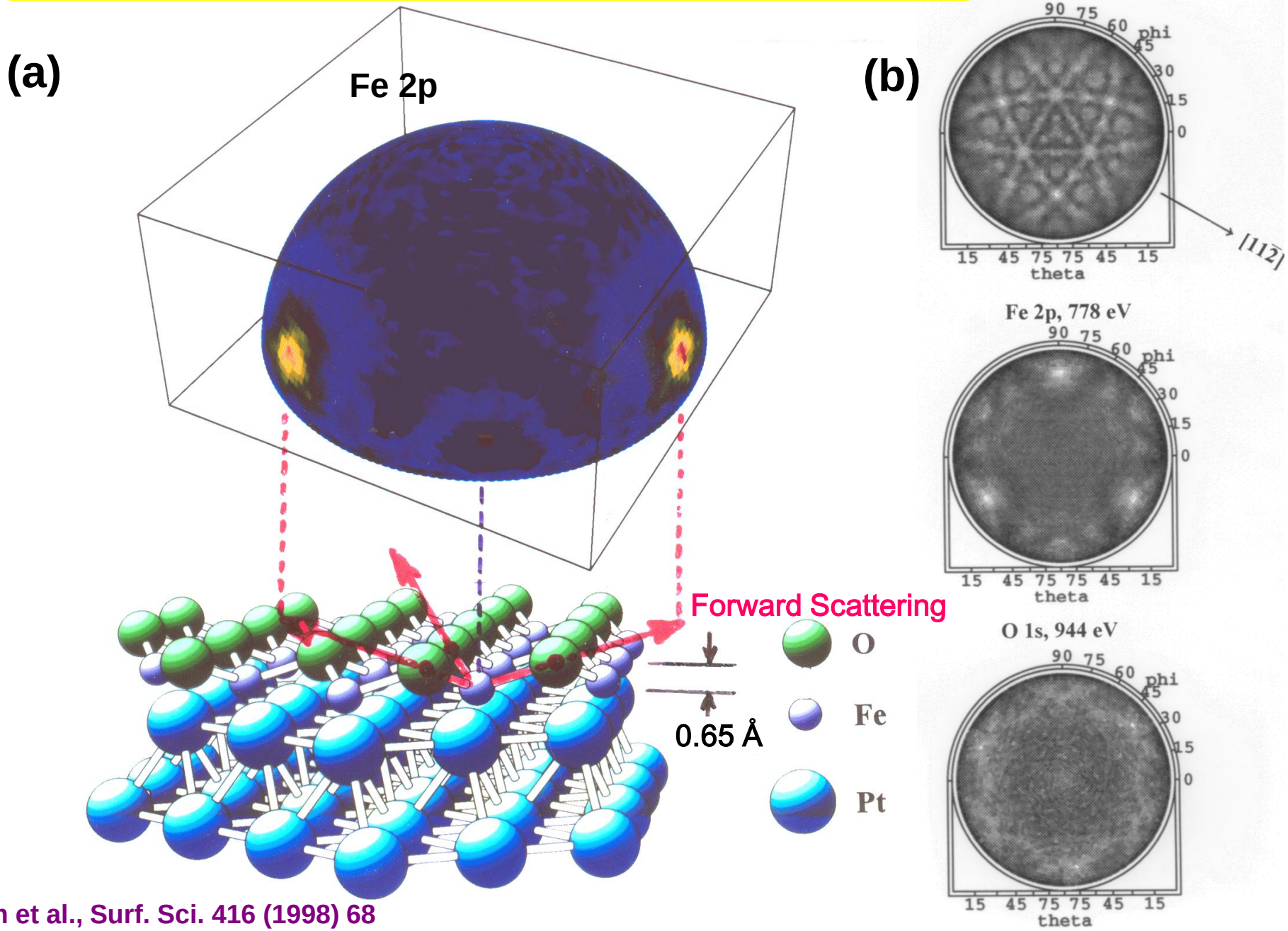

Kim et al., Surf. Sci. 416 (1998) 68

Energy dependence of photoelectron diffraction: Theory

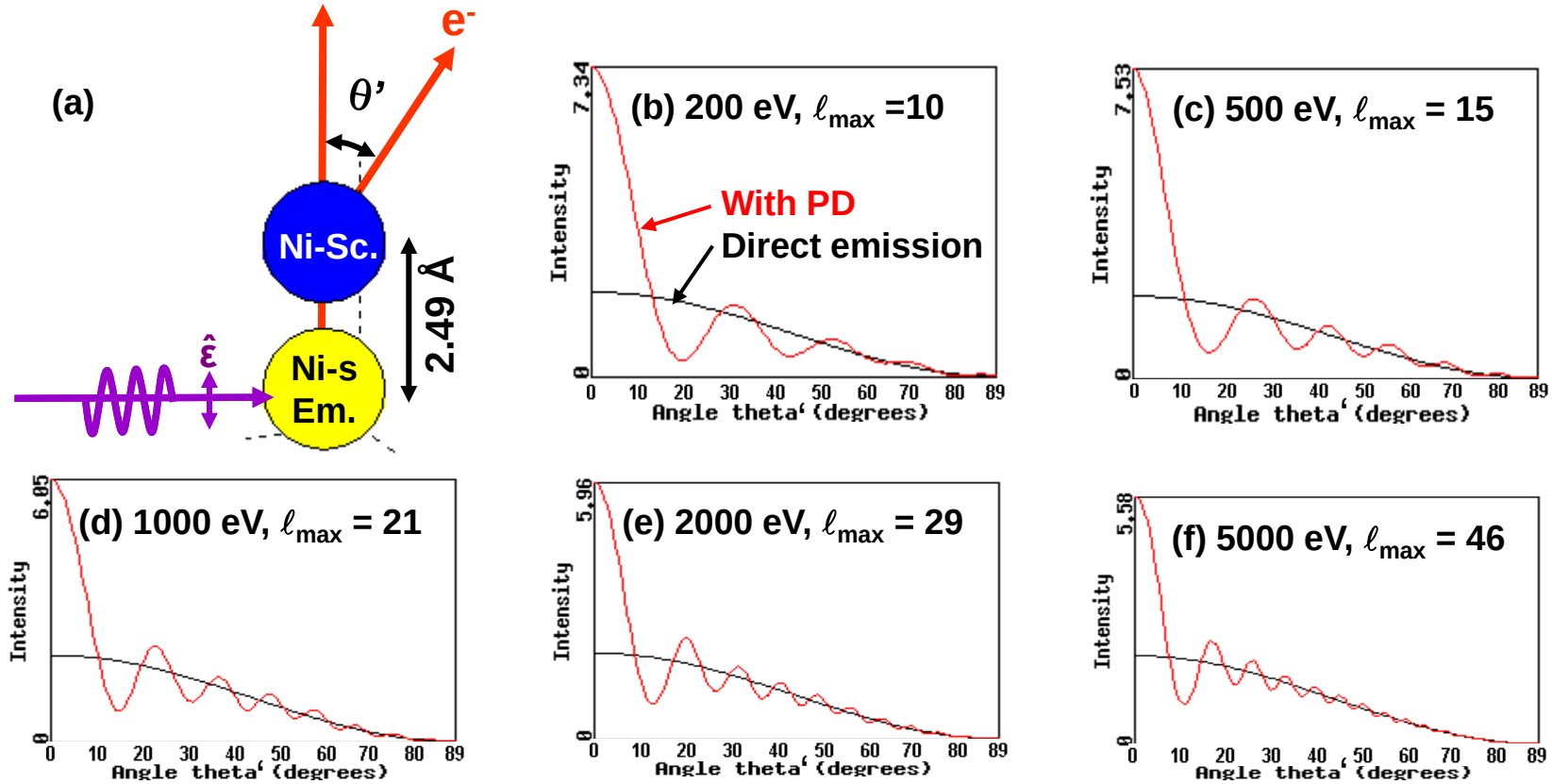

Much more forward peaked at higher energy, weaker in directions away from forward

Photoelectron Diffraction with soft and hard x-ray excitation: two viewpoints

The scattering of photoelectrons from localized sources can be described in real space (multiple scattering cluster) and reciprocal space (dynamical theory of electron diffraction)

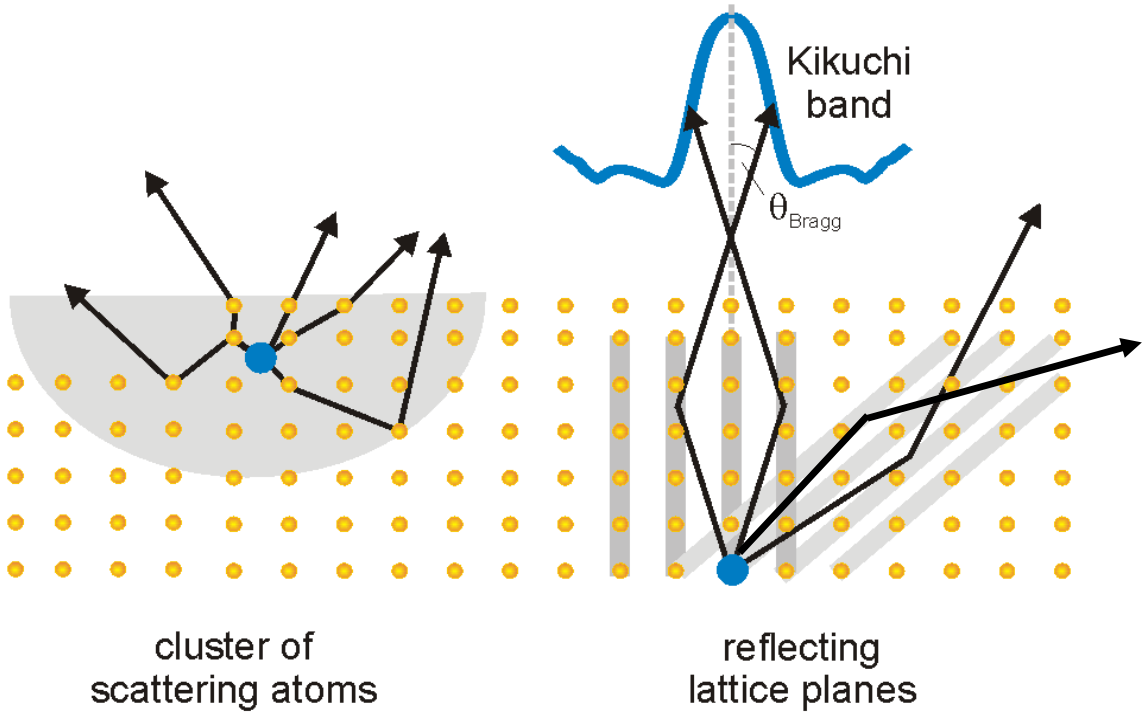

Soft x-ray excitation → Hard x-ray excitation

A. Winkelmann et al, New J. Phys 10 (2008) 113002

Photoelectron Diffraction with soft and hard x-ray excitation: two viewpoints, expt. vs. theory

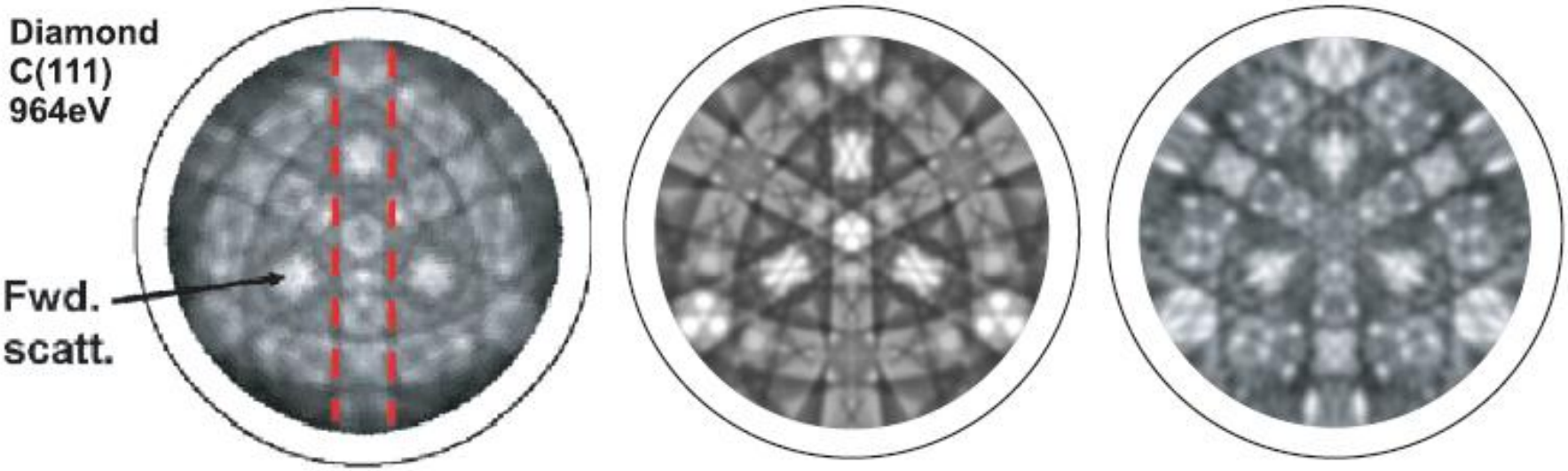

(a) experiment

Osterwalder et al.

(b) dynamical simulation

(c) multiple scattering simulation (EDAC)

A. Winkelmann et al, New J. Phys 10 (2008) 113002

Bulk sensitive HXPD of Si 1s

Native SiO_2 /Si(001)

hν = 5417 eV

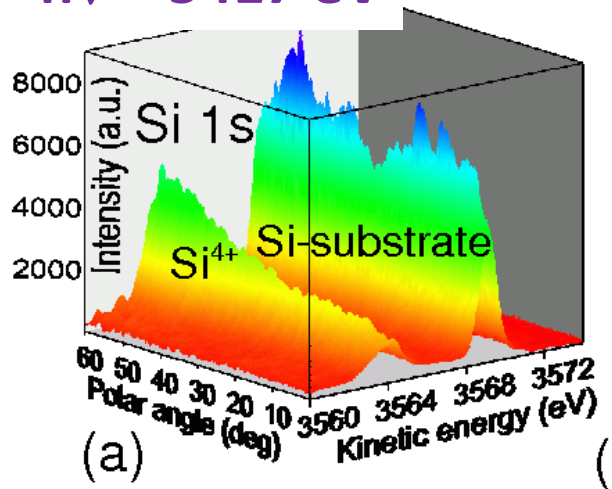

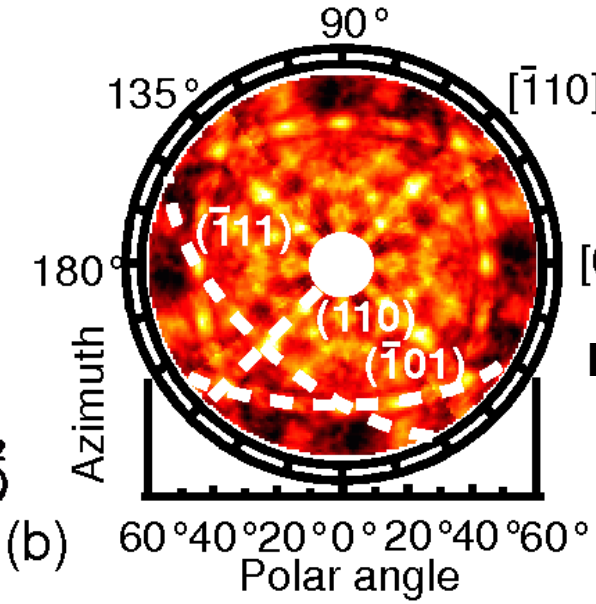

H-Si(001)

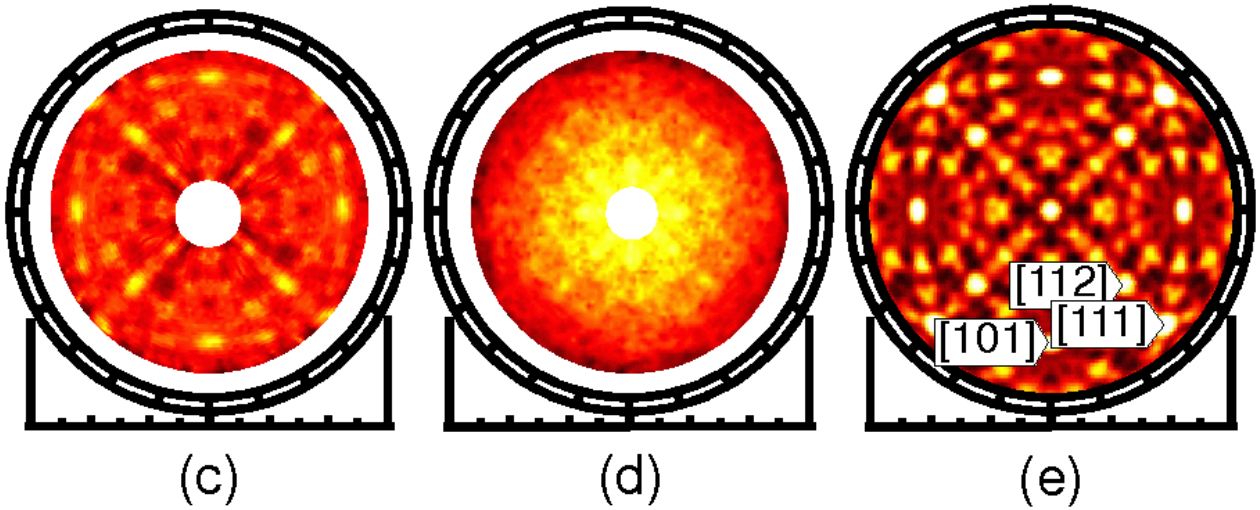

4.1 nm SiO_2/Si(001) **7.0 nmSiO_2/Si(001)** **Multiple scattering cluster simulation**

Pis et al., Applied Physics Express 3 (2010) 056701;
Kobata et al., SPring8: Surf. Interf. Anal.,http://onlinelibrary.wiley.com/doi/10.1002/sia.3760/pdf

Hard x-ray photoelectron diffraction--Theory: Sensitivity to lattice distortions and atomic site type?

Si(111)-6 keV: Impurity atom on lattice site (Si) vs. tetrahedral interstitial (T)

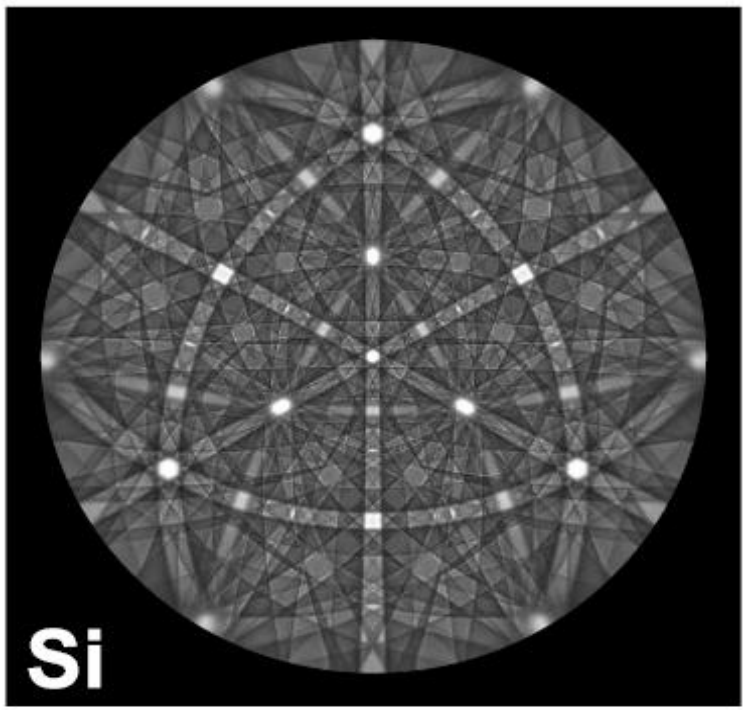

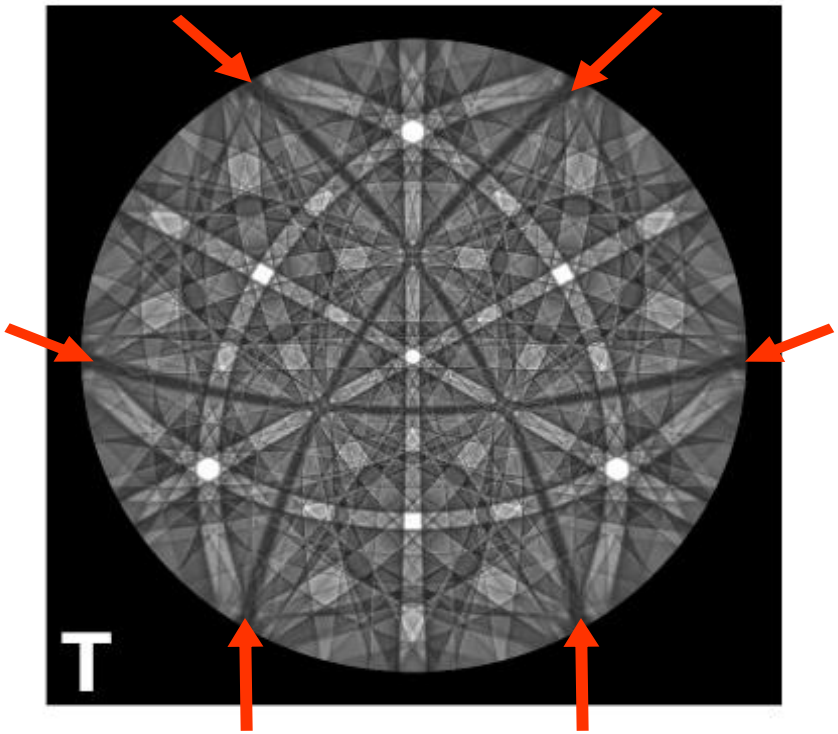

A. Winkelman, J. Garcia de Abajo, MPI Halle, CF, New Journal of Physics 10 (2008) 113002

Missing Kikuchi bands-->"forbidden reflections"

Basic Concepts and Experiments

Core-Level Photoemission

Intensities and Quantitative Analysis, the 3-Step Model
Varying Surface and Bulk Sensitivity
Chemical shifts
Multiplet Splittings
Electron Screening and Satellite Structure
Magnetic and Non-Magnetic Dichroism
Resonant Photoemission
Photoelectron Diffraction and Holography

Valence-Level Photoemission

Band-Mapping in the Ultraviolet Photoemission Limit
Densities of States in the X-Ray Photoemission Limit

Some New Directions

Photoemission with Hard X-Rays (throughout lectures)
Photoemission with Standing Wave Excitation
Photoemission with Spatial Resolution/Photoelectron Microscopy
Temporal Resolution
@ Higher Pressures

Diffraction and Holography: What's the Difference?

Holography:

Reference and scattered interfere→ phase relation preserved

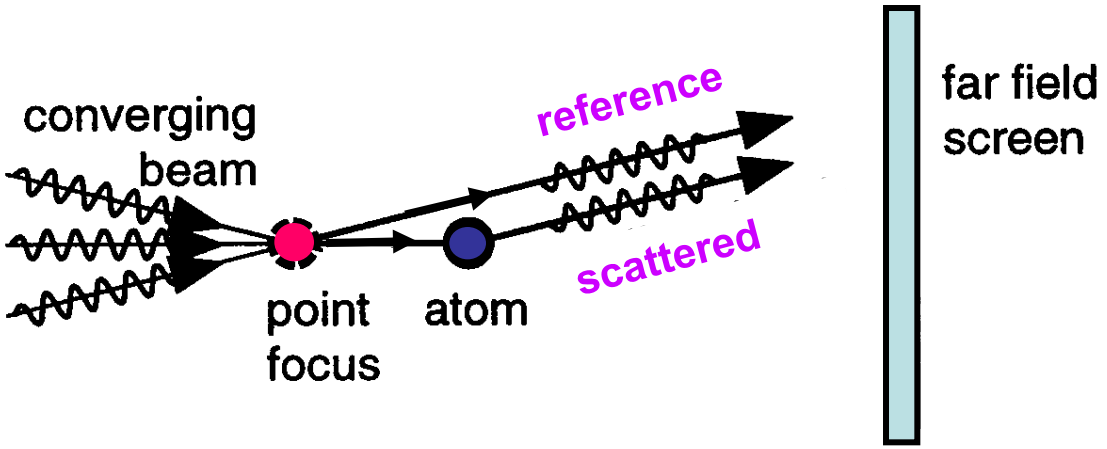

Diffraction:

Reference lost→ "The phase problem": solved for x-rays via "direct methods", multiple anomalous dispersion, isomorphous replacement

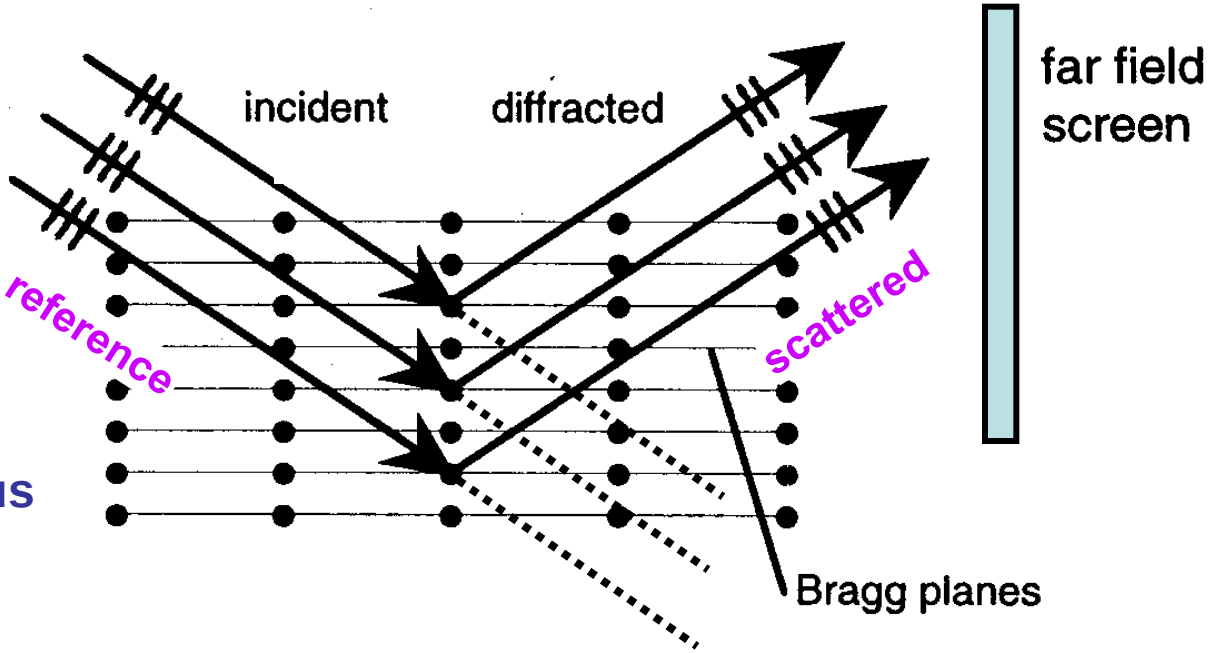

Photoelectron Holography: An Additional Trick

Holography:

Reference and scattered interfere→ phase relation preserved

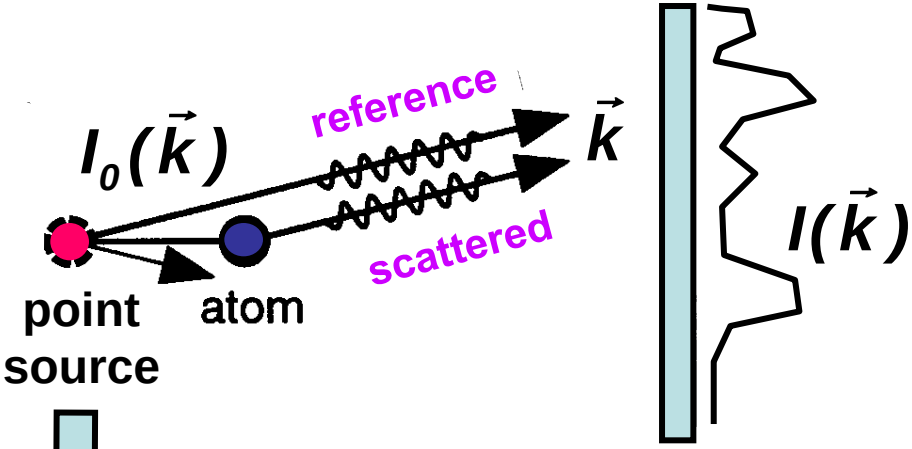

Use an "inside-source": atomic or nuclear emitter (Szöke, in "Short Wavelength Radiation: Generation and Applications", D. Attwood and J. Bokor, Eds., AIP Conference Proceedings No. 147 (1986))

$$\chi(\vec{k}) = [I(\vec{k}) - I_0(\vec{k})] / I_0(\vec{k})$$

Holographic image of scatterers =

$$U(\vec{r}) = \left| \iiint \chi(\vec{k}) \exp[i\vec{k} \bullet \vec{r} - ikr] d^3 k \right|$$

Differential photoelectron holography in Cu(001) —Cu 3p emission

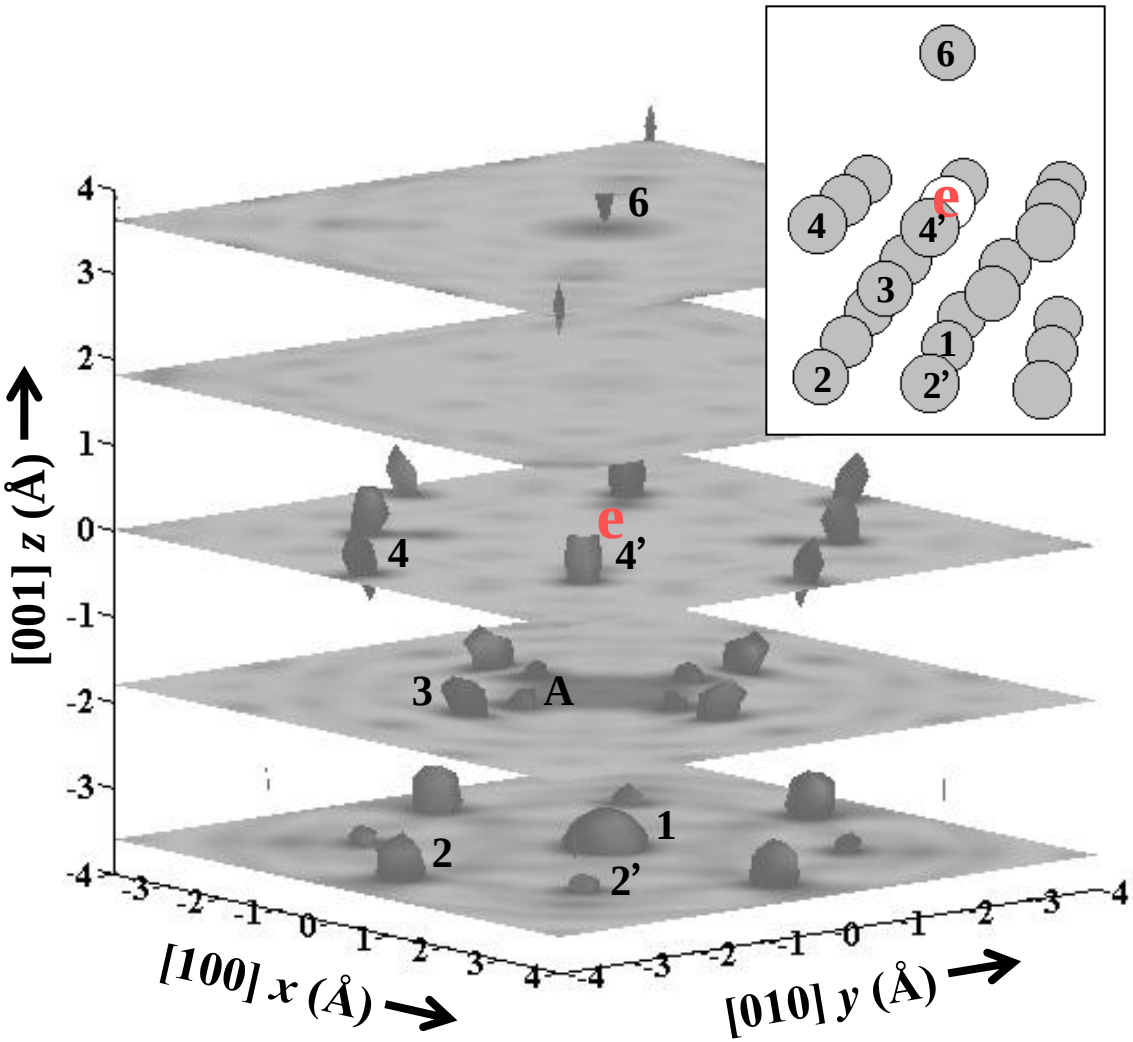

Omori et al., Phys. Rev. Lett. 88 (2002) 5504

Derivative photoelectron holography: As and Si emission from As/Si(111):

$$U(\vec{r}) = \left| \iiint \chi(\vec{k}) \exp[i\vec{k}\cdot\vec{r} - ikr] d^3k \right|$$

$$\text{with } \chi = \frac{I(\vec{k}) - I_0}{I_0}$$

and $I(\vec{k})$ from integration of logarithmic derivative

$$L(h\nu, \hat{k}) = \frac{I(h\nu + \delta, \hat{k}) - I(h\nu - \delta, \hat{k})}{\left[I(h\nu + \delta, \hat{k}) + I(h\nu - \delta, \hat{k}) \right] \delta}$$

$$I(\vec{k}) \equiv I(k, \hat{k}) = A \int L(h\nu, \hat{k}) d^3k$$

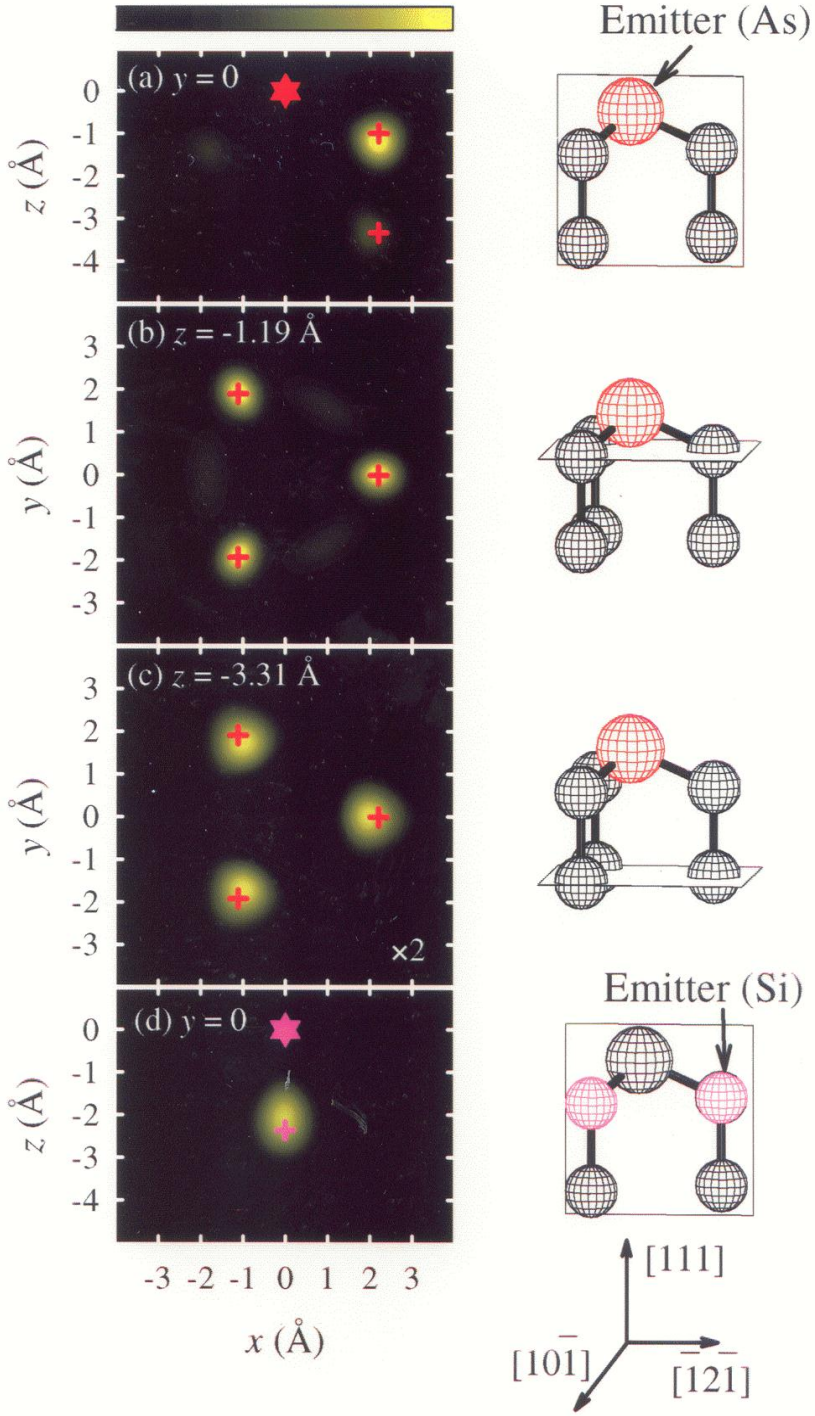

Luh et al. Phys. Rev. Lett., 81, 4160 (1998)

Basic Concepts and Experiments

Core-Level Photoemission

Intensities and Quantitative Analysis, the 3-Step Model
Varying Surface and Bulk Sensitivity
Chemical shifts
Multiplet Splittings
Electron Screening and Satellite Structure
Magnetic and Non-Magnetic Dichroism
Resonant Photoemission
Photoelectron Diffraction and Holography

Valence-Level Photoemission

Band-Mapping in the Ultraviolet Photoemission Limit
Densities of States in the X-Ray Photoemission Limit

Some New Directions

Photoemission with Hard X-Rays (throughout lectures)
Photoemission with Standing Wave Excitation
Photoemission with Spatial Resolution/Photoelectron Microscopy
Temporal Resolution
@ Higher Pressures

Typical experimental geometry for energy- and angle-resolved photoemission measurements

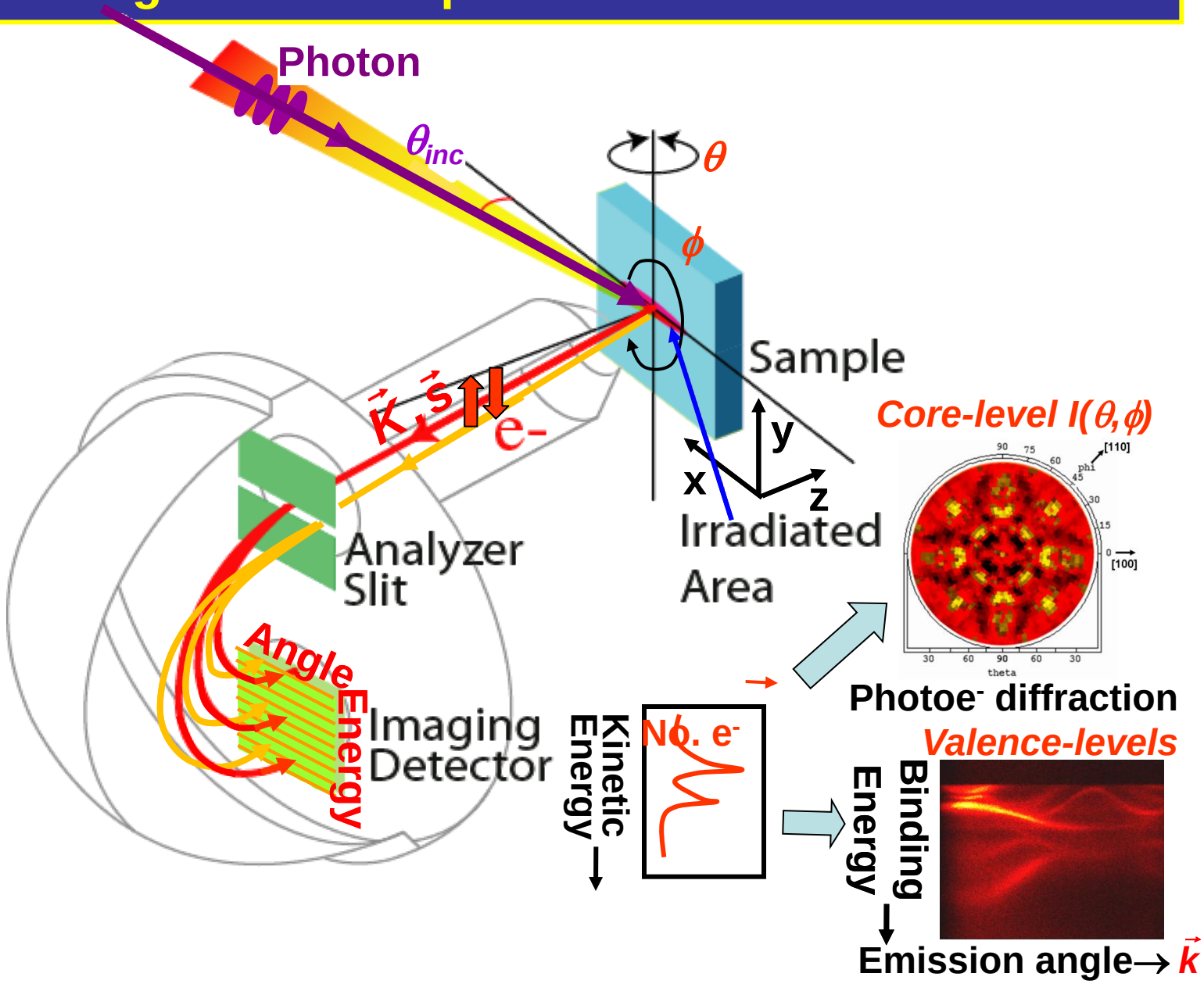

PHOTOELECTRON EMISSION – BASIC MATRIX ELEMENTS + SELECTION RULES:

• ATOMIC-LIKE (LOCALIZED) STATES ⇒ CORE:

$$\varphi_i(\vec{r}) = \varphi_{n_i l_i m_i}(r,\theta,\phi) = R_{n_i l_i}(r)\, Y_{l_i m_i}(\theta,\phi)$$

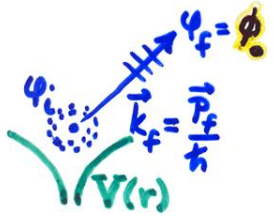

$$\varphi_f(\vec{r},\vec{k}_f) = \varphi_{E_f}(\vec{r},\vec{k}_f)$$

PHASE SHIFT OF l_f WAVE IN $V(r)$

$$= 4\pi \sum_{l_f, m_f} i^{l_f} e^{-i\delta_{l_f}} Y^*_{l_f m_f}(\theta_{k_f}, \phi_{k_f})\, Y_{l_f m_f}(\theta,\phi)\, R_{E_f, l_f}(r)$$

DIPOLE APPROX.: INT. $\propto |\langle \varphi_f | \hat{\varepsilon}\cdot\vec{r} | \varphi_i \rangle|^2 = |\hat{\varepsilon}\cdot\langle \varphi_f | \vec{r} | \varphi_i \rangle|^2 \Rightarrow$

- $\Delta l = l_f - l_i = \pm 1$ TWO CHANNELS
- $\Delta m = m_f - m_i = 0, \pm 1$ LINEAR POLARIZ.
- $\Delta m = \pm 1$, CIRCULAR POLARIZATION

EQUIVALENT WITHIN CONSTANT FACTOR

$$\vec{r} \leftrightarrow \vec{p} \leftrightarrow \vec{\nabla} V(r)$$

• BLOCH-FUNCTION (DELOCALIZED) STATES ⇒ VALENCE:

$$\varphi_i(\vec{r}) = u_{\vec{k}_i}(\vec{r})\, e^{i\vec{k}_i\cdot\vec{r}}$$

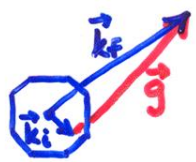

BRILLOUIN ZONE

$$\varphi_f(\vec{r}) = u_{\vec{k}_f}(\vec{r})\, e^{i\vec{k}_f\cdot\vec{r}}\ ;\ E_f = \frac{p_f^2}{2m} = \frac{\hbar^2 k_f^2}{2m}$$

USUALLY NEGLIG.

$$|\langle \varphi_f | \hat{\varepsilon}\cdot\vec{p} | \varphi_i \rangle|^2 = |\hat{\varepsilon}\cdot\langle \varphi_f | \vec{p} | \varphi_i \rangle|^2 \Rightarrow \Delta\vec{k} = \vec{k}_f - \vec{k}_i - \vec{k}_{h\nu} + \vec{k}_{PHONON}$$

$$= \vec{g}_{BULK}\ (\text{OR } \vec{g}_{SURF})$$

"DIRECT" TRANSITIONS

BUT LATTICE VIBRATIONS ⇒ SUM OVER $\vec{k}_{PHONON}$

⇒ FRACTION DIRECT ≈ DEBYE-WALLER FACTOR

$$\approx \exp[-g^2 \overline{u^2}]$$

Valence-band photoemission: Angle-Resolved Photoemission (ARPES)

$E_f(\vec{K}_f) =$

$E_f(\vec{k}_f) - V_0 \approx \hbar^2 K_f^2 / 2m_e$

$\vec{k}_{f,\parallel} = \vec{K}_{f,\parallel}$

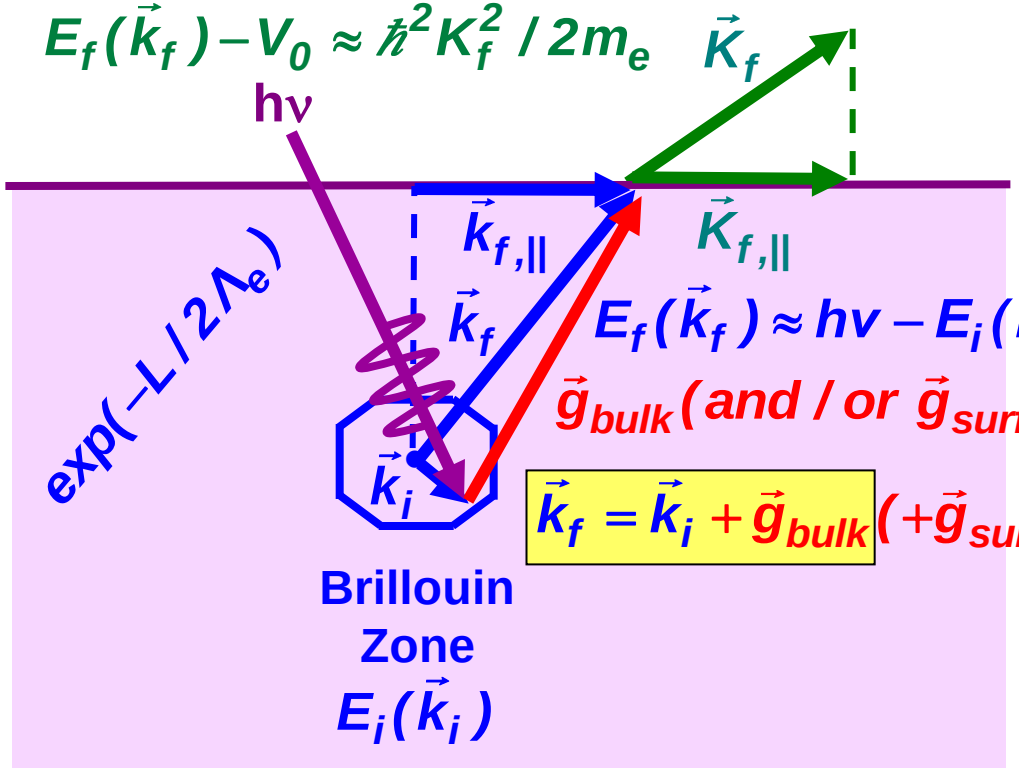

$E_f(\vec{k}_f) \approx h\nu - E_i(\vec{k}_i) \approx \hbar^2 k_f^2 / 2m_e$

$\vec{g}_{bulk}$ (and / or $\vec{g}_{surf}$)

$\vec{k}_f = \vec{k}_i + \vec{g}_{bulk} (+\vec{g}_{surf}) + \vec{k}_{h\nu} + \vec{k}_{phonon}$

High energy a/o
High temp.

$$I(E_f, \vec{k}_f) \propto \left| \hat{\varepsilon} \bullet \left\langle \varphi_{photoe}(E_f = h\nu + E_i, \vec{k}_f = \vec{k}_i + \vec{g}) \middle| \vec{r} \middle| \varphi(E_i, \vec{k}_i) \right\rangle \right|^2$$

"Direct" or k-conserving transitions

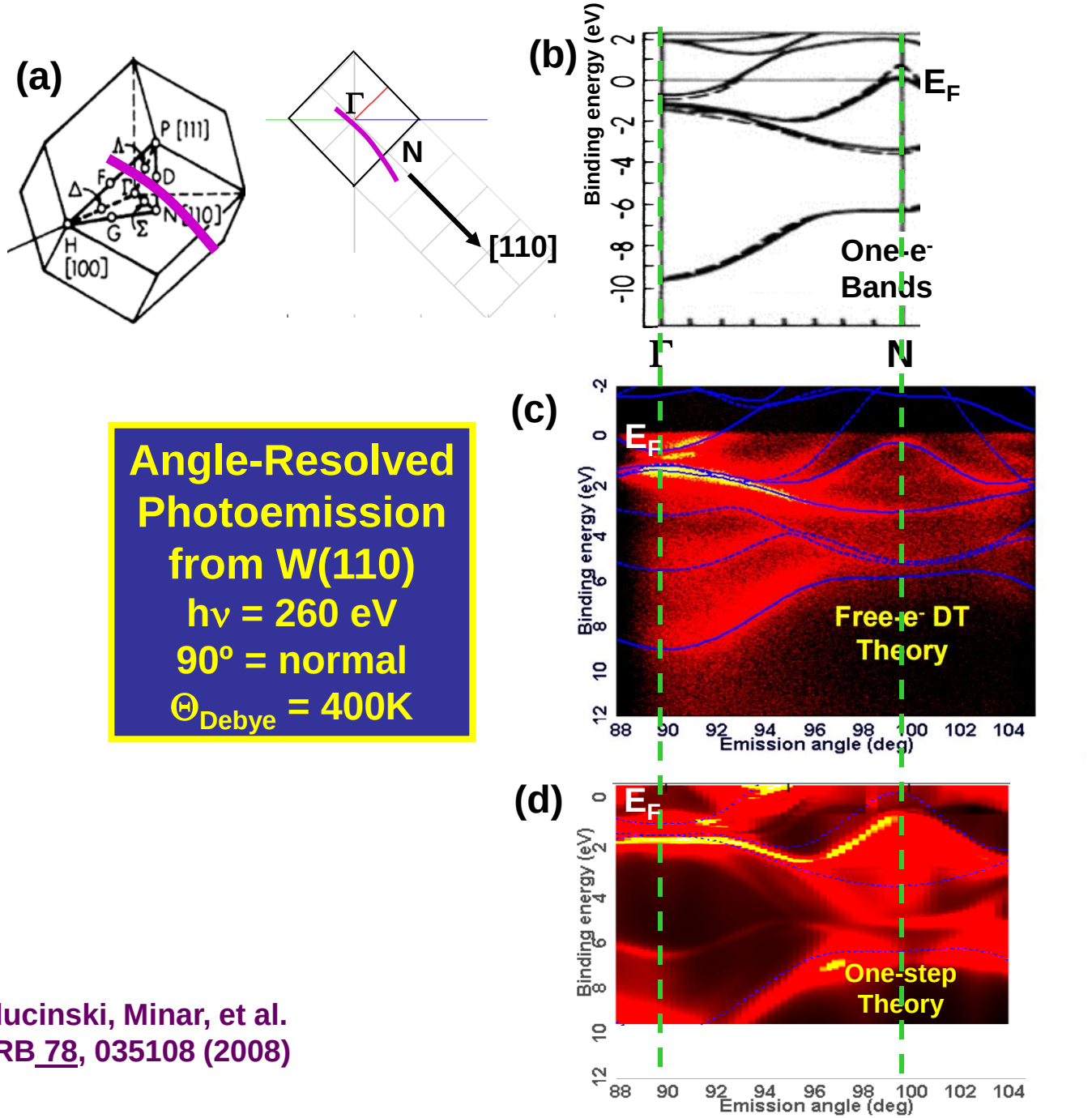

Angle-Resolved Photoemission from W(110)

$h\nu$ = 260 eV

90° = normal

Θ_{Debye} = 400K

Plucinski, Minar, et al.
PRB 78, 035108 (2008)

Typical experimental geometry for energy- and angle-resolved photoemission measurements

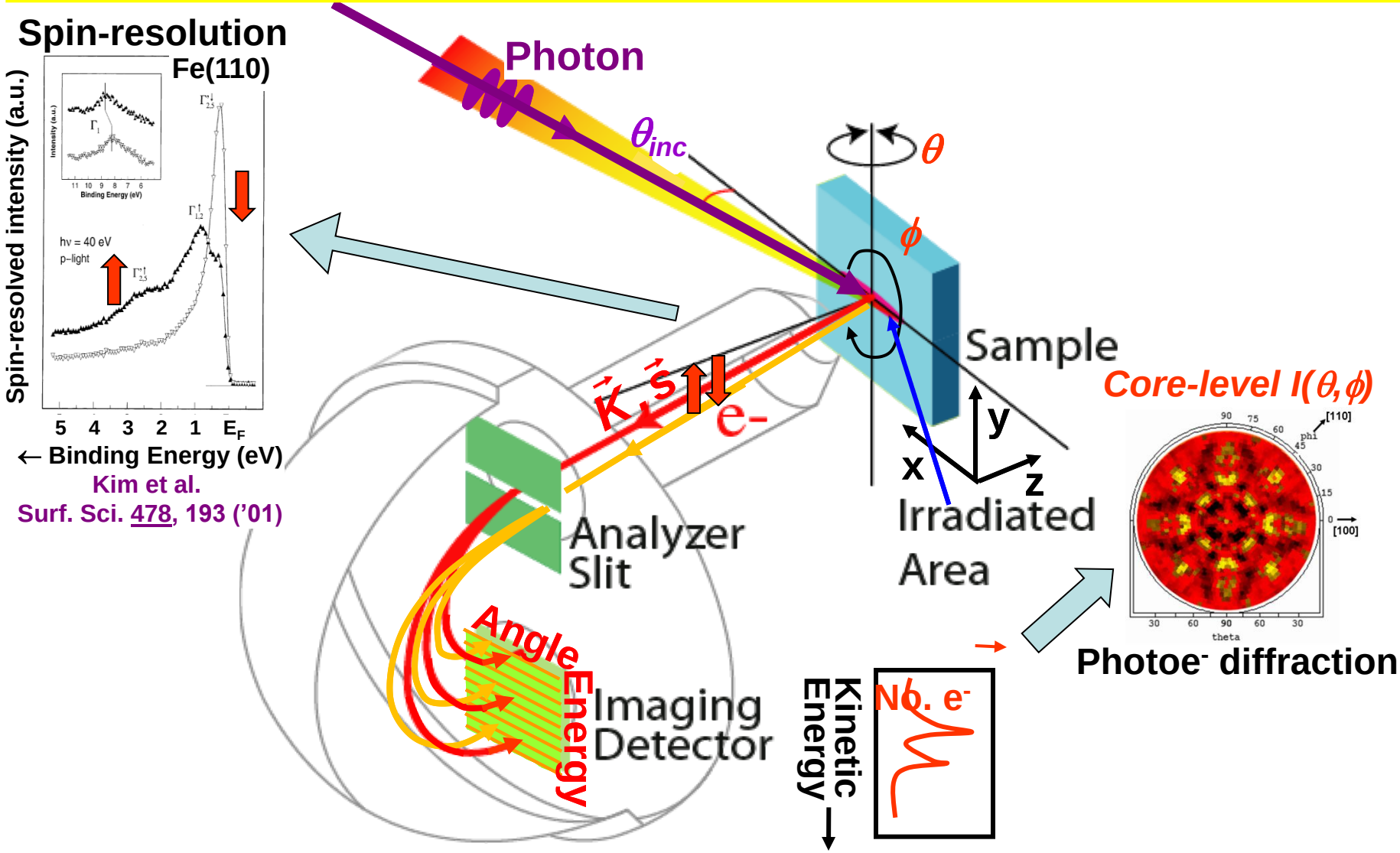

Band structure of Nickel

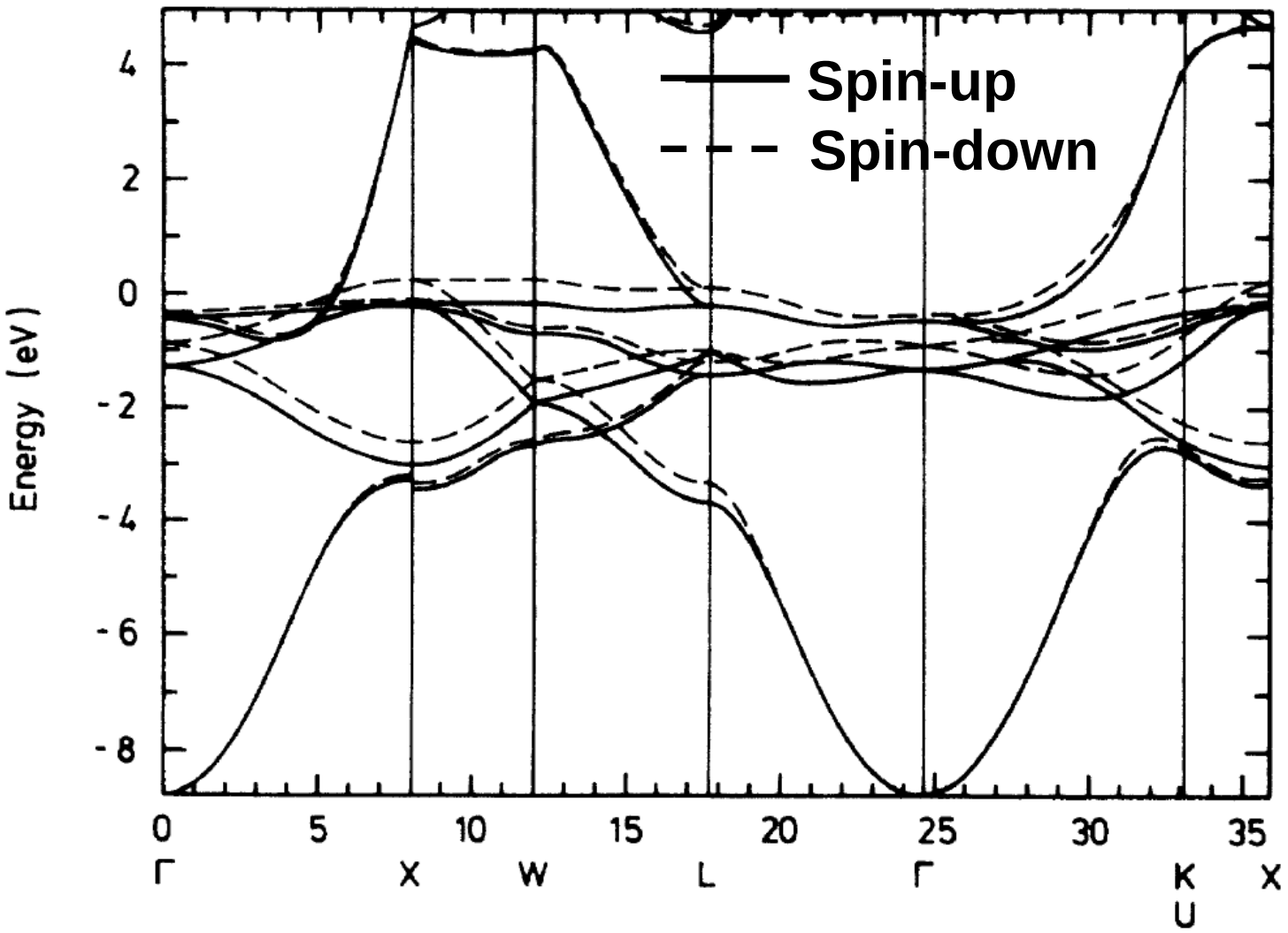

Huebner, Phys. Rev. B 42, 11553 (1990)

Angle-Resolved Photoemission from ferromagnetic Ni(111)

hν = 21.2 eV

Spin-split bands

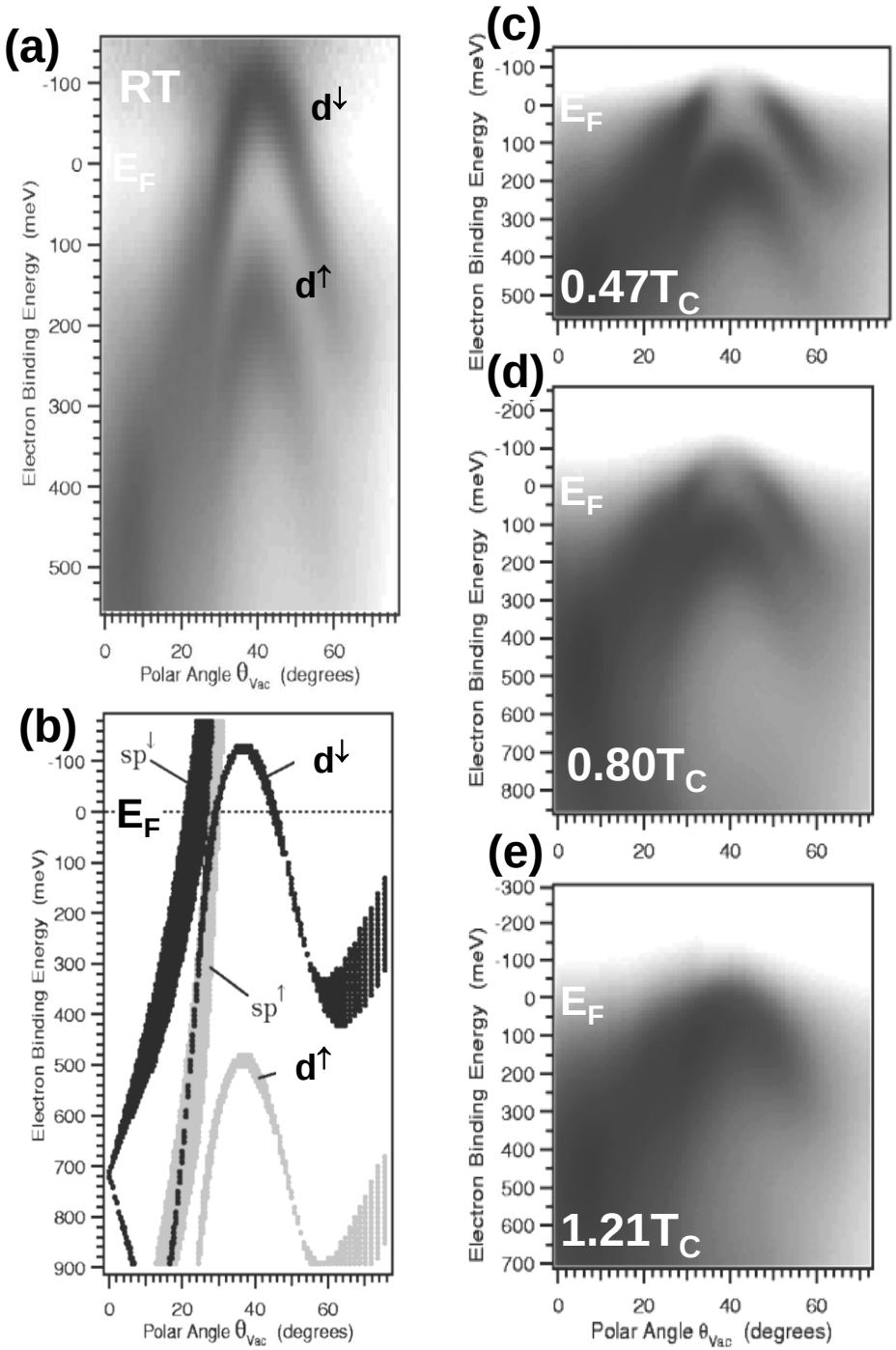

Kreutz et al.,
Phys. Rev. B 58 (1998) 1300

Basic Concepts and Experiments

Core-Level Photoemission

Intensities and Quantitative Analysis, the 3-Step Model
Varying Surface and Bulk Sensitivity
Chemical shifts
Multiplet Splittings
Electron Screening and Satellite Structure
Magnetic and Non-Magnetic Dichroism
Resonant Photoemission
Photoelectron Diffraction and Holography

Valence-Level Photoemission

Band-Mapping in the Ultraviolet Photoemission Limit
Densities of States in the X-Ray Photoemission Limit

Some New Directions

Photoemission with Hard X-Rays (throughout lectures)
Photoemission with Standing Wave Excitation
Photoemission with Spatial Resolution/Photoelectron Microscopy
Temporal Resolution
@ Higher Pressures

ARPES—How high can we go in energy and temperature?

$E_f(\vec{K}_f) =$

$E_f(\vec{k}_f) - V_0 \approx \hbar^2 K_f^2 / 2m_e$

$\vec{k}_{f,\parallel} = \vec{K}_{f,\parallel}$

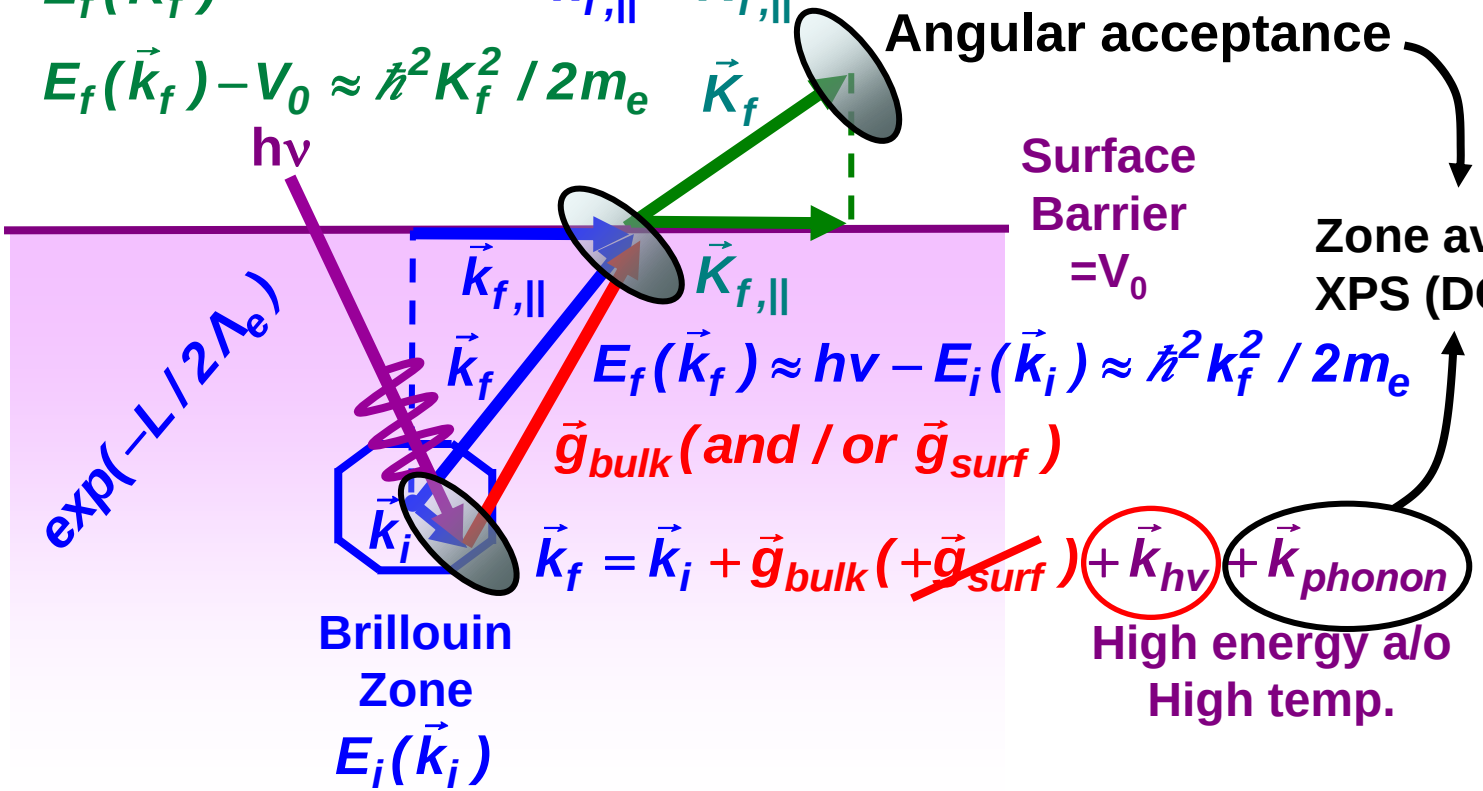

Fraction DTs ≈ Debye-Waller factor = $W(T) \approx \exp[-(k^f)^2 \langle u^2(T)\rangle]$

$\approx \exp[-C_1 (k^f)^2 T/(m\Theta_D^2)] \approx \exp(-C_2 E_{kin} T)$

ARPES → bands, quasiparticles (Low hν, Low T, High angul. Res.)

XPS → DOS (High hν, High T, Low angul. Res.)

Shevchik, Phys. Rev. B 16, 3428 (1977)
Hussain….CF, Phys. Rev. B 34 (1986) 5226

VALENCE-BAND PHOTOELECTRON INTENSITIES AND DENSITIES OF STATES

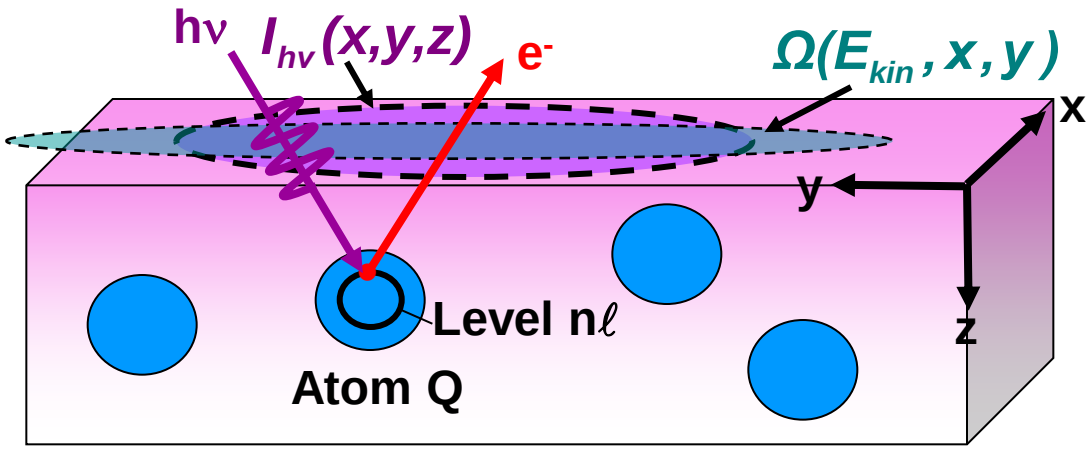

$$I(E_{kin}, Qn\ell) =$$

$$C' \int_0^\infty I_{hv}(x,y,z)\rho_{Qn\ell}(E_b,x,y,z)\frac{d\sigma_{Qn\ell}(hv)}{d\Omega}\exp\left[-\frac{z}{\Lambda_e(E_{kin})\sin\theta}\right]\Omega(E_{kin},x,y)dxdydz$$

$I_{hv}(x,y,z)$ = x-ray flux

$\rho_{Qn\ell}(E_b,x,y,z)$ = density of states, projected onto $Qn\ell$ character

$\frac{d\sigma_{Qn\ell}(hv)}{d\Omega}$ = energy-dependent differential photoelectric cross section for subshell $Qn\ell$

$\Lambda_e(E_{kin})$ = energy-dependent inelastic attenuation length

→ Mean Emission Depth

$\Omega(E_{kin}, x, y)$ = energy-dependent spectrometer acceptance solid angle

Valence spectra in the XPS Limit

Gold Valence Spectrum

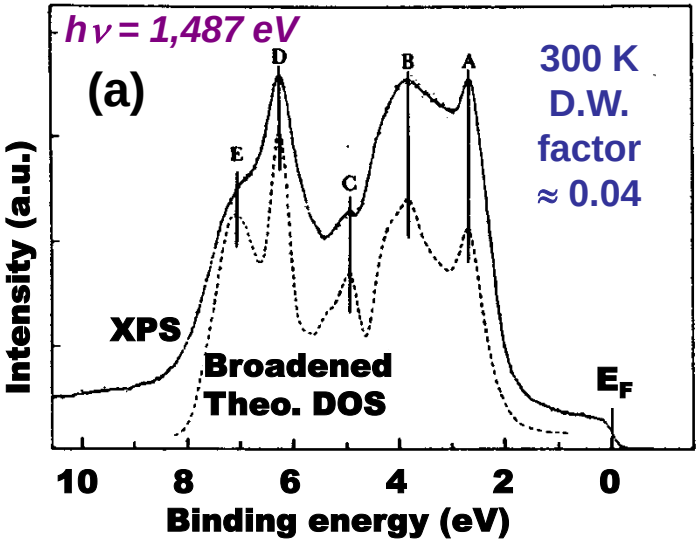

Gold Valence Spectrum

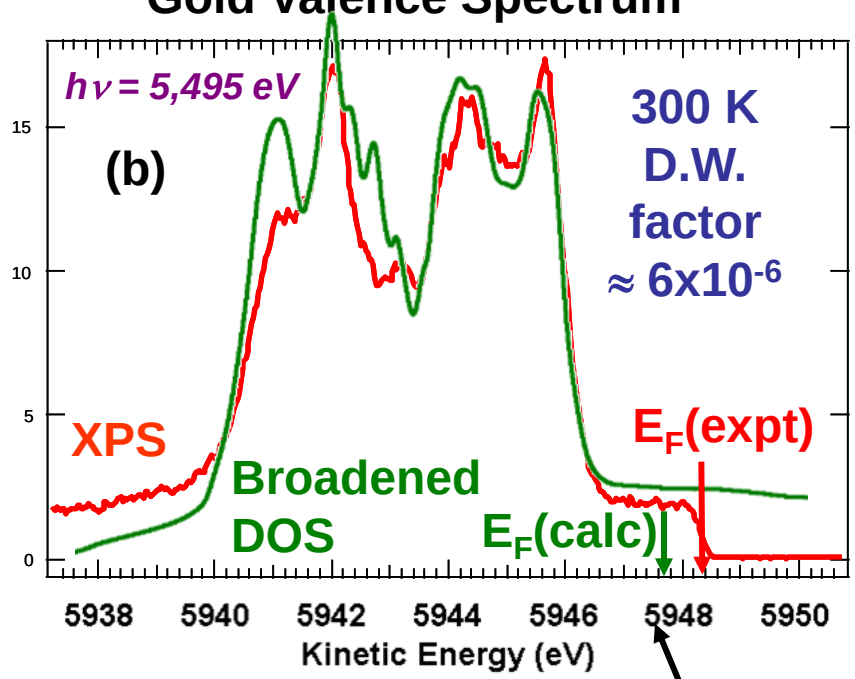

Silver Valence Spectrum

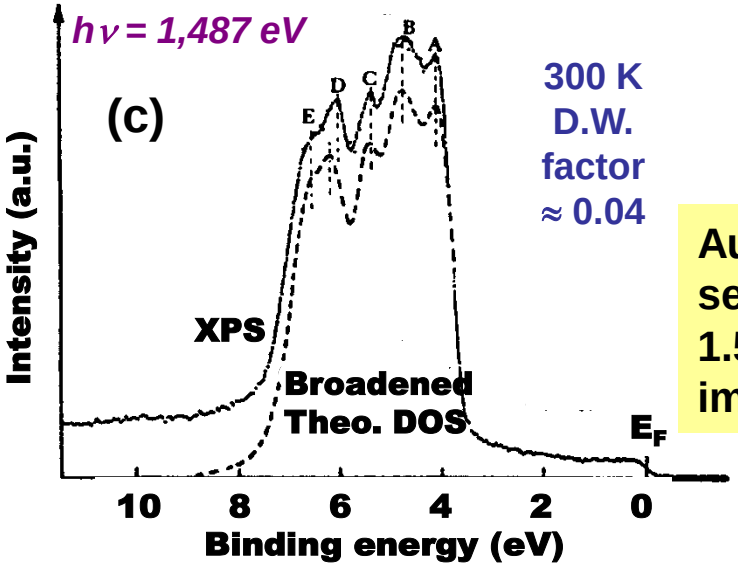

Au subshell photoelectric cross section ratios: Au6s/Au5d = 0.012 at 1.5 keV and 0.028 at 6 keV→6s more imp. at 6 keV x 2.5x

Screening/ self-energy correction

In the XPS Limit—Comparison to theoretical DOSs

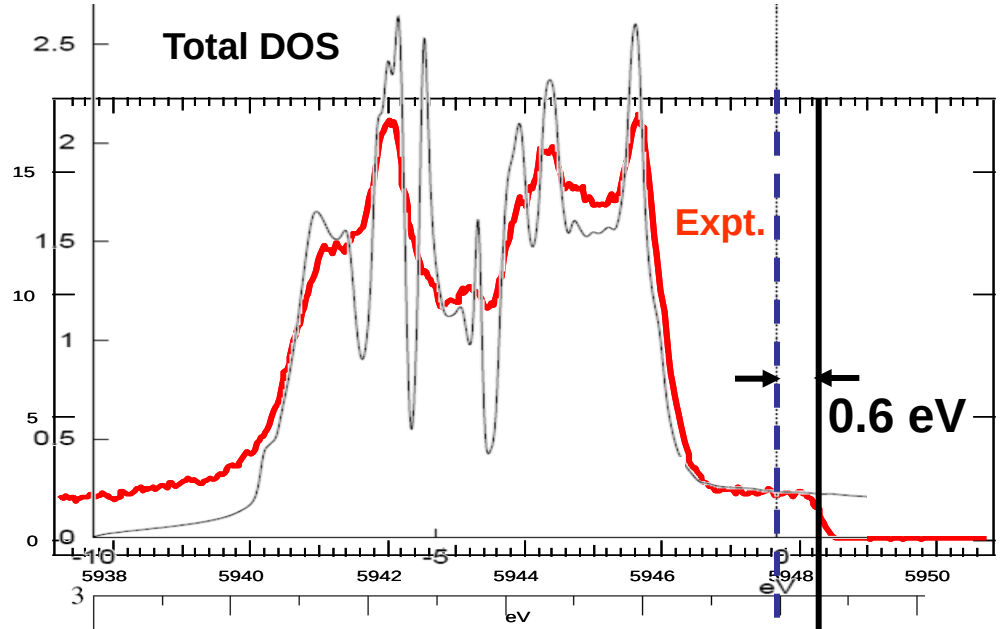

Takata et al., SPring8 @ 5.495 keV

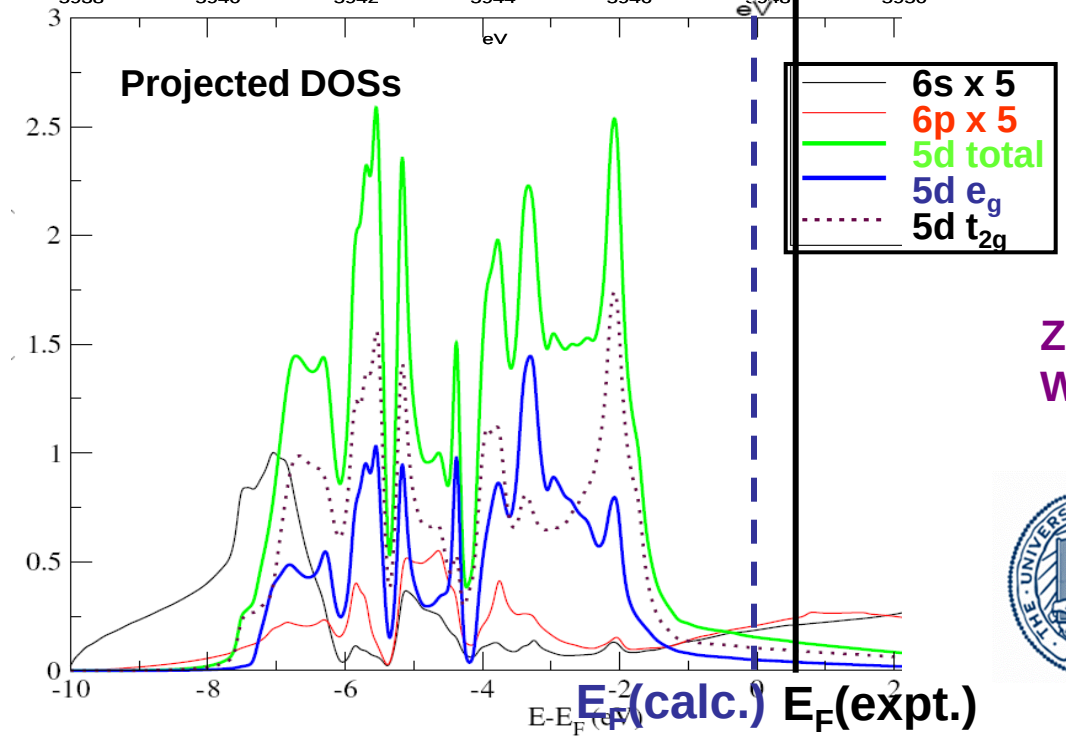

E_F(calc.) E_F(expt.)

Au subshell photoelectric cross section ratios: Au6s/Au5d = 0.012 at 1.5 keV and 0.028 at 6 keV→6s more imp. at 6 keV x 2.5x

Z. Yin
W.E. Pickett

XPS and HXPS in k space:

(a)

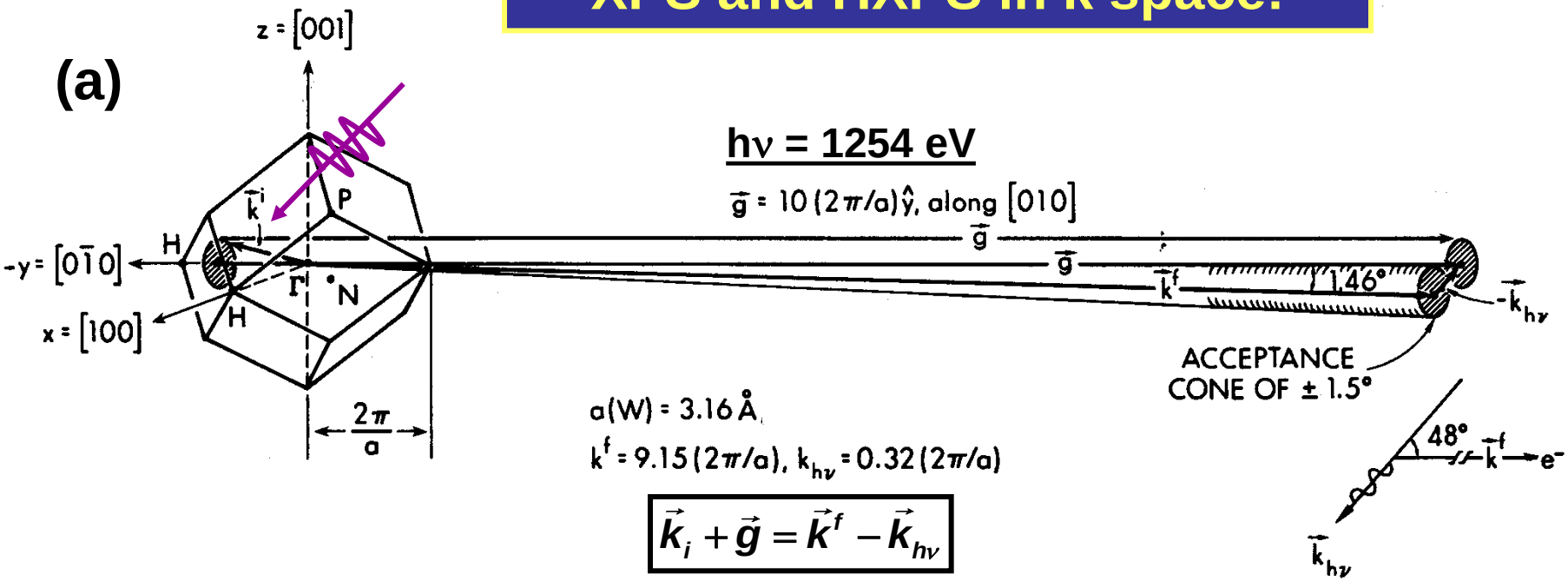

$$\vec{k}_i + \vec{g} = \vec{k}^f - \vec{k}_{h\nu}$$

(b)

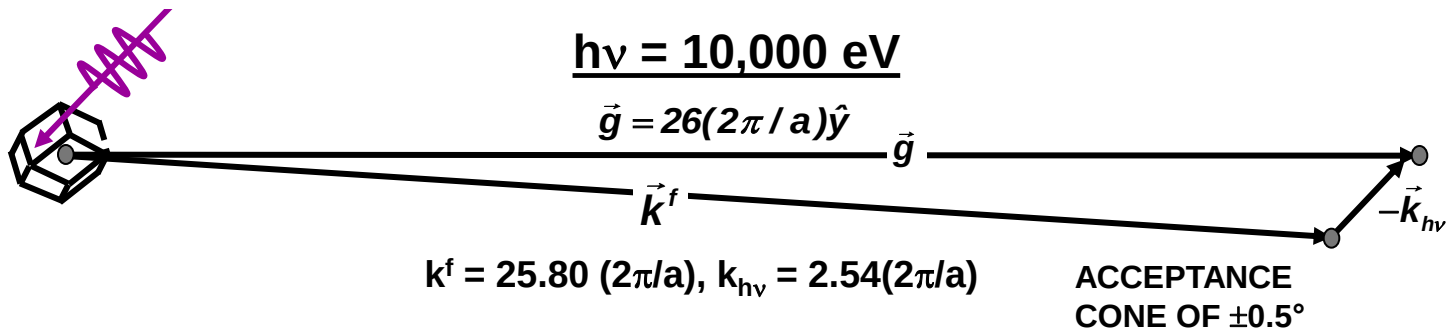

Phonon effects: Approximate fraction of "good" direct transitions

≈ Debye-Waller factor = *$W(T) \approx \exp[-g^2 \langle u^2(T) \rangle]$*

= Mean-squared vibrational displacement

The Photoelectric Effect, Einstein, 1905
Light can behave like a Particle!

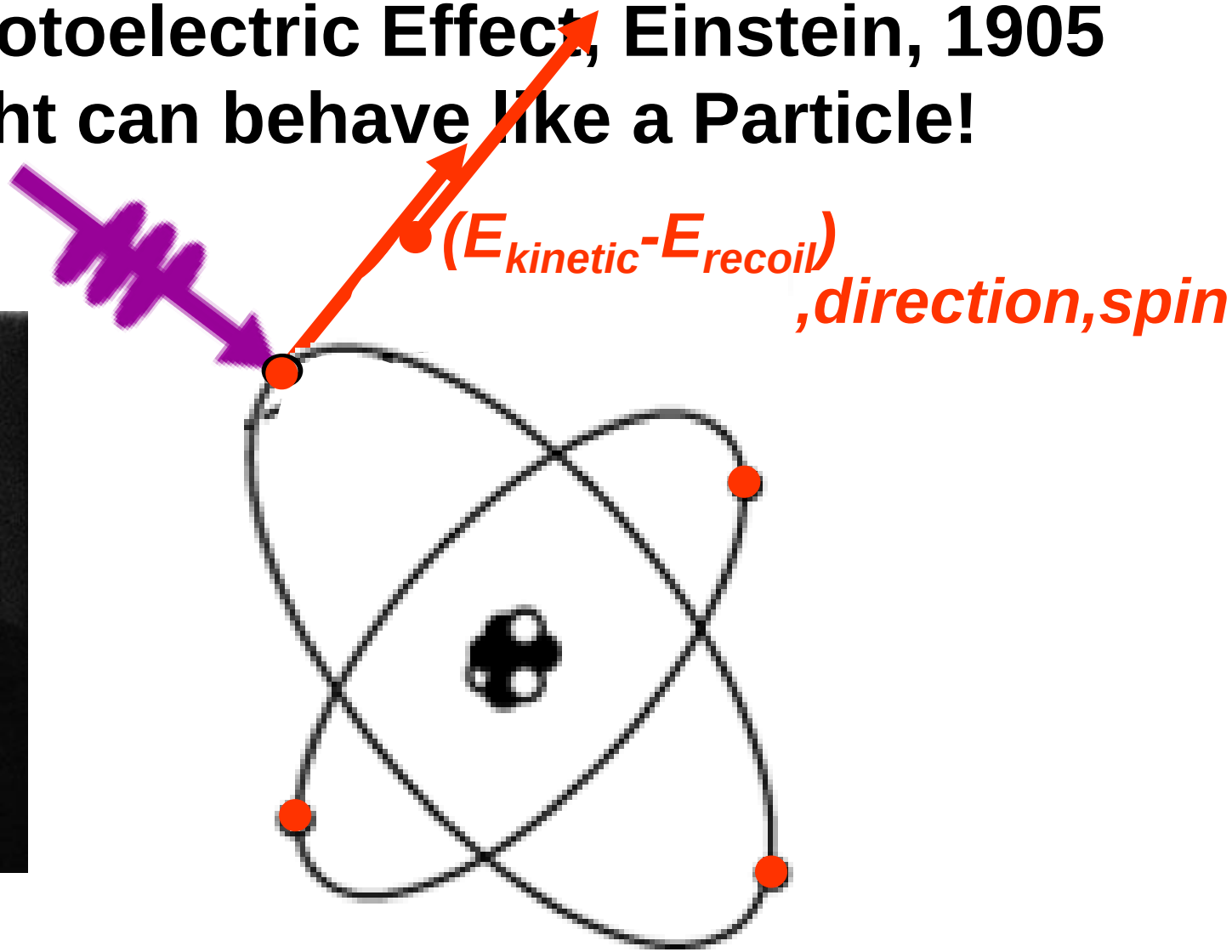

$$h\nu = E_{initial} - E_{final} = E_{binding} + (E_{kinetic} - E_{recoil})$$

Angle-Resolved Photoemission at High Energy-- How high can we go?:

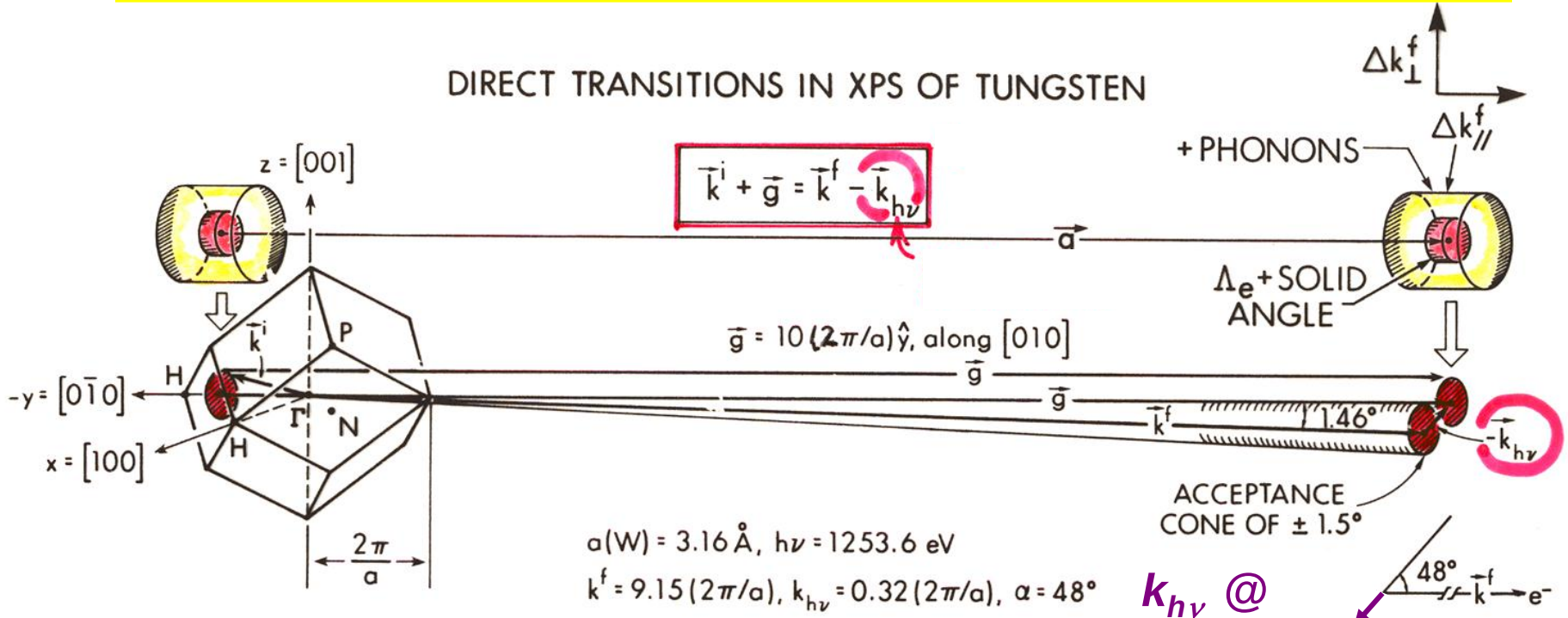

$k_{h\nu}$ @ 1,253 eV

Hussain et al., Phys. Rev. B 22, 3750 (1980)

Takata et al., Phys. Rev. B 75, 233404 (2007)

Additional effects at higher energies:

- **non-dipole--the photon momentum $k_{h\nu}$**
- **angular acceptance→B.Z. averaging**
- **lattice recoil, phonon creation→more B.Z. averaging, ~Debye-Waller factor** $= W(T) \approx \exp[-(k^f)^2 \langle u^2(T)\rangle]$

$$\approx \exp[-C_1 (k^f)^2 T/(m\Theta_D^2)] \approx \exp(-C_2 E_{kin} T)$$

….the "XPS limit" of full B.Z. averaging and D.O.S. sensitivity→core-like photoelectron diffraction

- **recoil leads to peak shifts and broadening:** $E_{recoil}(eV) \approx \left[\frac{m_e}{M}\right] E_{kin} \approx 5.5 \times 10^{-4} \left[\frac{E_{kin}(eV)}{M(amu)}\right]$

Alvarez et al., PR*B* 54, 14703 (1996)

Angle-Resolved Photoemission (ARPES) with soft x-rays: W(110) at 860 eV

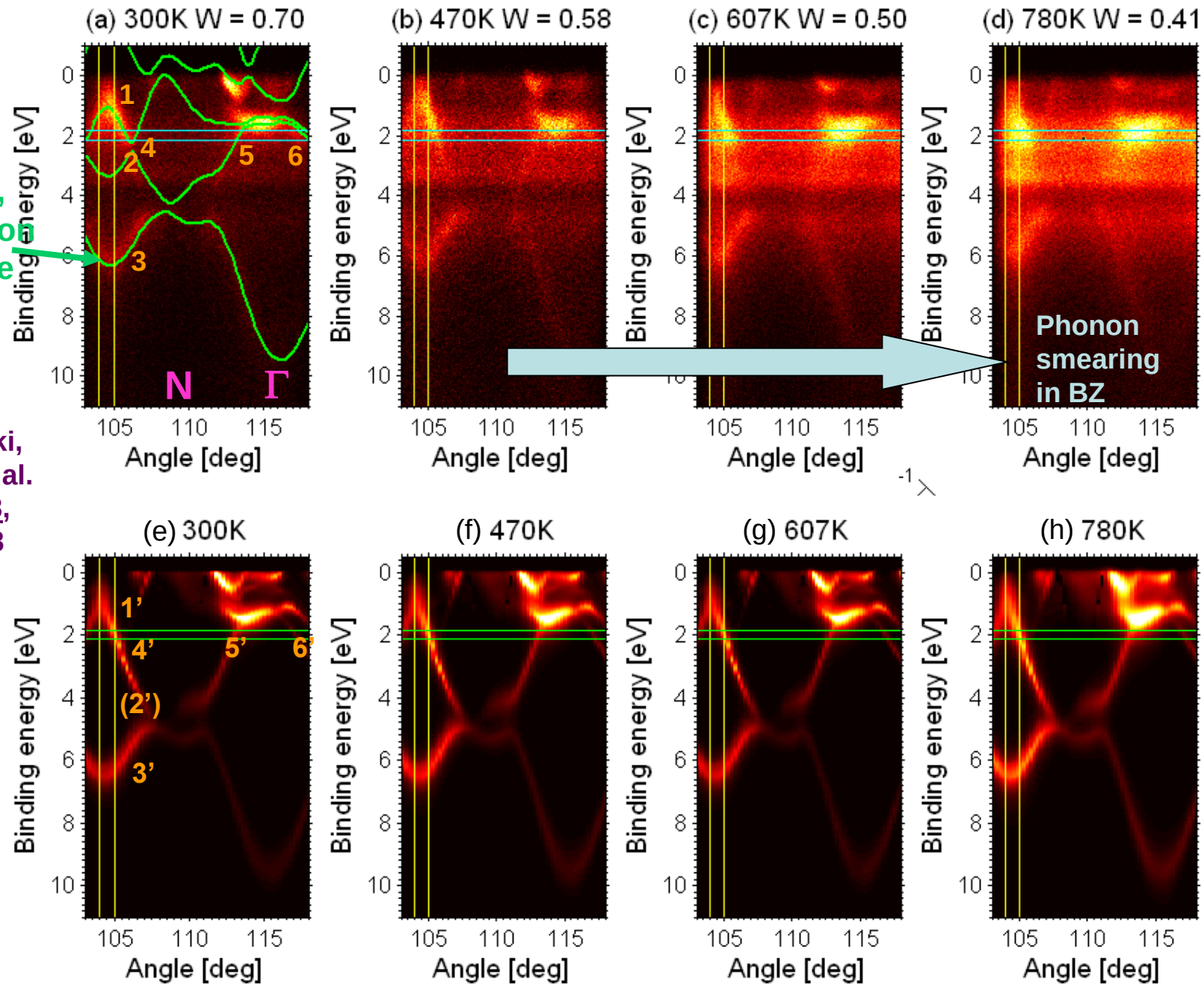

One-electron, free-electron final-state theory

Plucinski, Minar, et al. PRB 78, 035108 (2008)

Experiment and theory: W(110)--860 eV

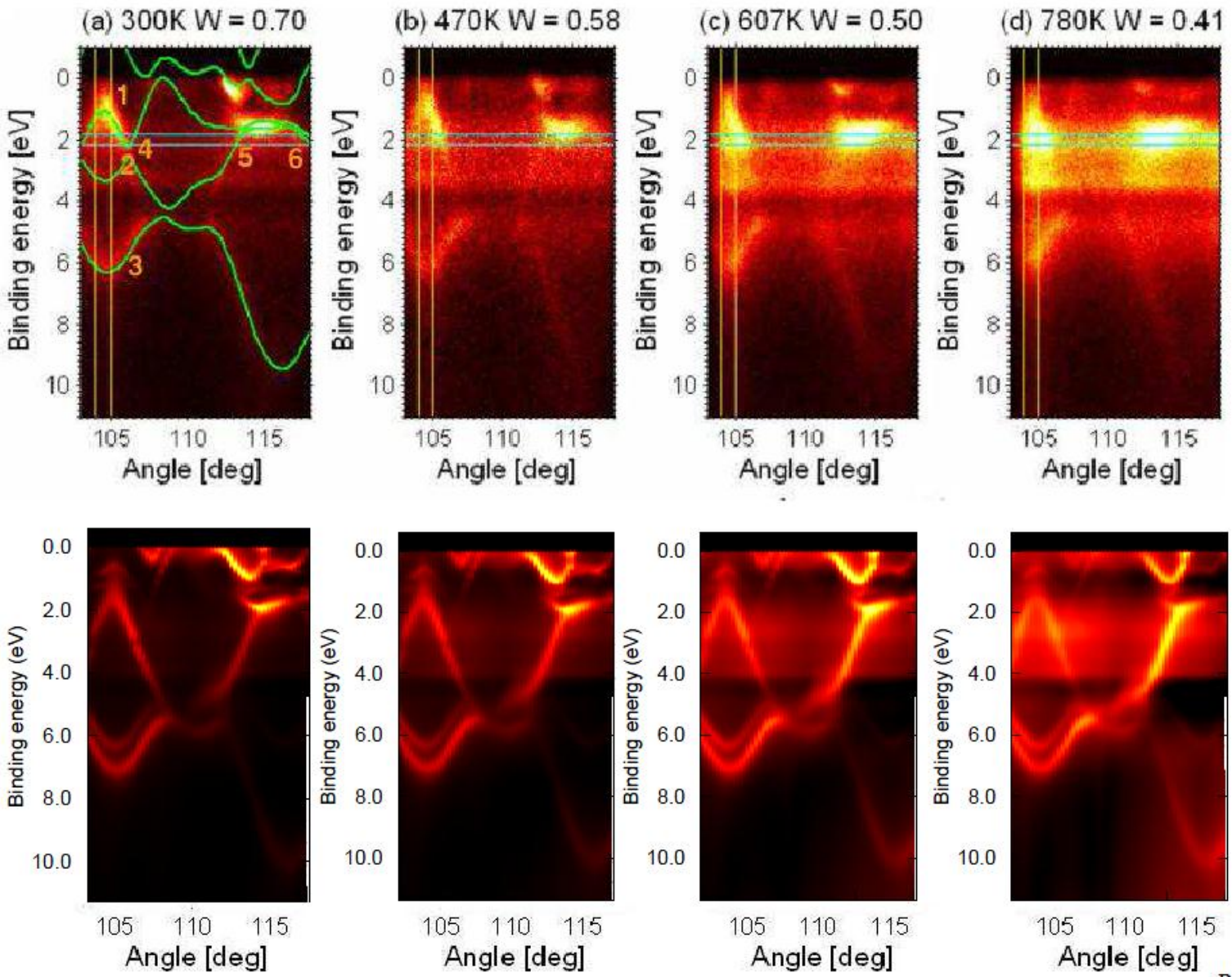

J. Braun, J. Minár and H. Ebert, submitted to PRL (2012)

The Debye-Waller Factor

Estimate of the Fraction of Direct Transitions and Max. Recoil Effect

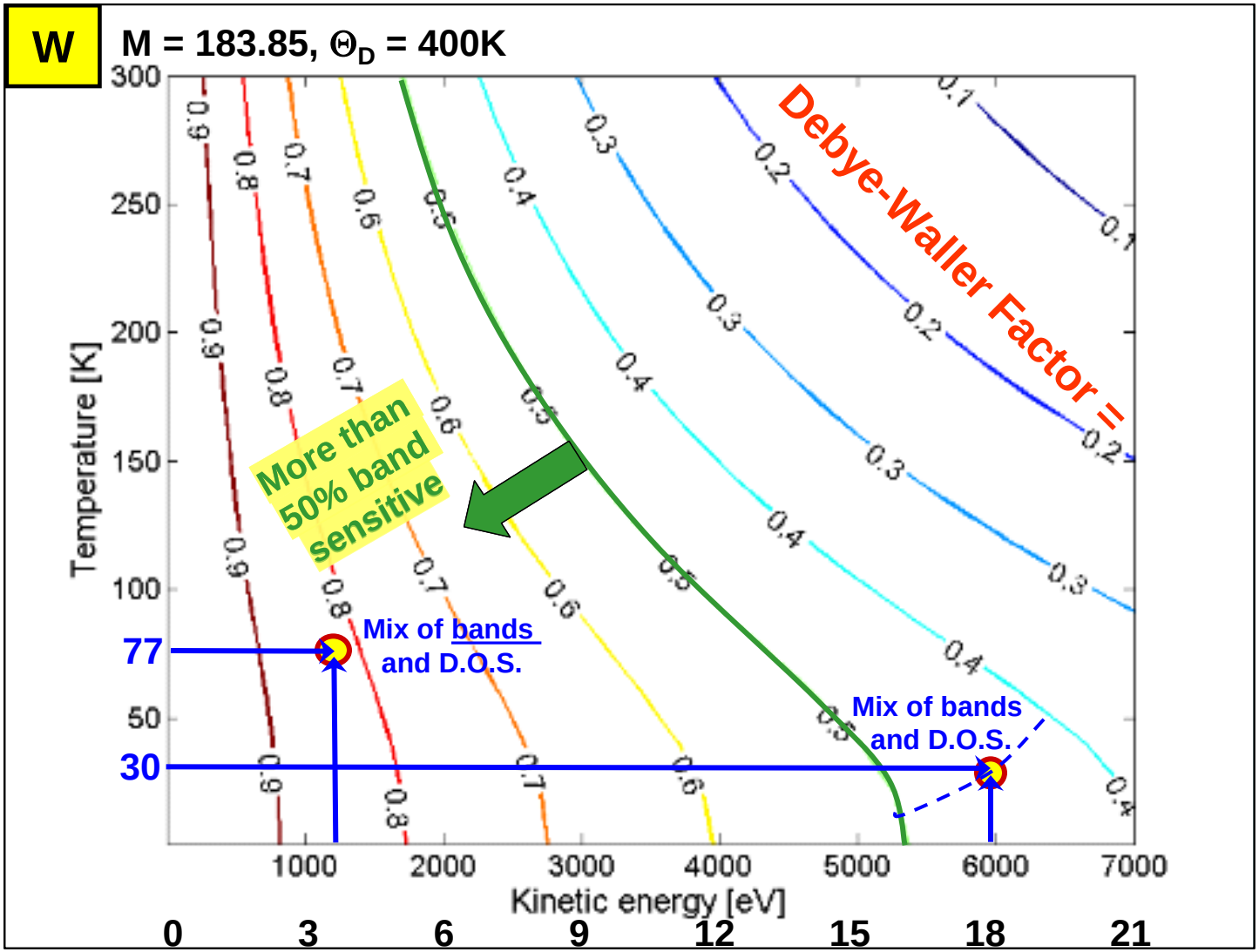

0 3 6 9 12 15 18 21

E^{max}_{recoil} (meV)

L. Plucinski, et al. PRB 78, 035108 (2008)

ARPES with a non-monochromatized lab. x-ray source: hν = 1253.6 eV, T = ~77K, W = 0.82

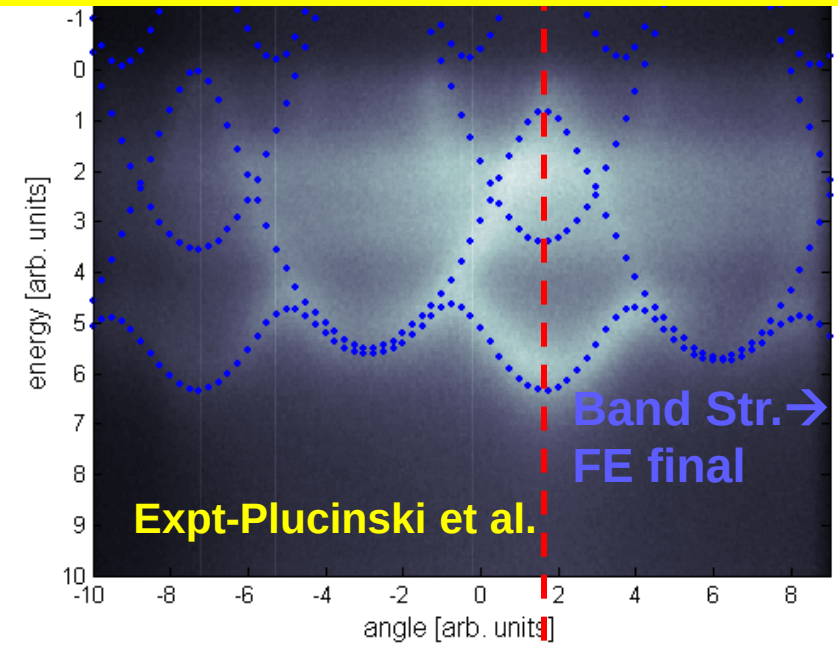

W(110) Normal emission 1283eV

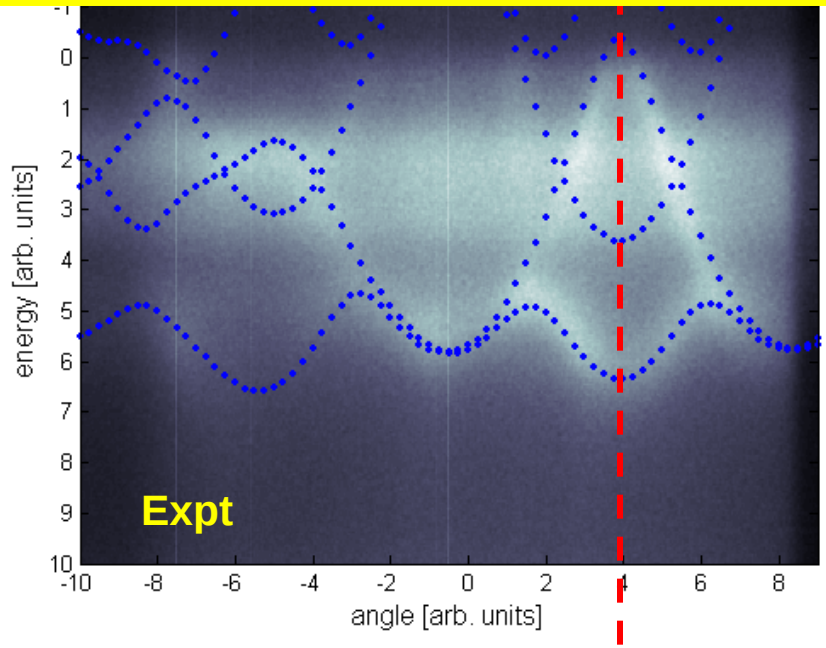

W(110) OFF-Normal emission 1283eV

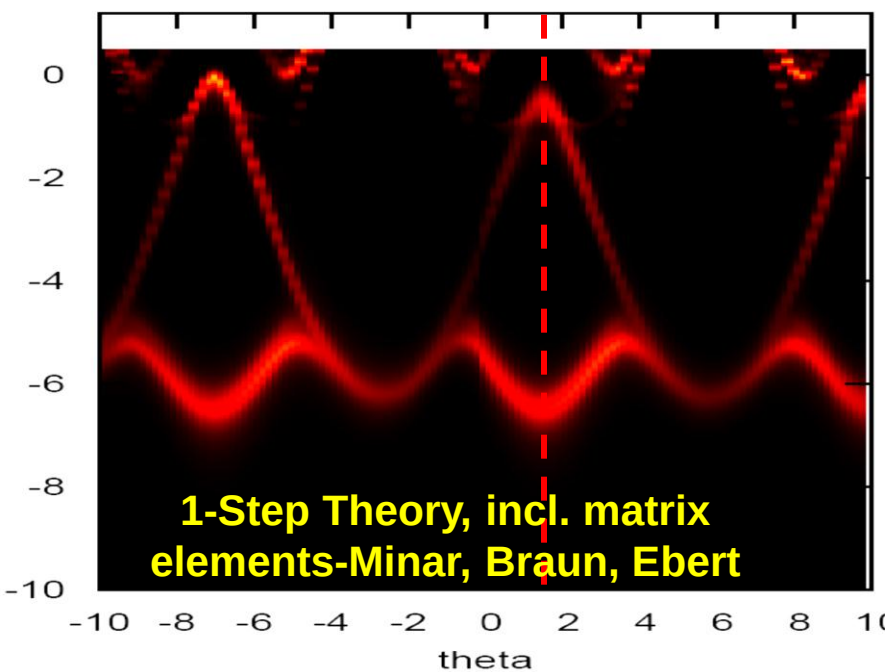

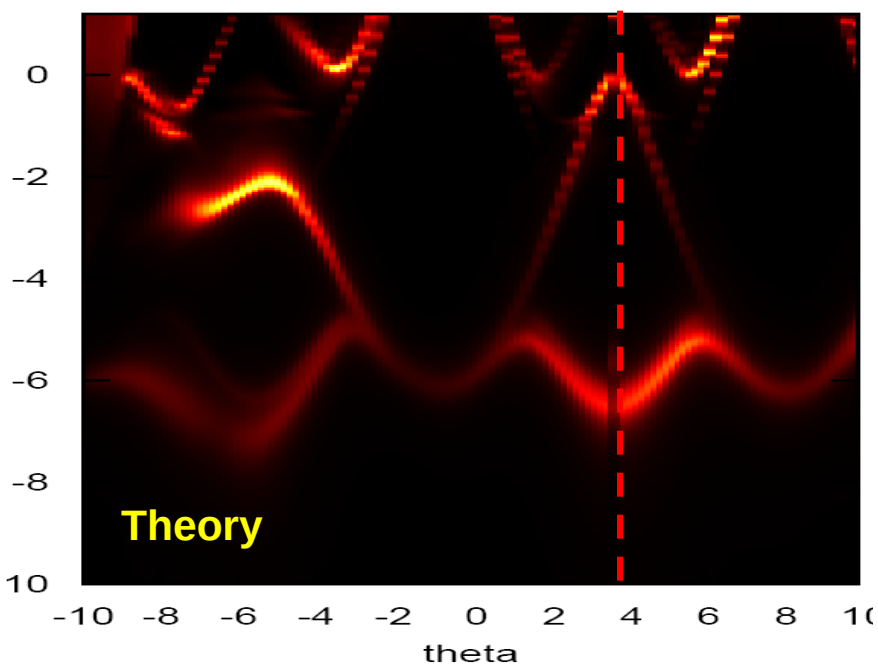

Hard x-ray ARPES for W(110): 6.0 keV, 300K and 30K

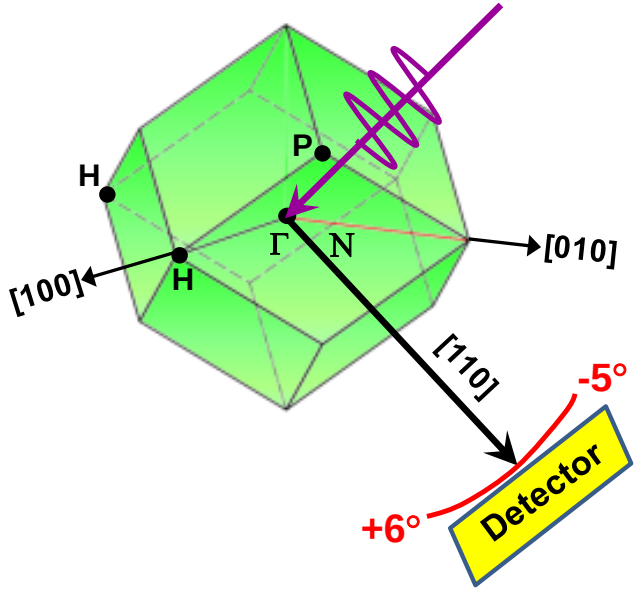

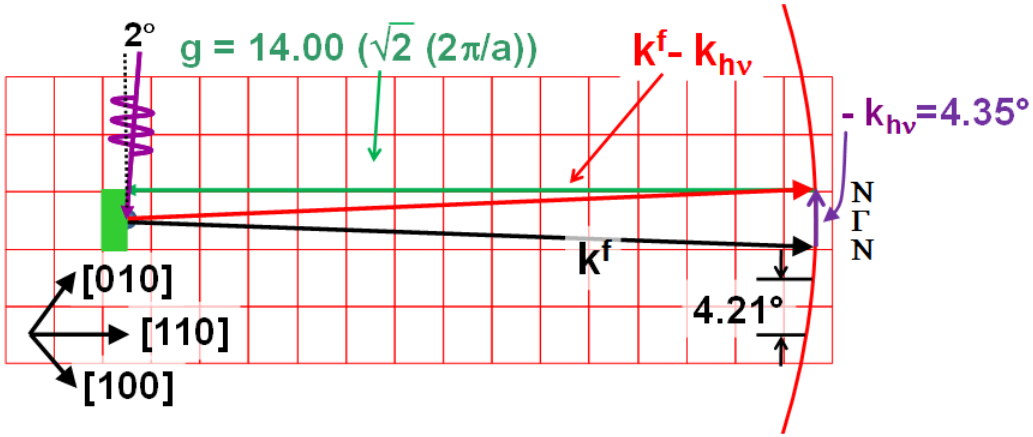

Gray, Minar et al., Nature Materials 10, 759 (2011)

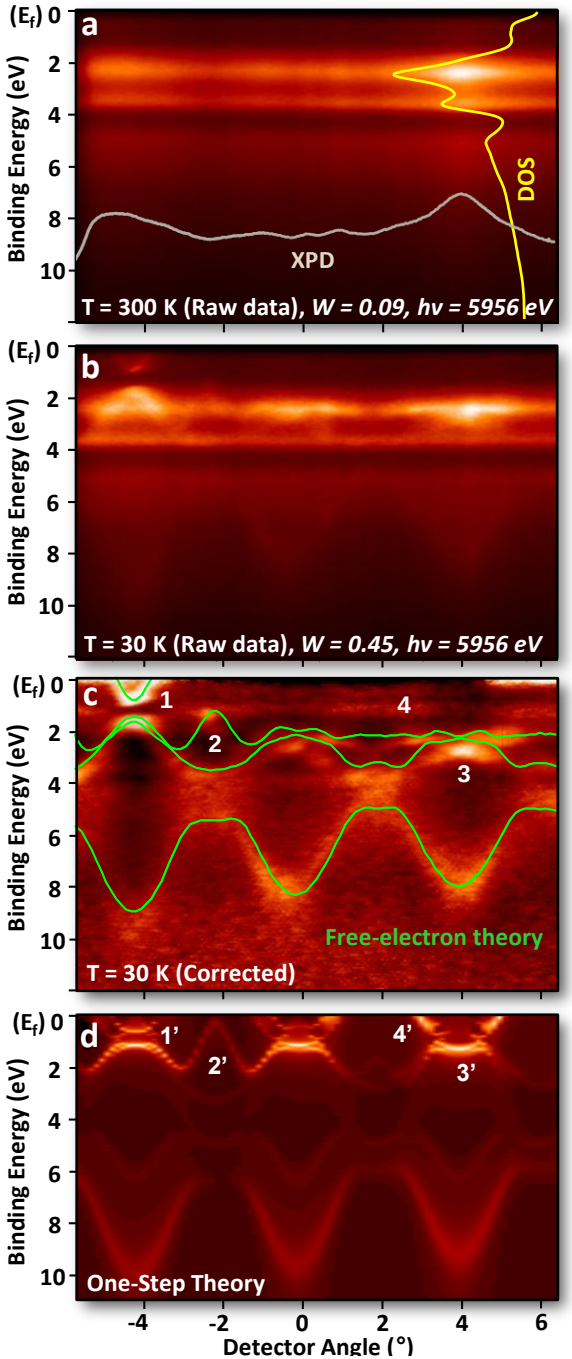

W(T,E$_{kin}$) = Approximate recoil-free fraction→fraction direct transitions

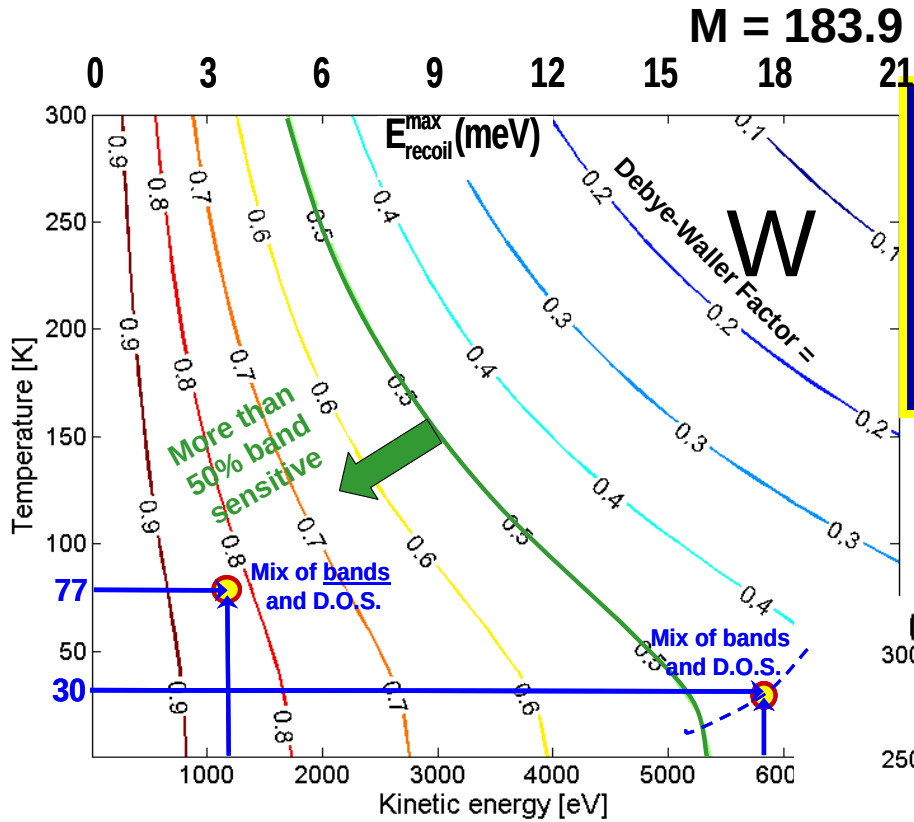

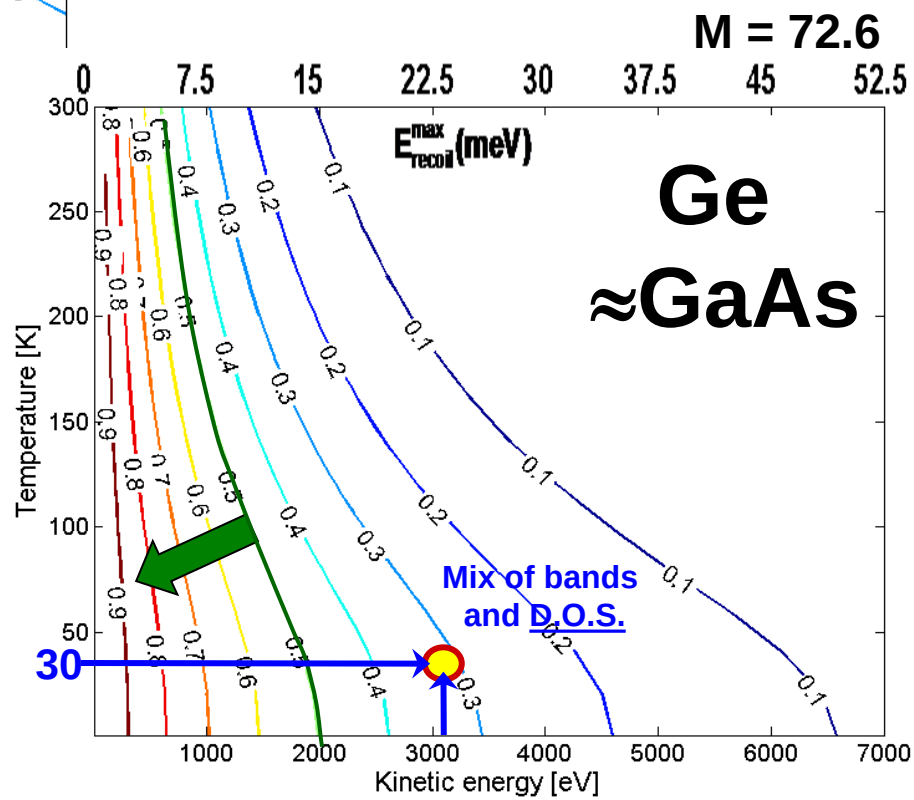

Plucinski

Hard x-ray ARPES from GaAs(001)-3.2 keV, 30 K, W = 0.31

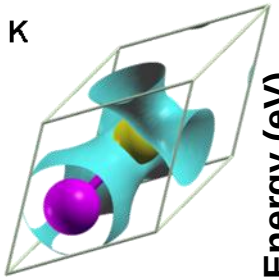

Band-like

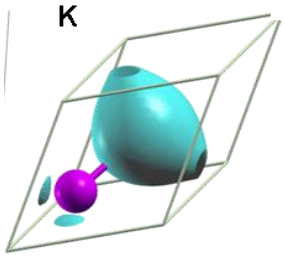

Core-like
As 4s
⇑
Charge densities

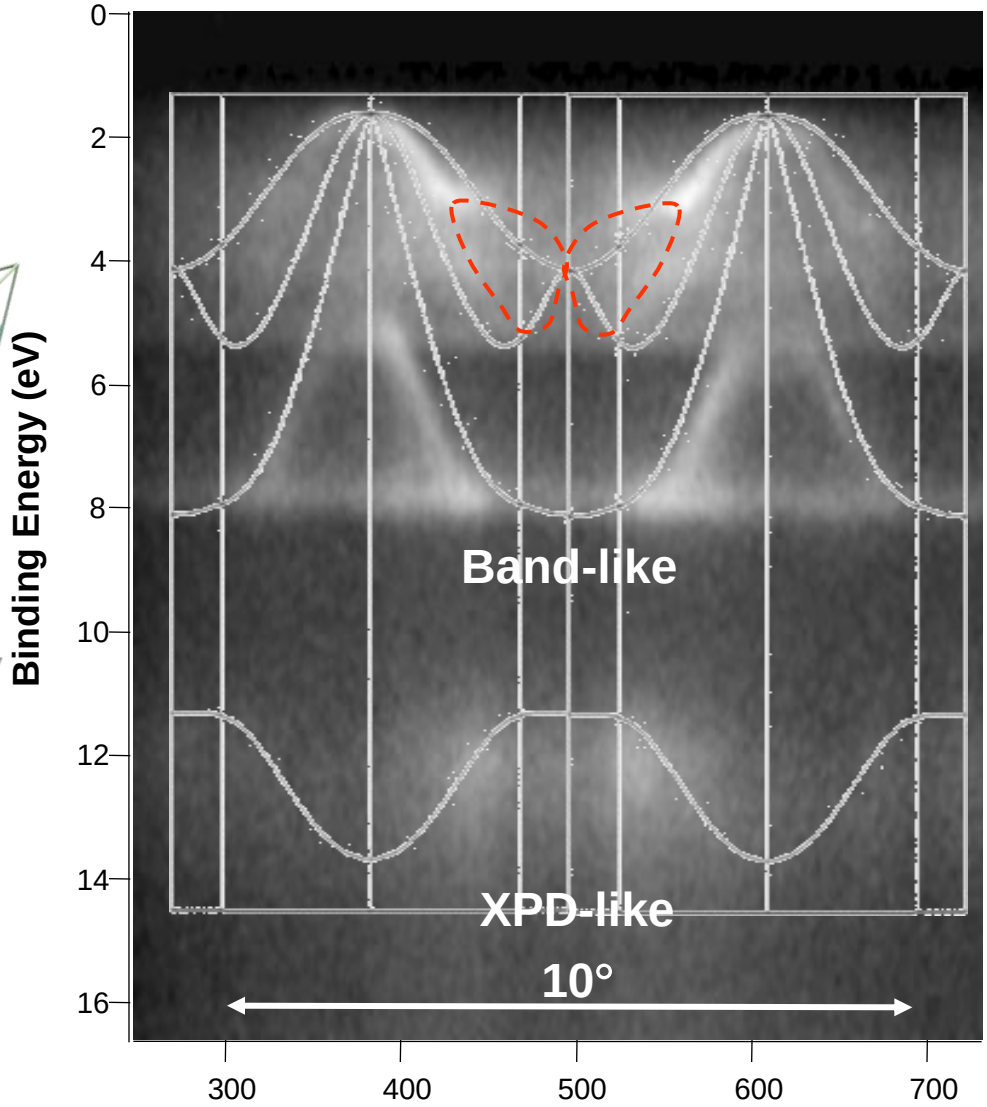

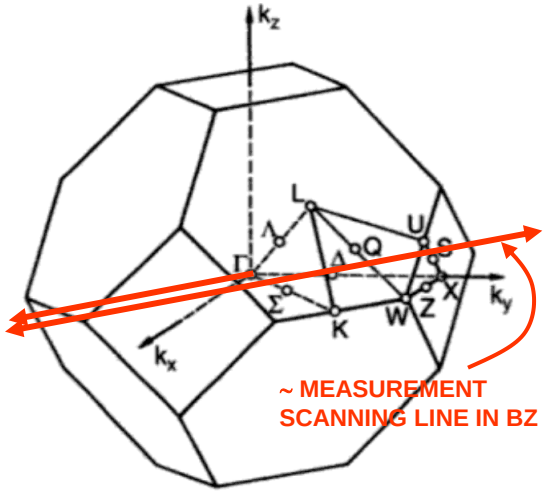

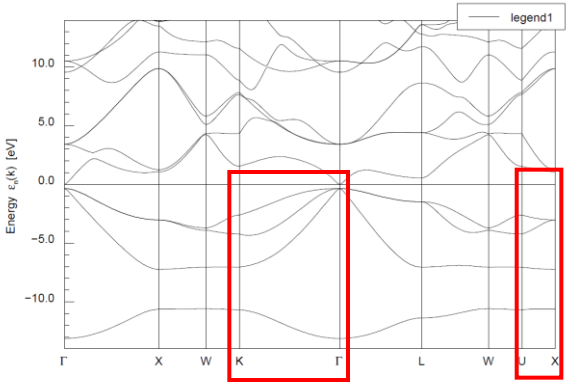

Expt.-Gray, Papp, Ueda, Yamashita, Kobayashi
Theory- Pickett, Ylvisaker

Hard x-ray ARPES for GaAs(001): 3.2 keV

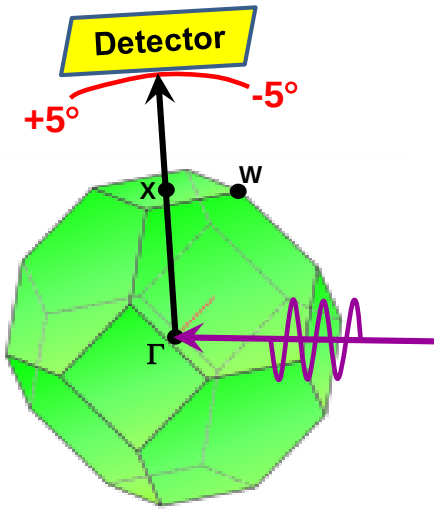

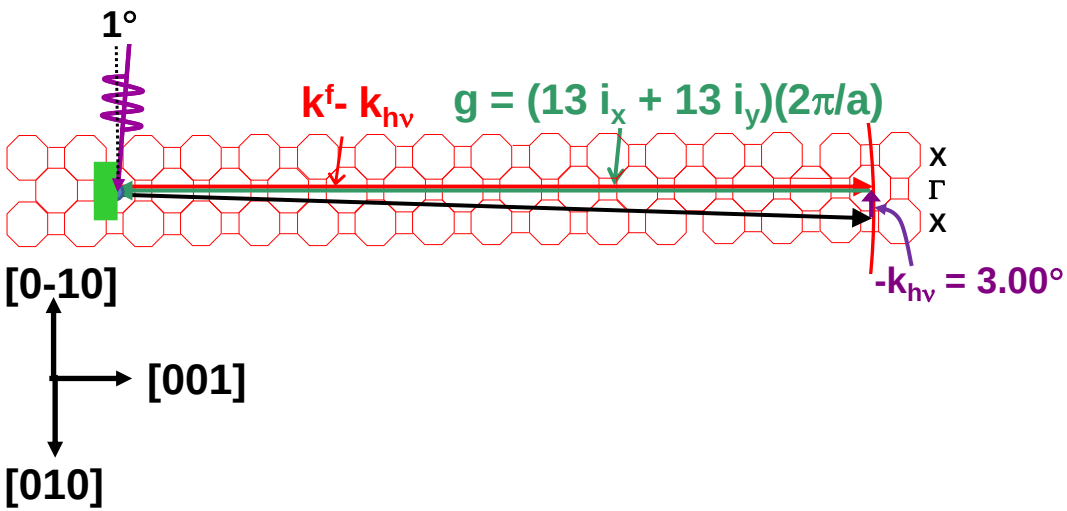

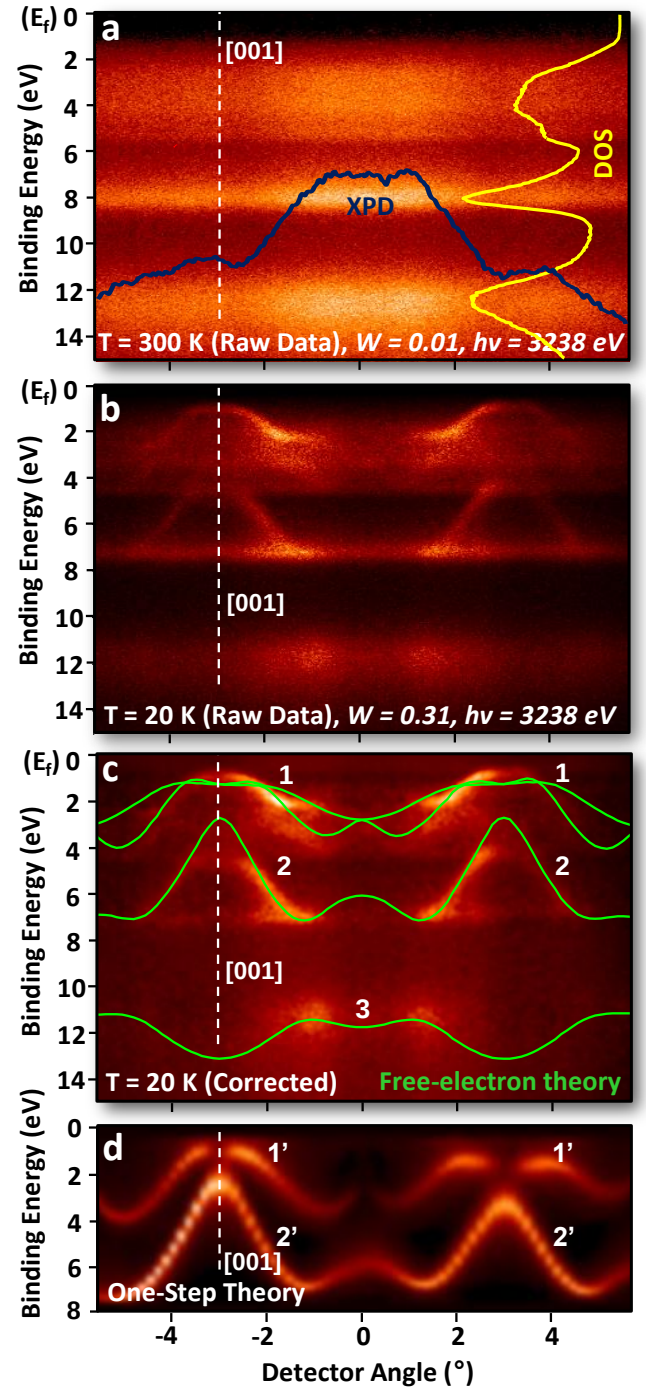

Gray, Minar et al., Nature Materials 10, 759 (2011)

Hard x-ray ARPES--GaAs and the dilute magnetic semiconductor $Ga_{0.97}Mn_{0.03}As$

How does Mn alter the electronic structure so as to produce ferromagnetic coupling? Two differing views:

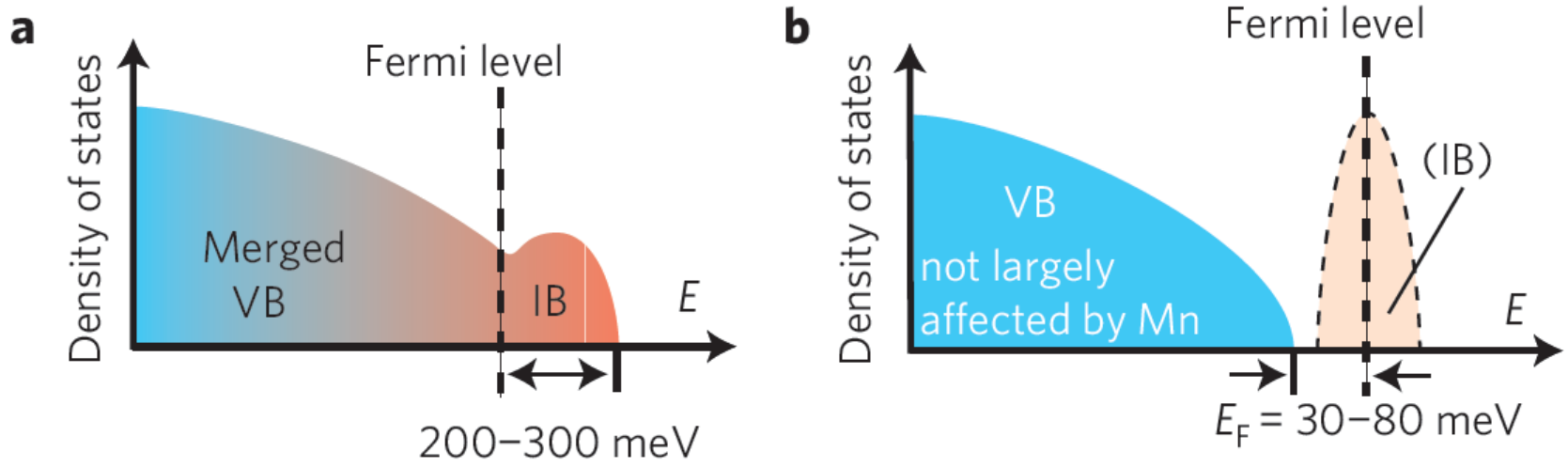

GaAs doped with Mn: a magnetic semiconductor
$Ga_{0.96}Mn_{0.04}As$--HXPS: T = 20K, Broad Survey

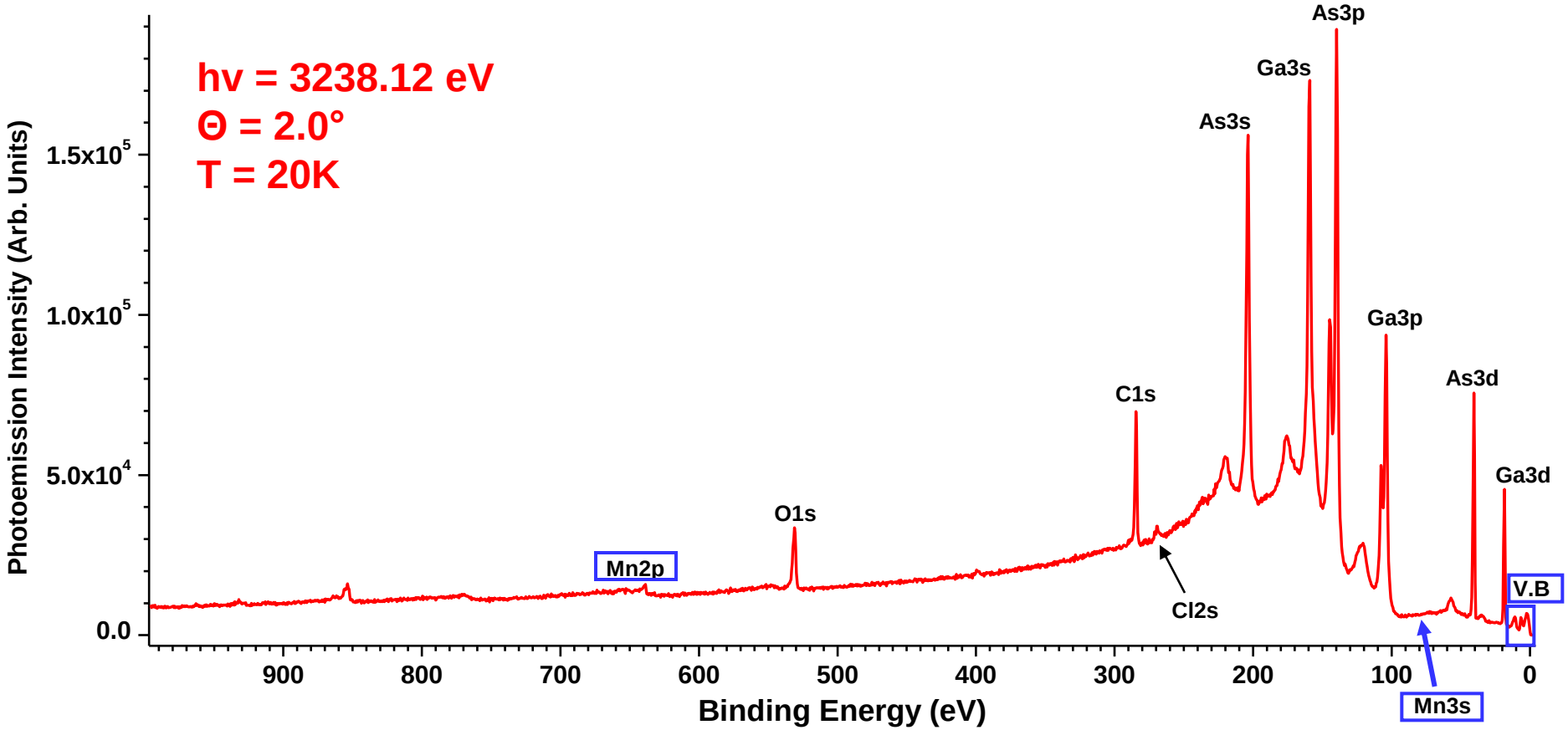

Samples: Stone, Dubon
Expt.-Gray, Papp, Ueda, Yamashita, Kobayashi
Theory- Pickett, Ylvisaker, Minar, Braun, Ebert

Hard x-ray ARPES--GaAs and DMS $Ga_{0.97}Mn_{0.03}As$ Comparing Experiment and One-Step KKR Theory

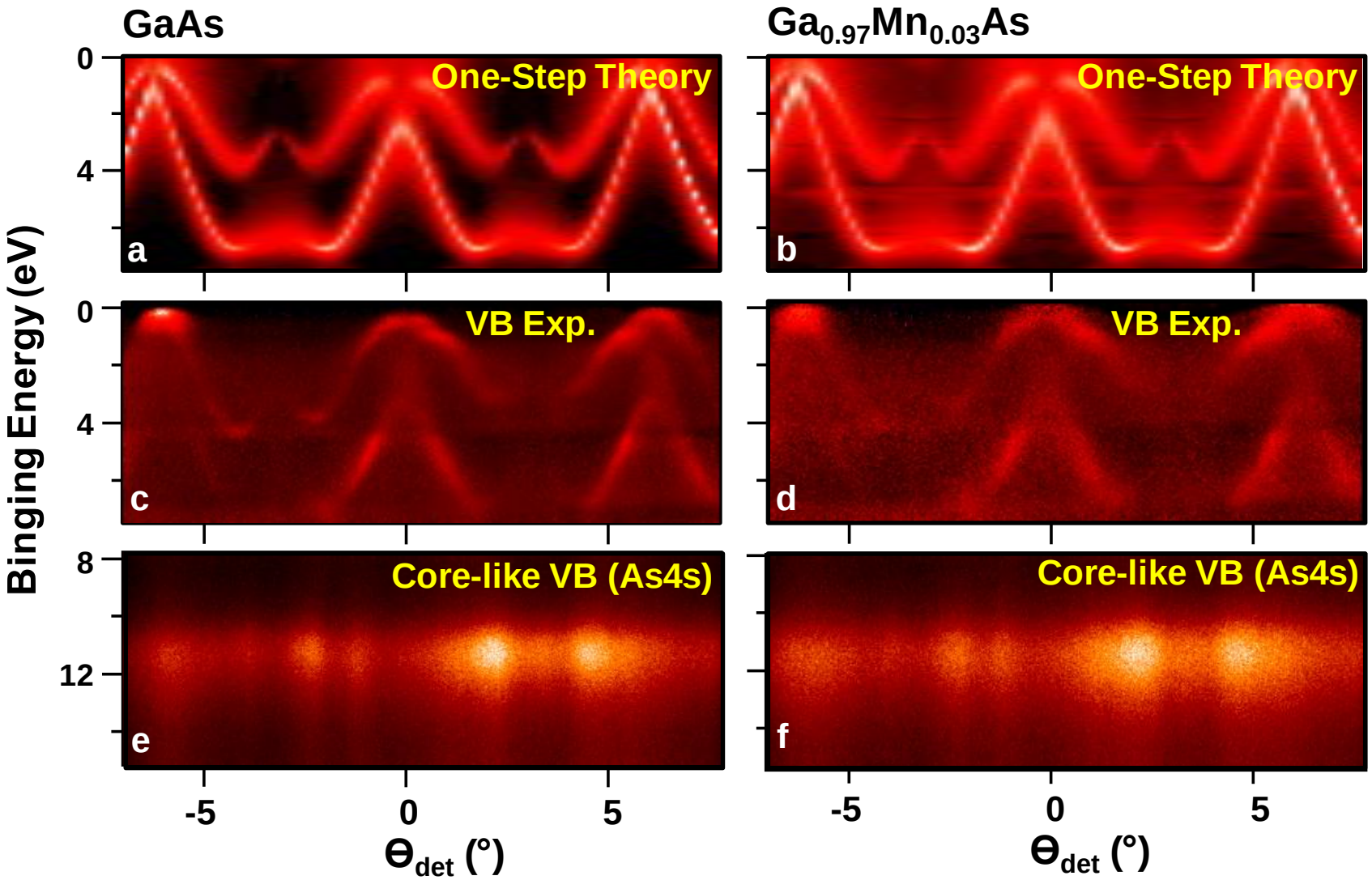

Gray, Minar, Dubon (sample) et al., TBP

Hard x-ray ARPES--GaAs and the dilute magnetic semiconductor $Ga_{0.97}Mn_{0.03}As$

How does Mn alter the electronic structure so as to produce ferromagnetic coupling? Two differing views:

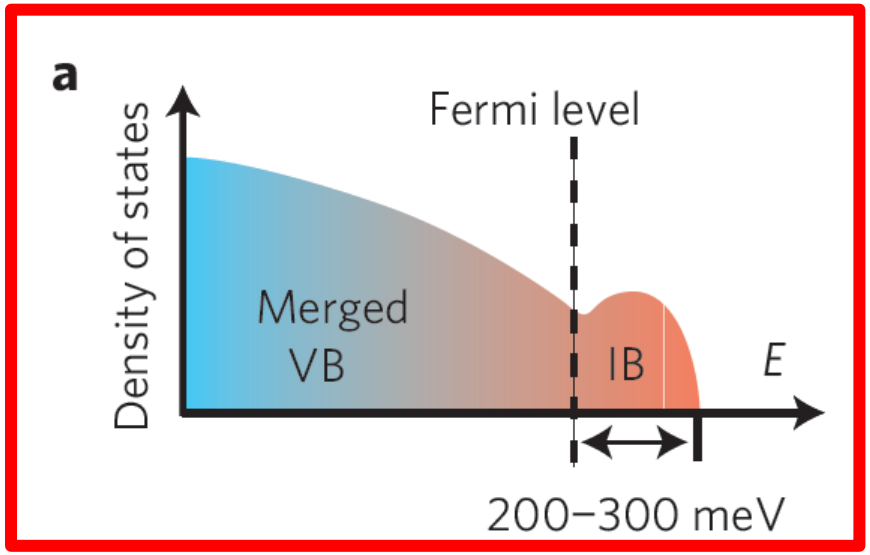

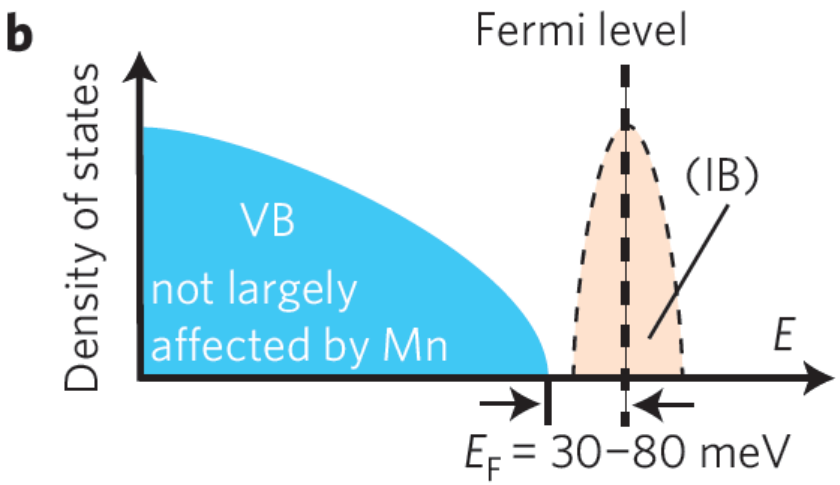

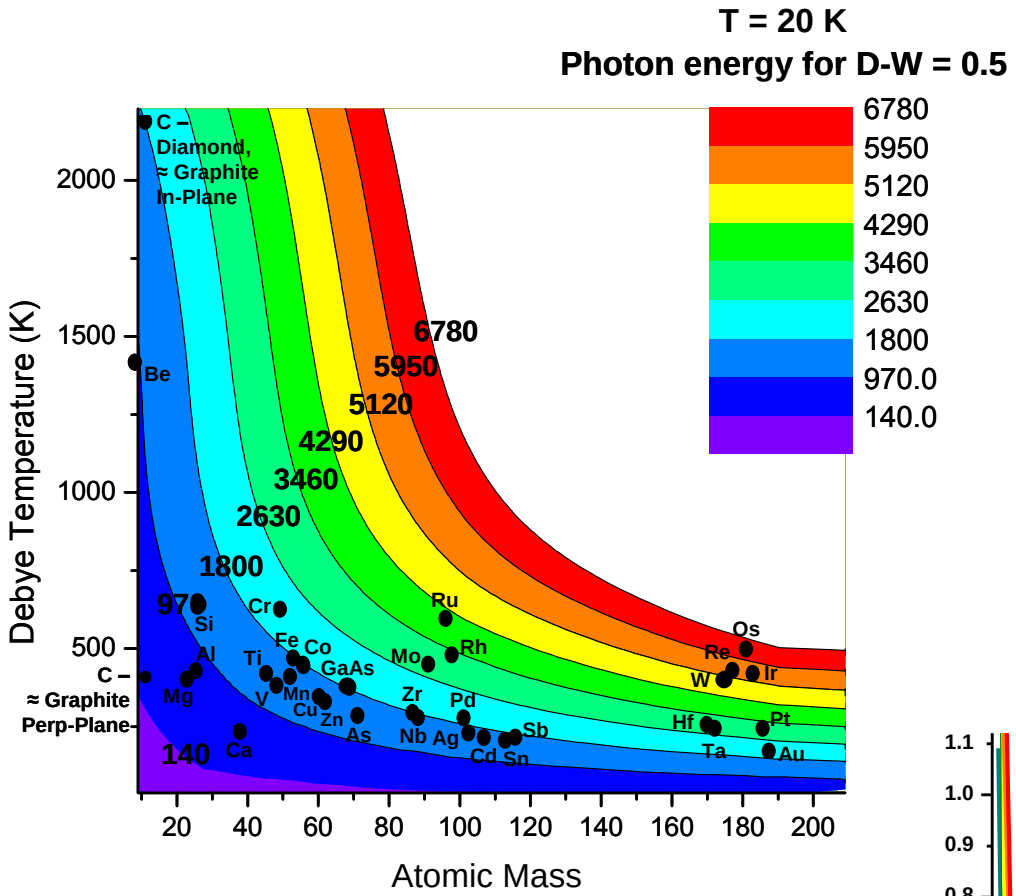

Photon energy for ca. 50% k-conserving transitions@ 20K

HARPES-How high can we go? Photoemission Debye-Waller Factors and Recoil Energies

Recoil energy as a fn. of atomic number and kinetic energy

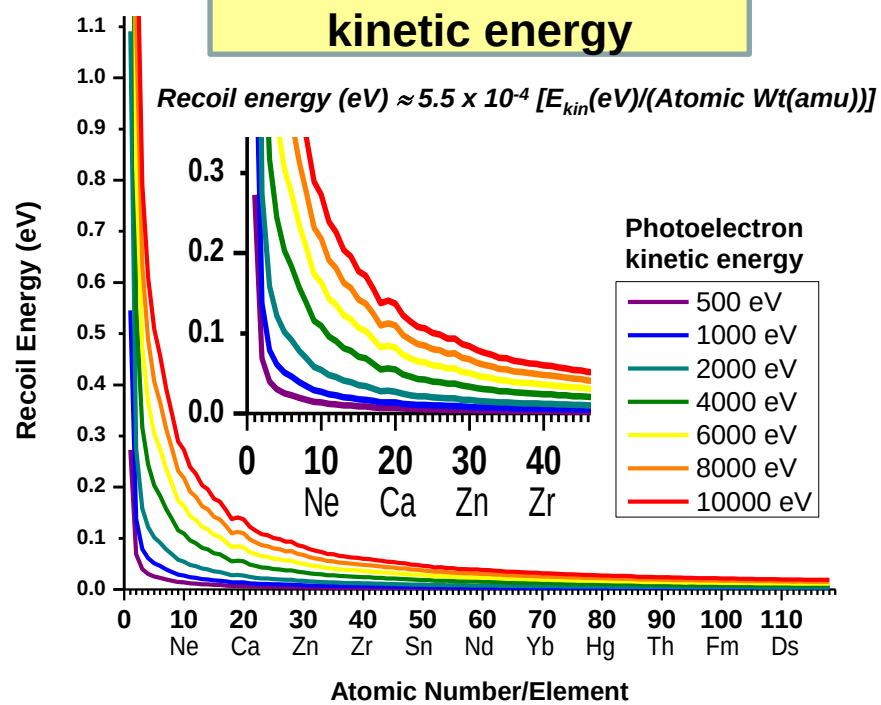

C. Papp. L. Plucinski, et al., Phys. Rev. B 84, 045433 (2011)

Basic Concepts and Experiments

Core-Level Photoemission

Intensities and Quantitative Analysis, the 3-Step Model
Varying Surface and Bulk Sensitivity
Chemical shifts
Multiplet Splittings
Electron Screening and Satellite Structure
Magnetic and Non-Magnetic Dichroism
Resonant Photoemission
Photoelectron Diffraction and Holography

Valence-Level Photoemission

Band-Mapping in the Ultraviolet Photoemission Limit
Densities of States in the X-Ray Photoemission Limit

Some New Directions

Photoemission with Hard X-Rays (throughout lectures)
Photoemission with Standing Wave Excitation
Photoemission with Spatial Resolution/Photoelectron Microscopy
Temporal Resolution
@ Higher Pressures

Typical experimental geometry for energy- and angle-resolved photoemission measurements

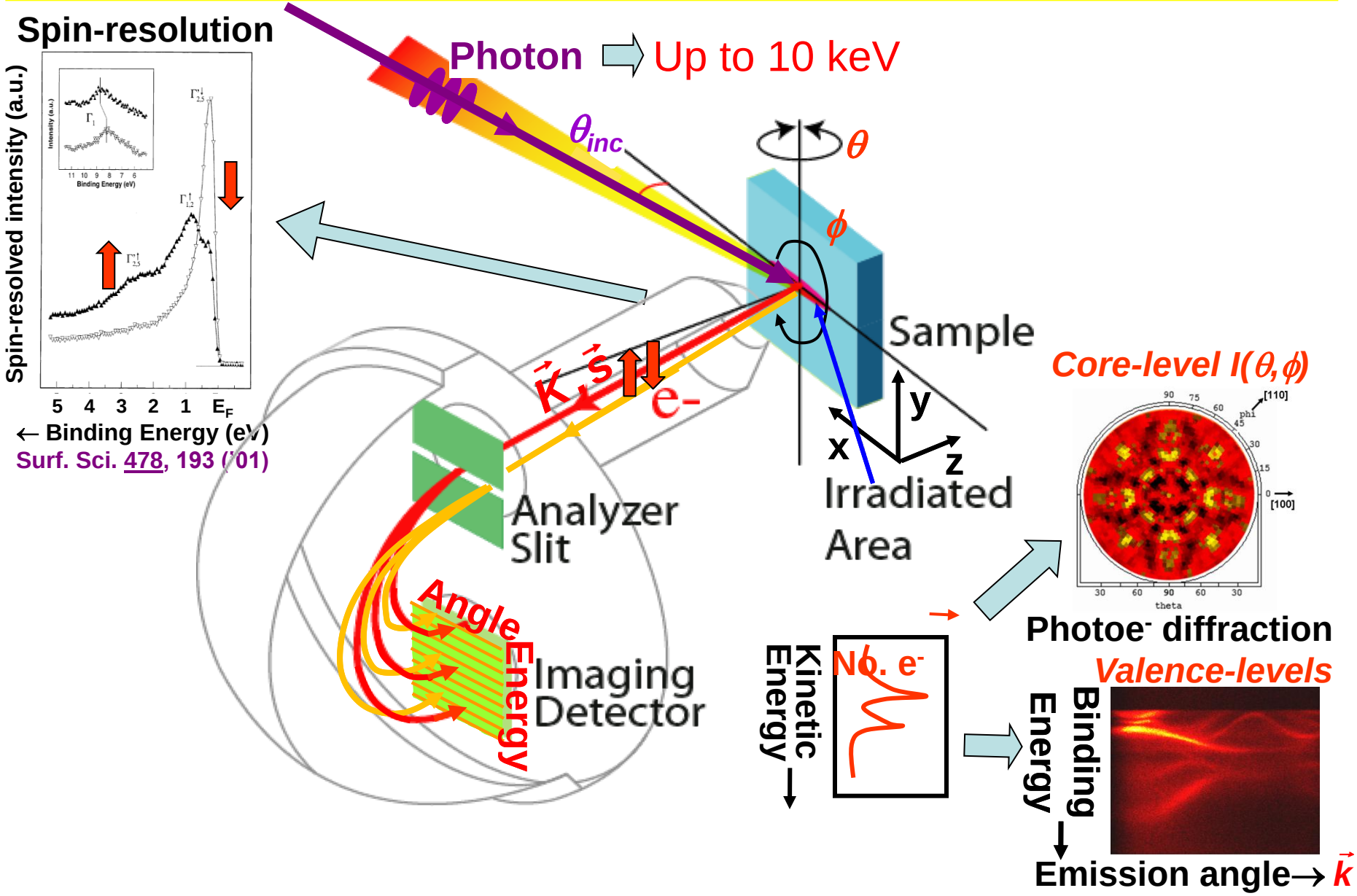

Surface sensitivity and why we may want to go to 5-10 keV in XPS

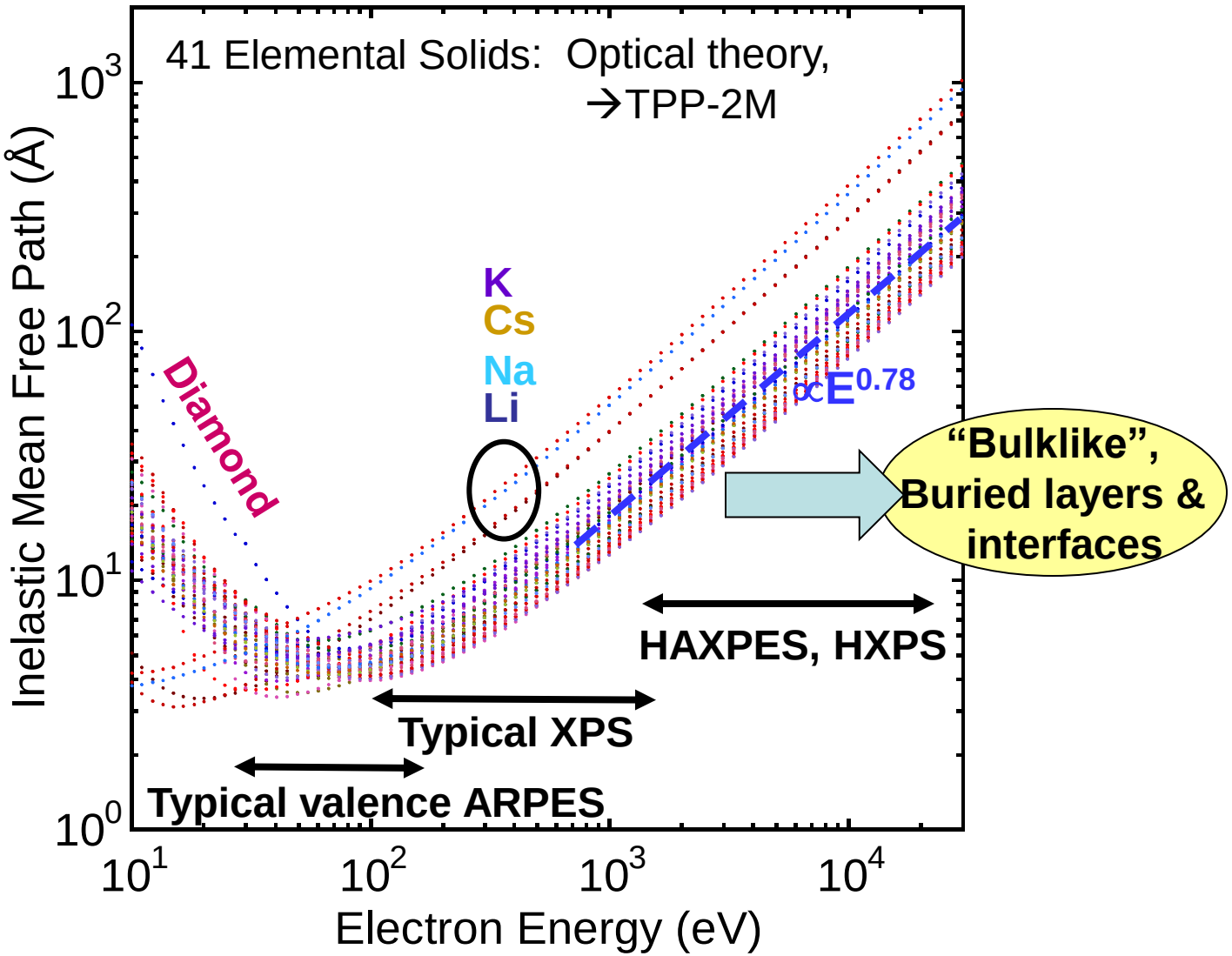

Tanuma, Powell, Penn, Surf. and Interf. Anal. 43, 689 (2011)

Varying surface sensitivity for lower electron takeoff angles

Simplest interpretation:

Average emission depth = $\Lambda_{inelastic} \sin\theta_{takeoff}$

How valid?

$E_{kin} \approx$ 500-1000 eV

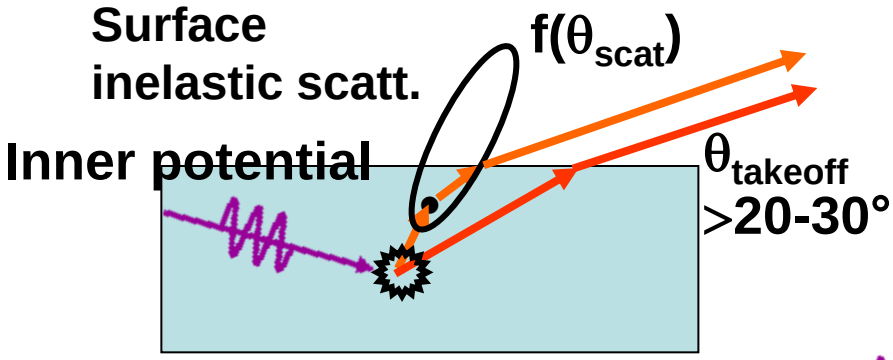

E.g.: A. Jablonski and C. J. Powell, J. Vac. Sci. Tech. A 21, 274 (2003):
→ Mean Emission Depth (MED) more relevant than $\Lambda_{inelastic}$

$E_{kin} \approx$ 10,000 eV

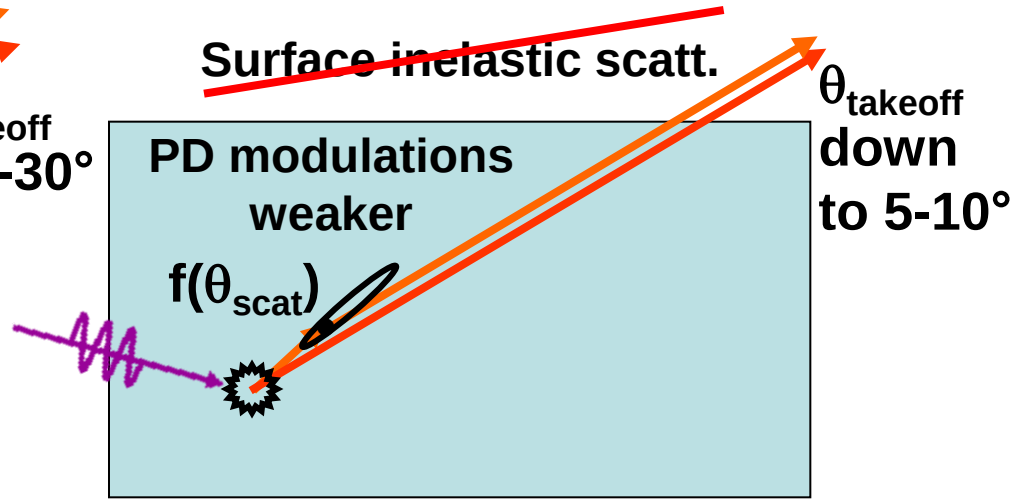

Approx. constant analyzer transmission

Simpler analysis

Cleaner bulk & surface distinction

C.S.F., Nucl. Inst. & Meth. A 547, 24 (2005)

Kover, Werner, Drube, et al., Surf. & Int. Anal. 38, 569 (2006)

Looking into nanoscale devices--Variable takeoff-angle Si 1s photoelectron spectra from NiGe(12-nm)/SiO_2(12-nm)/Si(100)

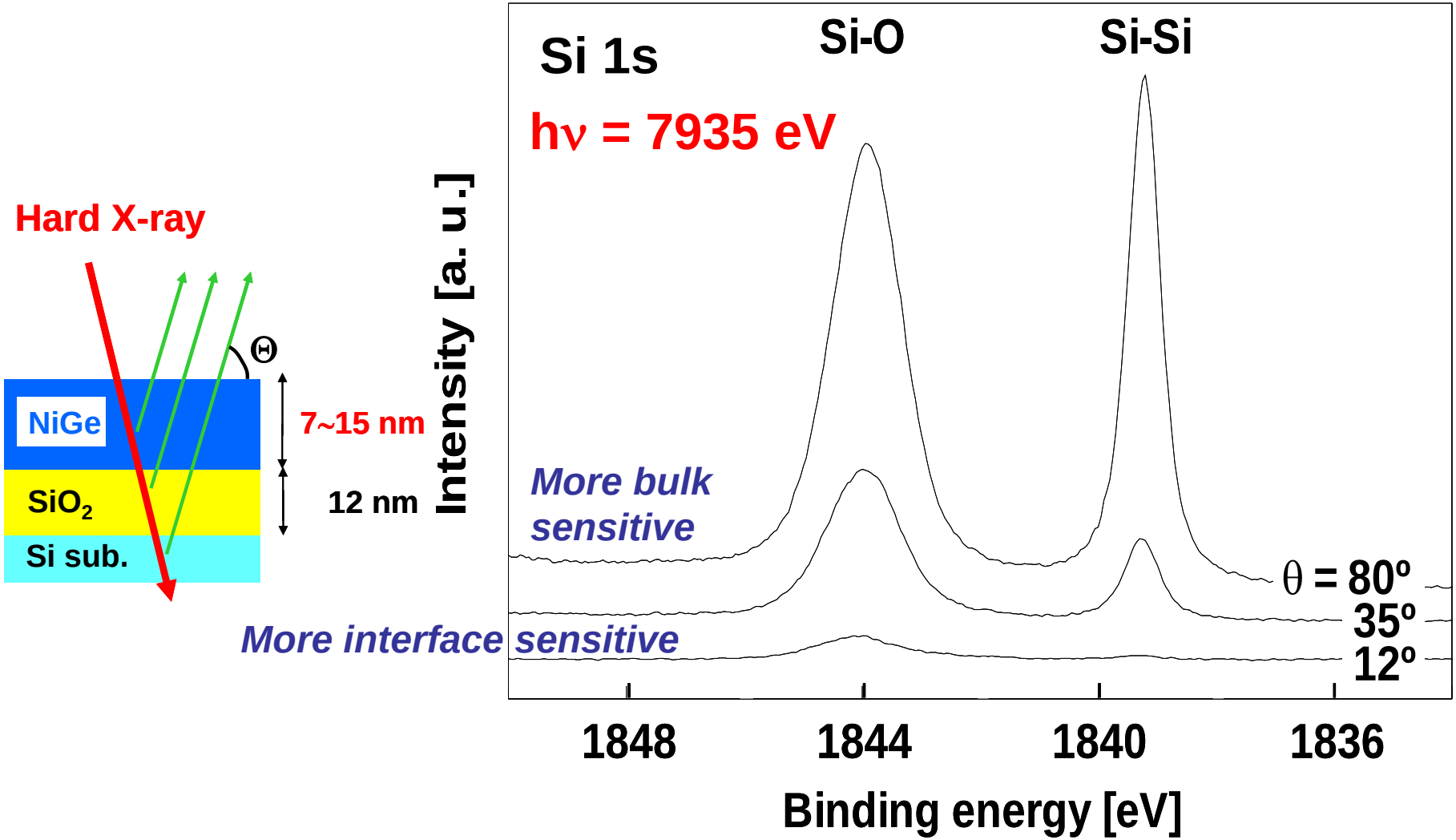

Hattori et al., Int. J. High Speed Electronics 16 (2006) 353

Hard x-ray photoemission--Quantitative analysis of peak intensities using theoretical cross sections: $La_{0.7}Sr_{0.3}MnO_3$, $h\nu$ = 7700 eV

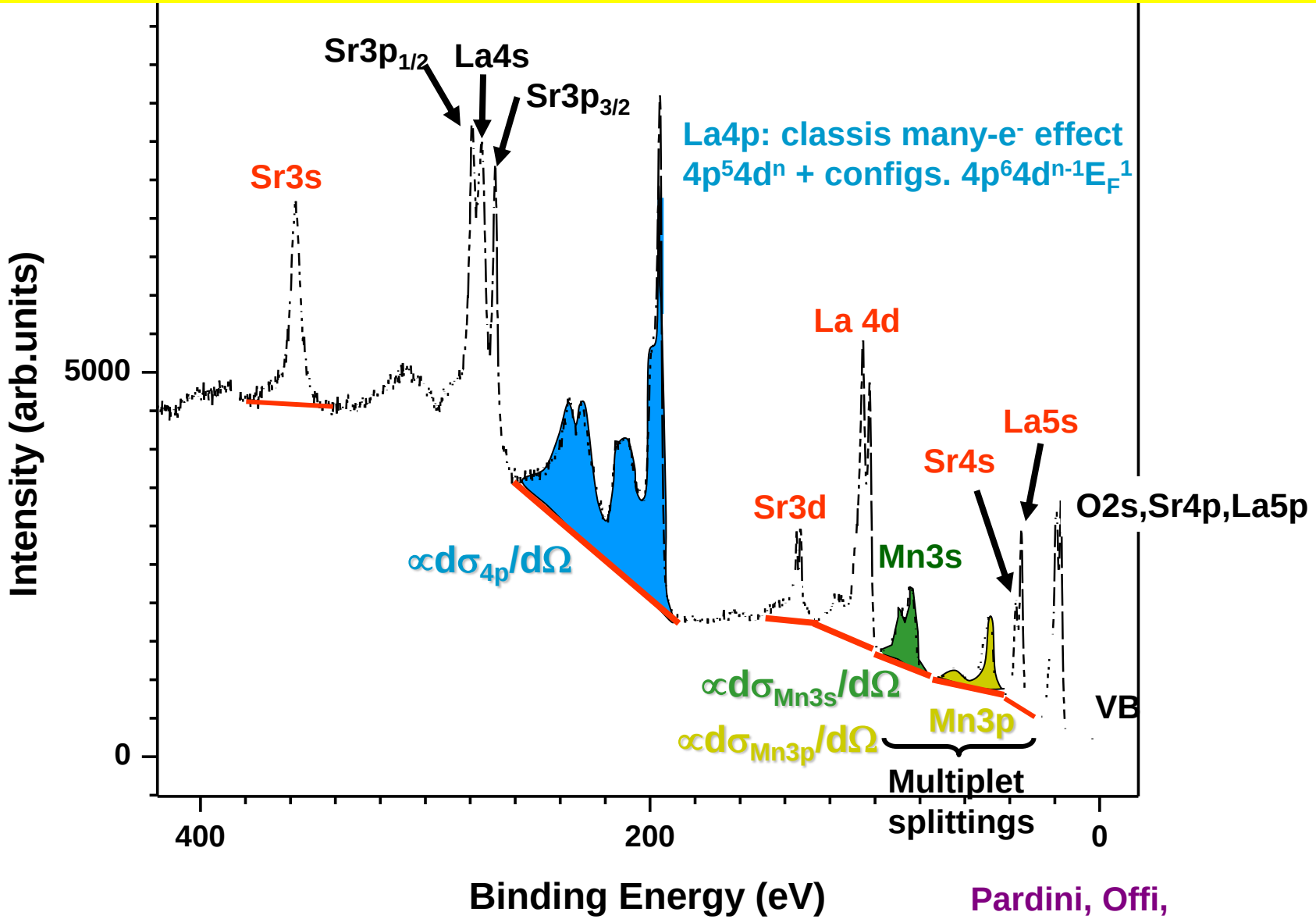

Pardini, Offi, Panaccione, CF, TBP

Quantitative analysis of peak intensities using theoretical cross sections (Scofield): $La_{0.7}Sr_{0.3}MnO_3$, $h\nu$ = 7700 eV

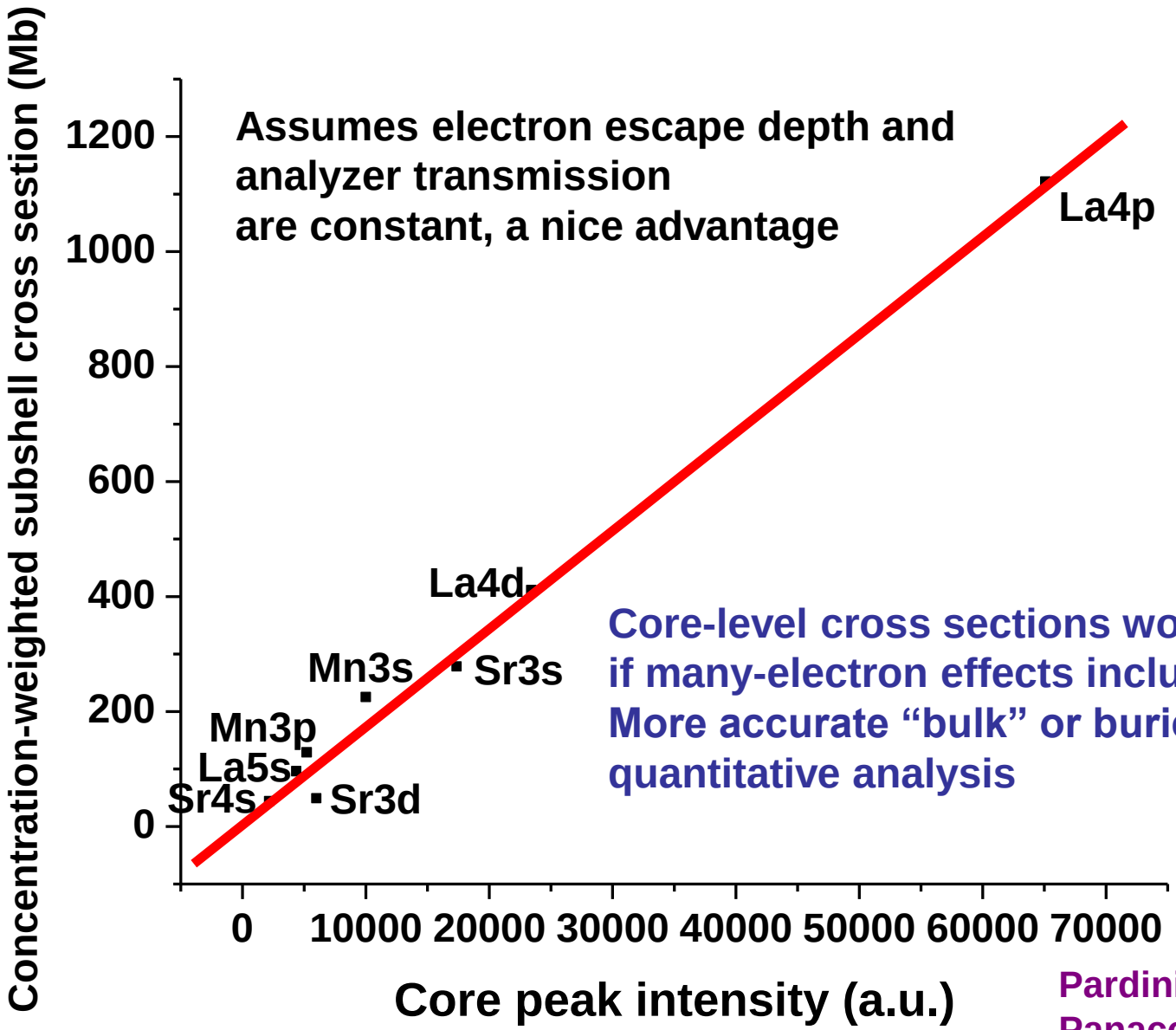

Core-level cross sections work very well, if many-electron effects included→ More accurate "bulk" or buried layer quantitative analysis

Pardini, Offi, Panaccione, CF, TBP

Electronic Structure of Strained Manganite Thin Films with Room Temperature Ferromagnetism Investigated by Hard X-ray Photoemission Spectroscopy: $La_{0.85}Ba_{0.15}MnO_3$

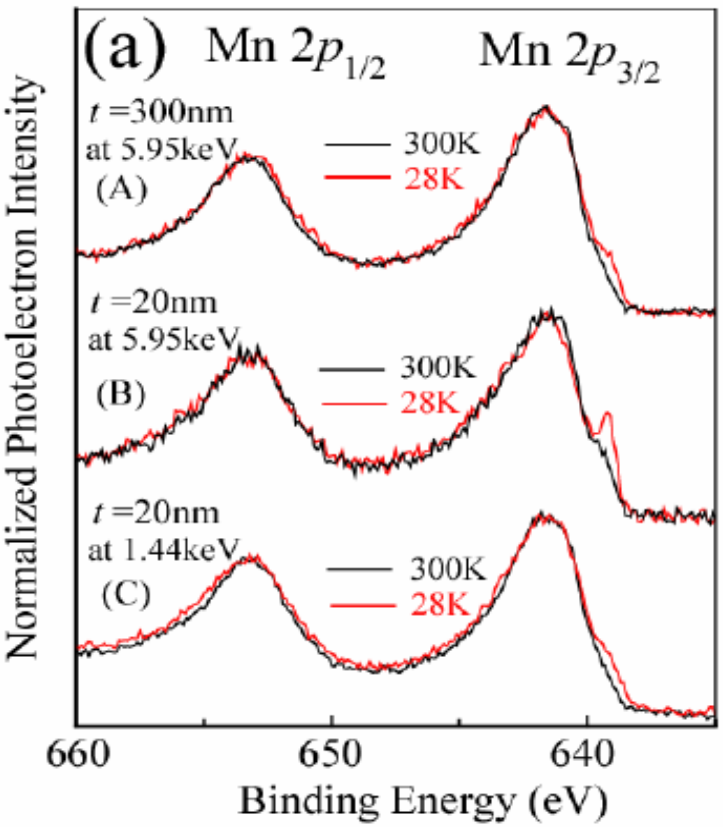

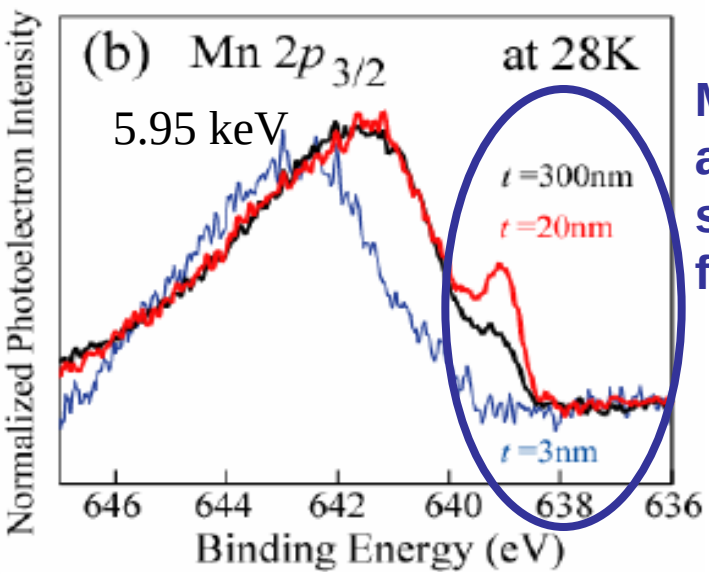

Magnetism-associated screening feature

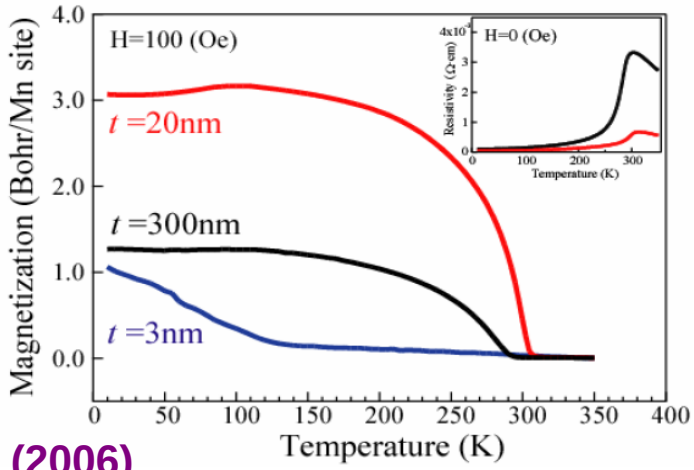

Tanaka et al., Spring8, Phys. Rev. B 73, 094403 (2006)

Temperature dependence of Mn2p spectra: $La_{0.7}Sr_{0.3}MnO_3$
New satellite structures in core spectra

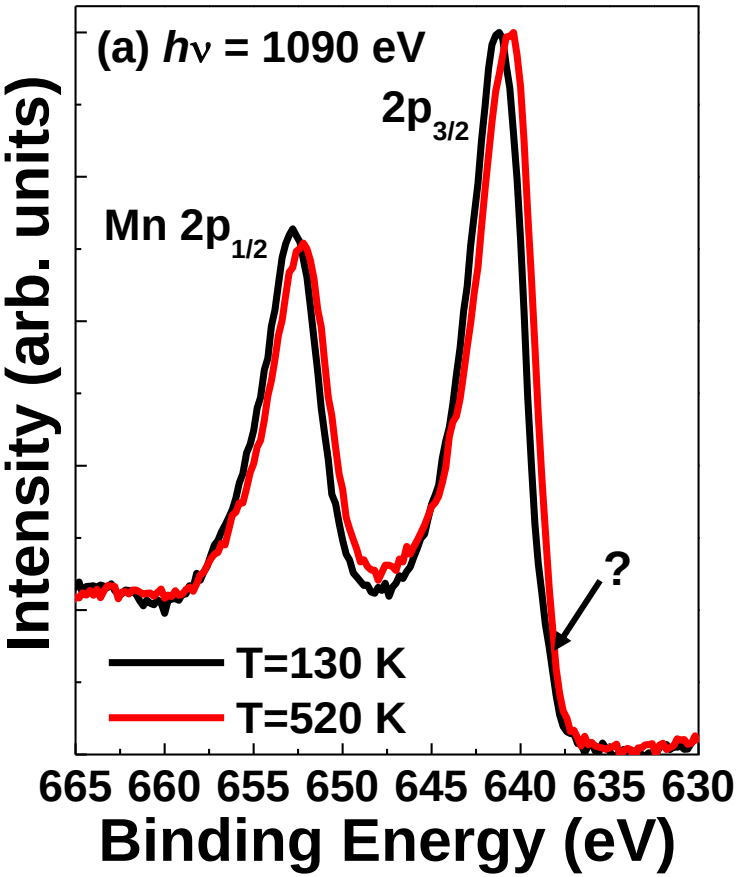

Mean depth: ~1 nm

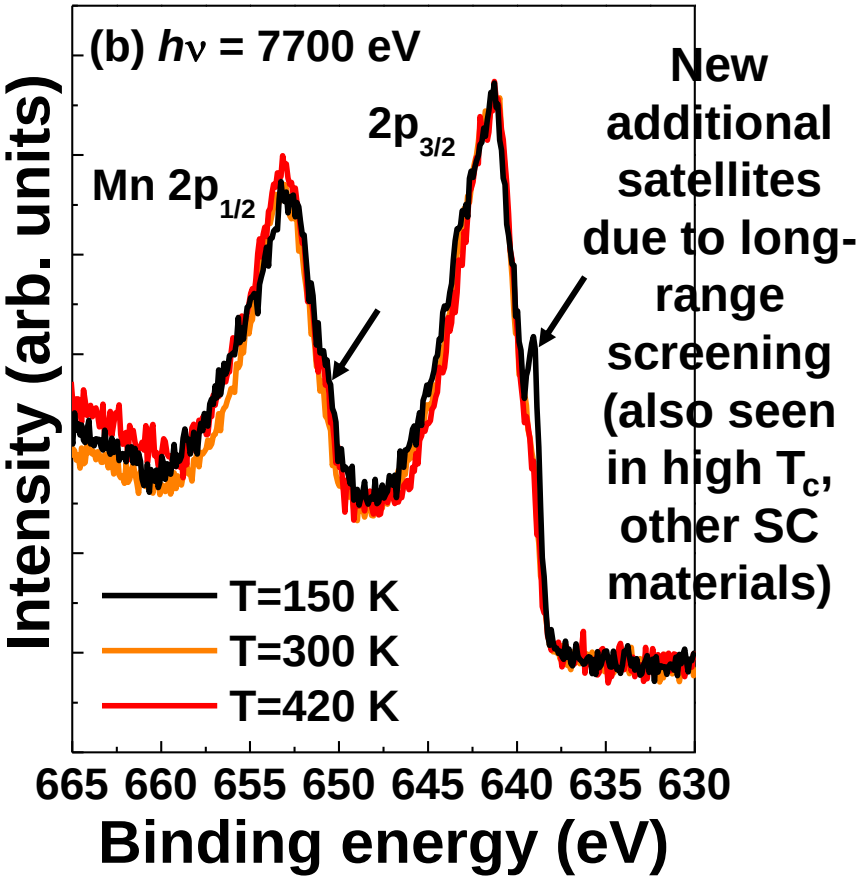

Mean depth: ~8 nm

→Suggests bulk electronic structure not reached until ca. 8 nm depth

Offi, Mannella, et al., Phys. Rev. B 2008, 77, 174422

Basic Concepts and Experiments

Core-Level Photoemission

Intensities and Quantitative Analysis, the 3-Step Model
Varying Surface and Bulk Sensitivity
Chemical shifts
Multiplet Splittings
Electron Screening and Satellite Structure
Magnetic and Non-Magnetic Dichroism
Resonant Photoemission
Photoelectron Diffraction and Holography

Valence-Level Photoemission

Band-Mapping in the Ultraviolet Photoemission Limit
Densities of States in the X-Ray Photoemission Limit

Some New Directions

Photoemission with: Hard X-Rays (throughout lectures)
Standing Wave Excitation
Spatial Resolution/Photoelectron Microscopy
Temporal Resolution
@ Higher Pressures

Typical experimental geometry for energy- and angle-resolved photoemission measurements

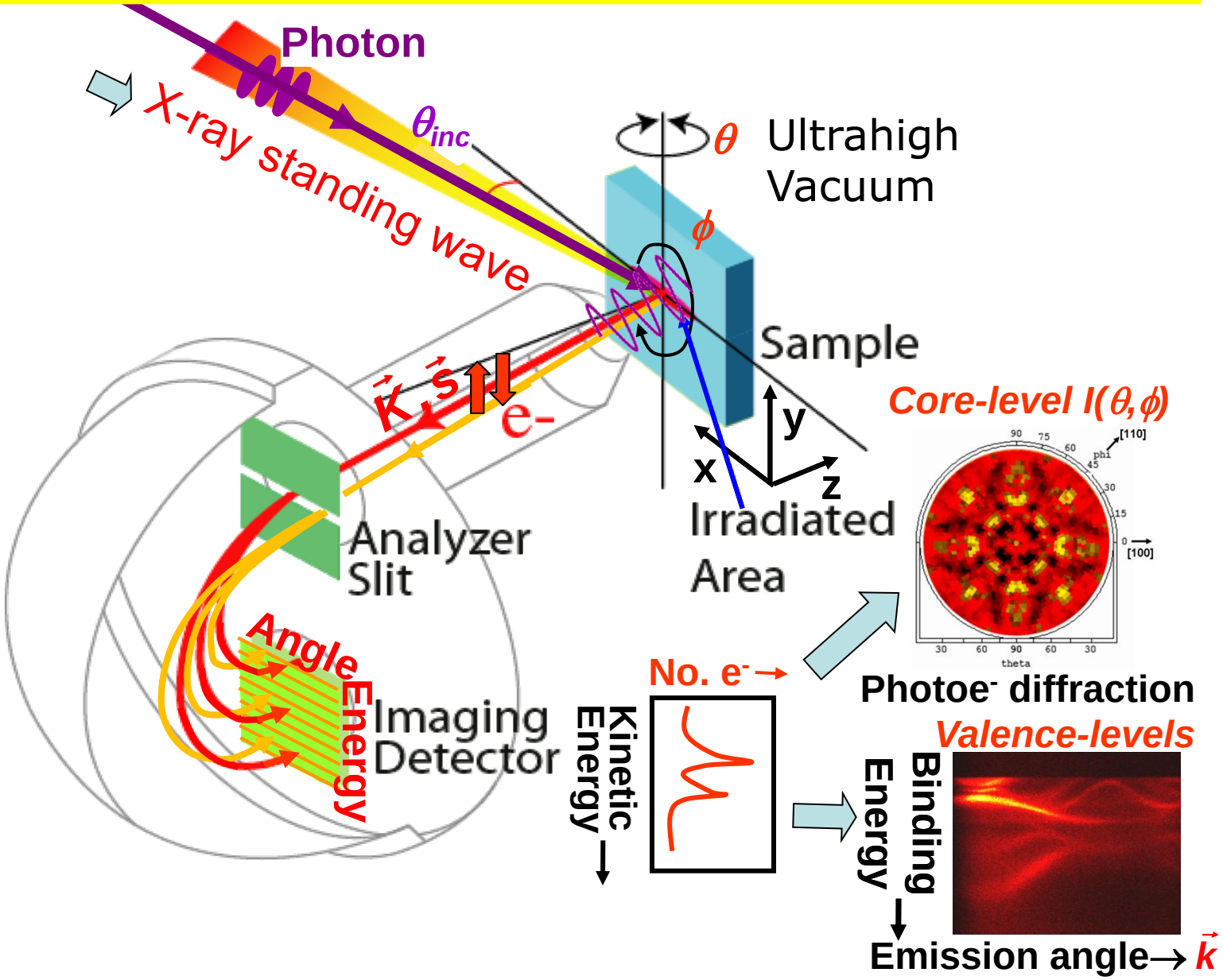

PHOTOELECTRON INTENSITIES—THE 3-STEP MODEL

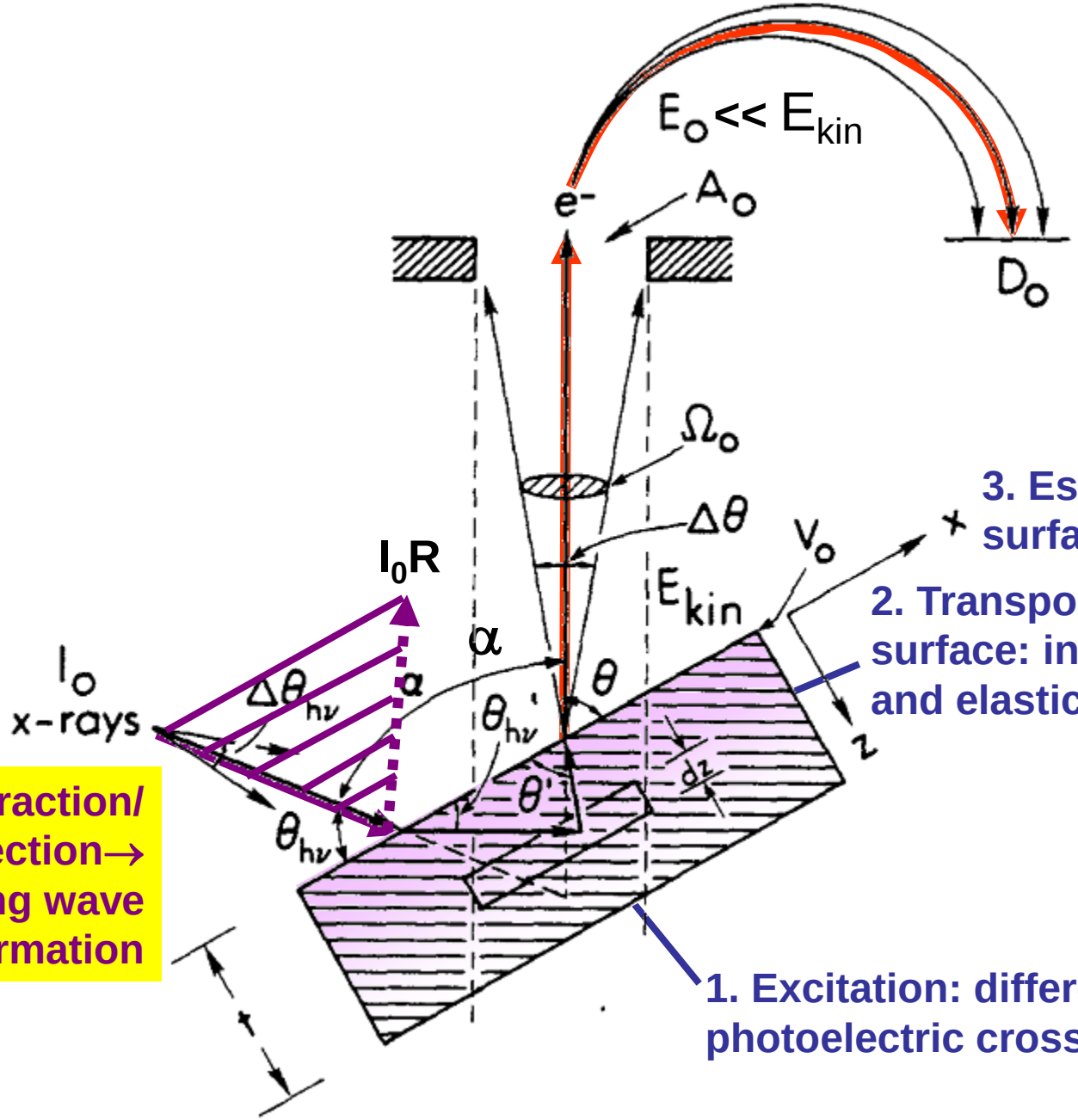

3. Escape across the surface barrier (V_0)

2. Transport to the surface: inelastic (Λ_e) and elastic ($f(\theta)$) scattering

+X-ray refraction/ reflection→ standing wave formation

1. Excitation: differential photoelectric cross section ($d\sigma/d\Omega$)

Standing wave formation:

$$I_{SW}(|E^2|) \propto |\phi_{inc} + \phi_{refl}|^2 = |\phi_{inc}|^2 + \underbrace{\phi_{inc}\phi_{refl}^* + \phi_{inc}^*\phi_{refl}}_{\text{SW modulation}} + |\phi_{refl}|^2$$

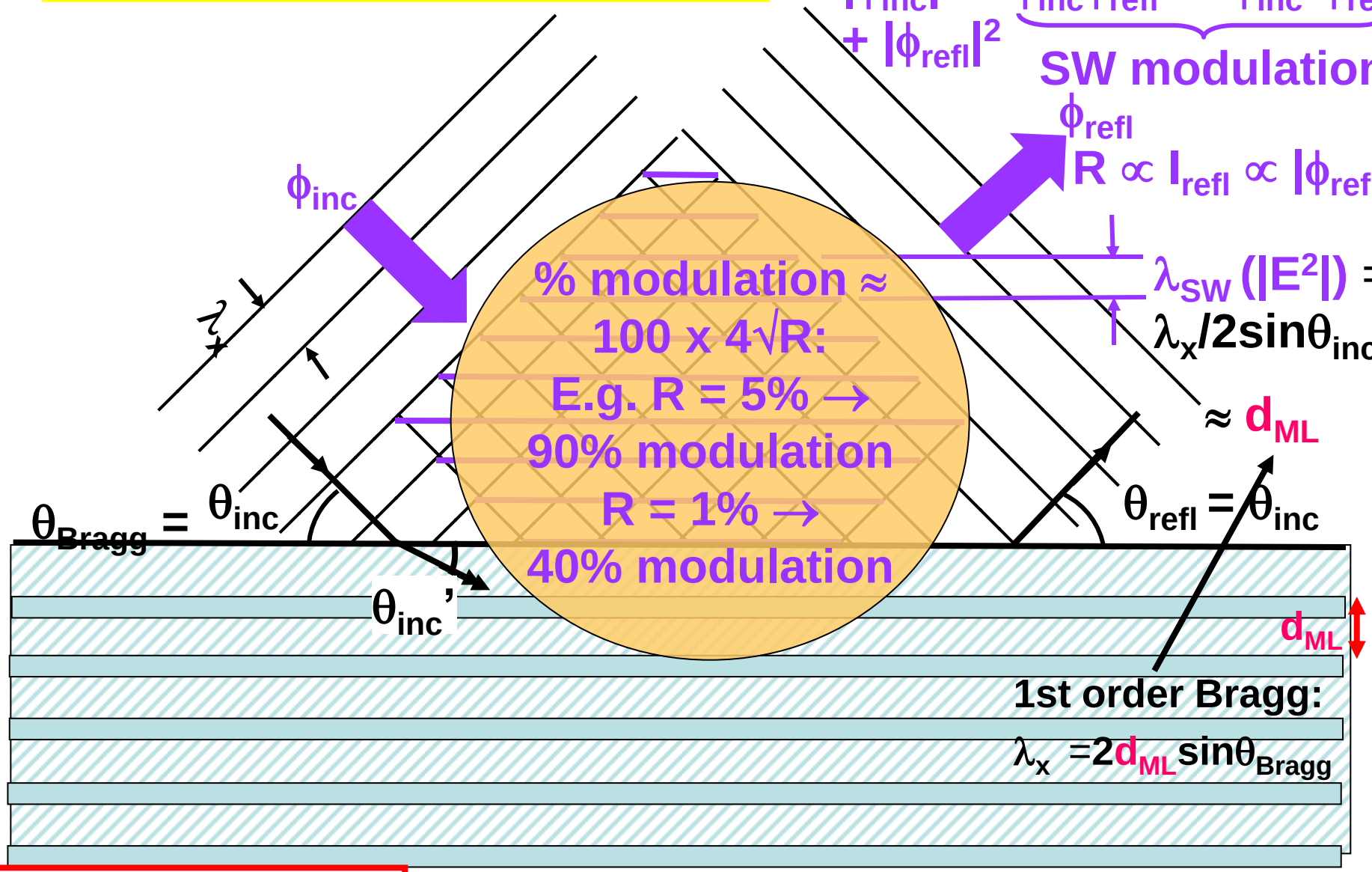

Periodic atomic planes: $d_{ML} \leq$ ~5 Å--Si(111)—≤3.74Å, LaB_{66}(001) --≤23.52Å→5.88Å, mica—10.0 Å; or **Synthetic multilayers:** $d_{ML} \approx$ ~20-40 Å

Standing wave formation in reflection from a surface, or single-crystal Bragg planes[+], or a multilayer mirror

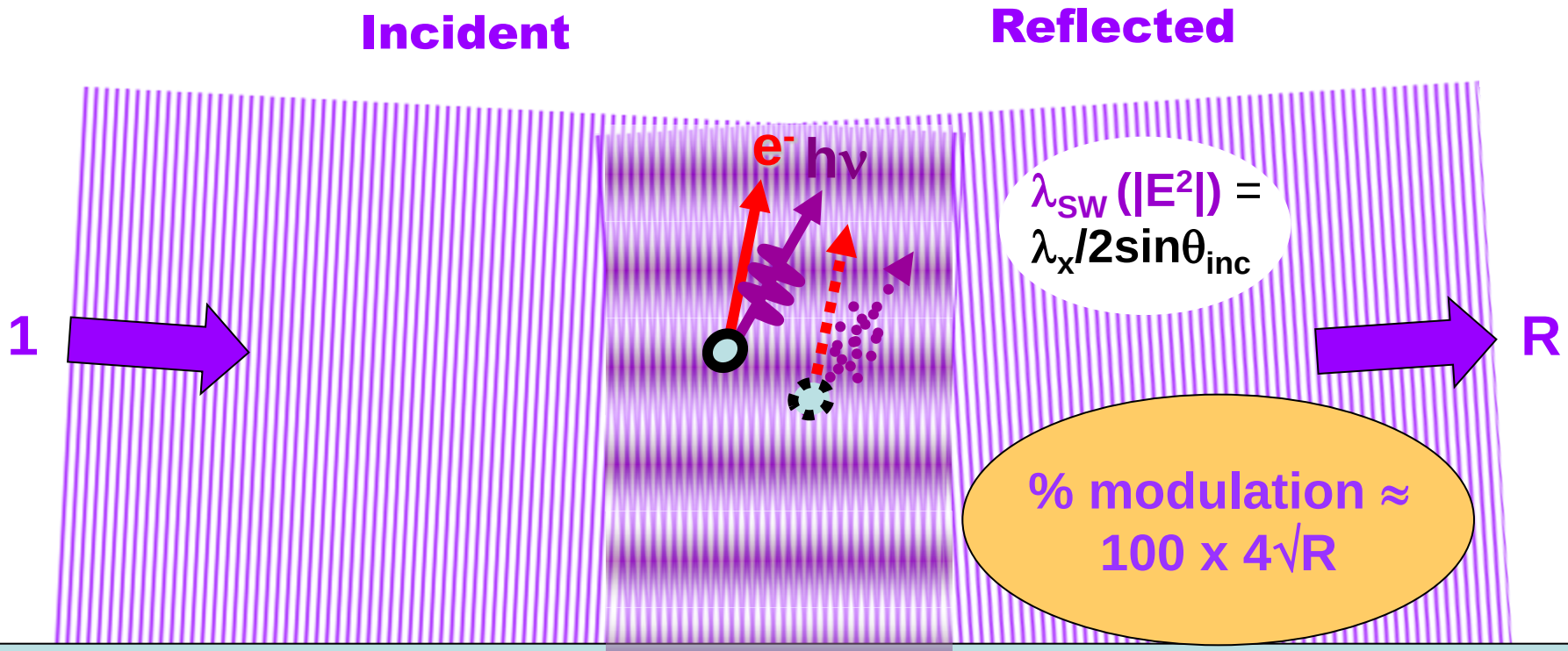

- ***Rocking curve:***

$$I(\theta_{inc}) \propto 1 + R(\theta_{inc}) + 2\sqrt{R(\theta_{inc})}\, f \cos[\varphi(\theta_{inc}) - 2\pi P]$$

XMCD—Kim, Kortright, PRL 86, 1347 (2001)

- ***Photon energy scan:***

$$I(h\nu) \propto 1 + R(h\nu) + 2\sqrt{R(h\nu)}\, f \cos[\varphi(h\nu) - 2\pi P]$$

with: f = coherent fraction of atoms, P = phase of coherent-atom position

- ***Phase scan with wedge-shaped sample ("Swedge" method):***

[+]Standing waves via Bragg reflection of hard x-rays: Batterman, Phys. Rev A 133, 759 (1964)

Standing Wave Behavior During a Rocking Curve Scan

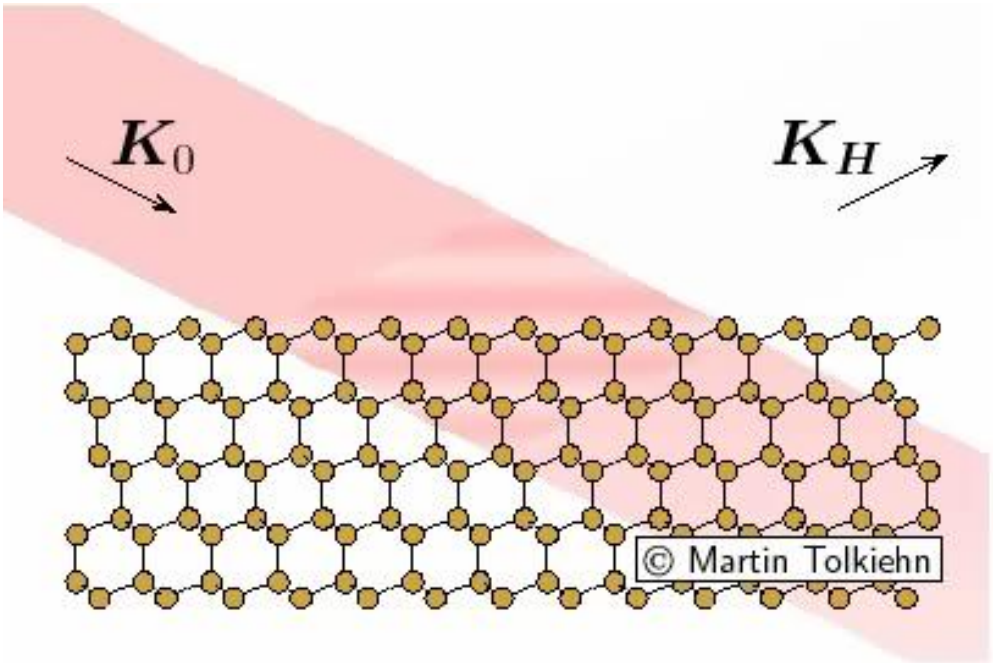

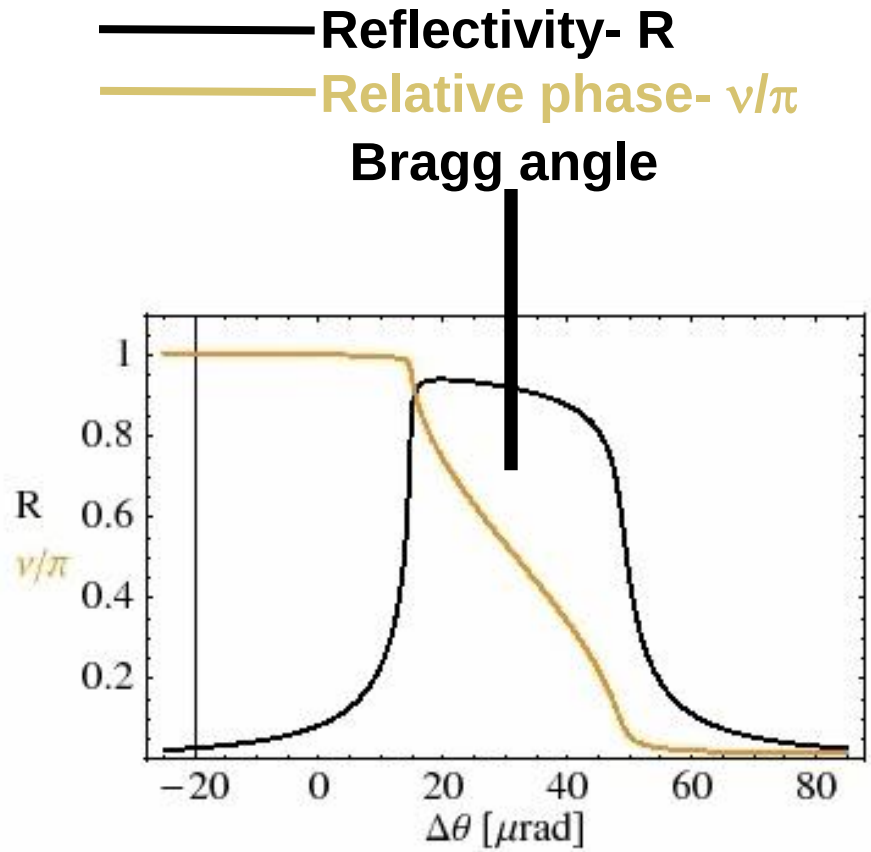

+Same general forms if photon energy is scanned

With thanks to Martin Tolkiehn, Dimitri Novikov, DESY

Site-specific valence electronic structure of SrTiO3

hν = 2.75 keV

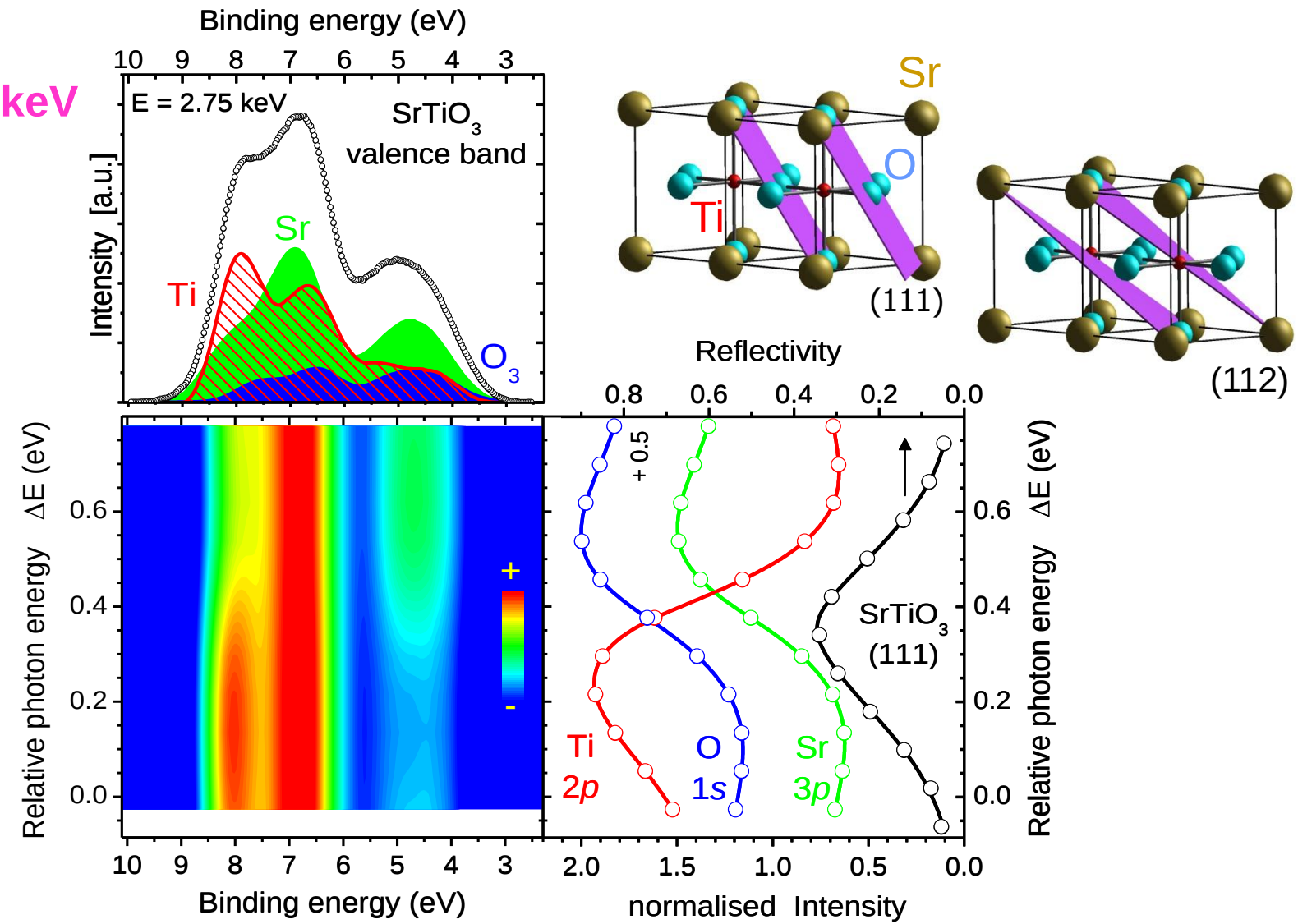

Valence band XSW *Core-level XSW*

Lee et al., Solid State Communications 150 (2010) 553,
Talk by Materlik

Case study: Standing wave/rocking curve analysis of an epitaxial $SrTiO_3/La_{0.67}Sr_{0.33}MnO_3$ interface: Resonant soft x-ray excitation

The Advanced Light Source

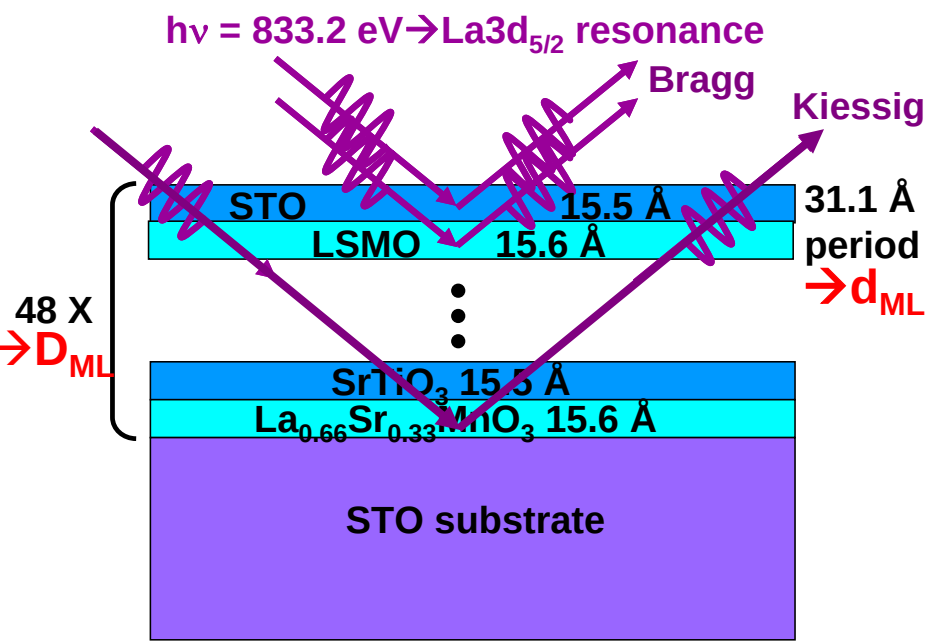

$$\lambda_x = 2d_{ML}\sin\theta_{Bragg}$$

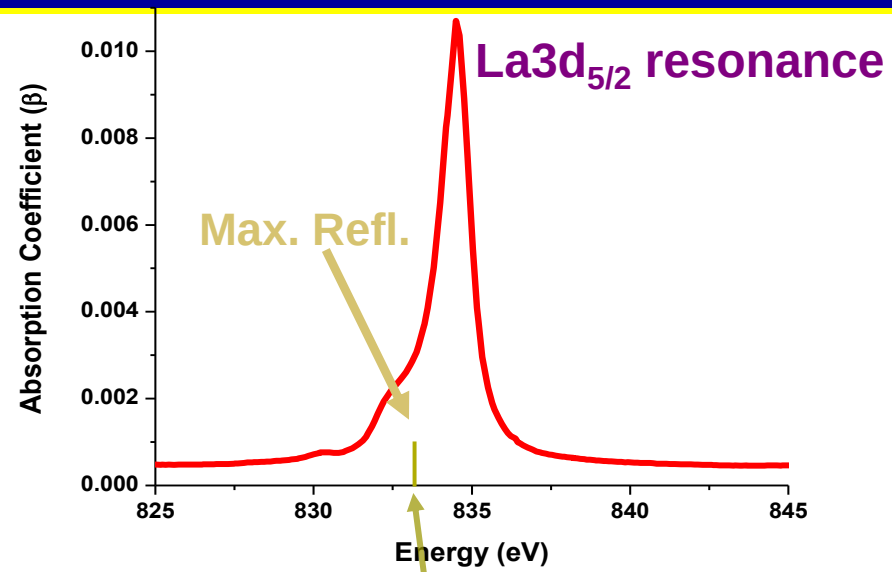

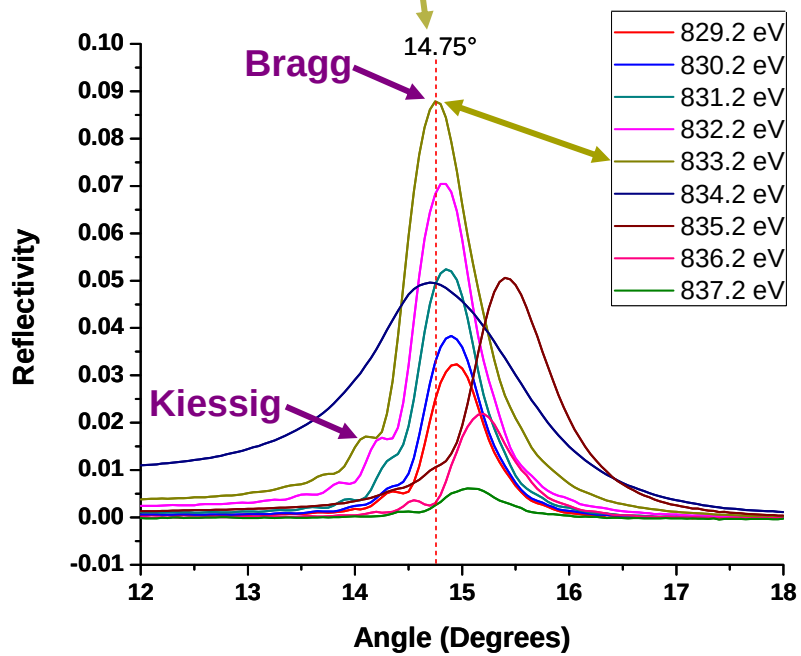

Gray et al., Phys. Rev. B 82, 205116 (2011)
Samples: Ramesh, Huijben

Standing wave/rocking curve analysis of an epitaxial $SrTiO_3/La_{0.67}Sr_{0.33}MnO_3$ interface: hard x-ray excitation

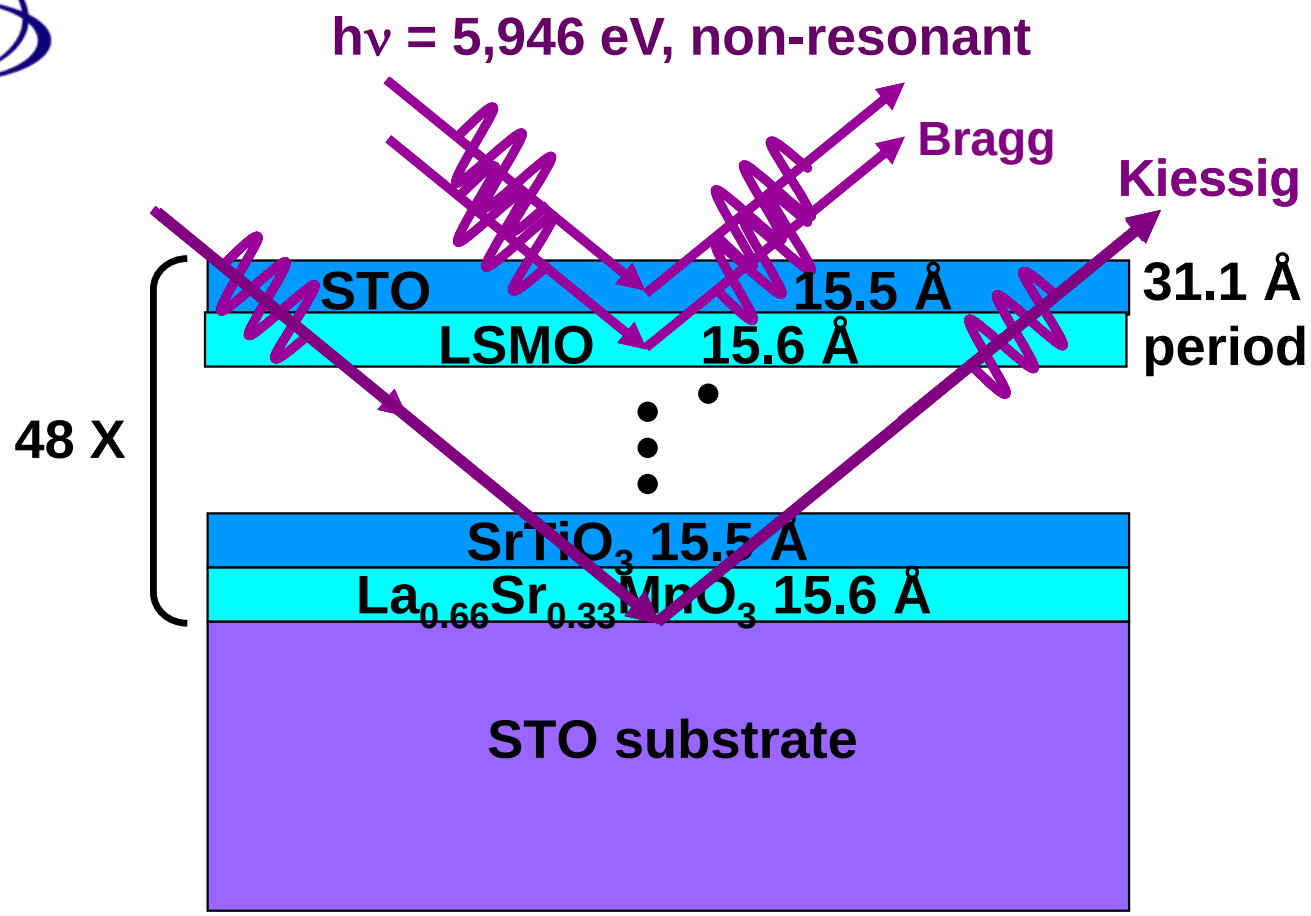

Gray et al., Phys. Rev. B 82, 205116 (2011)
Samples: Ramesh, Huijben

$SrTiO_3/La_{0.67}Sr_{0.33}MnO_3$ Multilayer
Analysis of Rocking Curves

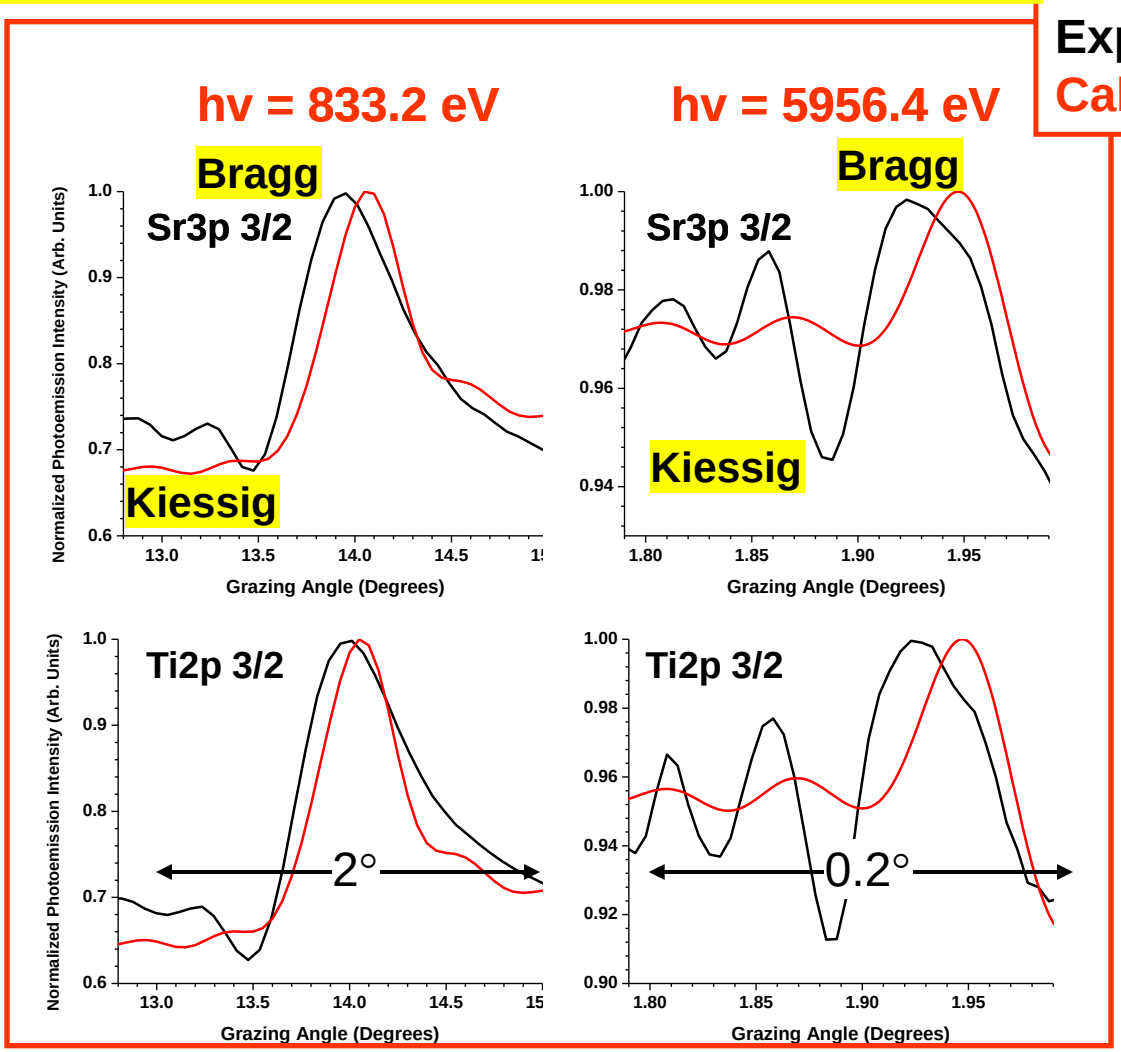

Ideal Bilayer Thickness Gradient Profile

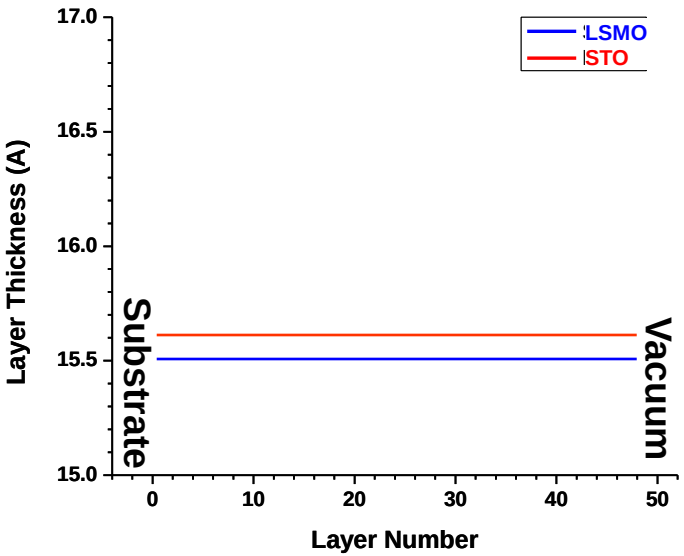

- Relative amplitude of the predicted Kiessig fringes does not agree with experiment
- Strong Kiessig fringes predicted on both sides of the rocking curves, esp. @ 5.9 keV

The Advanced Light Source

SPring-8

$SrTiO_3/La_{0.67}Sr_{0.33}MnO_3$ Multilayer
Analysis of Rocking Curves

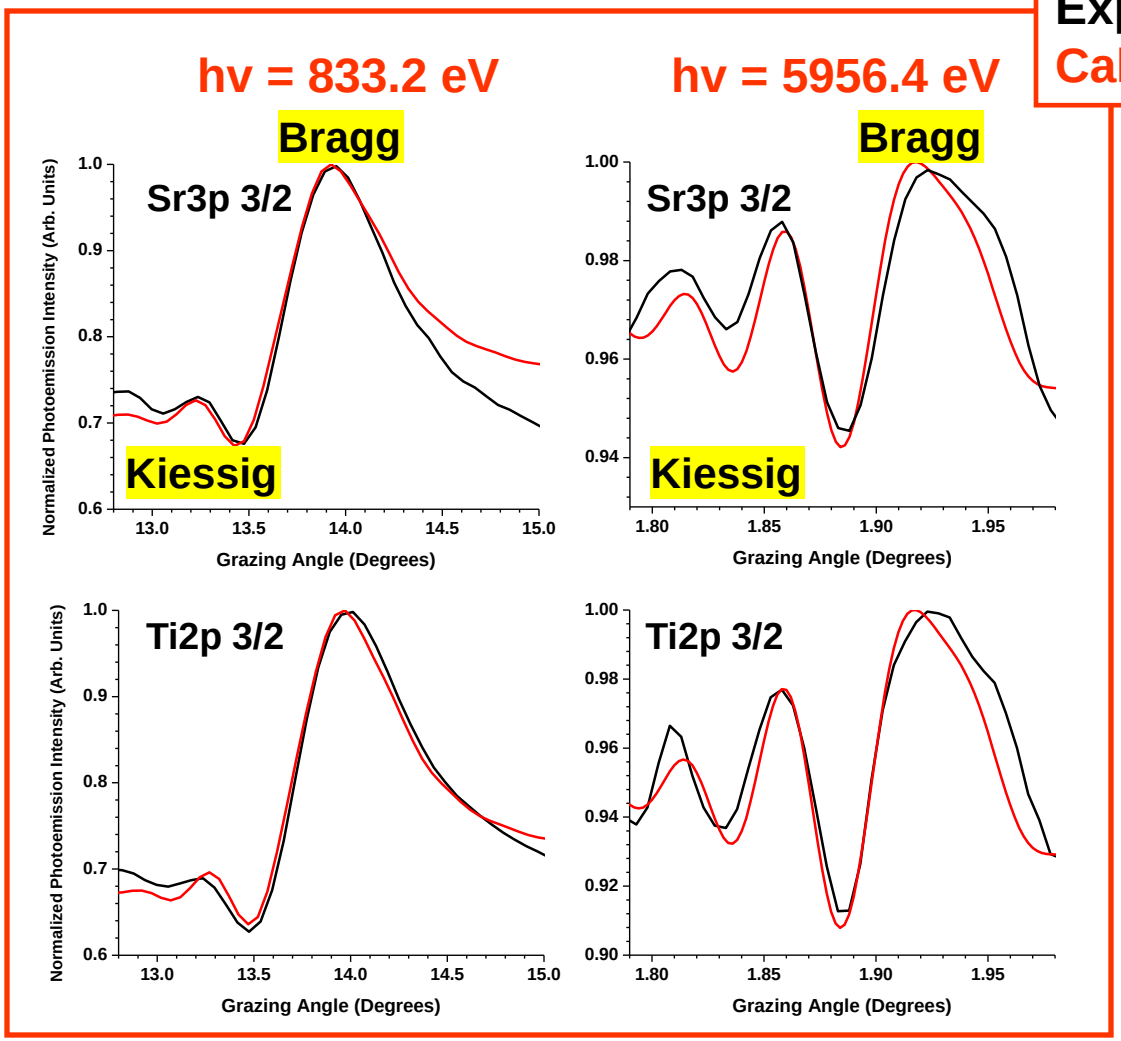

Bilayer Thickness Gradient Profile

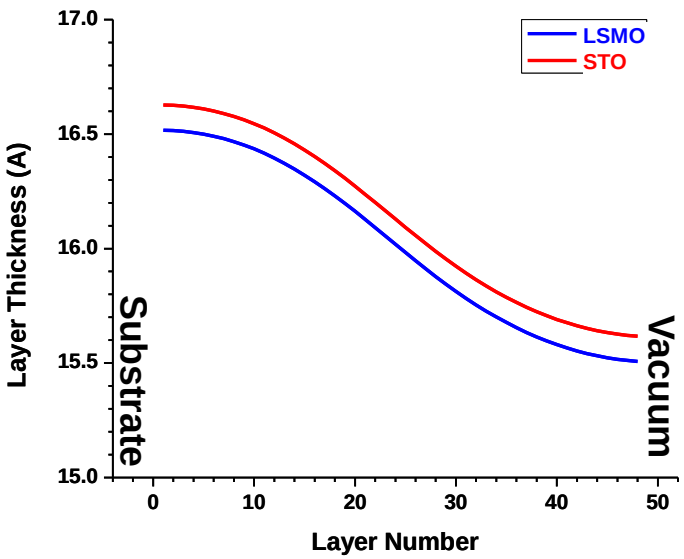

→Average multilayer d_{ML} changes by about -2 Å ≈ -6% or half a unit cell from top to bottom

BEST FIT

The Advanced Light Source

SPring-8

A. Gray

Fitting of Rocking Curves—All Elements Present, Soft and Hard X-rays

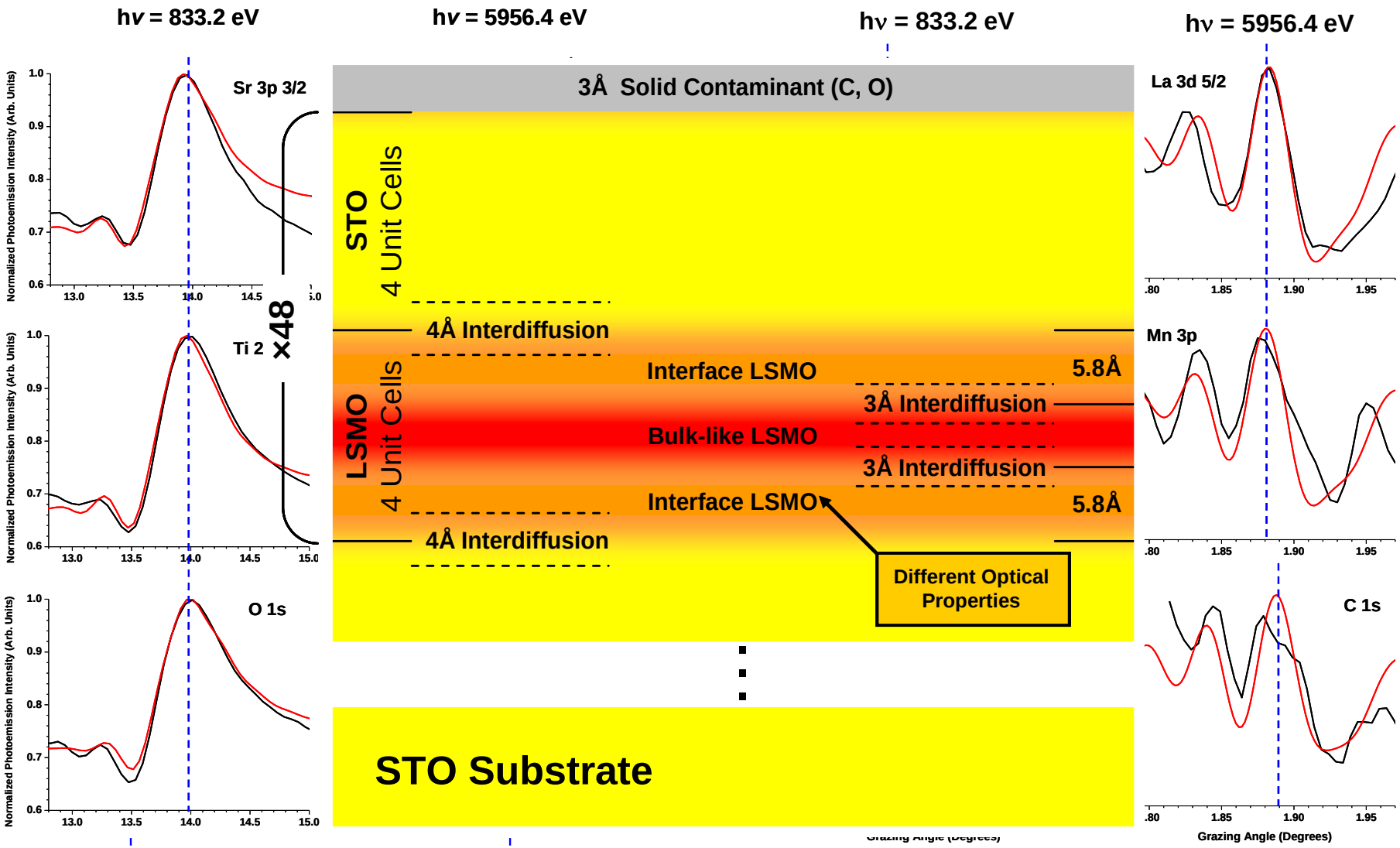

Gray et al., Phys. Rev. B 82, 205116 (2011)

STO/LSMO-Resonant soft x-ray standing wave/rocking curves at 833 eV: core photoelectron peaks compared to calculated standing-wave field

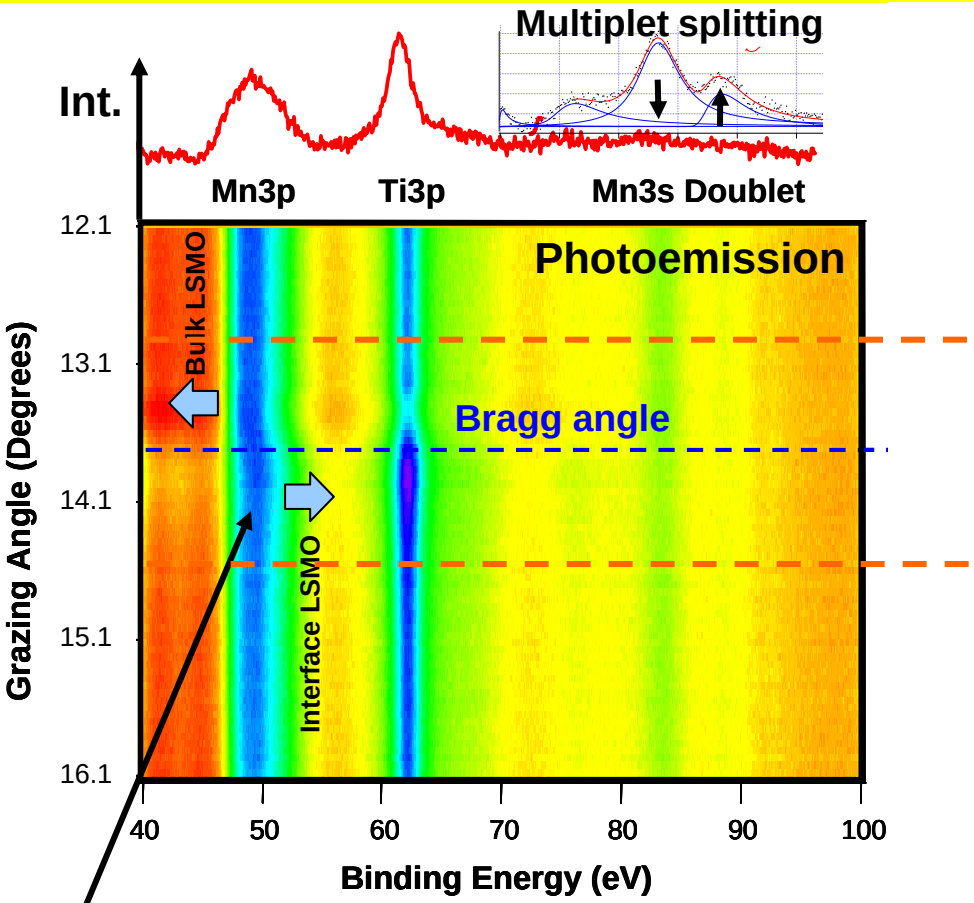

- Clear chemical/final-state shift at interface seen in Mn 3p
- No change in Mn 3s
- No change in Ti 3p—near surface

The Advanced Light Source

Gray, Yang et al., Phys. Rev. B 82, 205116 (2011)

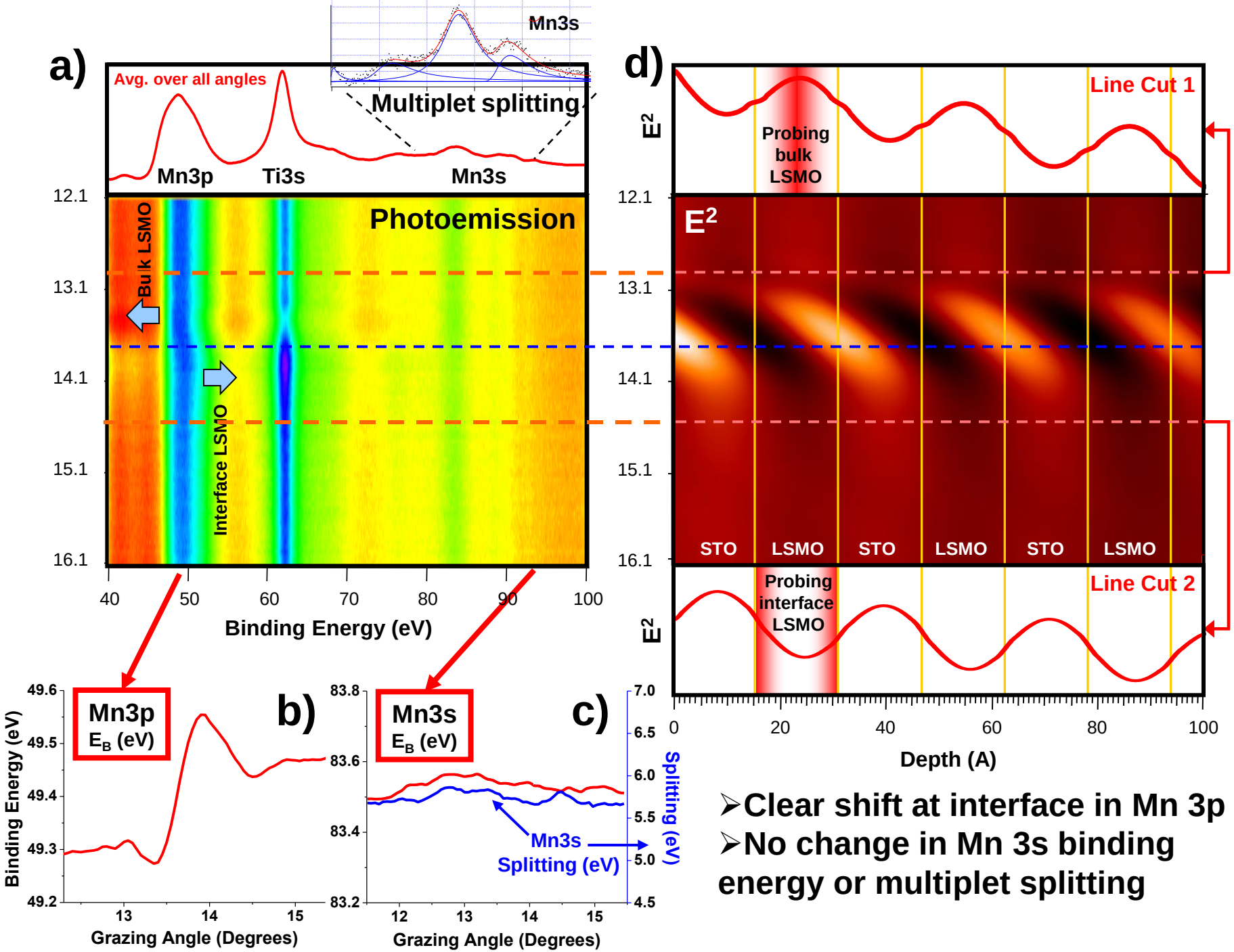

- Clear shift at interface in Mn 3p
- No change in Mn 3s binding energy or multiplet splitting

STO/LSMO-Explaining the Difference Between Mn 3p and Mn 3s behavior

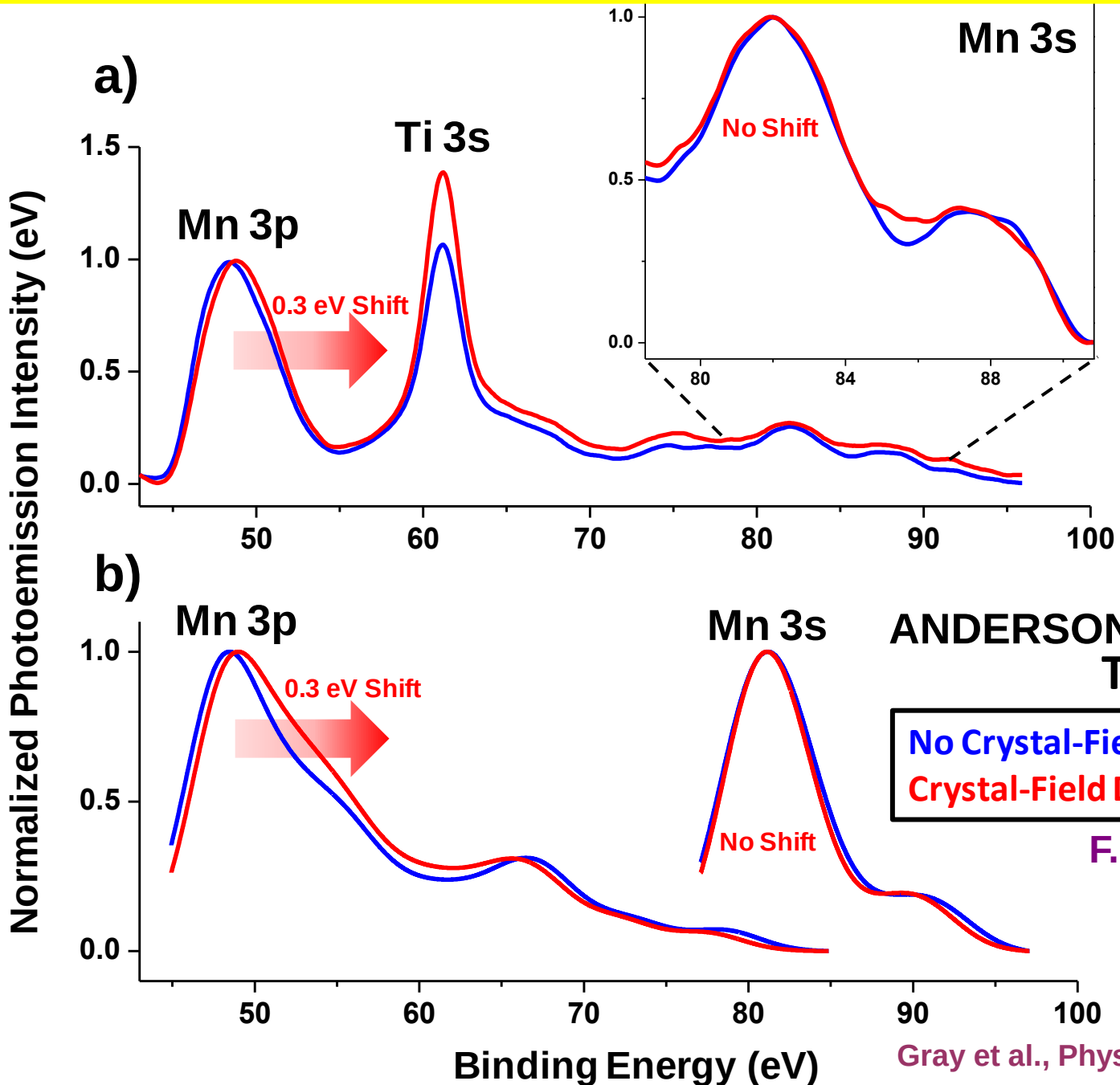

EXPERIMENT

Bulk LSMO
Interface LSMO

ANDERSON IMPURITY MODEL THEORY

No Crystal-Field Distortion
Crystal-Field Distortion (Ds = 0.2 eV)

F. de Groot

Gray et al., Phys. Rev. B 82, 205116 (2010)

X-ray photoemission: some key elements

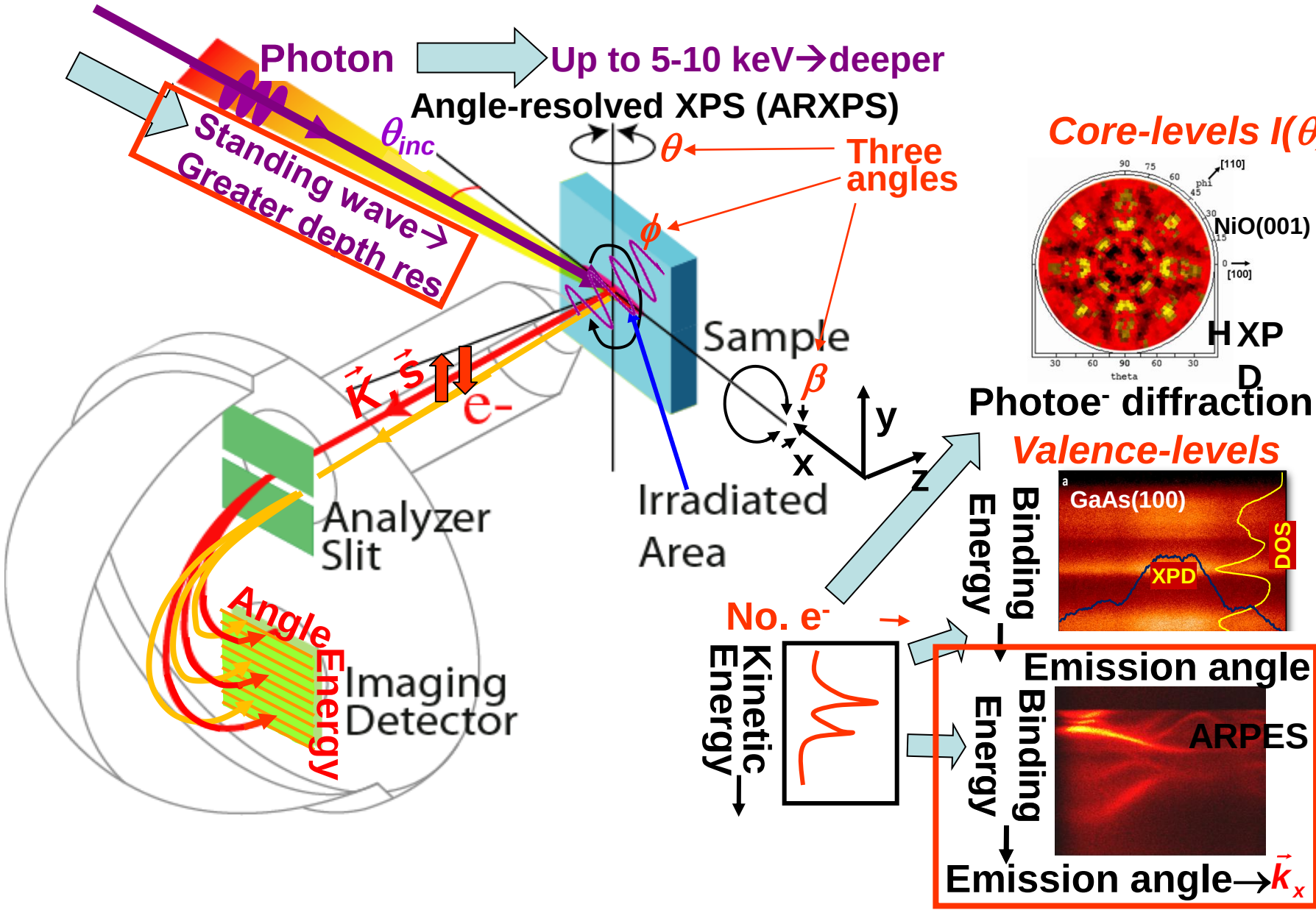

ARPES—How high can we go in energy and temperature?

$E_f(\vec{K}_f) =$

$E_f(\vec{k}_f) - V_0 \approx \hbar^2 K_f^2 / 2m_e$

$\vec{k}_{f,\parallel} = \vec{K}_{f,\parallel}$

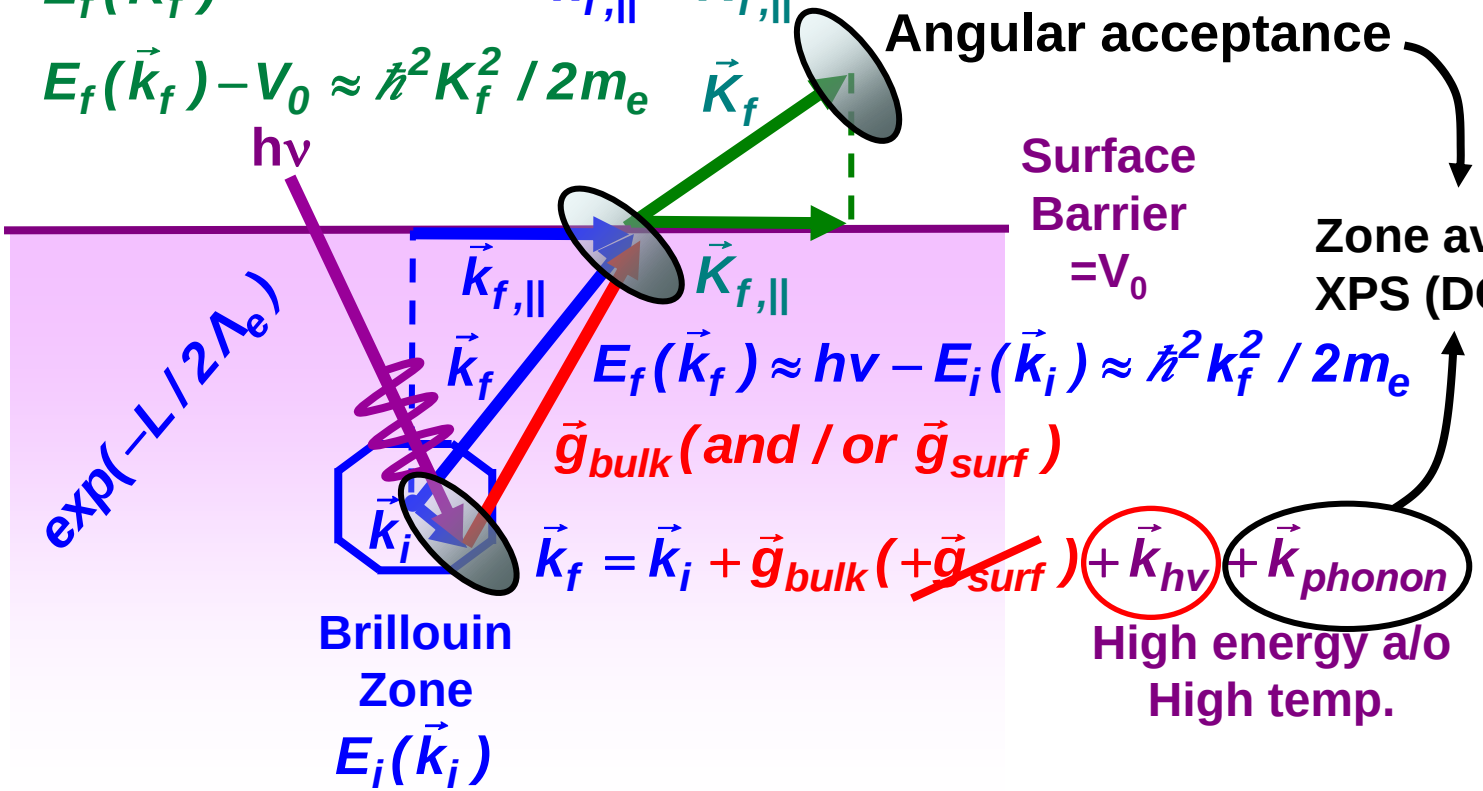

Zone averaging:
XPS (DOS) limit

Fraction DTs ≈ Debye-Waller factor = $W(T) \approx \exp[-(k^f)^2 \langle u^2(T)\rangle]$

$\approx \exp[-C_1 (k^f)^2 T/(m\Theta_D^2)] \approx \exp(-C_2 E_{kin} T)$

ARPES → bands, quasiparticles (Low hν, Low T, High angul. Res.)

Shevchik, Phys. Rev. B 16, 3428 (1977)
Hussain….CF, Phys. Rev. B 34 (1986) 5226

XPS → DOS (High hν, High T, Low angul. Res.)

$SrTiO_3$ and $La_{0.67}Sr_{0.33}MnO_3$ band structures and DOS

$SrTiO_3$-insulator

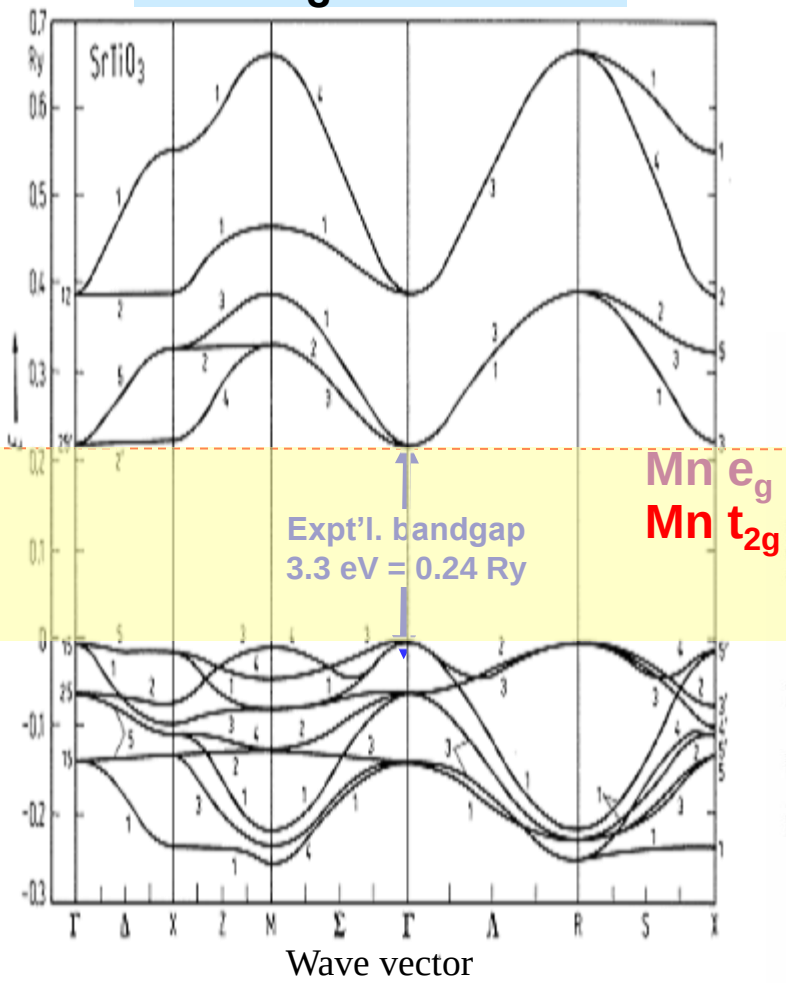

Mattheiss, PRB 6, 4718 (1972)

$La_{0.67}Sr_{0.33}MnO_3$-Half-Metallic Ferromagnetic metal

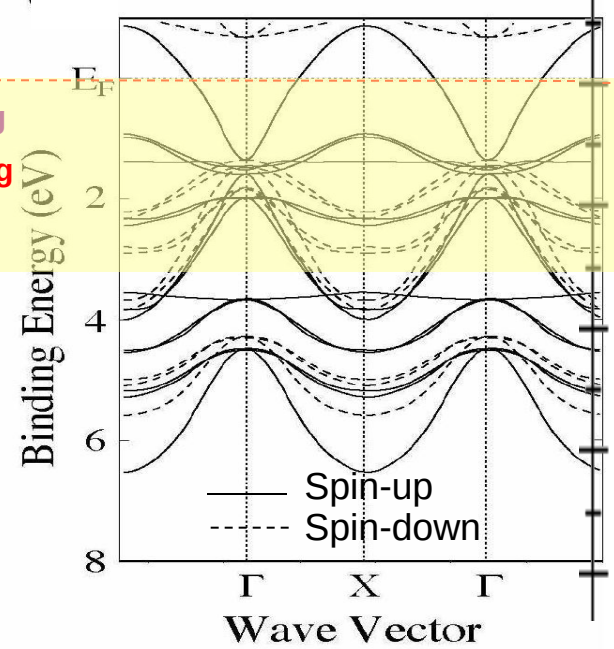

Chikamatsu et al., PRB 73, 195105 (2006)

Zheng, Binggeli, J. Phys. Cond. Matt. 21, 115602 (2009)

Projected DOSs

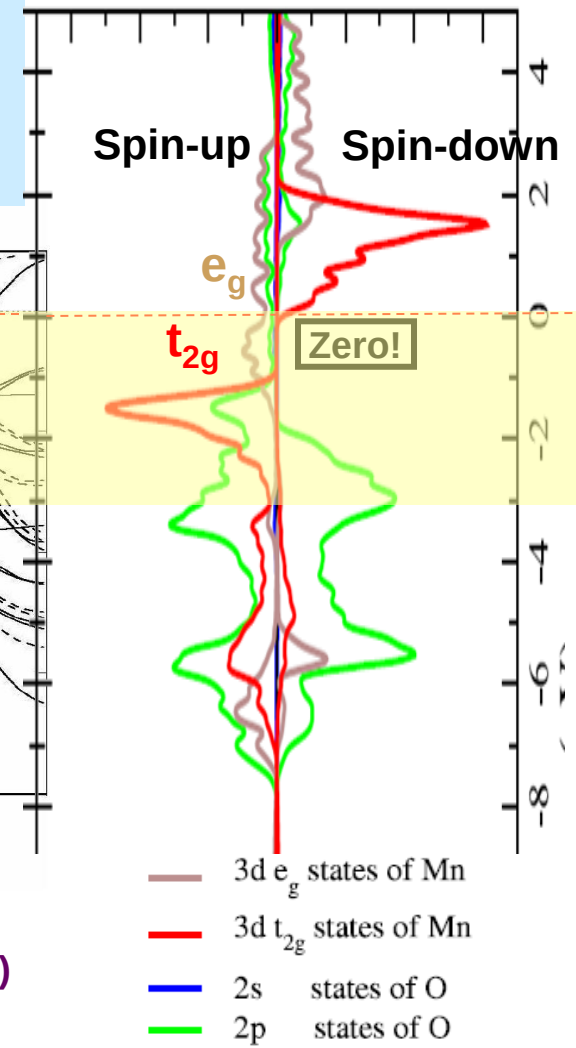

STO/LSMO-Standing wave/rocking curves of valence region: 833 eV, 300K
Debye-Waller ≈ 0.013→ DOS limit

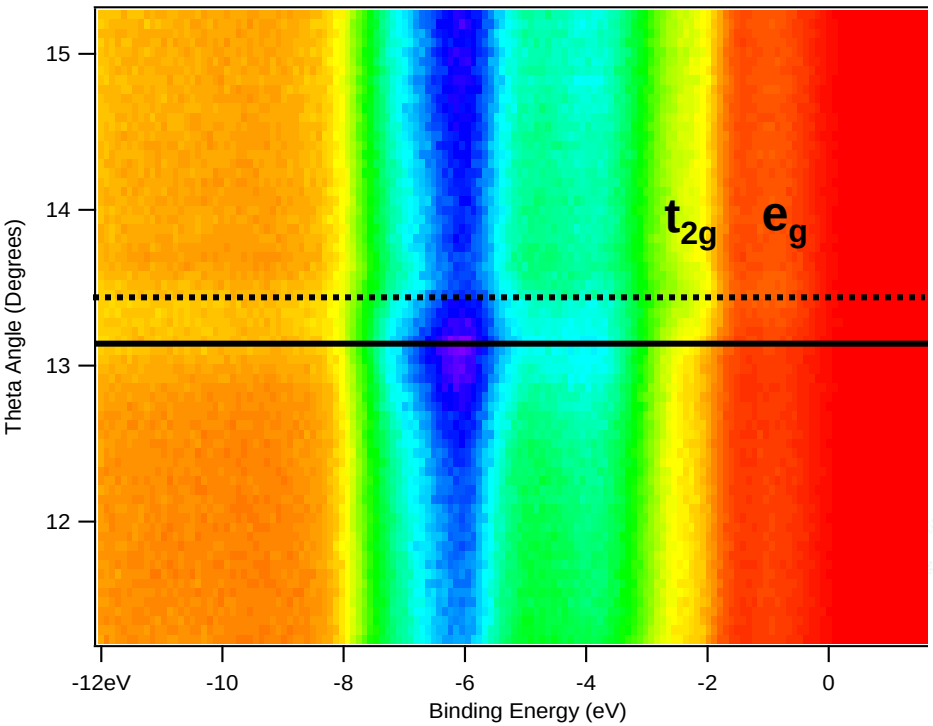

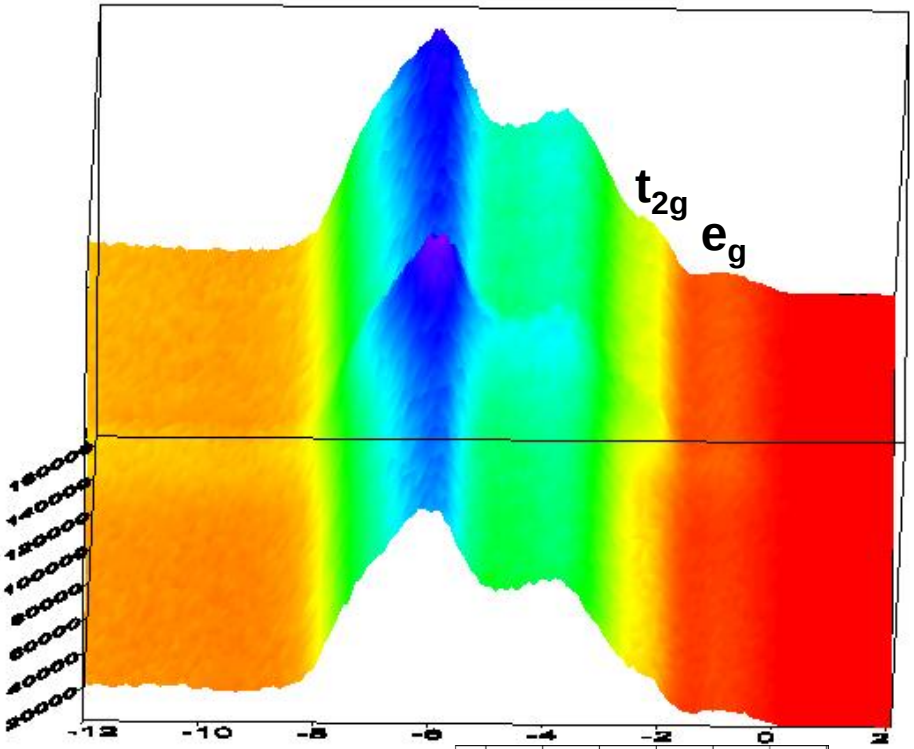

A. Gray et al., Phys. Rev. B 82, 205116 (2010)

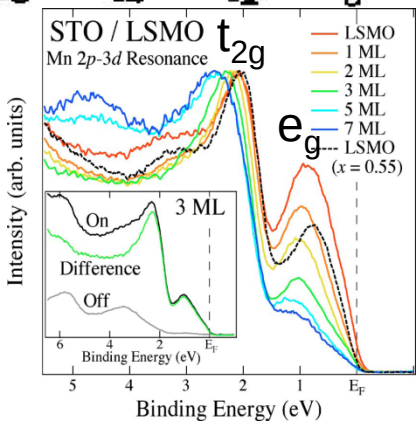

The Advanced Light Source

Prior resonant PS: Fujimori et al., J.A.P 99, 08S903 (2006)

Standing-wave angle-resolved photoemission

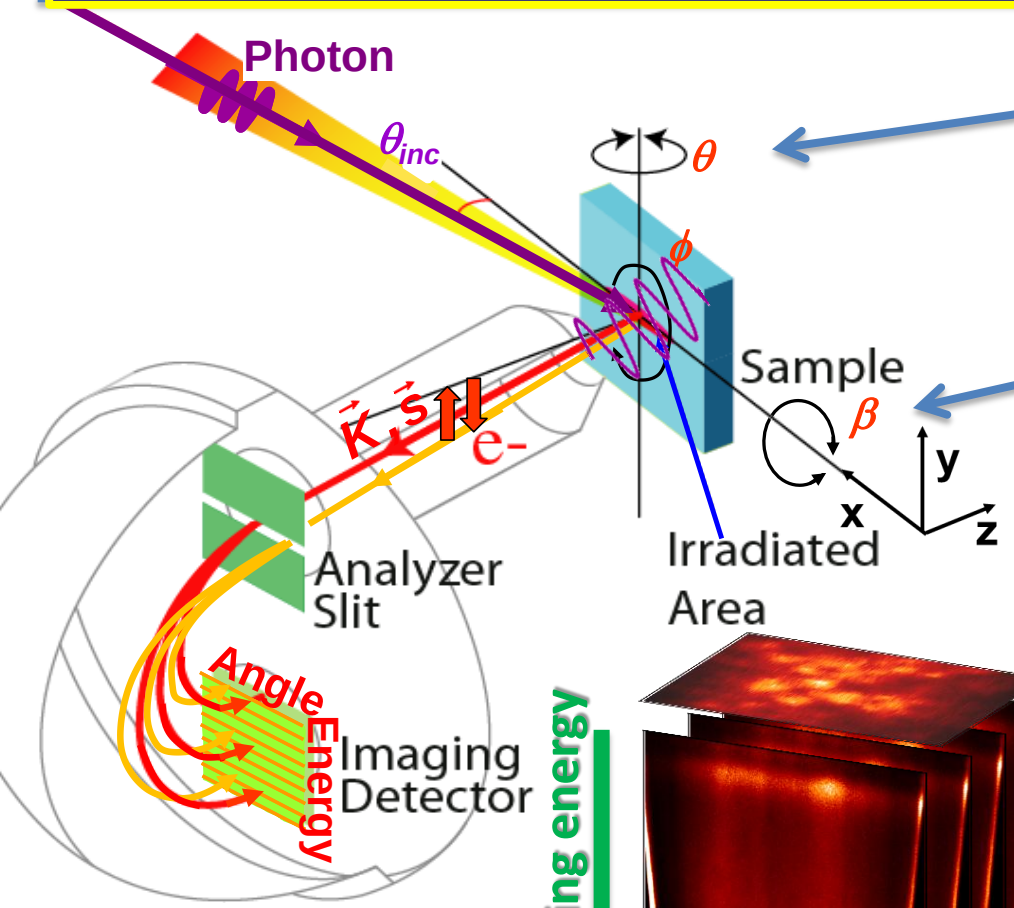

Variation of Θ:
Change of incidence angle
⇨Standing wave effect

Variation of β:
Change of takeoff angle
⇨ measure electrons with different **k**-vector

k-space mapping

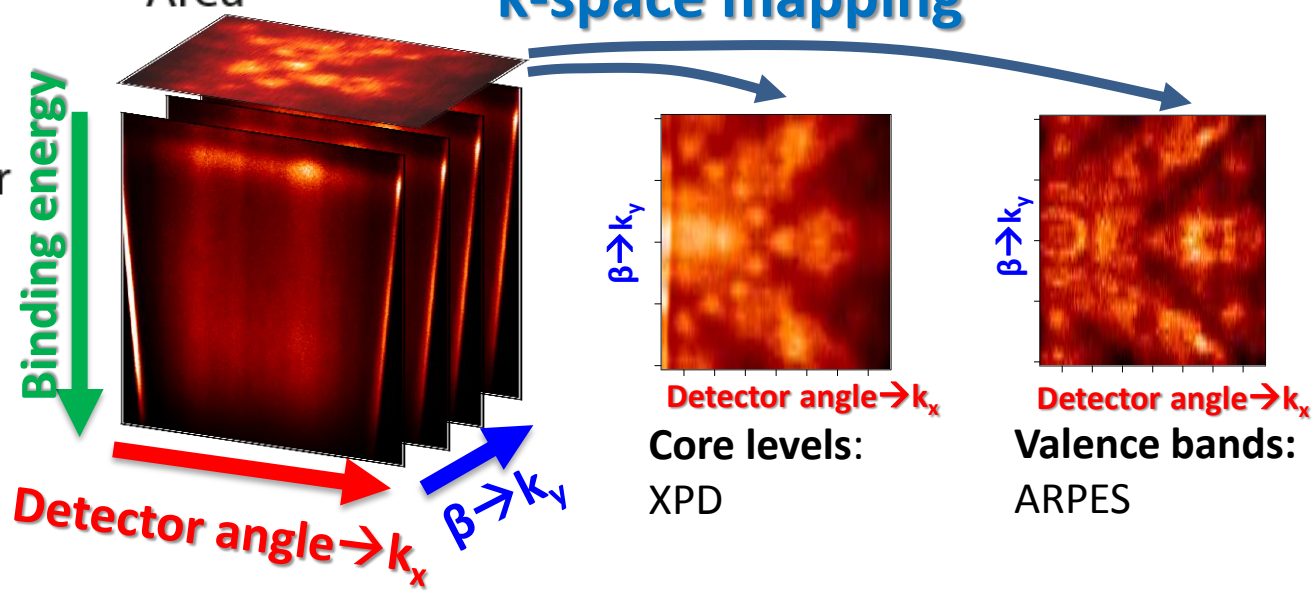

Core levels:
XPD

Valence bands:
ARPES

STO/LSMO Depth-resolved ARPES: hν=833 eV, 20K

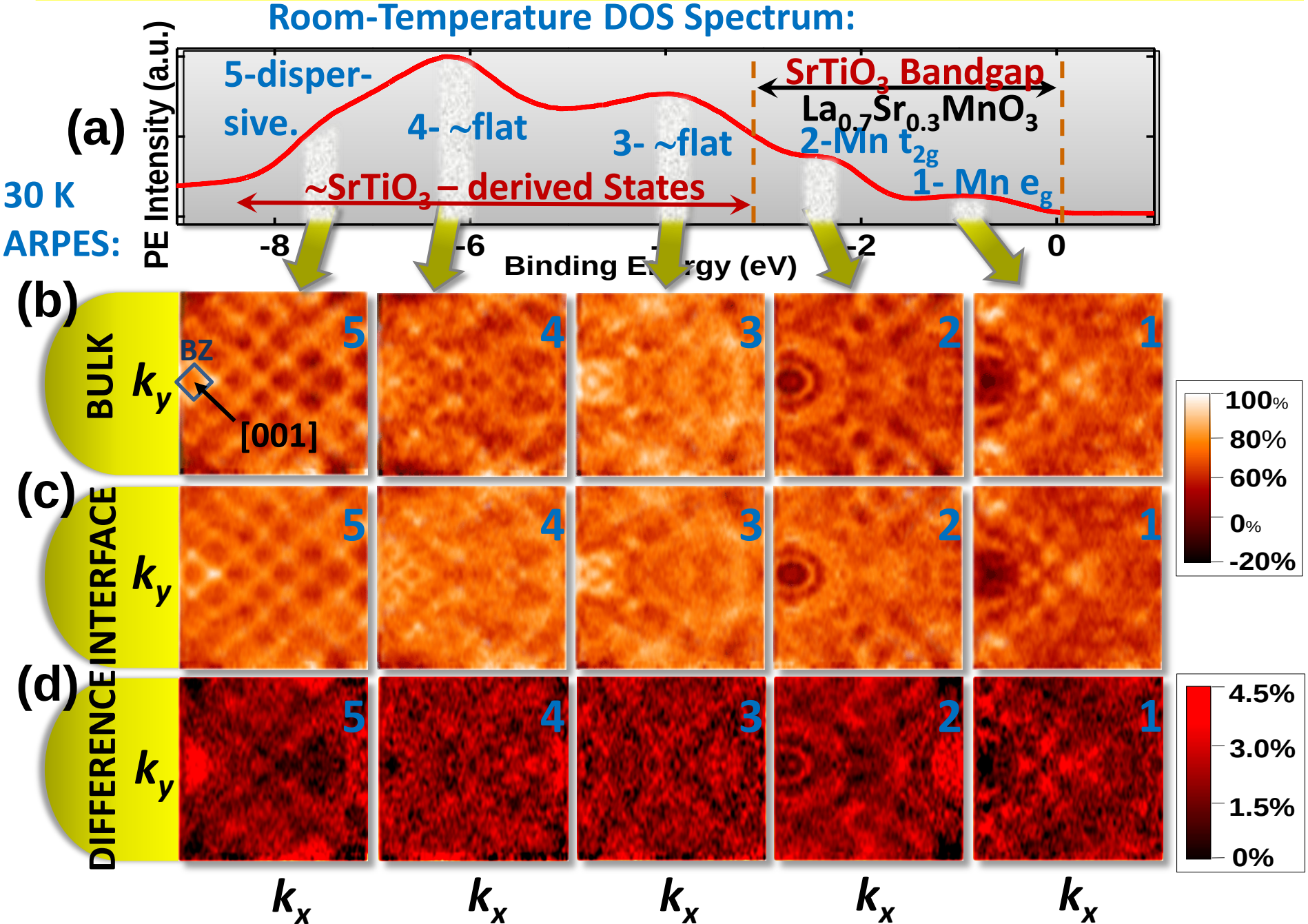

First comparison to one-step photoemission theory for LSMO

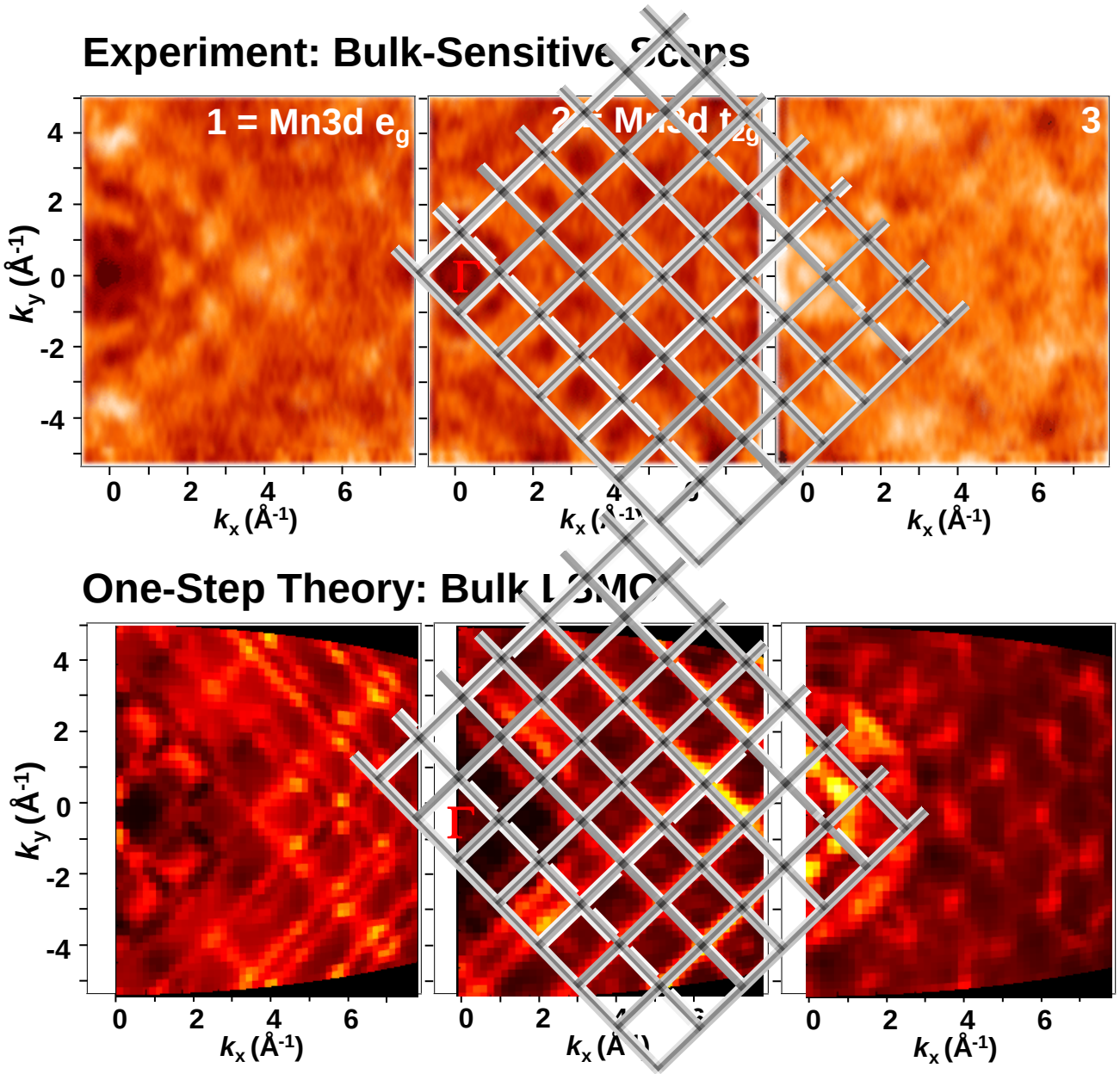

Theory from:
H. Ebert, J. Minar et al., Munich: one-step time-reversed LEED, with matrix elements

A. Gray, J. Minar et al., TBP

First comparison to one-step photoemission theory for STO/LSMO

Experiment:
t_{2g}: Bulk LSMO

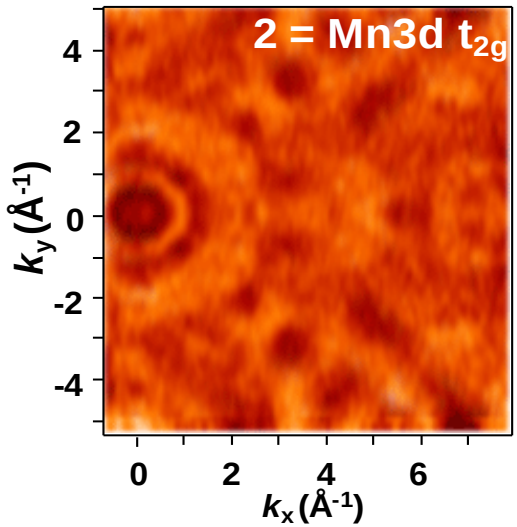

One-Step Theory, LDA+U, with SW E-field profile:
t_{2g}: Bulk LSMO **Interface LSMO**

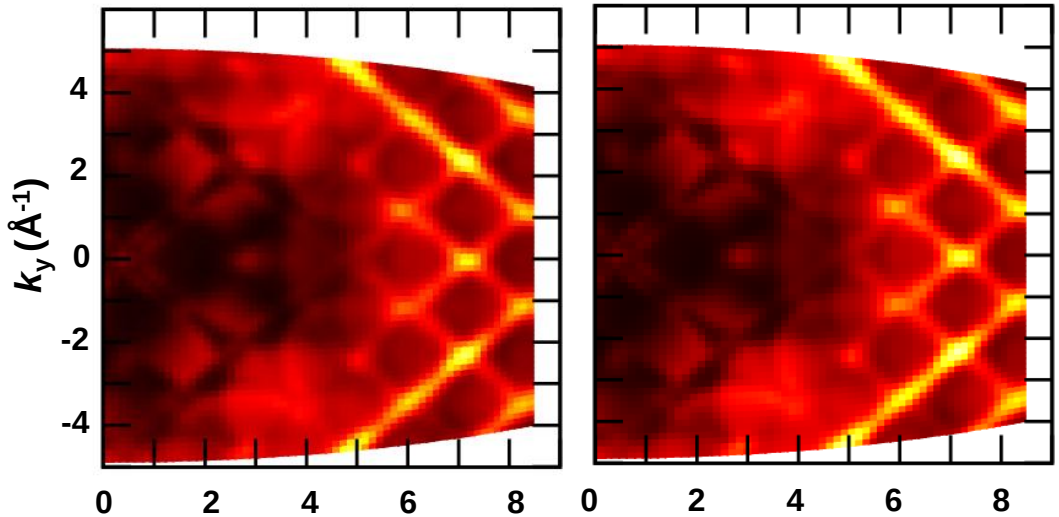

Bulk – Interface- ~5%

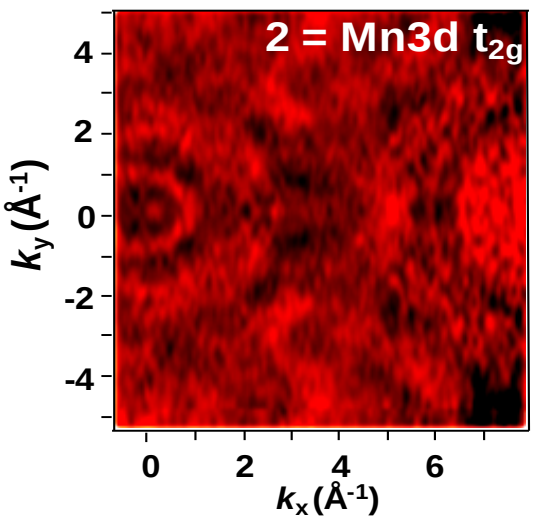

Bulk – Interface- ~8%

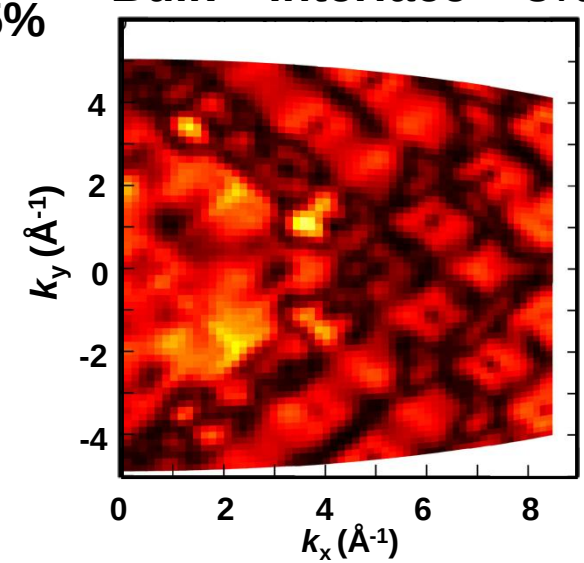

Calculations with more complex Interface relaxations in progress- Minar, Braun, Ebert

A. Gray, J. Minar et al., TBP

Standing wave formation in reflection from a surface, or single-crystal Bragg planes+, or a multilayer mirror

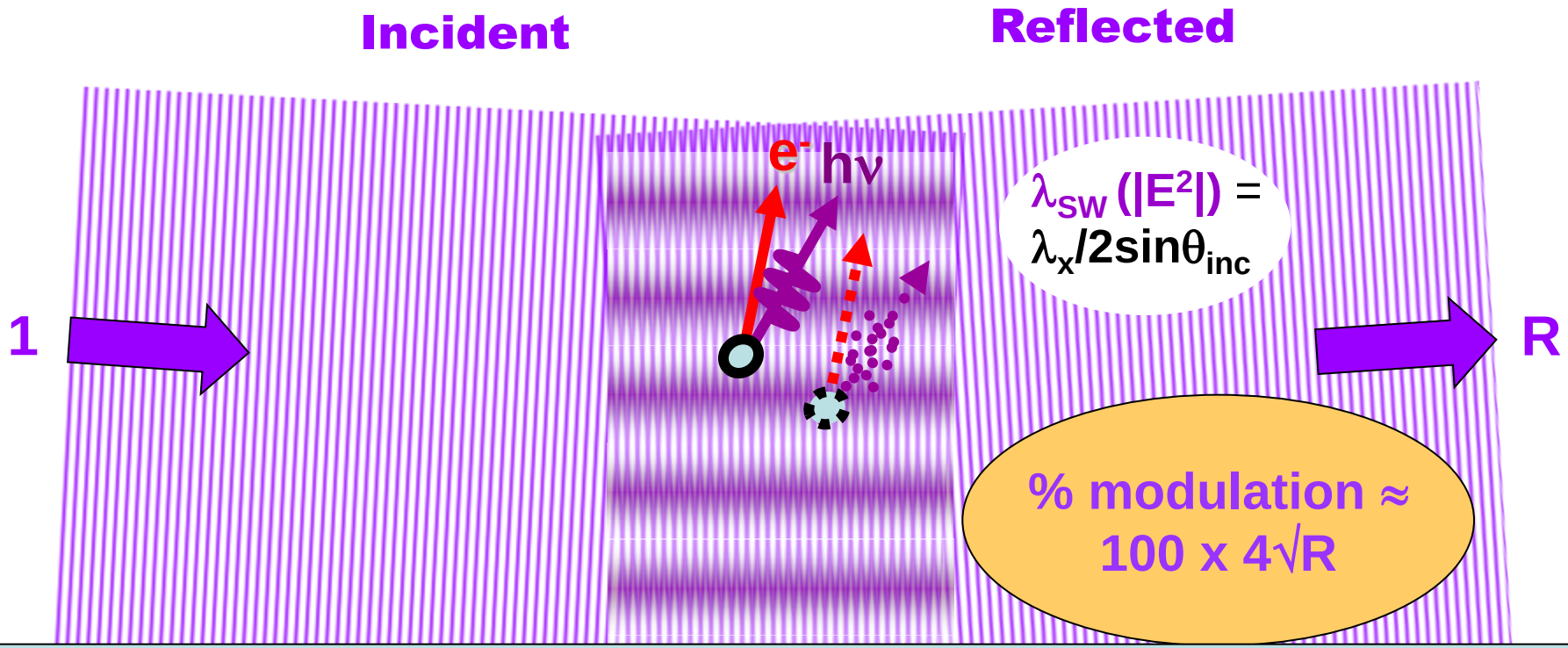

1. Rocking curve:

$$I(\theta_{inc}) \propto 1 + R(\theta_{inc}) + 2\sqrt{R(\theta_{inc})}\, f \cos[\varphi(\theta_{inc}) - 2\pi P]$$

2. Photon energy scan:

$$I(h\nu) \propto 1 + R(h\nu) + 2\sqrt{R(h\nu)}\, f \cos[\varphi(h\nu) - 2\pi P]$$

with: f = coherent fraction of atoms, P = phase of coherent-atom position

3. Phase scan with wedge-shaped sample ("Swedge" method):

Fe/Cr GMR—Yang,J. Phys. Cond. Matt. 14, L406 (2002); ; Co/CoFeB/Al_2O_3 TMR—Yang, J. Phys.: Cond. Matt. 18, L259 (2006); Fe/MgO TMR— Döring, Yang, Balke—PRB B 83, 165444 (2011) & 84, 184410 (2011

Probing Buried Interfaces: The Standing Wave-Wedge ("Swedge") Method

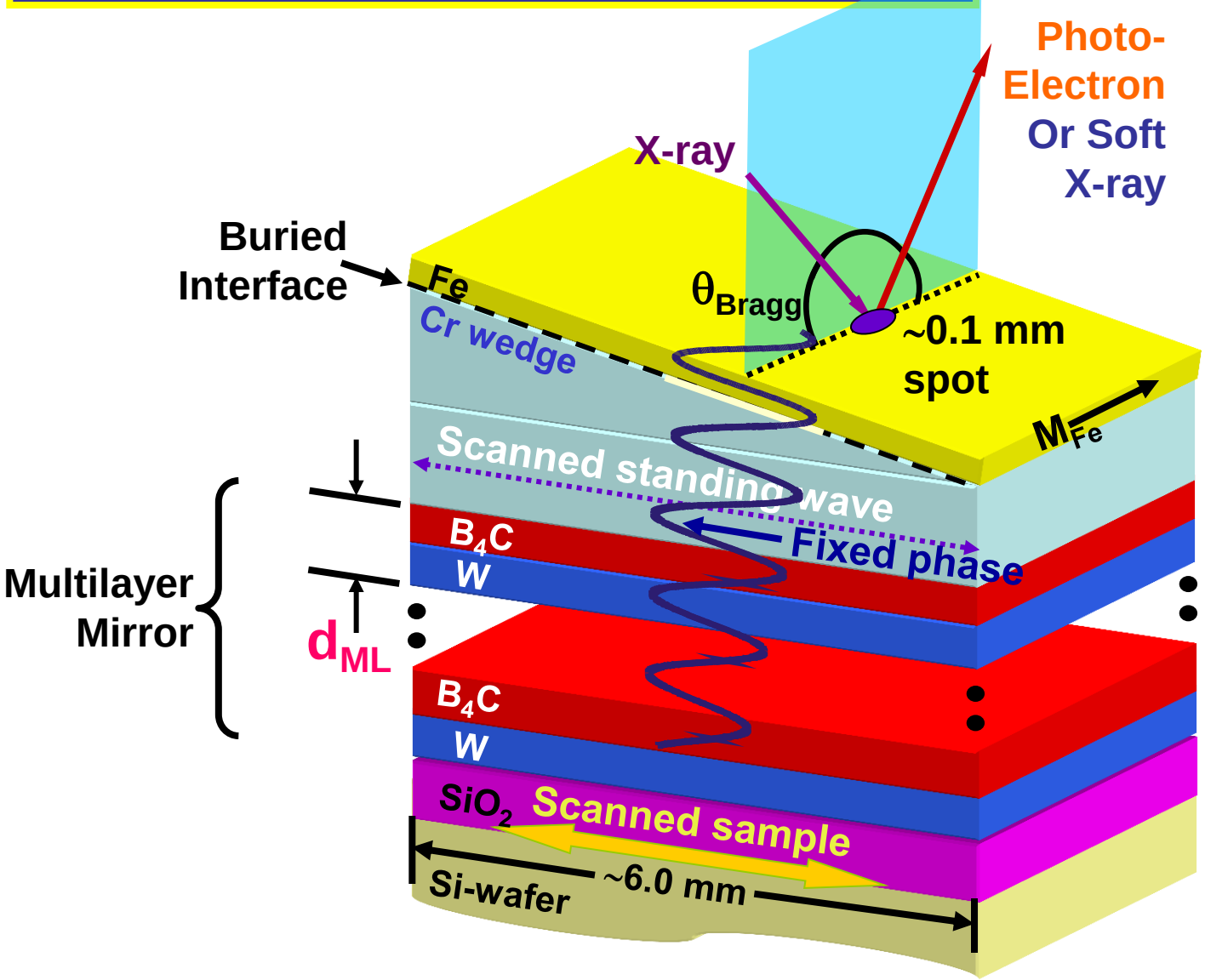

λ_{SW} ($|E^2|$) = $\lambda_x/2\sin\theta_{inc}$ $\approx$ d_{ML}

1st order Bragg:

$\lambda_x = 2d_{ML}\sin\theta_{Bragg}$

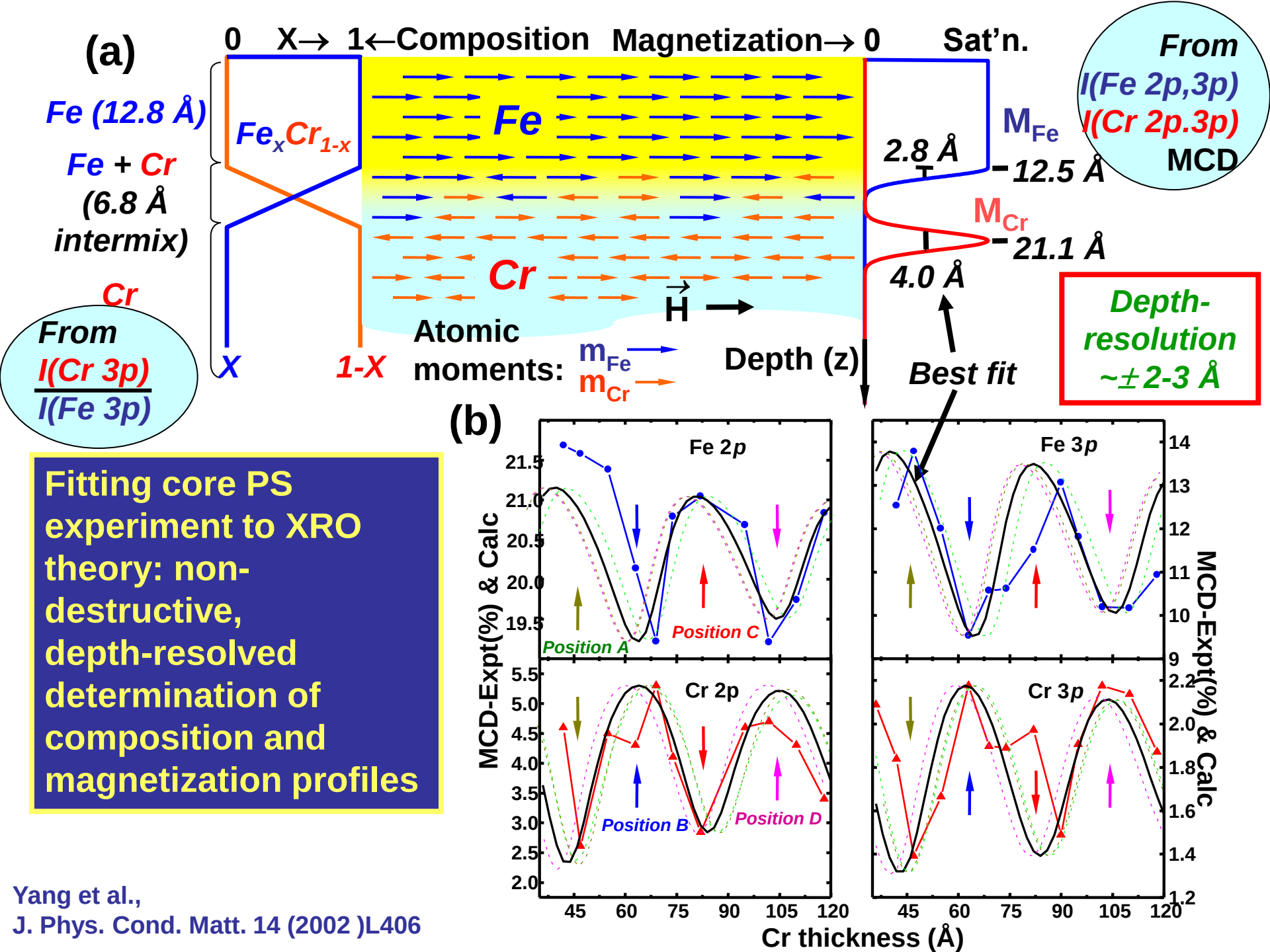

Fitting core PS experiment to XRO theory: non-destructive, depth-resolved determination of composition and magnetization profiles

Yang et al.,
J. Phys. Cond. Matt. 14 (2002)L406

Probing Buried Interfaces: The Standing Wave-Wedge ("Swedge") Method

Example: The MgO/Fe magnetic tunnel junction interface

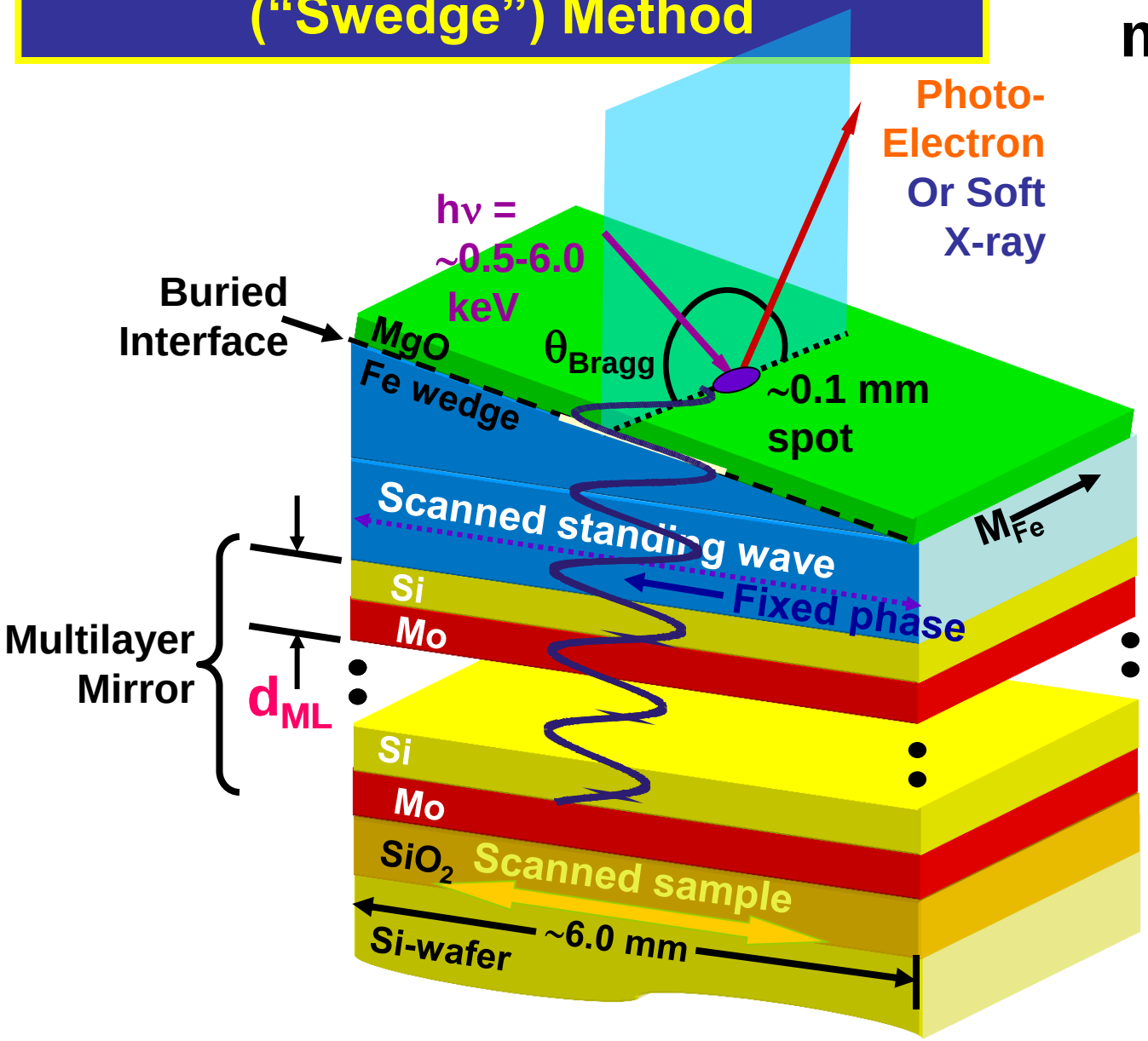

$\lambda_{SW}(|E^2|) = \lambda_x/2\sin\theta_{inc} \approx d_{ML}$

1st order Bragg: $\lambda_x = 2d_{ML}\sin\theta_{Bragg}$

Soft x-ray standing-wave wedge scans through a magnetic tunnel junction

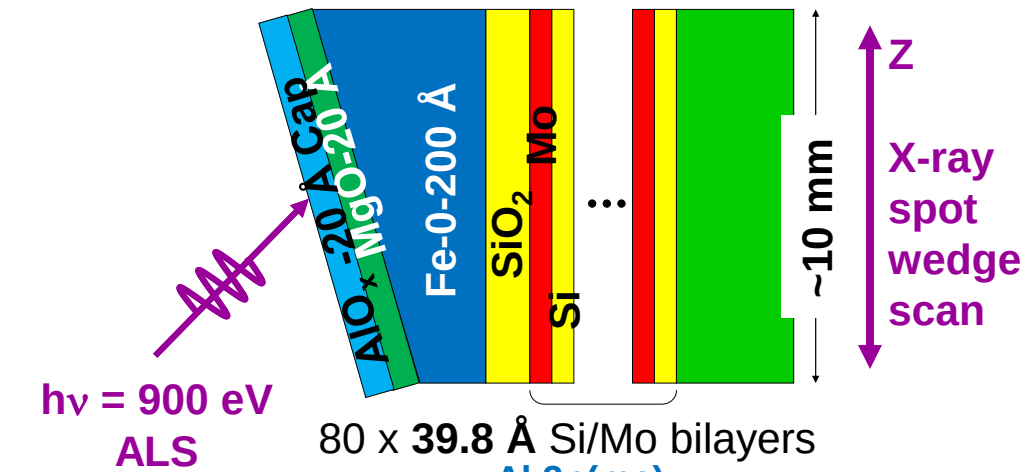

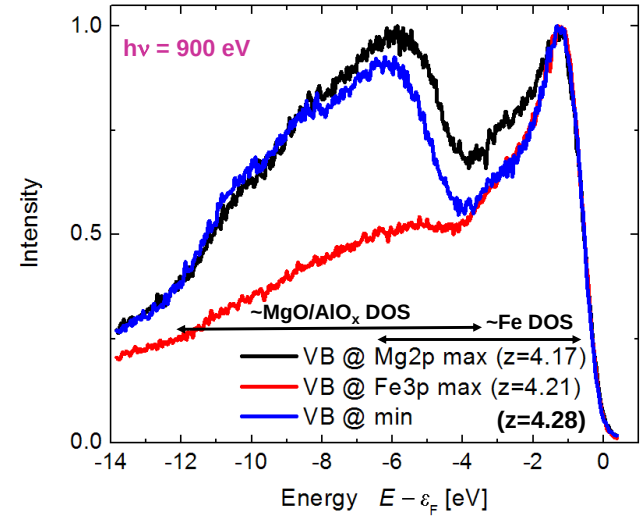

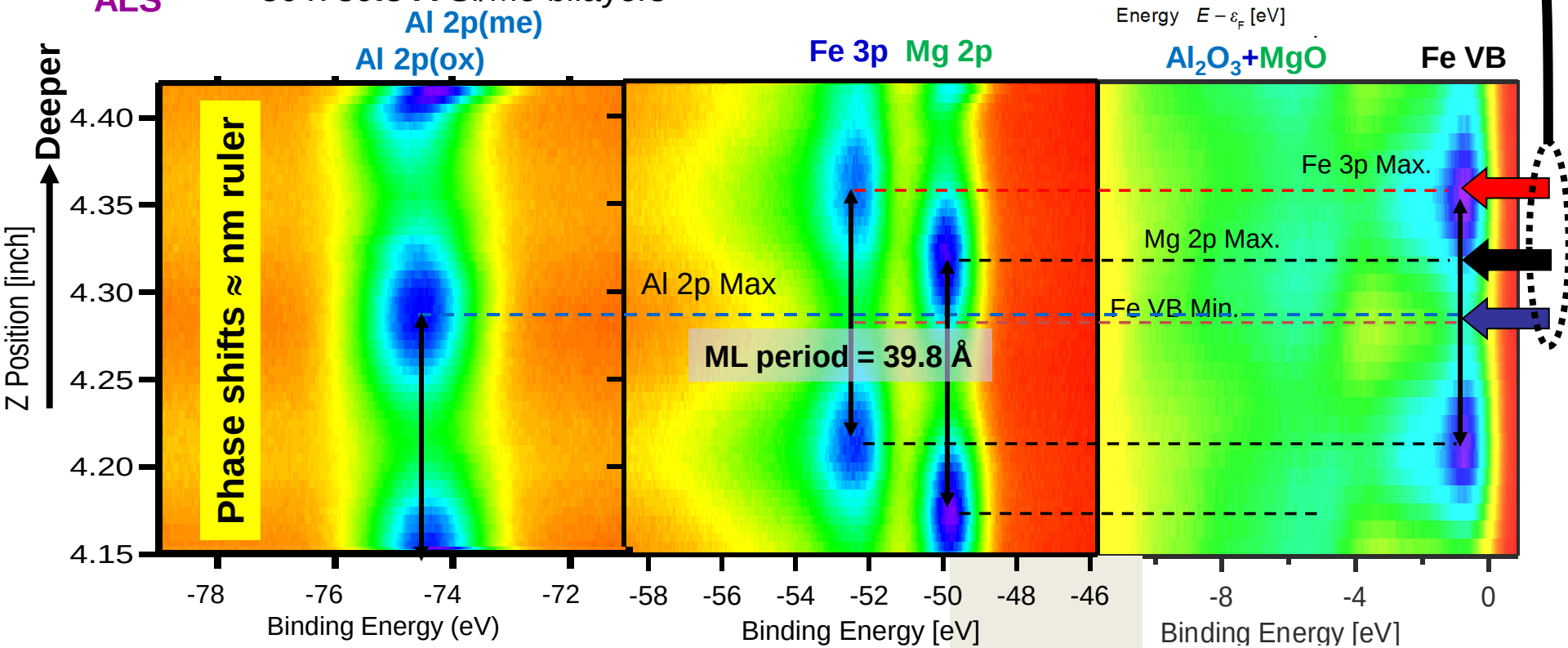

Balke, Yang et al., Phys. Rev. B 84, 184410 (2011)

(D)

Magnetic Circular Dichroism with Standing Wave Excitation-MgO/Fe, hν = 900 eV

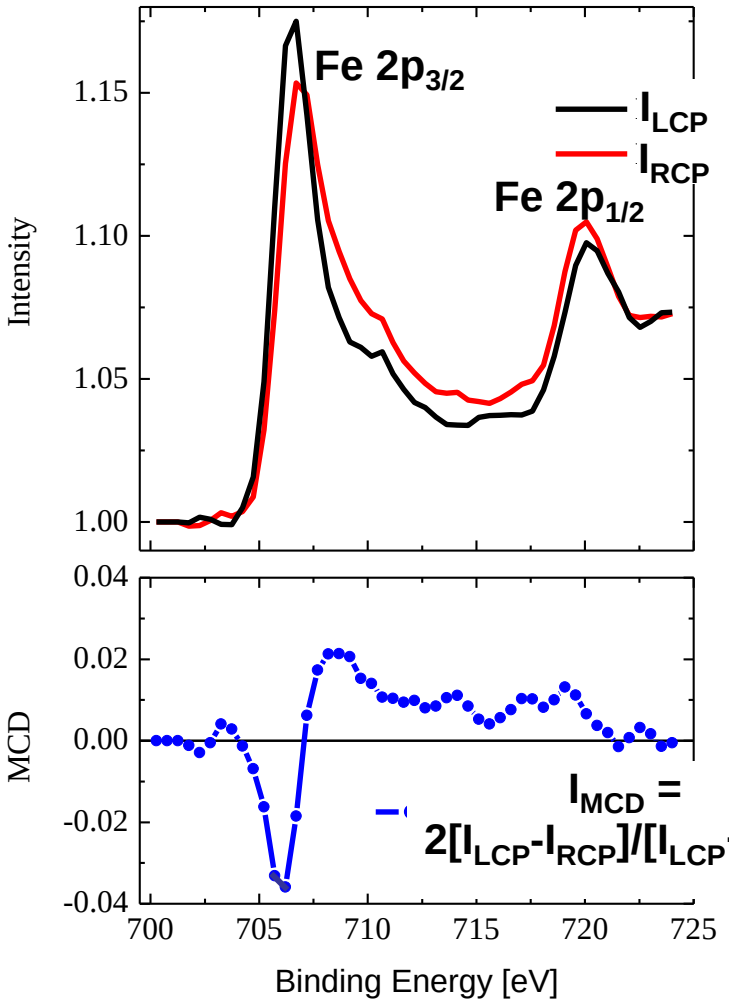

$I_{MCD} = 2[I_{LCP}-I_{RCP}]/[I_{LCP}+I_{RCP}]$

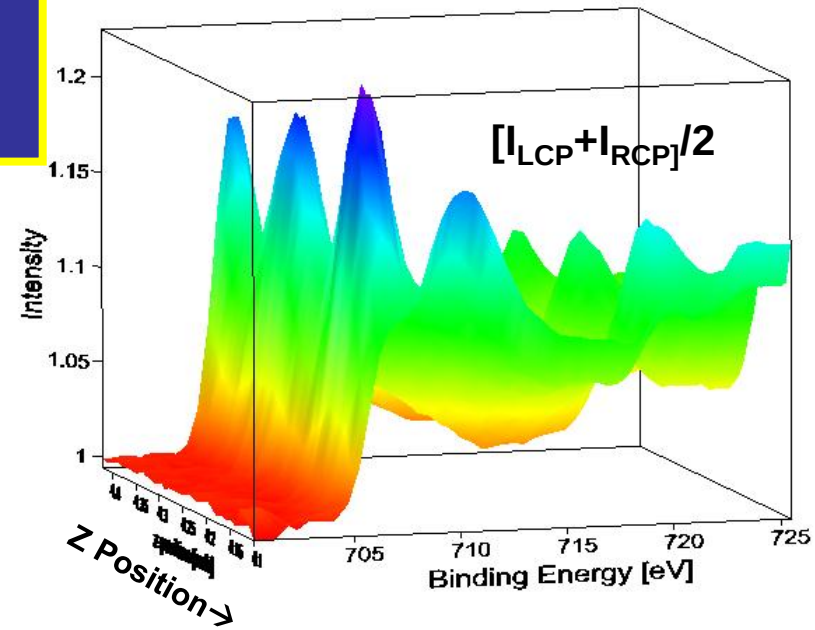

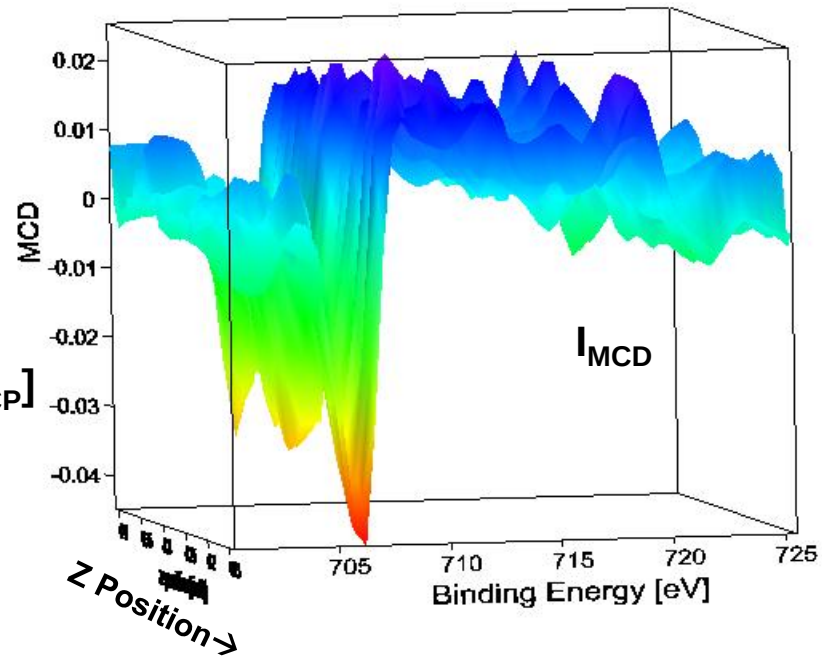

Yang, Balke et al., Phys. Rev. B 84, 184410 (2011)

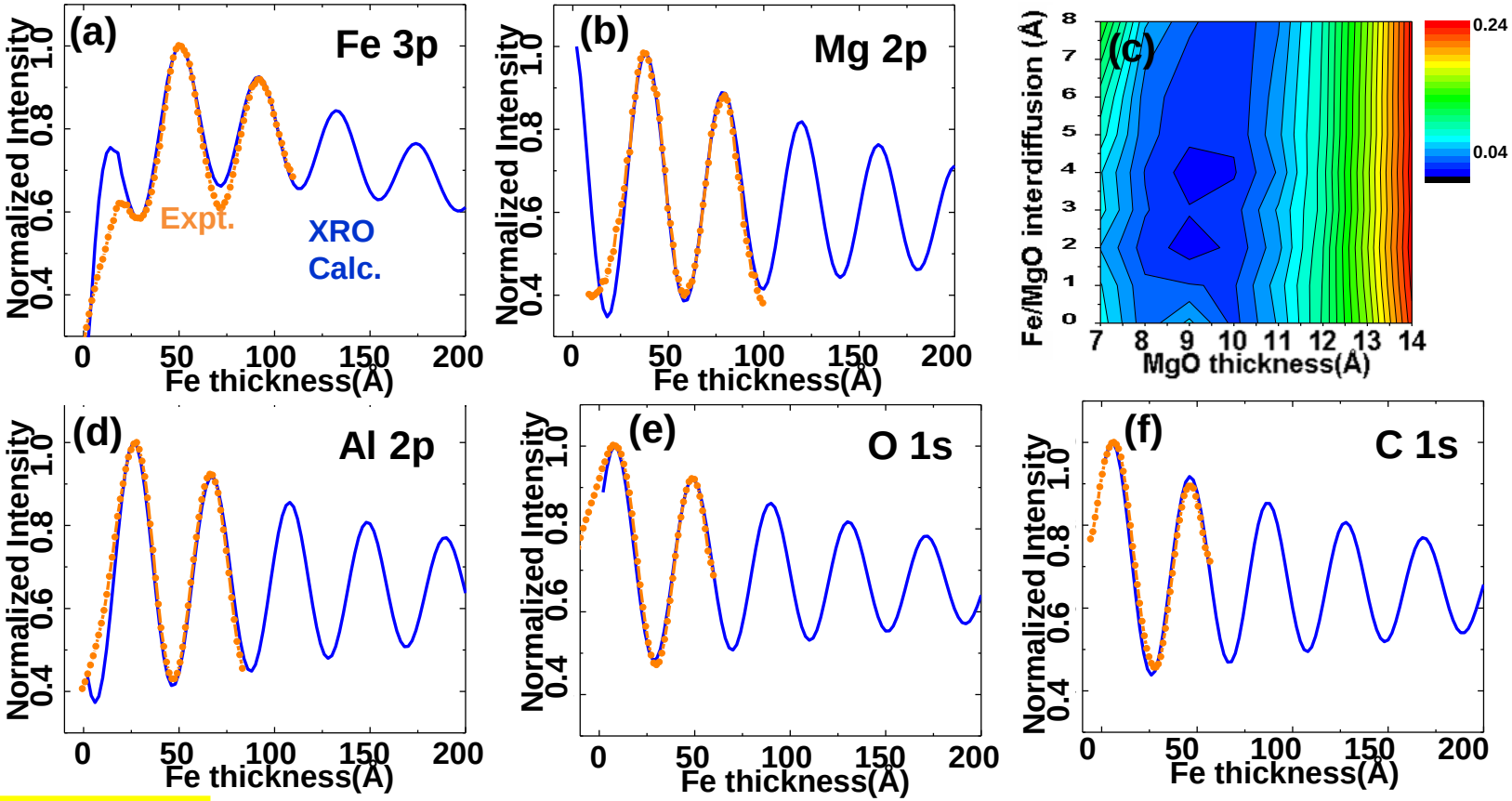

Standing wave/wedge analysis of an Fe/MgO tunnel junction multilayer: final fits of expt. to x-ray optical calcs.

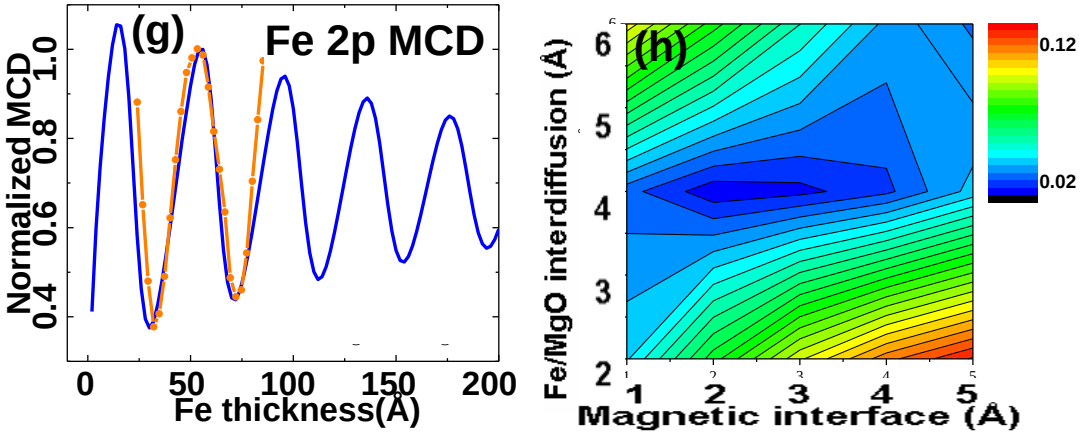

Balke, Yang et al., Phys. Rev. B 84, 184410 (2011)

Final profiles of concentration and magnetization

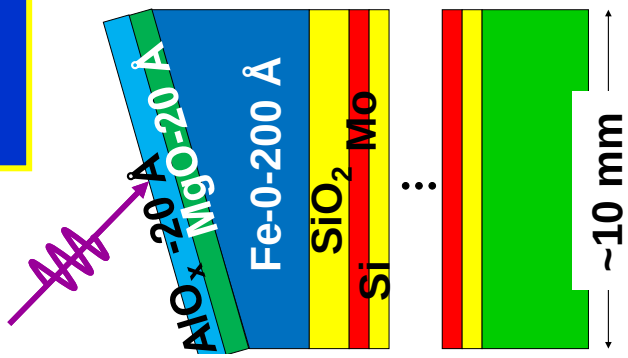

Concentration

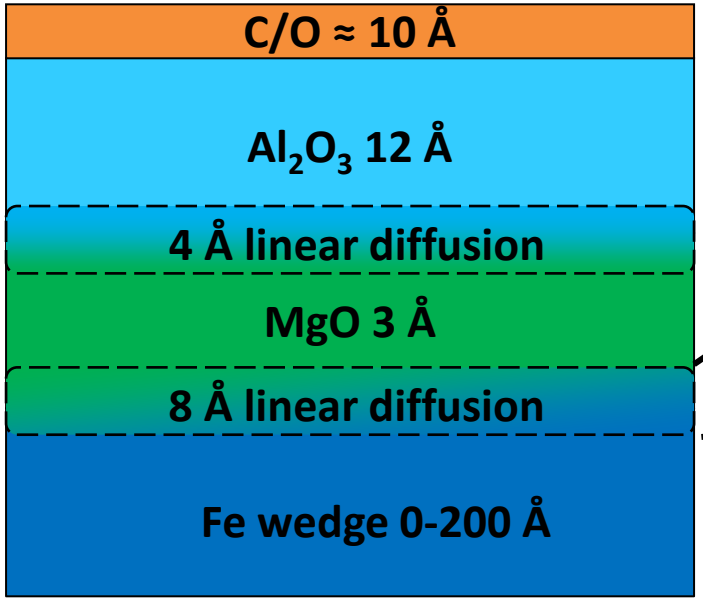

Magnetization

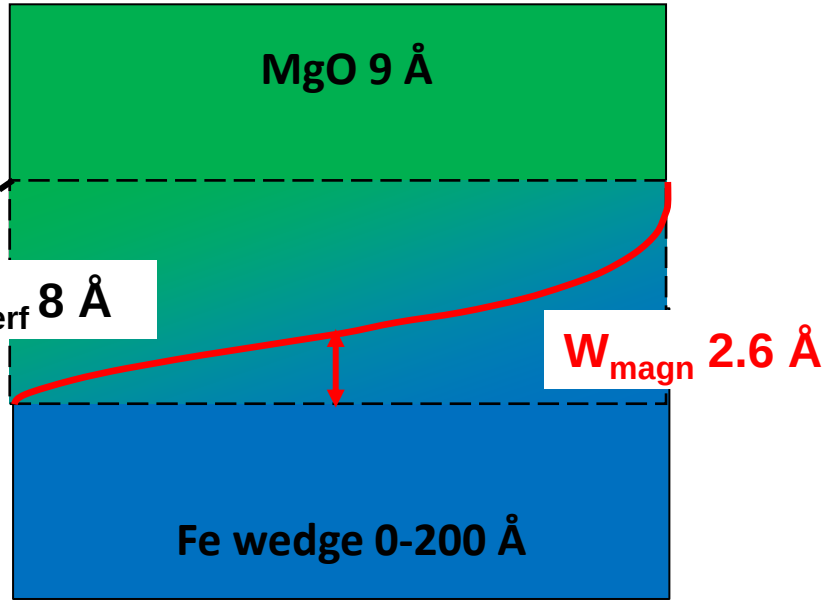

Yang, Balke et al., Phys. Rev. B 84, 184410 (2011)

MgO/Fe tunnel junction- the real interface

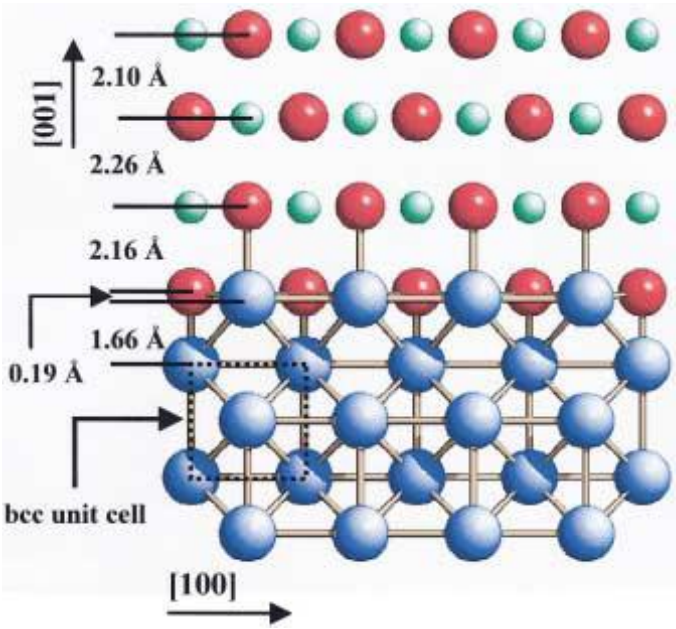

Meyerheim PRL 87, 076102 (2001).

- *Is there FeO at the interface?*
- *What is the density of states at the interface?*
- *Δ_1 controls tunneling? Can we see bands at epitaxial interfaces? (Future project)*

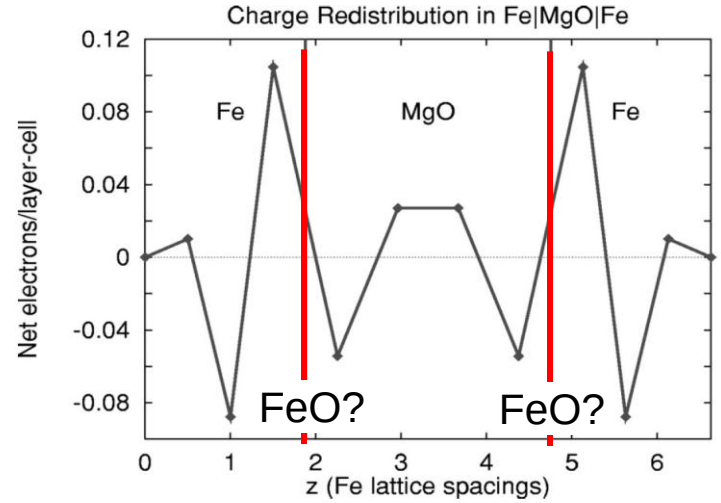

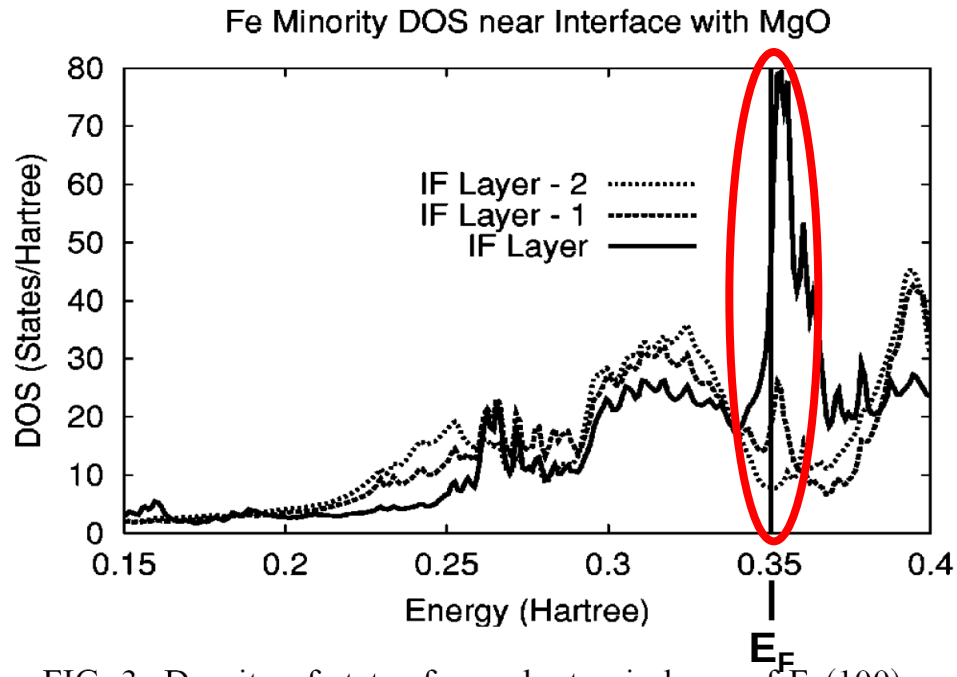

FIG. 3. Density of states for each atomic layer of Fe(100) near an interface with MgO. One hartree equals 27.2 eV.

Butler et al.,PRB 63, 054416 (2001);
Mathon & Umerski, PRB 63, 220403 (2001);
Mertig et al., PRB 73, 214441 (2006)

MgO/Fe tunnel junction-Δ_1 states dominant in tunneling for ideal interface

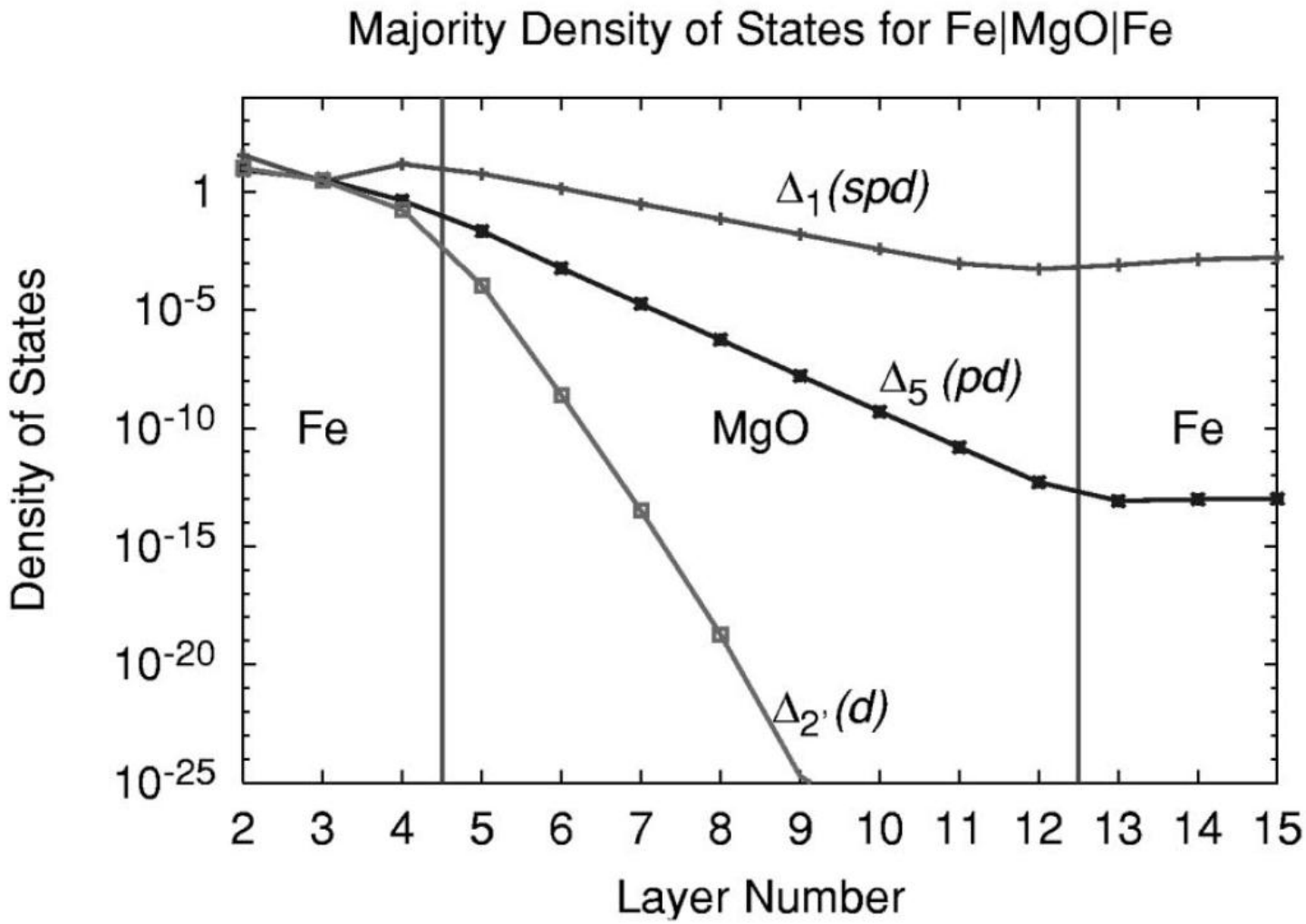

Butler et al.,PRB 63, 054416 (2001)

Standing wave/wedge derivation of depth-dependent densities of states: Fe/MgO tunnel junction

$\tilde{D}_L\left(E_{\text{kin,j}}\right)$ = matrix-element weighted density of states in layer L

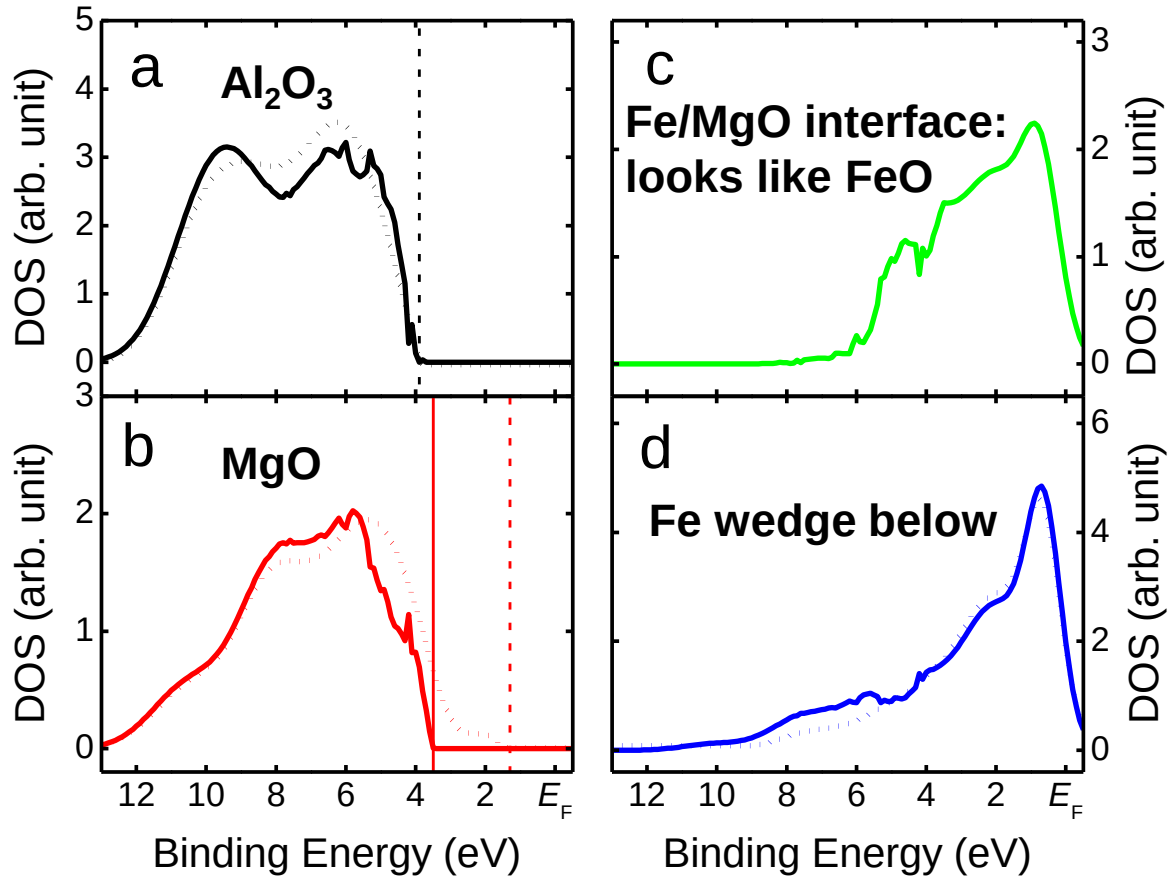

Yang, Balke et al., Phys. Rev. B 84, 184410 (2011)

Standing wave/wedge derivation of depth-dependent densities of states: Fe/MgO tunnel junction

→Oxidation at the Fe/MgO interface

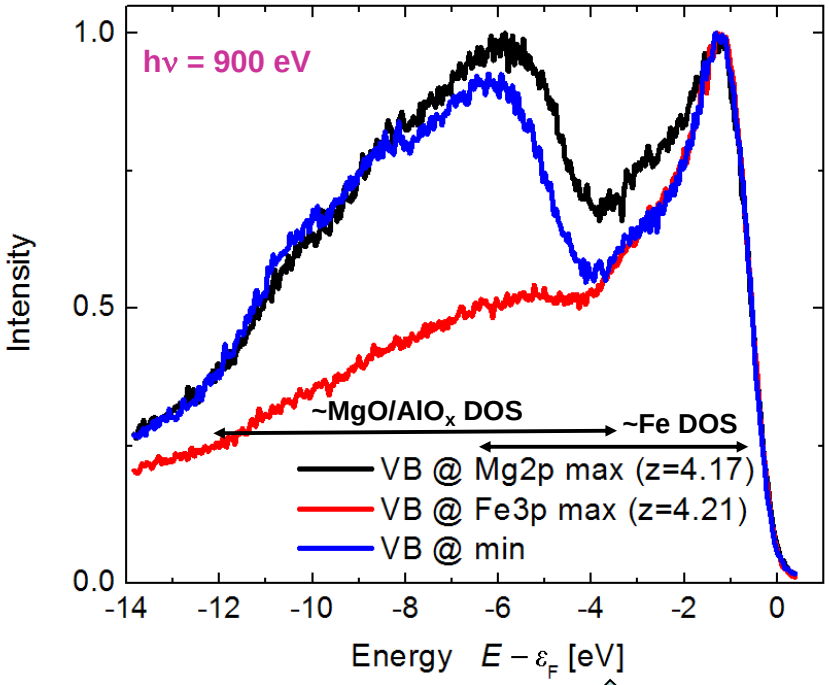

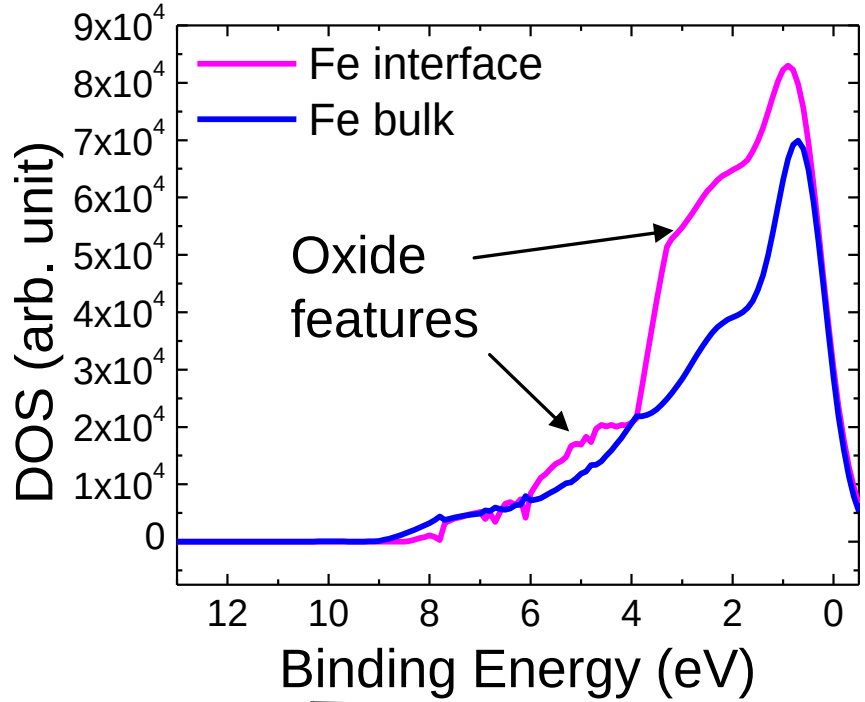

Self-consistent X-ray optical modeling of layer-resolved densities of states

Yang, Balke et al., Phys. Rev. B 84, 184410 (2011)

- Other material pairs in multilayer (B_4C/W, Si/Mo,…) + epitaxial multilayers (AlAs/GaAs, STO/LSMO→epitaxial samples

- Smaller periods (to ~25-30 Å) → smaller SW period, better resolution

- Lower $h\nu_{inc}$ →higher Bragg angles→perpend. component of M

- X-ray emission→ deeper layers, more sensitivity to SW position

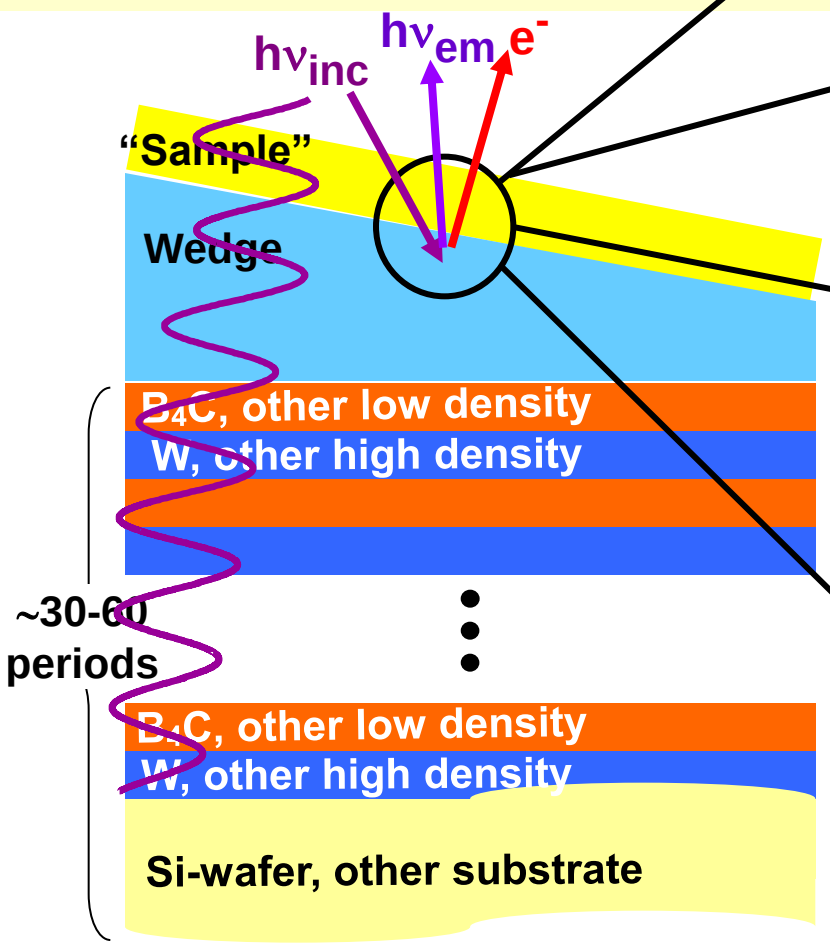

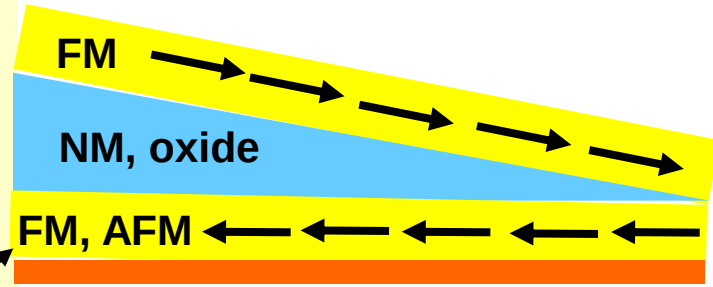

GMR, exchange biassing, tunnel junction, oxide multilayers

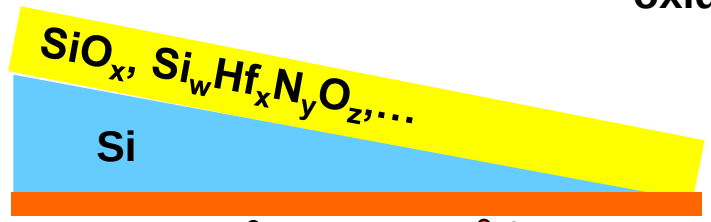

Ultrathin gate oxide, Oxynitride, other films

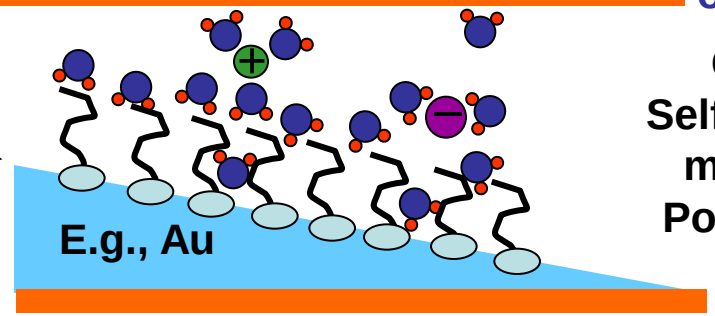

Clusters, Self-assembled monolayers, Polymer films, Proteins

Liquid layers, Conc. distributions

Microscope resolution

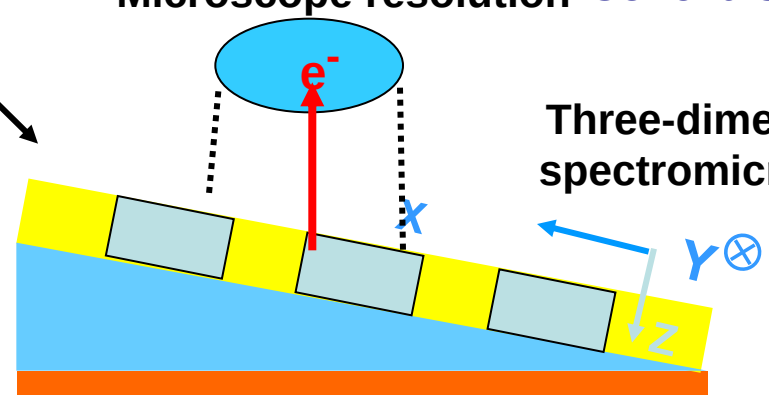

Three-dimensional spectromicroscopy

Basic Concepts and Experiments

Core-Level Photoemission

Intensities and Quantitative Analysis, the 3-Step Model
Varying Surface and Bulk Sensitivity
Chemical shifts
Multiplet Splittings
Electron Screening and Satellite Structure
Magnetic and Non-Magnetic Dichroism
Resonant Photoemission
Photoelectron Diffraction and Holography

Valence-Level Photoemission

Band-Mapping in the Ultraviolet Photoemission Limit
Densities of States in the X-Ray Photoemission Limit

Some New Directions

Photoemission with Hard X-Rays (throughout lectures)
Photoemission with Standing Wave Excitation
Photoemission with Spatial Resolution/Photoelectron Microscopy
Temporal Resolution
@ Higher Pressures

Kiskinova
Locatelli

Typical experimental geometry for energy- and angle-resolved photoemission measurements

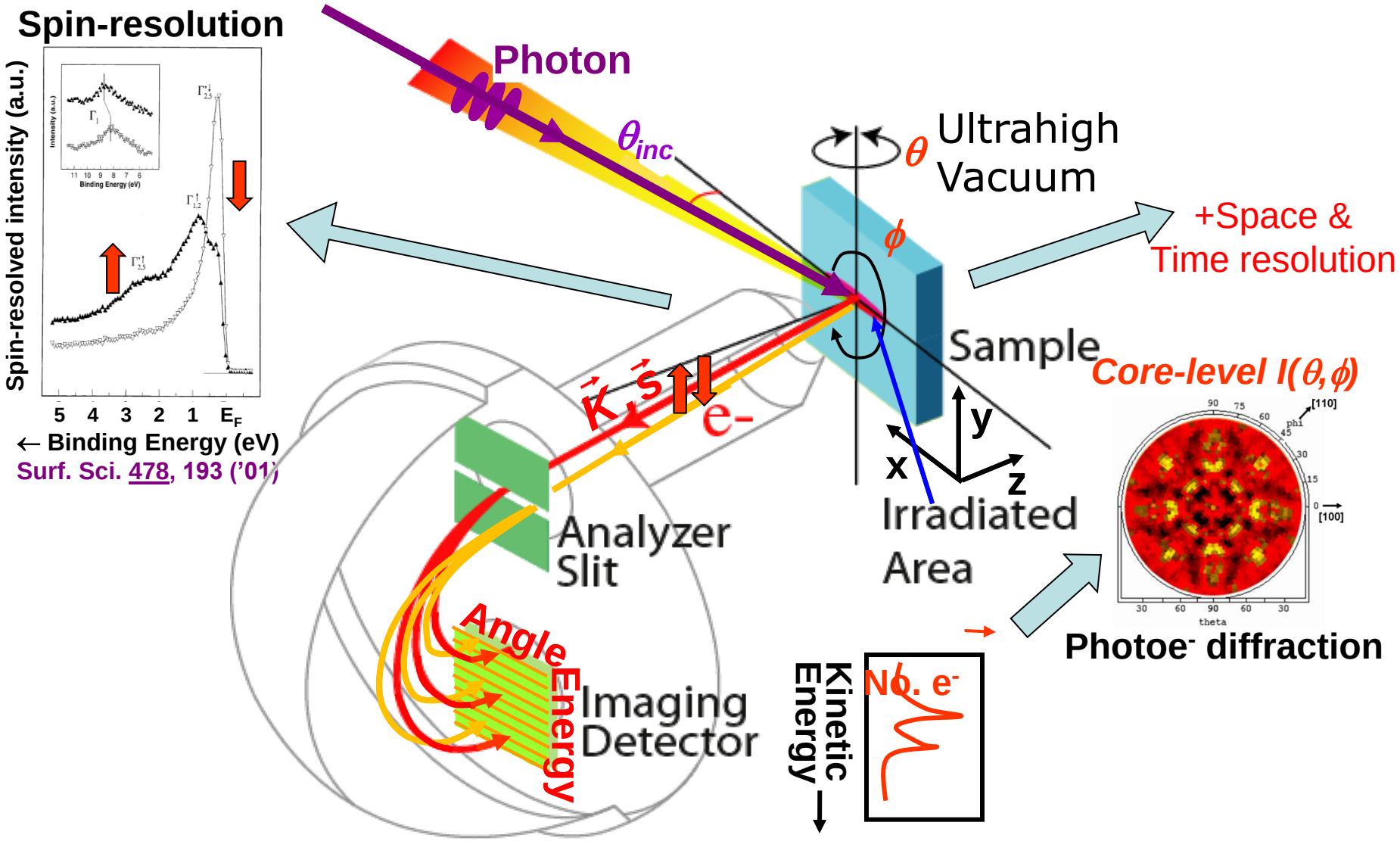

Imaging with soft x-ray photoemission microscopes—two types

Scanning X-ray Microscopy

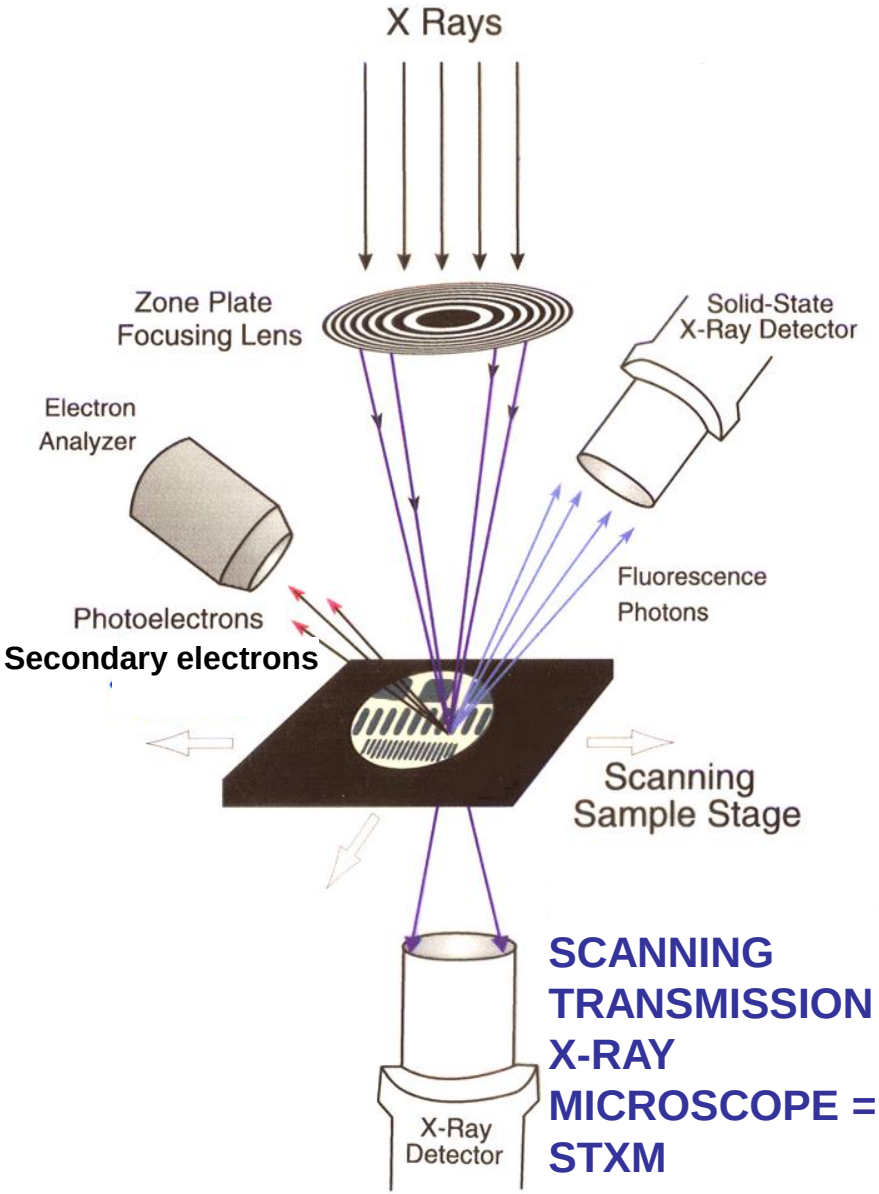

SCANNING TRANSMISSION X-RAY MICROSCOPE = STXM

X-Ray Photoelectron Microscopy

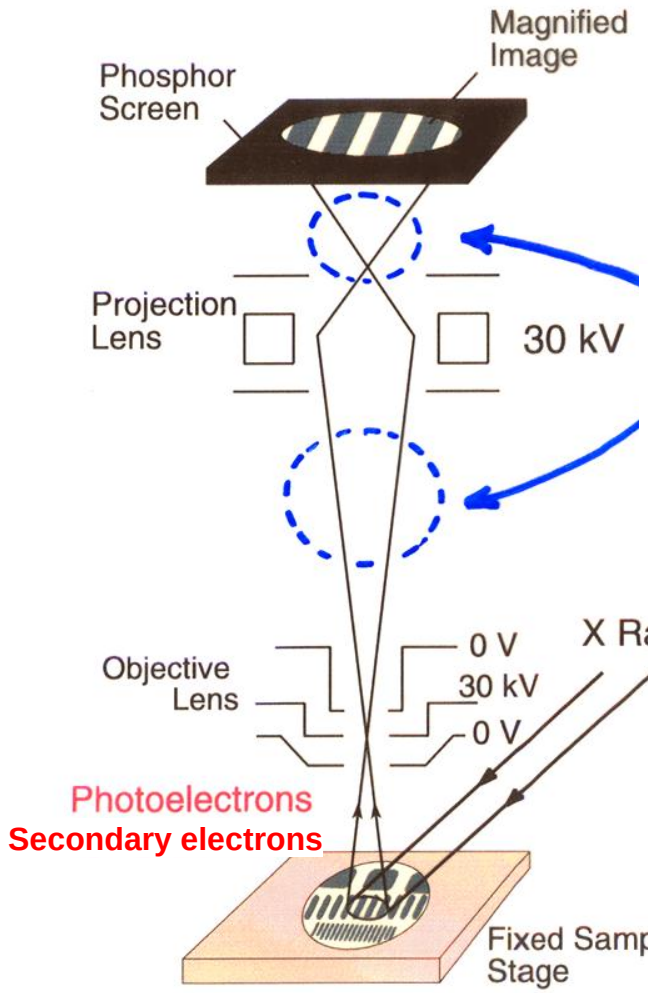

+ Energy Filter?

Kiskinova Locatelli

PHOTOELECTRON EMISSION MICROSCOPE = PEEM

Basic Concepts and Experiments

Core-Level Photoemission

Intensities and Quantitative Analysis, the 3-Step Model
Varying Surface and Bulk Sensitivity
Chemical shifts
Multiplet Splittings
Electron Screening and Satellite Structure
Magnetic and Non-Magnetic Dichroism
Resonant Photoemission
Photoelectron Diffraction and Holography

Valence-Level Photoemission

Band-Mapping in the Ultraviolet Photoemission Limit
Densities of States in the X-Ray Photoemission Limit

Some New Directions

Photoemission with Hard X-Rays (throughout lectures)
Photoemission with Standing Wave Excitation
Photoemission with Spatial Resolution/Photoelectron Microscopy
Temporal Resolution
@ Higher Pressures

Adding depth resolution to the photoelectron microscope via standing wave excitation

Spin-Polarized Photoelectron Microscope—BESSY, Berlin

Microscope field of view ~50 microns, approx. 1 period

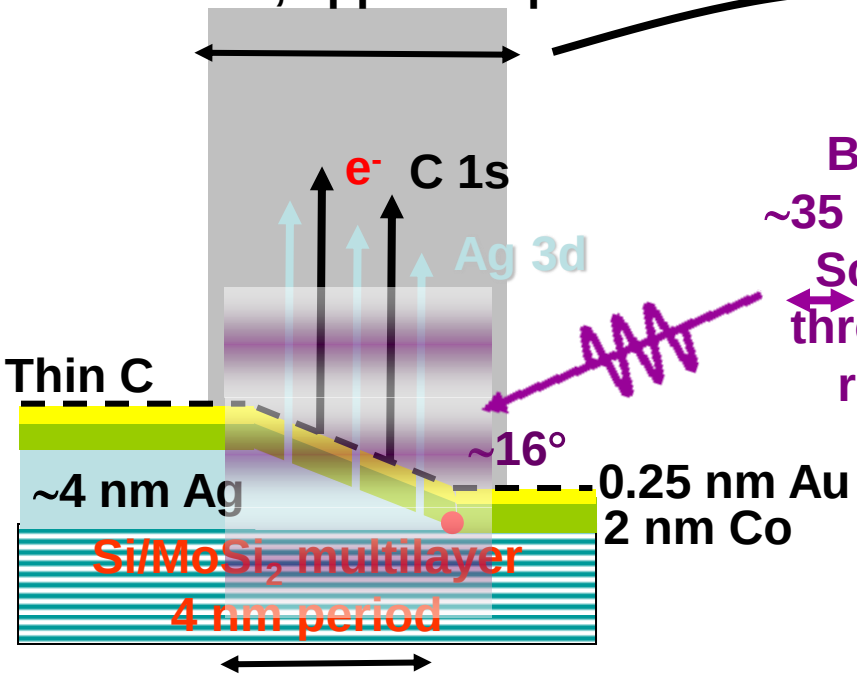

Step ca. 30 microns

Beam spot: ~35 x 10 microns Scanning hν through Bragg resonance

Imaging with element-specific photoelectron peaks

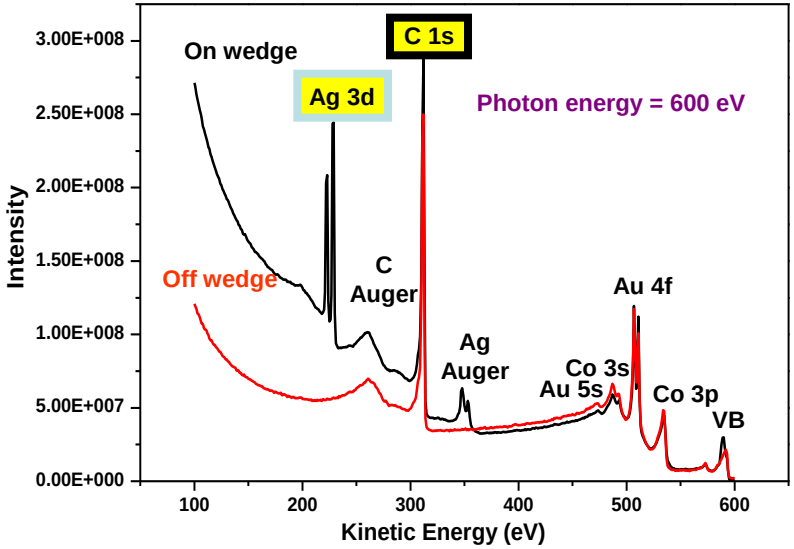

F. Kronast et al., Appl. Phys. Lett. 93, 243116 (2008)

Standing wave effects in a photoelectron microscope

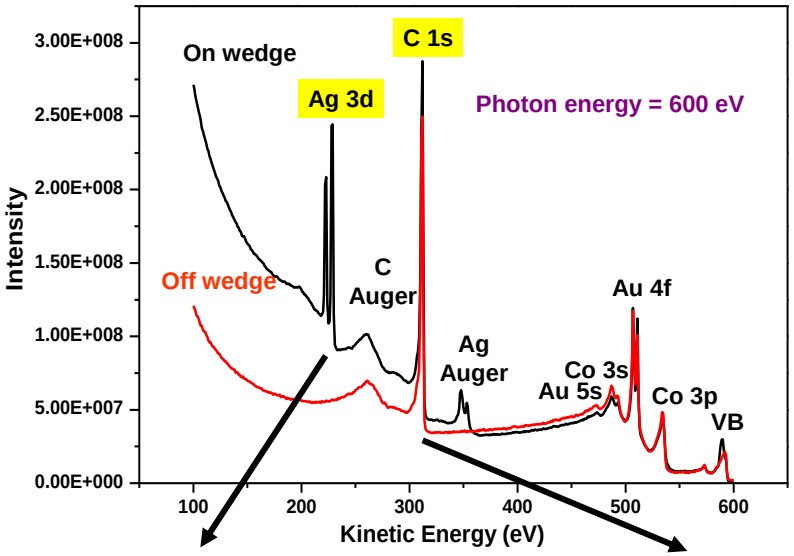

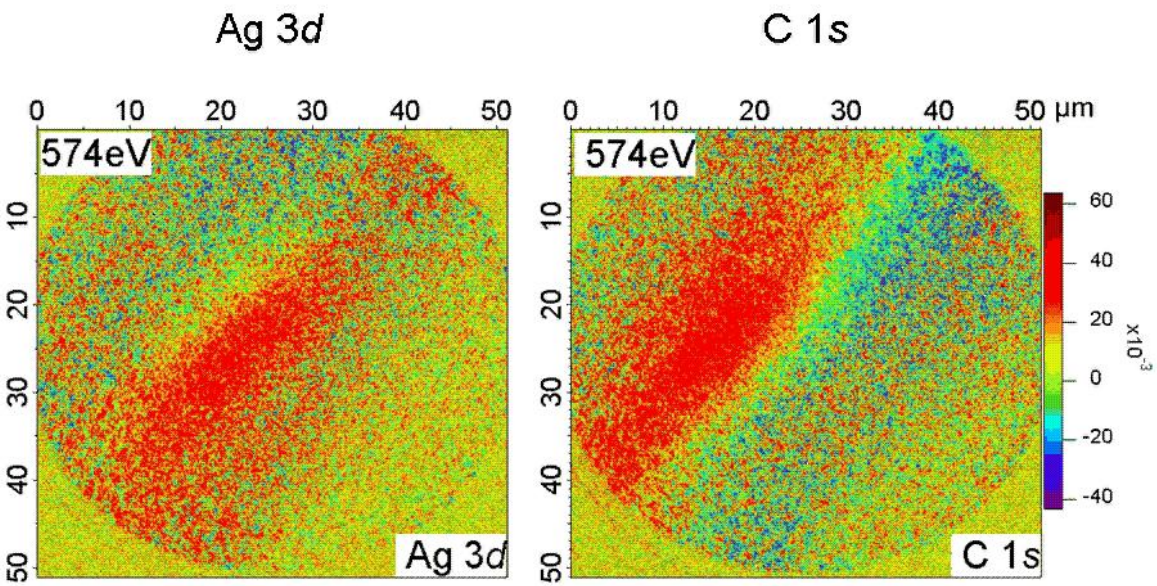

F. Kronast, H. Dürr, BESSY
D. Buergler, R. Scheiber,C. Schneider, Jülich
Yang, IBM, CF,
Appl. Phys. Lett. 93, 243116 (2008)

Third type: Imaging Zone-Plate X-ray microscope XM-1 @ ALS

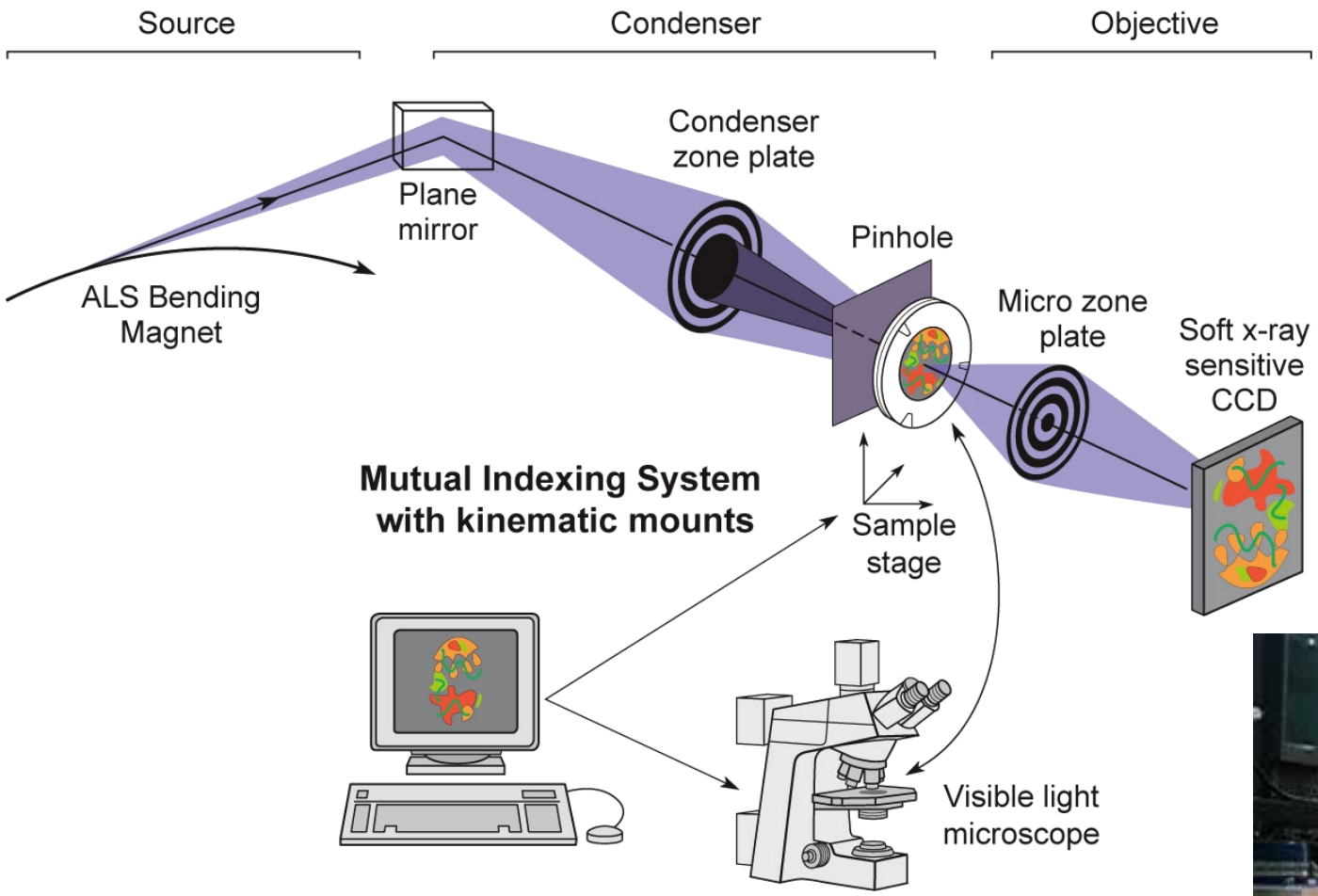

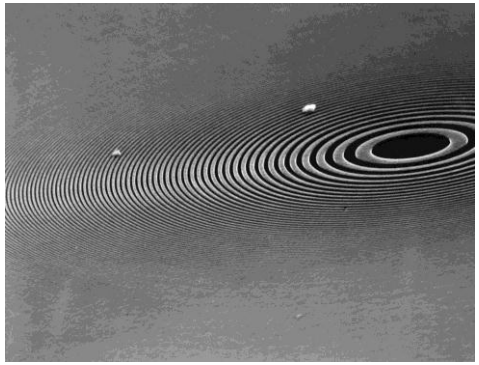

X-ray lens = zone plate
Outer rings 100 atoms apart

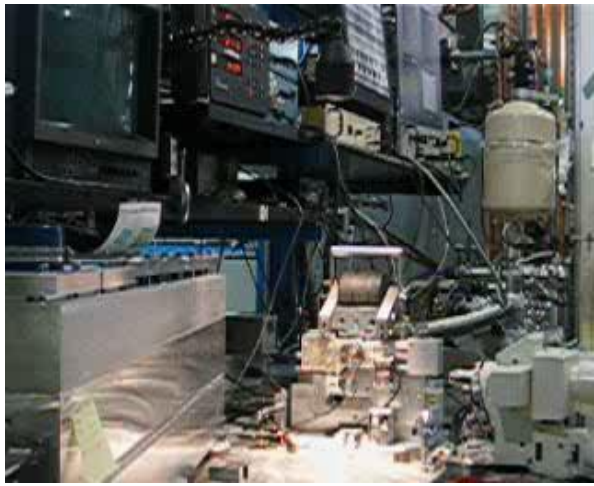

Fischer et al.

Nanometer-Scale Angle-Resolved Photoemission

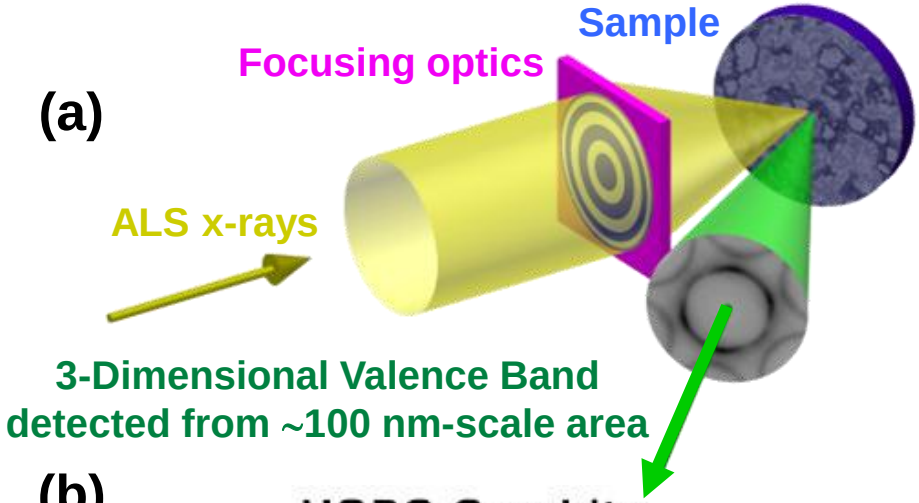

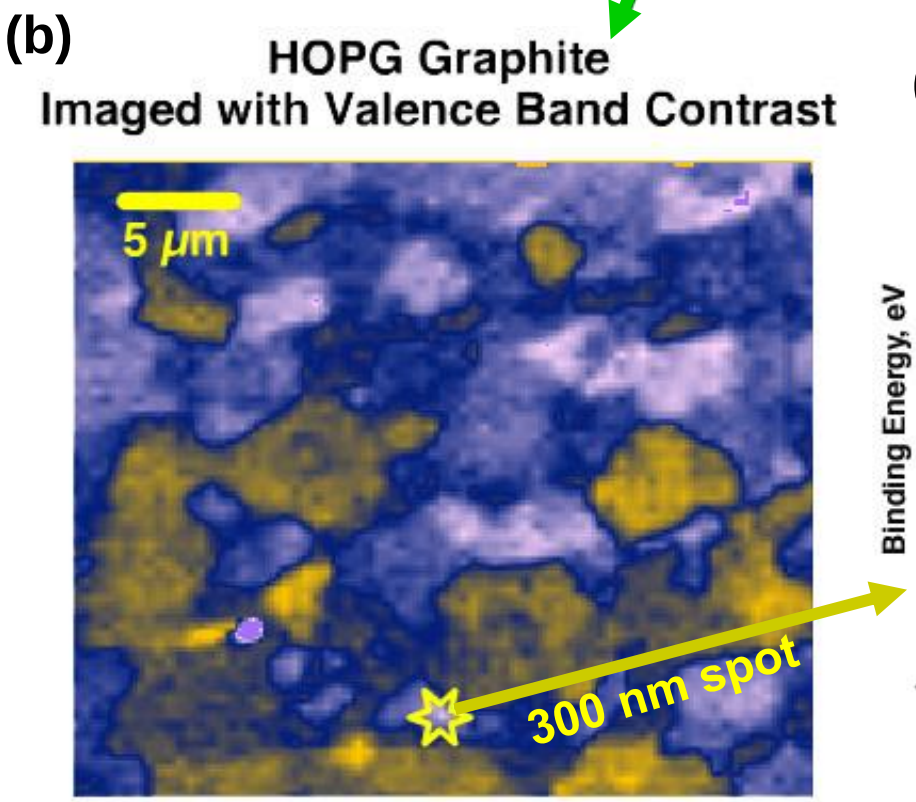

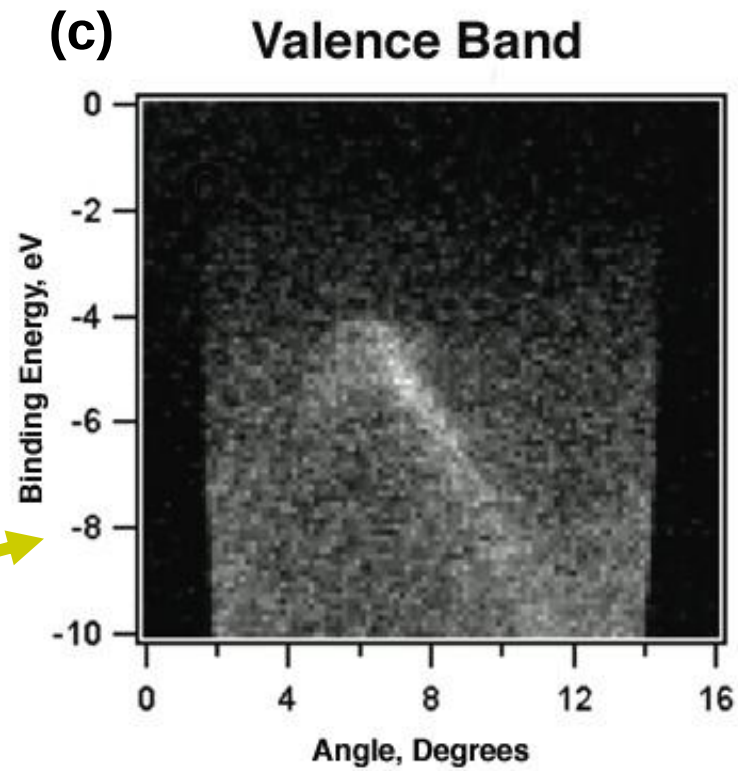

Rotenberg, Bostwick, ALS-LBNL

Basic Concepts and Experiments

Core-Level Photoemission

Intensities and Quantitative Analysis, the 3-Step Model
Varying Surface and Bulk Sensitivity
Chemical shifts
Multiplet Splittings
Electron Screening and Satellite Structure
Magnetic and Non-Magnetic Dichroism
Resonant Photoemission
Photoelectron Diffraction and Holography

Valence-Level Photoemission

Band-Mapping in the Ultraviolet Photoemission Limit
Densities of States in the X-Ray Photoemission Limit

Some New Directions

Photoemission with Hard X-Rays (throughout lectures)
Photoemission with Standing Wave Excitation
Photoemission with Spatial Resolution/Photoelectron Microscopy
⇒ Temporal Resolution
⇒ @ Higher Pressures

Surface sensitivity and why we may want to go to 5-10 keV in XPS

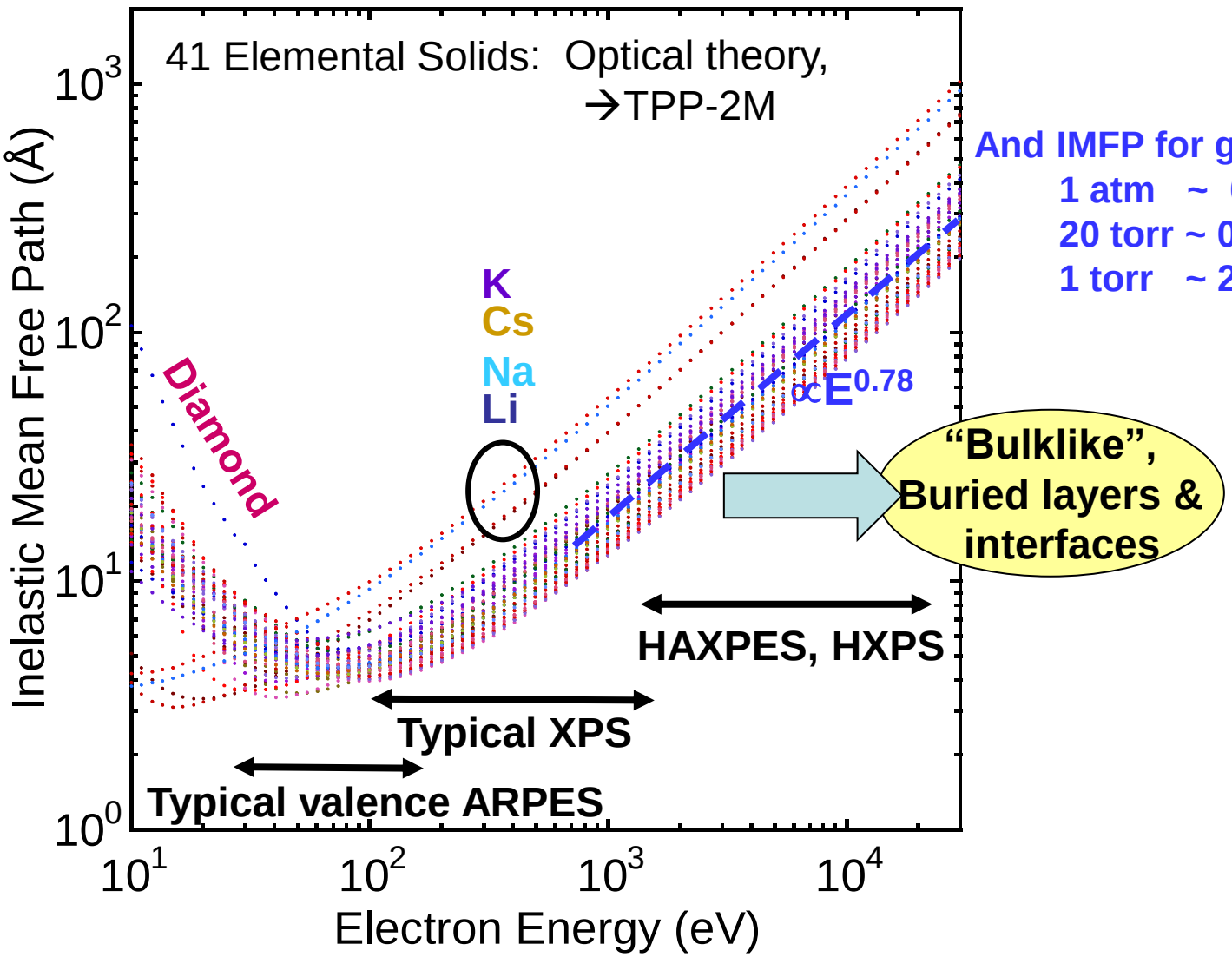

And IMFP for gases: N_2, e^- @ 500 eV
1 atm ~ 0.003 mm = 3 microns
20 torr ~ 0.1 mm = 100 microns
1 torr ~ 2 mm

Tanuma, Powell, Penn, Surf. and Interf. Anal. 43, 689 (2011)

Challenges for high-pressure photoemission: analyzer Pressure and short electron mean free fath

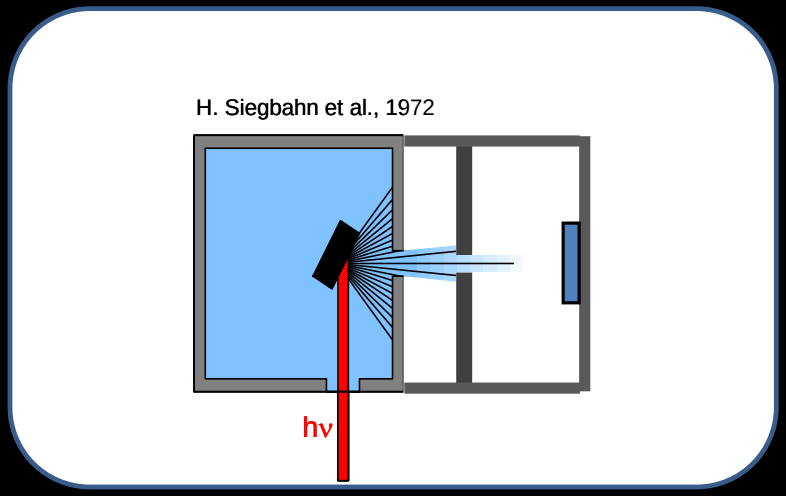

Very low efficiency

IMFP: N_2 @ 500 eV

1 atm ~ 0.003 mm = 3 microns
20 torr ~ 0.1 mm = 100 microns
1 torr ~ 2 mm

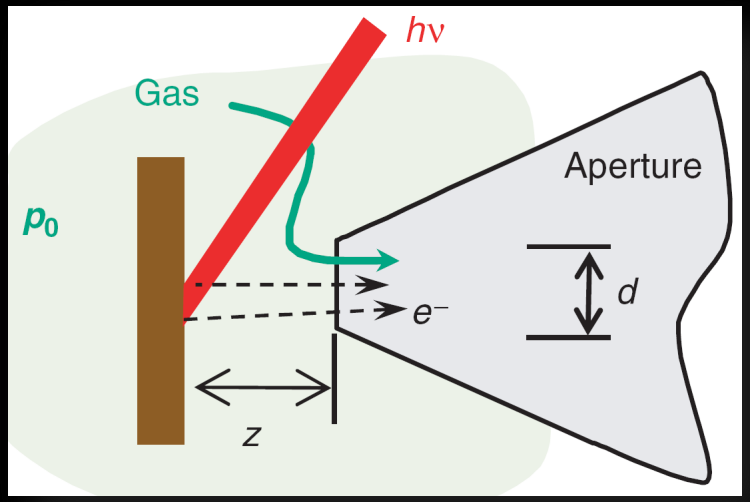

Smaller x-ray spot & z → Higher Pressure…

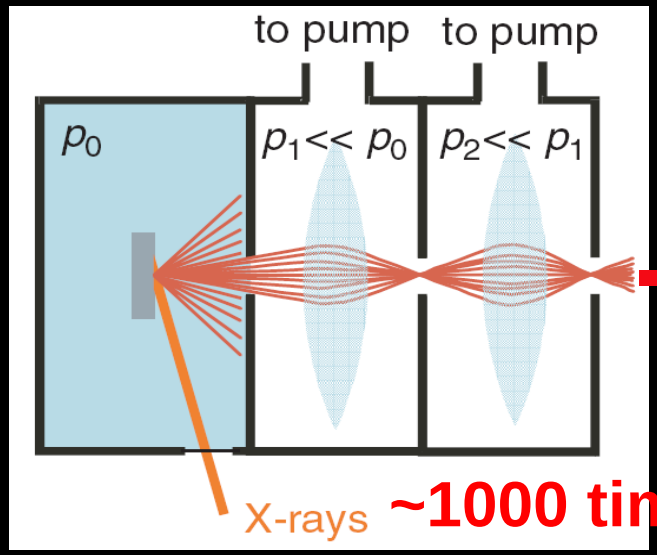

~1000 times

Detector

The first endstation at a SR facility (ALS, BL9.3.2):
D.F. Ogletree, H. Bluhm, G. Lebedev, C.S. Fadley, Z. Hussain, M. Salmeron, Rev. Sci. Instrum. 73 (2002) 3872.

A good review paper:
M. Salmeron and R. Schlögl, Surf. Sci. Rep. 63, 169-199 (2008).

Bridging the Pressure Gap: Chemical-State- and Time- Resolved Oxidation of Si at Multi-Torr Pressures

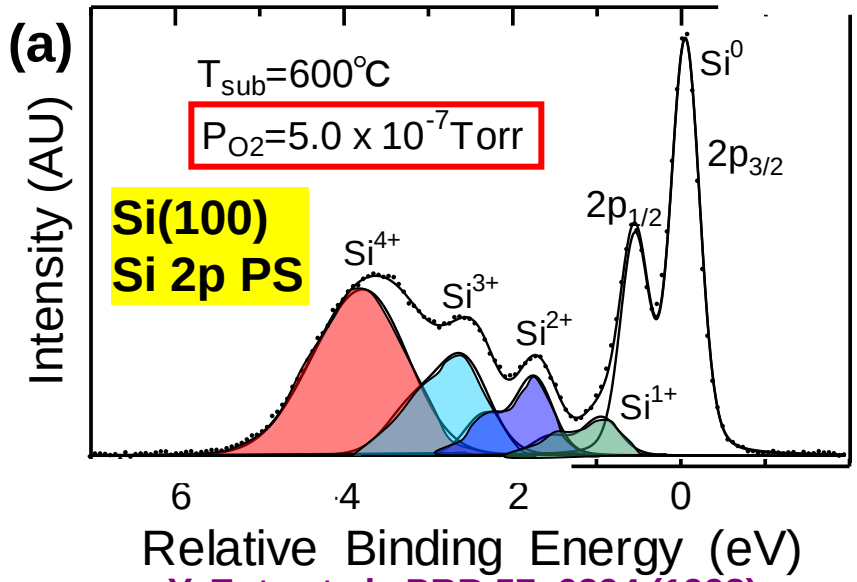

Y. Enta et al., PRB 57, 6294 (1998)

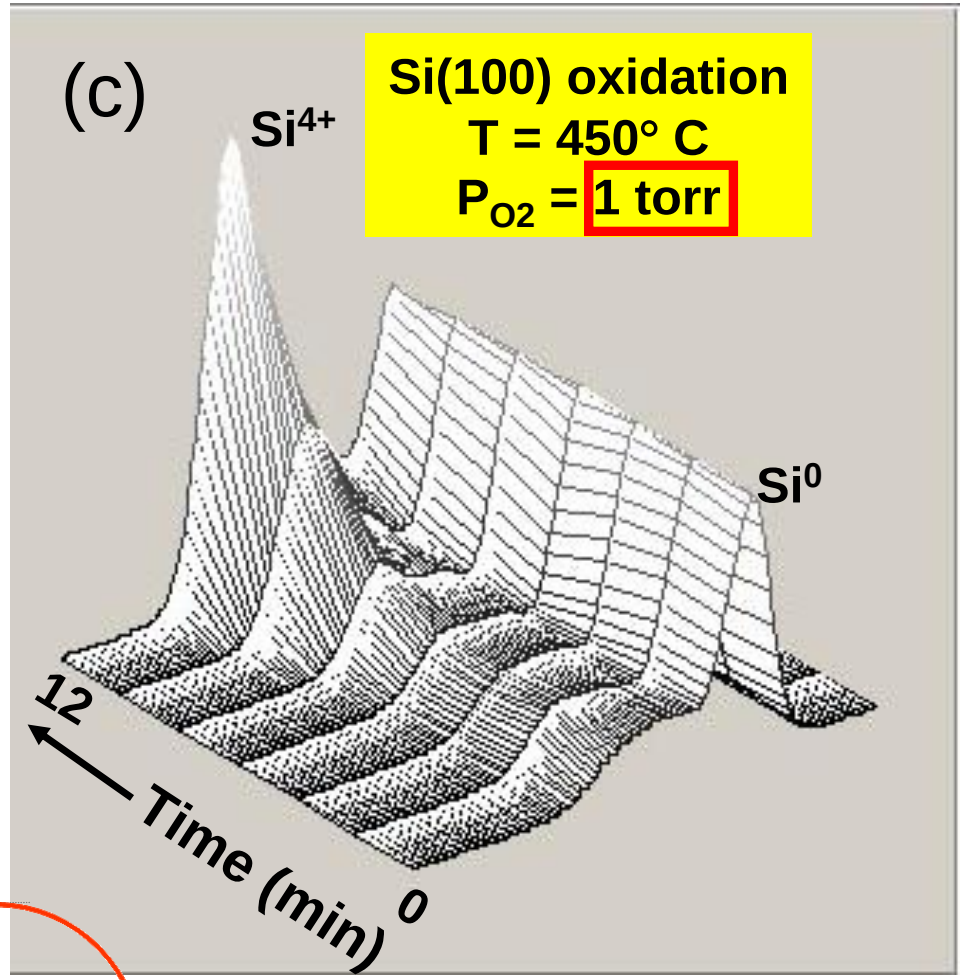

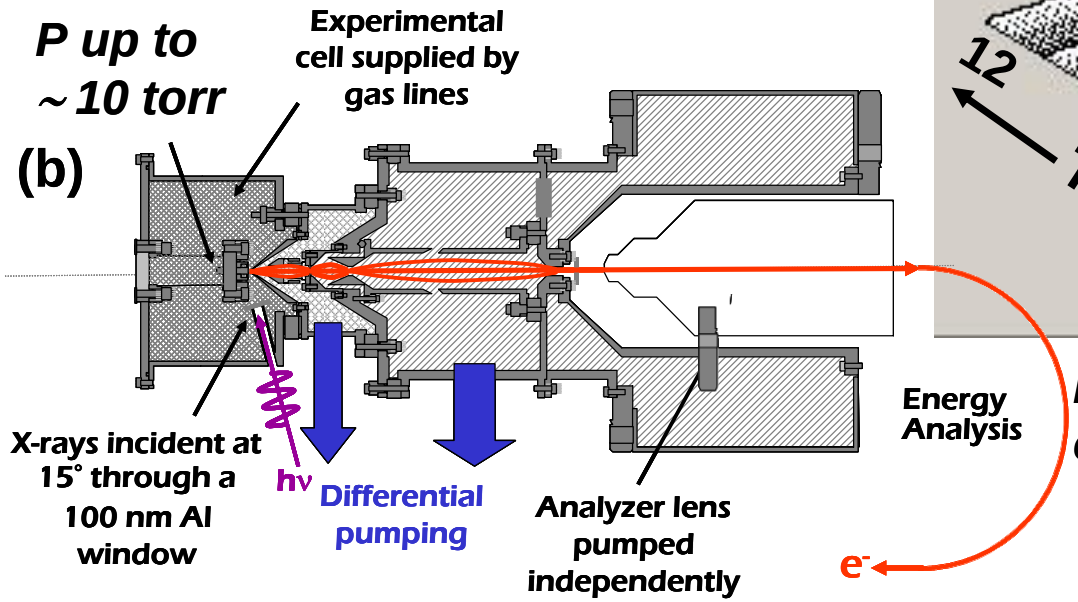

P ≈ 10^{-7} torr or better

Ogletree et al., Rev. Sci. Inst. 73, 3872 (2002)—SR, ALS
Bluhm, Salmeron, Schlögl—ALS, BESSY
Enta, Mun et al., Appl. Phys. Lett. 92, 012110 (2008); J. Appl. Phys. 103, 044104(2008)

Watching the oxide grow in real time: constant P, variable T

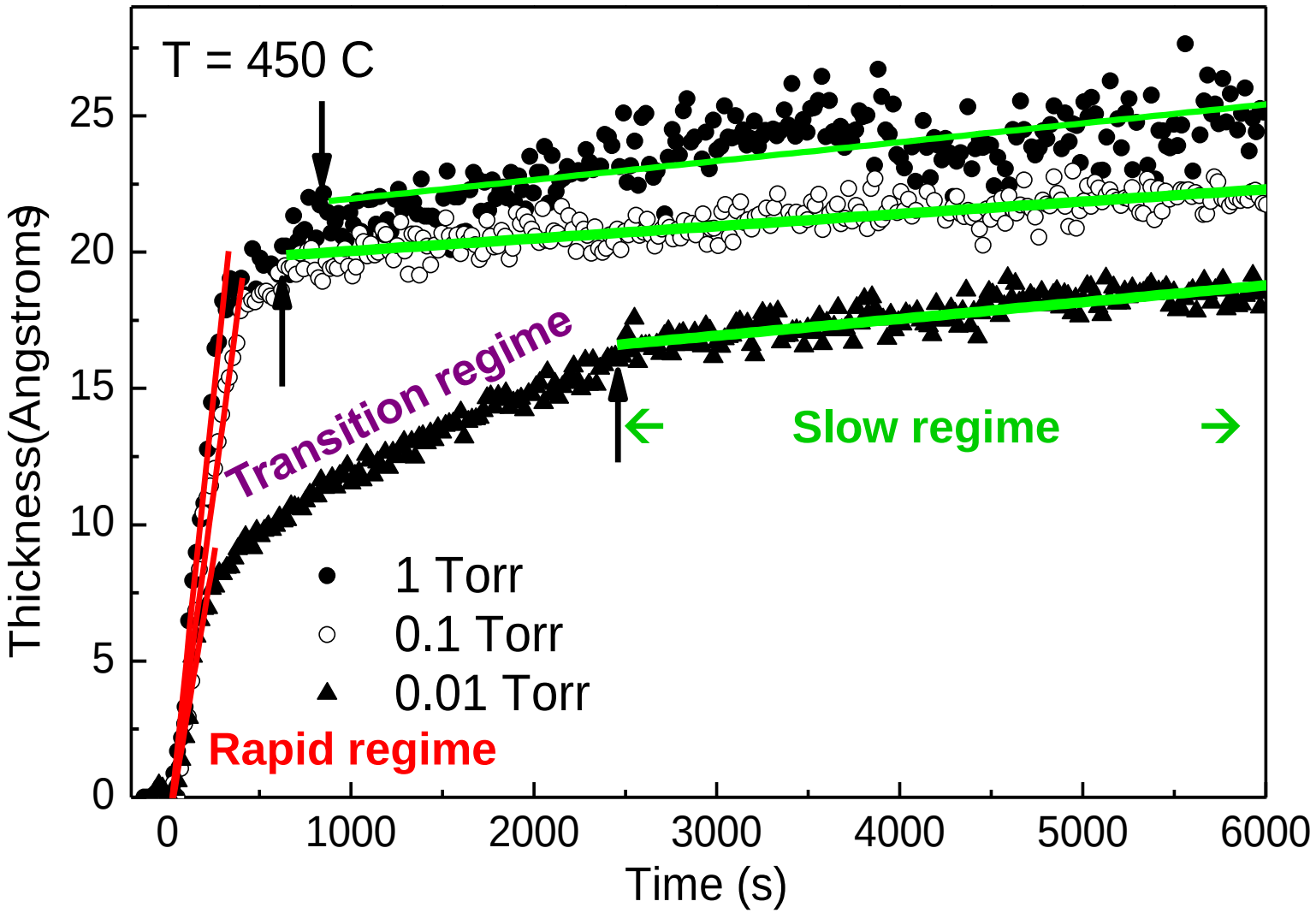

Time-resolved core-level XPS(→HXPS) as a monitor of a charge density wave in Mott insulator 1T-TaS_2

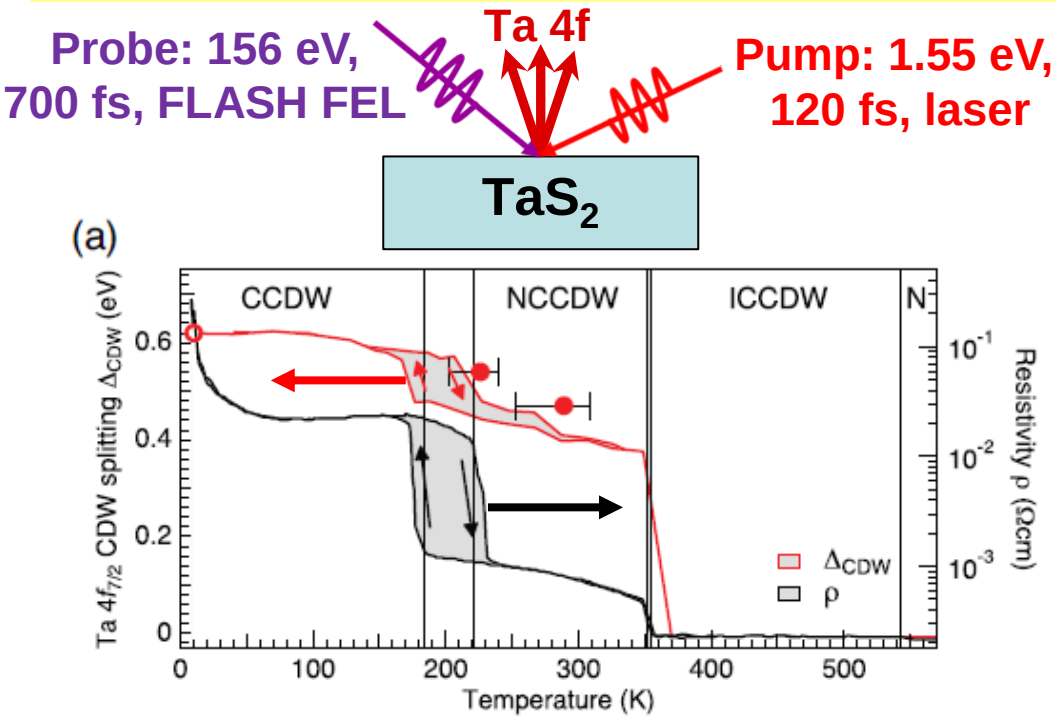

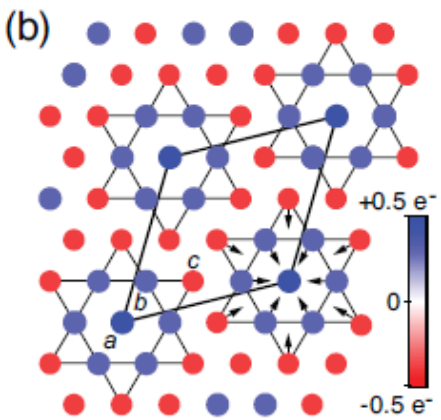

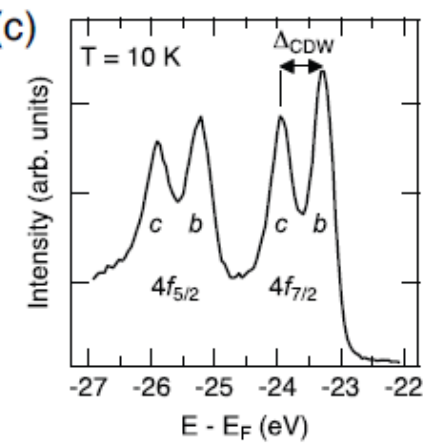

~~a~~:b:c = ~~1~~:6:6

Hellman et al., PRL 105, 187401 (2010)

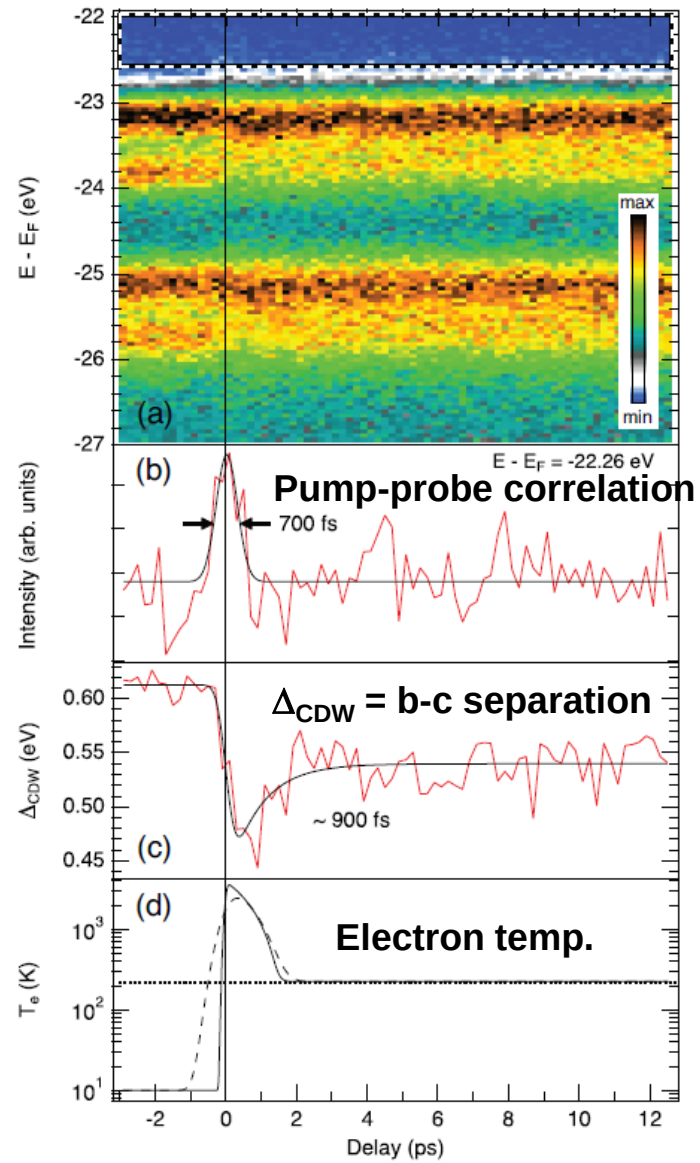

Typical experimental geometry for energy- and angle-resolved photoemission measurements

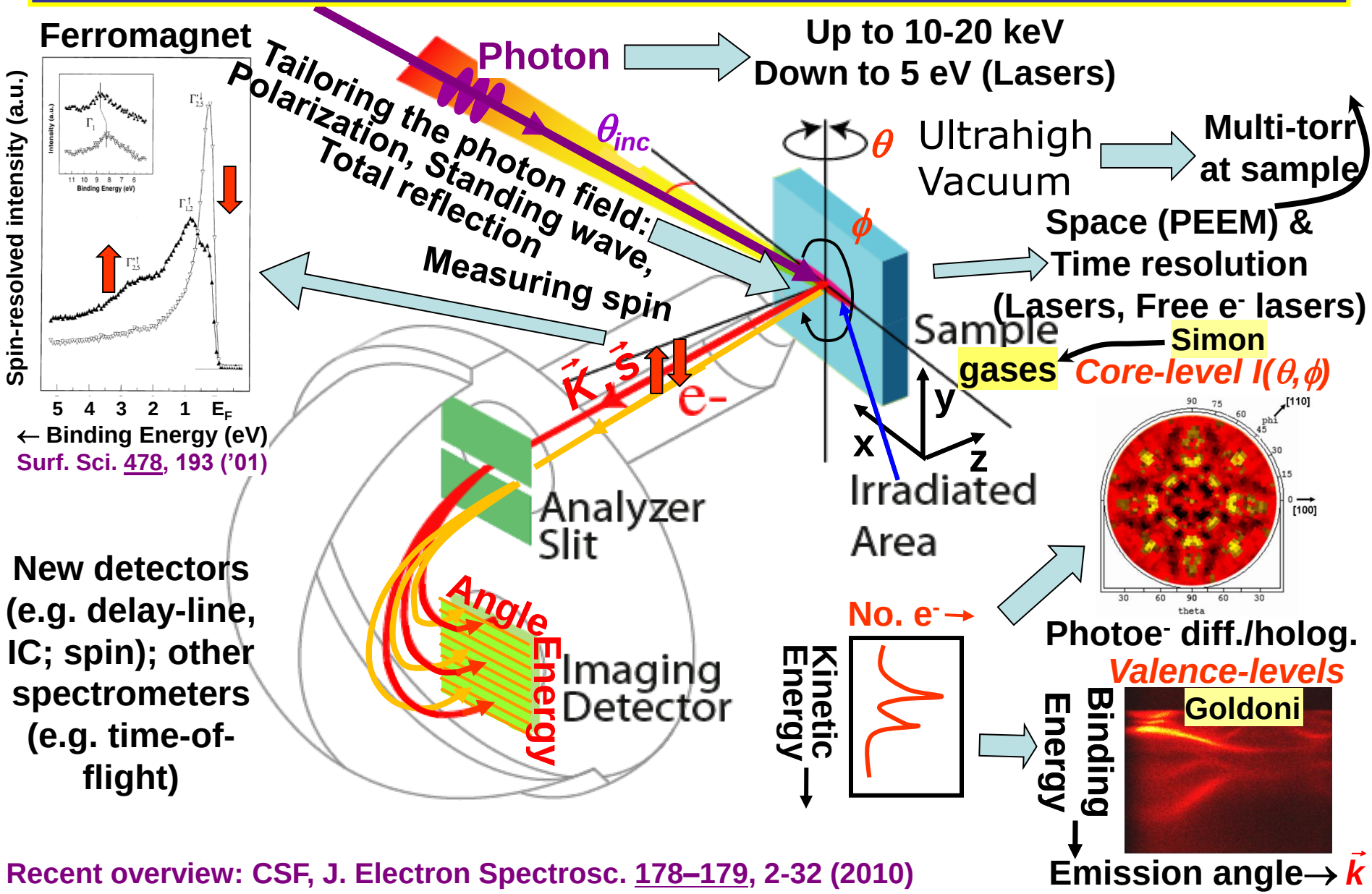

Recent overview: CSF, J. Electron Spectrosc. 178–179, 2-32 (2010)

Basic Concepts and Experiments

The photoelectric effect: 100+ years old! Much enhanced by synchrotron radiation, now moving to the harder x-ray regime and short-pulse FELs

Core-Level Photoemission— an element specific probe

Intensities and the Three-Step Model— quantitative near-surface analysis

Varying Surface and Bulk Sensitivity— vary energy or takeoff angle
standing waves

Chemical shifts— chemical state specific spectroscopy and stoichiometry

Multiplet Splittings— spin state, valence configuration(s)

Electron Screening and Satellite Structure— valence configuration(s)

Magnetic Circular Dichroism– long-range magnetic order

Resonant photoemisson– enhancing a given atom's contribution

Photoelectron Diffraction and Holography– element-specific atomic structure

Valence-Level Photoemission

Band-Mapping in the Ultraviolet Photoemission Limit– valence electronic states
Fermi surfaces, for many materials and nanostructures, ….

Densities of States in the X-Ray Photoemission Limit– densities of states with
greater bulk sensitivity, low temp. measurements→ band mapping

Some New Directions

Photoemission with Hard X-Rays– deeper probing of nanostructures,
densities of states, true bulk electronic structure

Photoemission with Standing Wave (SW) Excitation– selective probing of buried
interfaces and layers

Photoemission with: Spatial Resolution– nanoscale band mapping and
(several spectromicroscopies)

Temporal Resolution– lasers, FELs

@ Higher Pressures– several torr, Realtime kinetics

Miniussi et al., Ru T dependent lineshapes